Computer Model of the Refrigeration System of an Ice Rink

Gabriel Teyssedou

A Thesis

in

The Department

of

Building, Civil & Environmental Engineering

Presented in Partial Fulfillment of the Requirements
for the Degree of Master of Applied Science (Building Engineering) at
Concordia University
Montreal, Quebec, Canada

November 2007

Library and
Archives Canada

Published Heritage
Branch

395 Wellington Street
Ottawa ON K1A 0N4
Canada

Bibliothèque et
Archives Canada

Direction du
Patrimoine de l'édition

395, rue Wellington
Ottawa ON K1A 0N4
Canada

Canada

ABSTRACT

Computer Model of the Refrigeration System of an Ice Rink

Gabriel Teyssedou

During the past years, the increase of energy costs has led to the development of energy calculation models for the prediction of the energy performance of buildings. Ice rinks are buildings using significant quantities of energy because they have simultaneous refrigerating and heating needs. However, only a limited amount of information related to the simulation of ice rink refrigeration systems has been published so far.

This thesis presents the development of a computer model for the simulation of the refrigeration system of an ice rink by using the TRNSYS environment. Thermodynamic principles and empirical relations are used to identify the parameters of the compressor and heat exchangers from manufacturer's data and measurements collected in an ice rink located in Montreal. The model used to simulate the chiller is based on the ASHRAE Toolkit-I. The ice-concrete slab is simulated using an analytical and a correlation-based model. The controller model uses empirical relations to determine the number of compressors in operation based on the brine temperature.

The thesis present the analysis of the collected data and the mathematical description of the models developed for the refrigeration system. Simulations are performed using several days of measurements. The effects of a heat recovery system on the reduction of energy use and the corresponding CO_2 emissions are also investigated.

ACKNOWLEDGMENTS

TABLE OF CONTENTS

LIST OF FIGURES

LIST OF TABLES

NOMENCLATURE

Symbol	Meaning	Units
A	Area of the heat exchanger	m^2
AU_{cond}	Condenser's overall heat transfer coefficient	$W\ {}^\circ C^{-1}$
AU_{evap}	Evaporator's overall heat transfer coefficient	$W\ {}^\circ C^{-1}$
C	Capacitance	$J\ s^{-1}\ {}^\circ C^{-1}$
C_f	Clearance factor	-
C_{min}	Minimum capacitance	$J\ s^{-1}\ {}^\circ C^{-1}$
C_{max}	Maximum capacitance	$J\ s^{-1}\ {}^\circ C^{-1}$
c_p	Specific heat at constant pressure	$J\ kg^{-1}{}^\circ C^{-1}$
$\bar{c}_p$	Mean specific heat at constant pressure	$J\ kg^{-1}{}^\circ C^{-1}$
$c_{p,water}$	Specific heat of water	$J\ kg^{-1}{}^\circ C^{-1}$
f_c	Cut-off frequency	Hz
h	Enthalpy	$J\ kg^{-1}$
h_{fgo}	Enthalpy of vaporization	$J\ kg^{-1}$
h_{fo}	Enthalpy of the saturated liquid at the reference temperature	$J\ kg^{-1}$
$h_{ref,in}$	Enthalpy of the refrigerant at the inlet of a component	$J\ kg^{-1}$
$h_{ref,out}$	Enthalpy of the refrigerant at the outlet of a component	$J\ kg^{-1}$
k	Heat conductivity	$W\ m^{-1}{}^\circ C^{-1}$
$\dot{m}$	Mass flow rate	$kg\ s^{-1}$

$\dot{m}_{brine}$	Brine mass flow rate	kg s^{-1}
$\dot{m}_{ref}$	Refrigerant mass flow	kg s^{-1}
$\dot{m}_{water}$	Mass flow rate of water in the heating tank	kg s^{-1}
$m_{water,resurf}$	Mass of water spread during resurfacing	kg
I_t	Input signal	-
n	Number of compressors	-
N	Number of working points	-
O_t	Output signal	-
P	Pressure	Pa
P_0	Reference pressure	Pa
P_1	Compressor suction pressure	Pa
P_2	Compressor discharge pressure	Pa
$\dot{Q}_{cond}$	Rate of heat transfer in the condenser	W
$\dot{Q}_{evap}$	Rate of heat transfer in the evaporator	W
$\dot{Q}_{evap,i}$	Actual value of the refrigeration capacity	W
$\tilde{\dot{Q}}_{evap,i_i}$	Calculated value of the refrigeration capacity	W
$\dot{Q}_{ice}$	Cooling load on the ice sheet	W
$\dot{Q}_{max}$	Maximum rate of heat transfer	W
$\dot{Q}_{resurf}$	Cooling load of resurfacing	W
$\dot{Q}_{water}$	Rate of heat supplied by the heating tank to the water	W
r	Compression factor	-

R	Gas constant	J kg^{-1} °C^{-1}
t	Time	s
T	Period	s
T_{air}	Exterior air temperature	°C
T_{tank}	Temperature of the water in the tank	°C
$T_{air,out,cond}$	Air temperature at the condenser outlet	°C
$T_{air,out,lat}$	Air temperature after latent heat transfer at the condenser	°C
$T_{air,out,subcool}$	Air temperature after sub-cooling on refrigerant side	°C
$T_{aqueduct}$	Temperature of water in the aqueduct	°C
T_b	Brine temperature	°C
$T_{brine,in,pump}$	Brine temperature at the inlet of the pump	°C
$T_{brine,out,chill1}$	Brine temperature at the exit of chiller #1	°C
$T_{brine,out,chill2}$	Brine temperature at the exit of chiller #2	°C
$T_{brine,out,pump}$	Brine temperature at the pump outlet	°C
$T_{brine,out,sens}$	Brine temperature after the latent heat exchange	°C
T_c	Temperature cold reservoir	°C
T_h	Temperature hot reservoir	°C
T_{ice}	Ice temperature	°C
$T_{ice,after}$	Ice temperature after resurfacing	°C
$T_{ice,before}$	Ice temperature before resurfacing	°C

$T_{ref,in,evap}$	Refrigerant temperature at the inlet of the evaporator	°C
$T_{ref,in,exp,valve}$	Refrigerant temperature at the inlet of the expansion valve	°C
$T_{ref,out,comp}$	Refrigerant temperature at the compressor outlet	°C
$T_{ref,out,cond,de\sup}$	Refrigerant temperature after de-superheating	°C
$T_{ref,out,cond,lat}$	Refrigerant temperature after latent exchange at condenser	°C
$T_{ref,out,evap}$	Refrigerant temperature at the exit of the evaporator	°C
$T_{ref,out,evap,lat}$	Refrigerant temperature after latent exchange at evaporator	°C
T_0	Reference temperature	K
T_{sat}	Saturation temperature of the refrigerant	°C
T_{slab}	Temperature of the concrete slab	°C
$T_{vert,air}$	Vertical profile or air temperature	°C
U	Average overall heat transfer coefficient	W m^{-2} °C^{-1}
v	Specific volume	m^3 kg^{-1}
V	Volume	m^3
$\dot{V}$	Volumetric volume flow	m^3 s^{-1}
$\dot{V}_s$	Swept volume flow rate	m^3 s^{-1}
w_c	Center frenquency	Hz
$\dot{W}$	Power	W
$\dot{W}_i$	Actual value of the compressor electric input	W
$\tilde{\dot{W}}_i$	Calculated value of the compressor electric input	W

$\dot{W}_{lo}$	Constant part of electromechanical losses	W
$\dot{W}_{s}$	Compressor isentropic power	W

Greek symbol

α	Loss factor	-
ΔT_{m}	Logarithmic mean temperature difference	°C
ΔF_{g}	Radiative forcing of a gas	$W\,m^{-2}$
$\Delta T_{ref,cond}$	Refrigerant temperature difference at the condenser	°C
$\Delta T_{ref,evap}$	Refrigerant temperature difference at the evaporator	°C
$\Delta T_{subcool}$	Degree of sub-cooling	°C
$\Delta T_{sup\,heat}$	Degree of superheating	°C
Δx_{ice}	Ice thickness	m
$\bar{\gamma}$	Mean isentropic coefficient	-
ε	Heat exchanger effectiveness	-
ρ	Density	$kg\,m^{-3}$
ζ	Mean compressibility factor	-

Abbreviations

ANOVA	Analysis of variance
ARI	Air-Conditioning and Refrigerating Institute
ASHRAE	American Society of Heating, Refrigerating, and Air-Conditioning Engineers, Inc.

BLAST	Building loads analysis and system thermodynamic
BHP	Brake horse power
CAP	Capacity of one compressor
CFC	Chlorofluorocarbon
CCOHS	Canadian Centre for Occupational Health and Safety
COP	Coefficient of performance
CVF	Compaq Visual Fortran
DLL	Dynamic Link Library
DWS	Durbin-Watson statistic
EES	Engineering Equation Solver
EPA	Environment Protection Agency
GHG	Greenhouse gases
FDD	Fault detection and diagnoses
GWP	Global warming potential
HB	Heat balance
HBB	Heat balance on the brine side
HBR	Heat balance on the refrigerant side
HCFC	Hydrochlorofluorocarbon
HVAC	Heating, ventilating and air conditioning
IVF	Intel Visual Fortran
MAE	Mean absolute error
MPS	Microsoft Power Station
MVC	Microsoft visual C++

MVS	Microsoft Visual studio.NET
NCU	Number of compressors in use
NRCan	Natural Resources Canada
ODP	Ozone depletion potential
PID	Proportional integral derivative
PP	Power to the pump, lighting system and control panel
PCC	Power of one compressor-condenser unit
PRISM	Princeton Scorekeeping Method
RBT	Return brine temperature
RGT	Return gas temperature
SDT	Saturated discharge temperature
SEE	Standard error of estimate
SST	Saturated suction temperature
ST	Saturation temperature
TEWI	Total Environmental Warming Impact
TED	Total electric demand
UNEP	United Nations Environmental Protection
WMO	World Meteorological Organization

CHAPTER 1

INTRODUCTION

Everyday, huge amounts of energy are used by all sectors of our economy. From transport to industries, energy constitutes the base of our development. But currently, energy demand is growing at such a tremendous speed, that we are now facing a global challenge. The energy needs of millions of people must be satisfied with resources that are depleting everyday.

The energy issue has become so important owing to the fact that global energy demand is growing at two percent rate per year. This percentage is projected to double by 2035 with limited energy resources (Friedman and Homer-Dixon 2004). The consequence of this increase is that in the last decade energy costs have grown extremely fast. Societies must now find a way of maintaining the actual social economical growth while reducing the energy demand to ensure sustainable development.

1.1 Energy and environmental issues

The energy issue can be divided into two categories: supply and demand. At the moment, the largest part of the energy produced comes from the burning of fossil fuels. In addition, the majority of the scientific community agrees that the combustion of fossil fuels is partially responsible of global warming. Fuel combustion releases carbon dioxide, an important greenhouse gas (GHG) that contributes to the global warming of the planet.

By signing the Kyoto protocol in 1997, 154 countries agreed to encourage policies, programs and new technologies to reduce the emissions of six greenhouses gas responsible of global warming such as carbon dioxide (CO_2), methane (CH_4) and Hydrofluorocarbons (HFC). For instance, Canada was expected to reduce by 5.2% the emissions of GHG from 1990 levels by the year 2012 (Environment Canada 2005). Since 1990, Canada's GHG emissions have increased of 25%. Hence, to reach Kyoto's targets, the necessary reduction to respect the agreement is approximately of 30%.

Improving the management of the energy use is the second challenge that must be attained. Energy efficiency contributes to this goal and also reduces the greenhouse gas emissions. To achieve higher levels of energy reduction, efficient measures are more desirable in areas where significant amounts of energy are used.

Buildings are one of these areas. In Canada, about 30% of secondary energy (the energy used by final consumers) is used by building equipment (CANMET 2006). In 2001, the use of energy in buildings led to 135 MT of equivalent CO_2 emissions contributing by about 30% of the total emissions of Canada. Considering that 40% of existing buildings in Canada were constructed before the 1960's (NRCan 2003) using poor construction techniques, poor insulation and non optimized designs, the potential for energy savings in this sector is considerable.

Two types of buildings show a high potential of reduction of energy use: supermarkets and ice rinks. These buildings are similar because they both require significant amounts of heating and cooling simultaneously. Furthermore, supermarkets

and ice rinks are characterised by a positive assessment; meaning that the refrigeration system rejects enough heat that might satisfy the heating requirements of the building.

Several studies have been conducted in the field of energy efficiency of refrigeration systems. However, only a few publications covered the efficiency of refrigeration systems for ice rinks. There is a need of numerical models capable of predicting the energy use in those refrigeration systems.

1.2 Ice rinks issues

Ice rink refrigeration systems are not efficient due to the following reasons (Lavoie et al. 2000):

- In Quebec, 70% of the arenas are more than 20 years old and use low efficiency technology;
- Refrigeration systems often leak which means that they need to be refilled with expensive refrigerant;
- The refrigeration system is not integrated to the HVAC system of the building.

Lavoie et al. (2000) evaluated that, on an annual basis, arenas in Quebec consume on average 1,525,000 kWh/year of energy while rejecting 1,630,000 kWh/year of heat. Actual heating needs of arenas are approximately of 577,000 kWh/year, almost one third of the total heat rejected. Based on an evaluation of several energy efficient measures applied to refrigeration systems, the study has evaluated that the energy savings could reach 625,250 kWh/year (41% of the actual consumption). For the 435 arenas across Quebec, the possible energy savings are about 27 GWh/year, while the corresponding emissions reductions are 63 kT of equivalent CO_2.

While the energy use by the refrigeration systems has an indirect impact on the GHG emissions, the leaks of refrigerants have a greater and direct impact. In 90% of Quebec's arenas refrigerant R-22 is used, which is a high GHG emitter (Lavoie et al. 2000). Leaks of R-22 are evaluated to be of 60 kg per year per arena, which is equivalent to 114 tons of equivalent CO_2 (total of 49 kT for the 435 arenas).

The Montréal protocol signed in 1987 stipulates that starting in 2004 the production of R-22 must be phased out by 2030. Furthermore, in 1998, the Canadian government has adopted a regulation concerning the ozone-depleting substances with the aim to gradually reduce the use of HCFC. This is an important issue knowing that in the coming years, several refrigeration systems will be replaced with new generation systems that will have to operate with another refrigerant than R-22.

1.3 Thesis proposal and layout of the study

The purpose of this project consists in the development of a mathematical model of the refrigeration system with the goal of analyzing the energy use of the refrigeration system of an ice rink. TRNSYS (Klein et al. 2000) environment is used to perform the simulations of the refrigeration system. The model is calibrated using the data collected at a monitored ice rink in Montreal. The monitoring results are available from an ASHRAE project (Ouzzane et al. 2006) carried out by CANMET-Varennes with the collaboration of N. Galanis from Université de Sherbrooke, R. Sunyé from CANMET-Varennes and R. Zmeureanu from Concordia University. The impact of operating strategies on the energy use and the CO_2 emissions are also evaluated.

Since the TRNSYS environment has a modular structure, the refrigeration simulation is developed in such a way to allow for the change of models of a particular component of the refrigeration system. The following components are developed and integrated in the model of the refrigeration system:

i)   the ice-concrete slab is modeled by two approaches: an analytical solution, and an inverse model;

ii)   the chillers is defined using the ASHRAE Toolkit for Primary Equipment (Bourdouxhe et al. 1997), and using manufacturer's data for parameters identification;

iii)   the controller is defined by using empirical rules.

Components of the refrigeration system are programmed and compiled by using C++ language and the corresponding dynamic link library (DLL) models are generated and connected within TRNSYS. The simulation results obtained from the TRNSYS model are compared with measured temperatures and electric demand from the monitored ice rink. Finally, the potential energy savings due to the heat recovered from the condenser over the system life cycle are analyzed. An estimation of the reduction of greenhouse gases over the system life cycle is obtained.

CHAPTER 2

LITERATURE REVIEW

The literature review skims through the studies related to the refrigeration systems of ice rinks. The information in this field is limited and scarce. A few studies have been done in similar refrigeration domains and the results of these studies are presented.

This chapter introduces the vapour compression refrigeration cycle, which is the most used in Quebec's arenas. A discussion regarding the refrigerant industry is presented with a particular attention to the refrigerants used in ice rinks. Secondary coolants used in refrigeration systems are discussed as well. Operating conditions leading to more energy efficient systems in ice rinks are also discussed. The present literature review is focused on the use of TRNSYS and others simulation programs applied for the analysis of refrigeration systems.

2.1 Refrigeration systems

Refrigeration systems can be classified into two main categories: vapour compression systems and absorption systems (Çengel and Boles 2002). While compression systems use compressors to transform the refrigerant from a saturated mixture into superheated vapour, absorption systems operate with a generator. Because the vast majority of arenas employ vapour-compression systems (Lavoie et al. 2000), absorption systems will not be covered in this chapter.

A vapour compression refrigeration system is composed of four main components: a compressor, an expansion valve and two heat exchangers (evaporator and condenser) as presented in Figure 2.1 (Çengel and Boles 2002). Each number stands for a thermodynamic state of the cycle, and the arrows indicate the direction in which the working fluid circulates.
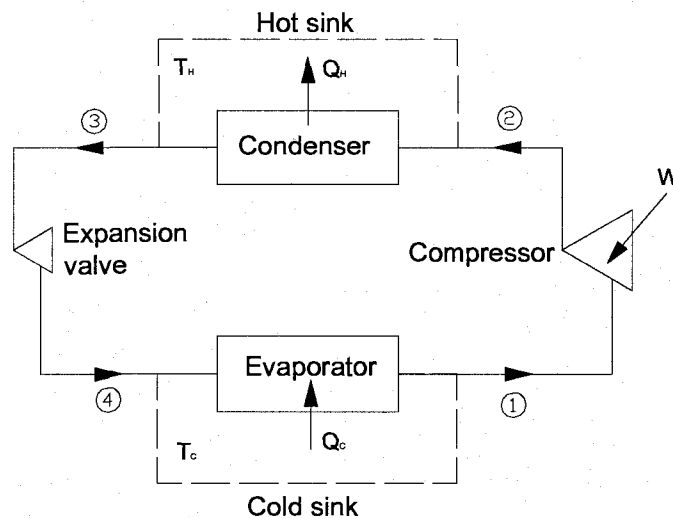
Figure 2.1: Vapour compression refrigeration cycle

Here, Q_C and Q_H are the heat absorbed and rejected by the system while W is the work input to the compressor. The vapour-compression refrigeration cycle can be divided into four processes:

a - heat absorption (Q_C) by the refrigerant from the cold sink while flowing through the evaporator (process 4-1);

b - compression of the refrigerant from low pressure to high pressure (process 1-2);

c - heat rejection (Q_H) when the refrigerant passes through the condenser (process 2-3);

d - expansion of refrigerant through the expansion valve (process 3-4).

Three types of compressors are commonly used in vapour compression refrigeration cycles: reciprocating, centrifugal and screw. Reciprocating compressors use a piston with a reciprocating motion in a cylinder as compressing element. The piston is driven by a crankshaft that allows the compression by increasing the pressure of the refrigerant. This type of compressor can be found in most of Québec's arenas (Lavoie et al. 2000).

A compressor can either be open or hermetic. Open compressors have an external driving motor connected by a driven shaft, whereas hermetic models have a driving motor sealed inside the compressor housing. Hence, in hermetic compressors, the motor has a direct contact with the refrigerant. These models are more often recommended when using toxic or dangerous refrigerants to avoid leaks. In Quebec ice rinks, open compressors are more often used (Lavoie et al. 2000).

2.2 Refrigerant and environmental issues

During the past decade, several studies have demonstrated the relation between the depletion of the ozone layer and the use of refrigerants that contain chlorine. Following the discovery in 1985 of a hole in the ozone layer over Antarctica, governments recognized the necessity to eliminate the production of chlorofluorocarbons (CFCs). These ozone-depleting substances contain either chlorine or bromine. The Montréal protocol, adopted in 1987, will gradually phase-out the consumption and production of CFCs and halogenated hydrocarbons (UNEP 2006). In 2000, they were in fact eliminated from the market. The protocol also called for a complete elimination of

hydrochloroflurocarbons (HCFCs) by 2030. HCFCs are still tolerated today because they have a shorter lifetime than CFCs. In fact, HCFCs are largely destroyed in the lower atmosphere.

Depending on the molecular composition of a refrigerant, the related consequences on the environment are different. In order to characterize the environmental effects, the scientific community has introduced several measuring factors. Each factor targets a specific consequence allowing to compare the refrigerants based on identified criteria. Commonly used refrigerants with their associated chemical formula and environmental factors are presented in Table 2.1.

Table 2.1: ODP and GWP values for most used refrigerants (Calm and Hourahan 2001)

Number	Structure	ODP	GWP 100 years	Atmospheric life (years)
11	CCl_3F	1.0	4600	45
12	CCl_2F_2	0.8200	10600	100
115	$CClF_2CF3$	0.4	7200	1700
22	$CHClF_2$	0.034	1700	11.9
134a	CH_2FCF_3	0	1300	13.8
123	$CHCl_2CF_3$	0.012	120	1.4

[1]100 years time horizon

Table 2.1 introduces the ozone depletion potential (ODP) index that is used to measure the capacity of a refrigerant to destroy the ozone layer (EPA 2006). This factor is defined as the ratio impact between the mass of any gas over the same amount of refrigerant CFC-11. Hence, by definition, the CFC-11 has an ODP of one. Chlorine is the main element that increases the ODP factor, thus all refrigerants containing this element in their composition have an ODP between 0.01 and 1.

Table 2.1 also introduces the global warming potential (GWP) of some refrigerants. The GWP is a weighting factor comparing the global warming effect of 1 kg of a gas with the global warming effect of 1 kg of CO_2. The GWP of a gas is obtained by integrating over a period of time the radiative forcing of the gas (ΔF_g) and the fraction of the greenhouse gas remaining in the atmosphere after a time period, compared with carbon dioxide (EPA 2006).

The Total Equivalent Warming Impact (TEWI), introduced in the early 1990s is an indicator that allows to evaluate the CO_2 emissions of a refrigeration system or heat pump (CETIAT 2000). It considers both the global warming effect of the refrigerant leaked into the atmosphere (direct impact) and the global warming effect due to the energy used over the lifetime of the refrigeration system (indirect impact). Therefore, TEWI is more accurate than the GWP factor in refrigeration applications because it provides a more complete measure of the impact of a refrigerant over its lifetime.

2.3 Refrigerants in ice rinks

According to a study carried out by Lavoie et al. (2000) on ice rinks across Quebec, 90% of the refrigeration systems use refrigerant R-22, while the remaining use ammonia. Due to its low operating costs, refrigerant R-22 is preferred to ammonia even if ammonia has no effect on the ozone layer, has a significantly higher heat transfer coefficient and it is more economical. Although ammonia is probably the best refrigerant from an economical and physical point of view, it is also a powerful respiratory irritant that can affect people at very low concentrations (CCOHS 2003).

In average, an arena use approximately 750 kg of HCFC-22. Each kilogram of R-22 that leaks from the refrigeration system is equivalent to an emission 1900 kg of CO_2 (WMO 1999). Lavoie et al. (2000) have evaluated that almost 10% of the refrigerant in the arena's system leaks every year to the atmosphere.

2.4 Secondary coolant in ice rinks

Almost all refrigeration systems in ice rinks use secondary coolants to transport and transfer heat from a medium to another. The secondary coolant is cooled by passing through the evaporator of the refrigeration system, and then it absorbs heat by passing through the heat exchanger installed in the concrete slab under the ice sheet. While transferring heat from the ice sheet to the heat exchanger, the secondary coolant does not change phase. The mass flow rate is established as a function of the desired ice temperature, the number of passes through the concrete slab and the thermal load on the ice sheet.

Two coolants are generally used in refrigeration applications: Calcium Chloride (CaCl) and glycol. In Québec's arenas, Calcium Chloride is more often used. In terms of energy efficiency, Calcium Chloride is a better choice than glycol because it has a higher heat transfer coefficient. Properties of secondary coolants are presented in Table 2.2 (ASHRAE 1998a).

Table 2.2: Characteristics of main secondary coolants (ASHRAE 1998a)

Secondary coolant	Concentration (by mass) %	Freezing point °C	Heat transfer coefficient W/(m^{2}K)
Propylene glycol	39	-20.6	1164
Ethylene glycol	38	-21.6	2305
Calcium chloride	22	-22.1	3214

Hence, systems operating with CaCl require smaller chillers and a smaller brine pump for the same heat transfer needs than systems using glycol. Smaller chillers and pumps are less expensive and use less energy leading to more economical systems. Although Calcium Chloride is the most energy efficient coolant, it is highly corrosive. This results into a shorter lifetime for the refrigeration system if it is not properly maintained.

The secondary coolant circulates inside propylene or cooper pipes that are inside the concrete slab under the ice sheet, installed with two, four or six passes before returning to the evaporator. The material and diameter of the coolant pipes are factors that influence the energy demand of the system. In Quebec arenas, 90% of the systems use two passes configuration while the rest use four passes network (Lavoie et al. 2000).

2.5 Energy efficient strategies for ice rink refrigeration systems

Studies that examine the efficiency and performance of ice rink refrigeration systems are scarce. Most of these studies have been carried out by the refrigeration industry and information is rarely shared or accessible. Government and universities research centers have published a few studies. The following pages present a summary of the work accomplished in the sector of ice rink efficiency.

2.5.1 Ice temperature control

Each activity in an ice rink has its own optimum ice temperature, which is related to the hardness of the ice surface. Table 2.3 presents the optimum ice temperature for different types of ice sports (CANMET 2003a).

Table 2.3: Ice temperature for different activities (CANMET 2003a)

Activity	Optimum temperature
Hockey	-6 °C to -5 °C
Artistic skating	-4 °C to -2 °C
Free skating	-2 °C to -2 °C
No activity	-2 °C to -1 °C

To avoid a continuous regulation of the refrigeration system, ice rink managers usually operate at a constant low ice temperature. Consequently, the ice temperature is often unnecessary low, which increases the electric demand of the system. A better energy strategy would consist of the use of variable ice temperatures as a function of the activity. However, the direct control of the ice temperature is not a simple task, since the control system must be tuned to consider several factors influencing the stability of the refrigeration system. A study carried out by CANMET (2003a) shows that the use of a floating ice temperature can lead to energy savings up to 2% of the annual energy use. More important savings can be realized by raising the ice temperature during the unoccupied hours (overnights and mornings) and by scheduling activities requiring higher ice temperatures in the morning and during the evenings. Ice temperature control is the key for a better control of the energy demand of ice rinks.

2.5.2 Ice and concrete slab

The heat transfer through the ice and concrete slab depends on the overall thermal resistance. The thicker the ice sheet and concrete slab, the greater is the thermal resistance. As revealed by CANMET (2003b), the ice and concrete slab thicknesses have considerable impact on the energy use of the refrigeration system. A reduction of 1 mm of the ice slab thickness leads to energy savings of 400 kWh/year, while a reduction of 1

13

mm of the concrete slab thickness leads to energy savings of 80 kWh/year. The thickness

of ice sheet is usually maintained in a range varying between 20 to 40 mm. The thickness

of concrete slab is generally of 25 mm above the cooling pipes as shown in Figure 2.2.
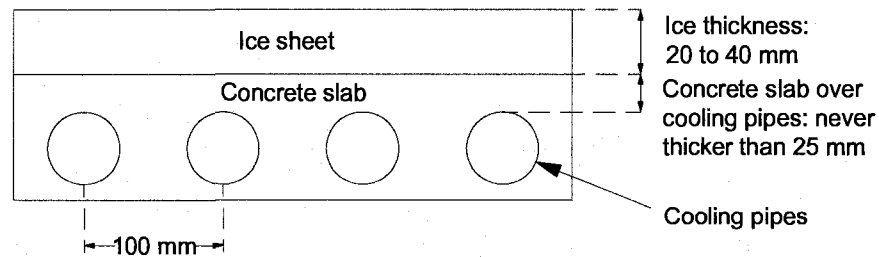
Figure 2.2: Schematic of the ice sheet, concrete slab and cooling pipes

The use of different ice thicknesses might be considered depending on the

activity. Indeed, hockey requires thicker ice than free skating. CANMET (2003b)

suggests maintaining an optimal ice thickness of 25 mm. The concrete slab above the

coolant pipes should never be thicker than 25 mm.

2.5.3 Compressors

The optimization of the performance of a refrigeration system depends on the

ability to control the power needed by compressors. Because the refrigeration load of an

ice rink is not constant, compressors must be able to operate in a wide range of

conditions. A system retrofit carried out on an ice rink in Québec has shown that screw

compressors were more adapted for this type application (Tremblay 2001). When a small

cooling load is required, screw compressors can be used at 10% of their maximum load,

while reciprocating compressors can only operate at 50% of their maximum load.

For reciprocating compressors, the control of the condensing pressure (also called head pressure) constitutes an energy efficient strategy widely discussed in the literature. Usually, ice rinks are designed to operate at a high and constant head pressure. This ensures a safe and reliable operation at high outdoor temperatures. Brownell (1998) compared the efficiency of ice rink refrigeration systems operating with a fixed and a floating head pressure. The study reveals that a floating head pressure can lead to a reduction of the compressor power input and therefore, to the increase of the COP of system. However, in some cases, a floating head pressure can increase the condenser power input. This situation occurs when at high pressure the outdoor temperature is not sufficiently low to properly condensate the refrigerant. The author concludes that by combining a variable speed compressor and a variable speed fan at the condenser, it is possible to develop an efficient strategy to reduce the energy use.

A study conducted by the Center for Energy and Environment (1998) targets the ideal condensing pressure leading to higher efficiency. The study recommends operating at a constant head pressure of 1030 kPa. The study also reveals that by reducing the condensing pressure by 140 kPa up to 170 kPa the resulting cost savings can reach 900 to 1800 $US per year for an arena operating nine months per year. Most of the arenas can operate with a low condensing pressure without modifying the condenser for mild and cool weathers.

2.5.4 Evaporators on the brine side: series against parallels

Ice rinks refrigeration systems generally have more than one evaporator connected in series or in parallel on the brine side. When operating at 50% of the

refrigeration plant capacity, it is better to connect evaporators in series on the brine side because this configuration uses less energy (McQuay 2002). However, the total pressure drop for the series arrangement is usually greater than for parallel arrangement. Therefore, evaporators in series lead to higher electric input for the brine pump.

McQuay (2002) has compared the energy input of chillers connected in series versus parallel in an office building. The study found that chillers in series consume less energy because the system has much more flexibility to operate under different load conditions. If chillers are connected in parallel, it is more difficult to regulate the refrigeration system. In fact, in a parallel configuration it is better to operate both chillers all the time, even if the plant load is less than 50% (McQuay 2002).

2.5.5 Brine pump

In ice rinks, the pumping needs may change as a function of the thermal load. However, constant speed pumps are generally chosen to provide the highest refrigeration capacity, contributing on average to 15% of the total energy used by the refrigeration system (CANMET 2003c). Well sized pumps are able to satisfy the peak loads without consuming large amounts of energy the rest of the time. It is possible to use a lower power pump to provide adequate cooling 75 to 95% of the time (Center for Energy and Environment 1998).

The pumping power can significantly be reduced by using a variable speed pump, by cycling single or multiple pumps or by using a two-speed motor to power the pump. Moreover, pumping power can be reduced by using low specific gravity brine (Dumas

1996). The effect of smaller pump is also important on the total load of the chiller. A smaller pump releases less heat to the brine, which reduces the load on the evaporator and the power demand of the chiller.

2.5.6 Pipe network

The configuration of the pipe network below the ice sheet influences the ice quality and the electric demand of the refrigeration system. While the majority of actual systems use two passes configurations, there is a trend for designing distribution systems with four passes. Compared to traditional two passes and constant speed pump systems, four passes arrangements with a variable speed pump can lead to energy savings of 93,000 kWh per year, representing 14% of the total energy consumption (CANMET 2003c). Table 2.4 shows the energy consumption for different combinations of pumps and coolant network configurations.

Table 2.4: Energy savings depending on the brine pipes configuration (CANMET 2003c)

System configuration	Energy consumption
4 passes/two-speed pump	577,000 kWh (-14%)
5 passes/one-speed pump	586,000 kWh (-12%)
4 passes/one-speed pump	595,000 kWh (-11%)
2 passes/variable-speed pump	622,000 kWh (-7%)
2 passes/two-speed pump	622,000 kWh (-6%)
4 passes/one-speed pump (actual system)	670,000 kWh (Ref.)

It has been noticed that systems using more than four passes have less uniform ice temperature. This occurs because the potential for heat transfer (temperature difference between the brine and the ice) is less important during the fifth and sixth pass.

2.6 Computer modelling of thermal systems

The aim of simulating a refrigeration system is to evaluate the energy use under different scenarios and then identify the optimum operating conditions. The literature review reveals that steady-state models are largely documented and are widely used, while transient models are rarer. Transient models are far more complicated due to the behaviour of the heat exchangers during the transient regime.

2.6.1 Energy estimating methods

A computer simulation is performed by using a software which can be based either on a forward or an inverse approaches. The forward approach, also known as the classical approach, is particularly useful when the system is under design. This approach presumes detailed knowledge not only of the various natural phenomena affecting the system behaviour but also of the magnitude of various interactions (ASHRAE 2005). Software such as BLAST (Hittle 1977), DOE-2 (1982), EnergyPlus (2001) and TRNSYS (Klein et al. 2000) are based on a forward approach. On the other side, when the system already exists, the inverse model or data-driven approach can be useful. By using utility bills or measurements, a mathematical model is determined and used to predict the future energy consumption of the system. An inverse model is simpler and more accurate than the equivalent forward model because the model is generated from the actual behaviour of a particular system. However, the model is only reliable for a specific system and for a certain range of operating conditions. This approach is used by the software called PRISM (1986) to extract the energy signature of houses and estimate the annual normalized energy used.

2.6.2 Modeling and simulating approaches

A simulation model is articulated on components connected together or on a pre-defined system. Component-based and system-based models can be classified into two categories: empirical and analytical models. Empirical models, commonly called black box models, are based on measurements performed on existing components or systems, and are developed using different statistical techniques (ASHRAE 2005). This type of model is easier to develop because no physical knowledge of the system is necessary. The empirical model is only reliable for the range of values obtained from the measurements. Analytical models, also known as white box, are based on the physical laws governing the components or the systems (ASHRAE 2005). This type of model requires less data for tuning and the model is valid for a wide range of operating condition. On the other hand, the model needs a good understanding of the physical phenomena taking place, which can demand significant work and the use of assumptions.

Simulated systems can be described by using either a component-based or a system-based model. If a system is modeled based on a component approach, every component is mathematically described separately and connected together by appropriate energy and mass transfer equations. This approach is more flexible because it allows the user to independently control the characteristics of each component of the system. However, this method requires more time if complex systems are described. The system-based approach consists in the use of predefined black-boxes defining systems. The user can control the general behaviour of the system without acceding to the particular characteristics of the components. This results into faster modeling, which is simpler to use by inexperienced users.

2.7 Literature survey of refrigeration simulation models

With the increase in energy costs, the need for the prediction of the energy performance of refrigeration systems has become important and has led to the development of a number of refrigeration models. This section presents some of the models developed. On the other hand, literature on refrigeration models for the ice rinks is scarce especially in the modelling and validation aspects.

Research groups have developed several simulation models for chillers for different applications: commercial, industrial and residential. Analytical and empirical models have been often used to simulate simple chillers. However, in more complex systems, combined models (both empirical and analytical) have presented greater accuracy (ASHRAE 2005). These models are advantageous because they combine both the physics and the particular behaviour of the system. In previous studies by Ge and Tassou (2000), Aprea and Renno (2004) and, Gordon and Choon (1994), the refrigeration system was composed of components, which were modeled with combined models separately and then linked together to obtain the complete model of the system.

2.7.1 Supermarket refrigeration simulation

Since supermarket refrigeration systems share several characteristics with ice rink refrigeration systems, some mathematical models developed for supermarkets are briefly presented in this section.

Ge and Tassou (2000) have developed a mathematical model to simulate a supermarket refrigeration system by using TRNSYS. The model includes a multi-

compressor pack, a multi-fan air-cooled condenser, a vertical multi-deck display cabinet with a direct expansion evaporator coil and a thermostatic expansion valve. The compressor model is based on the energy balance and efficiency parameters which are provided by the manufacturer. The model is part empirical, part analytical. It calculates the refrigerant mass flow passing through the compressor by using the following relation:

$$\dot{m}_{ref} = \frac{n_v \dot{V}}{v} \tag{2.1}$$

where V is the volumetric flow, v is the specific volume and n_v is the volumetric efficiency (given by Equation 2.2), which relates the discharge and suction pressure:

$$n_v = C_c \left(1 - C_e \left[\left(\frac{P_2}{P_1} \right)^{1/n} - 1 \right] \right) \tag{2.2}$$

where C_c, C_e and n are constants. In the energy balance of the compressor, the heat loss to the ambient through the shell surface (Q_{shell}) is taken into account:

$$\dot{W}_{comp} = \dot{m}_{ref} \cdot \left(h_{ref,out} - h_{ref,in} \right) + \dot{Q}_{shell} \tag{2.3}$$

The heat exchangers models are based on the effectiveness-number of heat transfer units (NTU) approach for dry coils:

$$\varepsilon = 1 - e^{-NTU} \tag{2.4}$$

This equation is only valid for sensible heat exchanges, thus the superheated and sub-cooled phases are simulated separately from the latent heat exchange that occurs with two-phase fluids. The thermostatic valve is modeled by analyzing all the forces acting on the valve to determine the mass flow rate.

Arias and Lundqvist (2005) have developed a model for a supermarket refrigeration system based on a system approach. The refrigeration system is simulated by using the software CyberMart, which models the heat exchanger with the effectivess (ε) and the number of transfer units NTU. It is important to note that this study considers neither the sub-cooling nor the superheating in the heat-exchangers. Hence, the heat transfer coefficients of the evaporator and the condenser are assumed to be constant during the simulation. The life cycle costs (LCC) as well as the total equivalent warming impact (TEWI) are evaluated by using methods included in CyberMart. The model is validated by using measurements from a monitored supermarket in Sweden. The annual energy consumption obtained from the simulation and measurements differs by 2.5%.

2.7.2 Simulation of industrial refrigeration systems

A model developed by Jolly and Tso (2005) uses a component approach to simulate a refrigeration system in a shipping container. The model is one of the most complete because it considers the following features: coil geometry of heat exchangers, mass transfer in the evaporator and effects of changes of relative humidity in the heat exchanger. Furthermore, the model provides a list of compressors with correction factors for different degrees of superheating. Each component is modeled separately, based on the physical behaviour of the device or based on manufacturer's data. For the compressor, the behaviour is simulated by using a correlation relating the evaporating temperature (T_e) and condensing temperature (T_c):

$$Y = C_0 + C_1 T_e + C_2 T_c + C_3 T_e^2 + C_4 T_e T_c + C_5 T_c^2 + C_6 T_e^2 T_c + C_7 T_e T_c^2 + C_8 T_e^2 T_c^2 \quad \text{(2.5)}$$

where Y represents either the mass flow rate, the capacity or the power demand. The equations developed are then combined into an algorithm that allows for evaluating the performance of the refrigeration system. The resulting model is then compared with data from an experimental unit. The simulated cooling capacity, evaporating and condensing pressures, compressor suction pressure, temperature and power draw, pressure losses in suction lines and compressor pressure ratio are compared with measurements. Results show that the model over-predicts the system's cooling capacity. Evaporating and condensing pressures are validated with the experimental results.

2.7.3 Refrigeration control strategies

Ge and Tassou (2000) used two control models. They used an on-off control model that reproduces the actual control system used in supermarkets. They also simulated the refrigeration system using a proportional plus integral derivative (PID) controller in order to determine the possible energy savings. The results show that the use of a variable head pressure instead of a constant head pressure at the discharge point can lead to a reduction of energy consumption up to 22%. Moreover, the study shows that a PID control can lead to smaller power fluctuations on small load periods. The PID controls the speed of the compressor so the power input increases smoothly with the charge. This measure leads to a reduction of 10% of the energy consumption.

Different control strategies are considered in a study carried out by Buzelin et al. (2005). The authors investigate alternative solutions in order to reduce the energy consumption of industrial refrigeration systems. To reach this goal, they study the effect

of a closed-loop control system against the traditional on-off control system. Both control strategies where tested and compared on an experimental setup. The authors found that by using a closed-loop control strategy, the reduction of energy use could reach 25%. By controlling the exit pressure of the compressor, the system can more easily maintain a constant temperature, thus the periods of work are shorter resulting in energy savings. The gain is particularly important for long time intervals.

Several studies have shown that controlling the head pressure and the compressor speed could lead to important energy reductions (Koury et al. 2001, Brownell 1998). A numerical simulation of a variable speed refrigeration system has been carried out by Koury et al. (2001). In their work, the authors present both a transient and a steady state model for the heat exchangers (condenser and evaporator). Steady state models were used to simulate the expansion valve and the compressor. Neither the compressor nor the expansion valve models consider mass variation of refrigerants. Since heat exchangers are very sensitive to transient states, a distributed model, which consists in a division of the heat exchanger into various small control volumes, is used. Energy, mass and momentum balance are applied to each volume together with the local heat-transfer coefficients. This method is particularly useful when the two-phase flow is considered in the heat exchanger. The behaviour of the system is simulated for three different conditions: the start-up of the system, the response of the system due to a step variation in the rotational speed of the compressor and the response of the system due to a step variation of the sectional area of the expansion valve while the system is under steady-state conditions. The study revealed that a traditional on-off control system increases the energy consumption and reduces the life of the compressor. However, by varying the

rotational speed of the compressor, it is possible to improve the general performance of the system (Koury et al. 2001, Brownell 1998). Variation of the rotational speed of the compressor leads to a strong variation of the refrigerant superheat degree at the evaporator exit. Since the thermostatic valve has slow response, it is more adequate to choose an electronic valve when manipulating a variable speed compressor (Outtagarts et al. 1995). The results obtained during step variations of the compressor speed are particularly interesting. The increase of the compressor speed results in an increase of the mass flow rate and the reduction of the temperature of the secondary coolant. This causes an increase of the superheating of the refrigerant at the evaporator exit and reduces the COP of the system.

2.7.4 Comparing different models of refrigeration systems

A study carried out by Sreedharan and Haves (2001) evaluates different modeling approaches for their applicability for fault detection and diagnosis (FDD) of vapour compression chillers. FDD involves two steps: detecting that a fault is present, and then isolating and diagnosing it. Three chillers models are compared: ASHRAE Primary Toolkit Model (Bourdouxhe et al. 1997), Gordon-Ng Universal Chiller Model (Ng et al. 1997) and CoolTools/DOE-2 Model (PG & E 2001).

Toolkit and the Gordon-Ng are analytical models, while the CoolTools is an empirical model. All three models are for steady-state regimes. The Toolkit is a component-based model whose equations are solved iteratively, while the Gordon-Ng model is a system-based model of the chiller. The CoolTools model is an empirical

model of the chiller based on polynomial curve fitting. This model is not flexible, and as a consequence it is not convenient for the simulation of an ice rink refrigeration system. Since, component-based models are more flexible than system-based models, the Toolkit and the Gordon-Ng models are more interesting for the current application.

The Gordon-Ng and Toolkit models are established based on the energy balance and the first law of thermodynamics. However, they differ in their approach and assumptions. Table 2.5 compares the assumptions used by the Toolkit and the Gordon-Ng models (Sreedharan and Haves 2001).

Table 2.5: Comparison of ASHRAE Toolkit and Gordon-Ng models (Sreedharan and Haves 2001)

Toolkit	Gordon-Ng
Neglects energy losses to environment in the energy balance	Includes energy losses to environment in the energy balance
Assumes isentropic compression	Estimates entropy generation
Requires refrigerant thermo-physical properties	Does not require refrigerant properties
Evaporator and condenser water flow rates are treated as variables (although the effect of flow rate on the convective heat transfer coefficient, and hence on the AU's is ignored)	Evaporator and condenser water flow rates are treated as constants (and incorporated into the thermal resistance parameter), although there is a variable condenser flow rate version of the model
Evaporator and condenser AU's are determined separately	A single effective thermal resistance is determined for the whole chiller
Electromechanical losses are proportional to the compressor power	Combined evaporator and compressor leaks are constant, independent of the compressor power

Sensible heat exchanges are ignored in both models; consequently no superheated or sub-cooled refrigerant is modeled. This hypothesis is very crude for the condenser: it neglects all the effects of de-superheating, which results in an underestimated mean temperature difference between the refrigerant and the water or air (Sreedharan and Haves 2001). The ASHRAE Toolkit compensates this error by overestimating the corresponding heat transfer coefficient (AU).

The model developed by Gordon and Ng is relatively simple: it includes the essential thermodynamic equations to predict the functional relations among the key variables. Only a few numbers of selected measurements are necessary to determine the three coefficients necessary to predict the chiller performance. The Gordon-Ng model has the advantage of being linear in parameters. This allows more robust parameter estimation methods and facilitates estimation of the uncertainty in the parameter values. The ASHRAE Toolkit model is more interesting when temperature measurements of the refrigerant are available. Compared to the Gordon-Ng model, the Toolkit has the possibility to predict the performance of the compressor, the condenser, the evaporator separately with more confidence (Sreedharan and Haves 2001). The Toolkit model assumes isentropic compression at full and part load compressions. No heat losses are considered between the system and environment.

A study carried out by Sreedharan (2001) compares the ability of three models (Toolkit, Gordon-Ng., CoolTools) to reproduce the behaviour of a centrifugal chiller operating in a commercial office building and of a centrifugal chiller in a laboratory. The author concluded that all three models have almost similar levels of accuracy. Table 2.6 summarizes the modeling results (Sreedharan 2001).

Table 2.6: Comparison of electric demand of a chiller using the AHSRAE Toolkit, Gordon-Ng, CoolTools/DOE models (Sreedharan 2001)

Model	Prediction error (kW)	
	Laboratory chiller	Building chiller
ASHRAE Toolkit	1.34	4.09
Gordon-Ng	1.38	4.01
DOE-2/CoolTools	1.92	4.24

2.8 Conclusions of the literature survey

Several models of refrigeration systems have been found in the literature mainly for buildings and industrial applications. However, models for the simulation of ice rink refrigeration systems are practically inexistent in the public domain.

Refrigeration models usually combine manufacturer data, polynomial equations and thermodynamic equations. Models using correlations are only valid within the range of the working points that the equations were developed for. Therefore, these types of models have to be used with precaution because the extrapolation may lead to significant errors. Furthermore, some models are based on a system approach, which is less flexible than a component approach. From a simulation perspective, the component approach is more convenient for the ice rink refrigeration system, since each component can be analyzed separately.

Based on the literature review, the ASHRAE Toolkit-I is the only model using a component-based approach and combining both thermodynamics equations and empirical relations. The Toolkit is an analytical model, which uses a few correlations to determine the parameters of the compressor from manufacturer data. This model is the most appropriate for the present study. Modifications will be brought to the ASHRAE-Toolkit in order to consider the sensible heat exchanges in the heat exchangers.

Different simulation programs are available on the market; some software packages are based on an inverse approach while others use a forward approach. Both forward and inverse approaches will be integrated in the simulation. TRNSYS (Klein et

al. 2000) is probably the software offering the greatest flexibility in this domain. TRNSYS allows the development of new components or the modification of the pre-established components by changing the source code or by changing the components parameters as obtained from the manufacture's catalogues. In addition, the version 16 of TRNSYS has the ability to manage external dynamic link libraries (DLL), providing an easier way to the user to incorporate external models in the TRNSYS library with an exported DLL.

2.9 Objective of the study

The objective of this study is to create a computer model of an existing ice rink refrigeration system, based on first principles, manufacturer's data and field measurements. The model is developed within the TRNSYS environment, and the mathematical models for chillers and heat exchangers are based on the ASHRAE Toolkit. The model is validated by using monitored data from an ice rink.

Chapter 3 presents the analysis of the measurements collected at the monitored ice rink. The effects of several parameters on the power input to the refrigeration system are analyzed. Typical conditions of operation of the monitored ice rink are also defined.

Chapter 4 presents the mathematical model for reciprocating chillers based on the ASHRAE Toolkit. Modifications are brought to the Toolkit to eliminate some limitations in their application for this study. The Toolkit is used to identify the parameters of the compressor and to simulate the chiller. The Toolkit model for chillers is integrated to TRNSYS model as an external DLL.

Chapter 5 presents the development of a thermodynamic model for the refrigeration system of the ice rink by using Engineering Equation Solver (EES) (Klein and Alvarado 1999). The purpose of this model is to identify the parameters of the heat exchangers based on the monitored data.

Chapter 6 presents the development of two models to simulate the ice-concrete slab: an analytical model and a correlation model. Both models are compared and verified by using measurements from the monitored ice rink. This chapter also presents the development of a controller used to determine the number of compressors in operation. Based on the analysis of the collected data, empirical rules are defined for the controller. The slab models and the controller model are integrated to the TRNSYS environment as externals DLLs.

Chapter 7 presents the simulation of the refrigeration system in TRNSYS environment. Simulations are performed for different days and the results are compared with the measurements made at the monitored ice rink. In particular, brine temperatures during each stage of the process are compared with measurements as well as the simulated power input of the system. Finally, the potential energy savings by heat recovery from the condenser are estimated when they are used for heating the sanitary hot water along with the reduction of CO_2 emissions.

CHAPTER 3

DESCRIPTION OF THE MONITORED ICE RINK

This study is based on measurements collected by Ouzzane et al. (2006) in a monitored ice rink located in Montreal. The different components of the ice skating rink used in this study, and its refrigeration system and operation mode are presented. The measurements collected are presented and analyzed to characterize the performance of the refrigeration system.

3.1 Description of typical ice rinks

This investigation looks at an interior artificial ice surface surrounded by stands and generally used for sports (hockey, free skating, speed skating or figure skating) and on occasion as an auditorium. As most entertainment facilities, ice rinks have a high rate of occupancy. They are often used eighteen hours per day, seven days a week during eleven months each year (ASHRAE 1998b). Arenas are buildings with large floor surfaces that vary between 2000 and 4600 meters square depending on the occupancy capacity. Generally, the ice surface corresponds to 50% of the total surface occupied by the floor area of the arena (ASHRAE 1998b). The ice temperature is maintained in a range between -6.5°C and -2°C. The brine temperature that circulates inside the pipe network below the ice sheet varies from -11.5°C to -7°C. In Québec, 90% of arenas use two pass brine loops under the ice slab while the rest use four passes. Furthermore, 70% of arenas in the province are more than 20 years old (Lavoie et al. 2000).

3.2 Description of the monitored ice rink

The present research is based on the measurements collected at the Camillien-Houde ice rink, located in the centre of Montreal (Ouzzane et al. 2006). The arena was constructed in the early 1980's with the following dimensions: 42 meters wide, 64 meters long and 9.36 meters high. The ice surface (61 m × 26 m) is used eleven months per year. The layout of the building is presented in Figure 3.1.
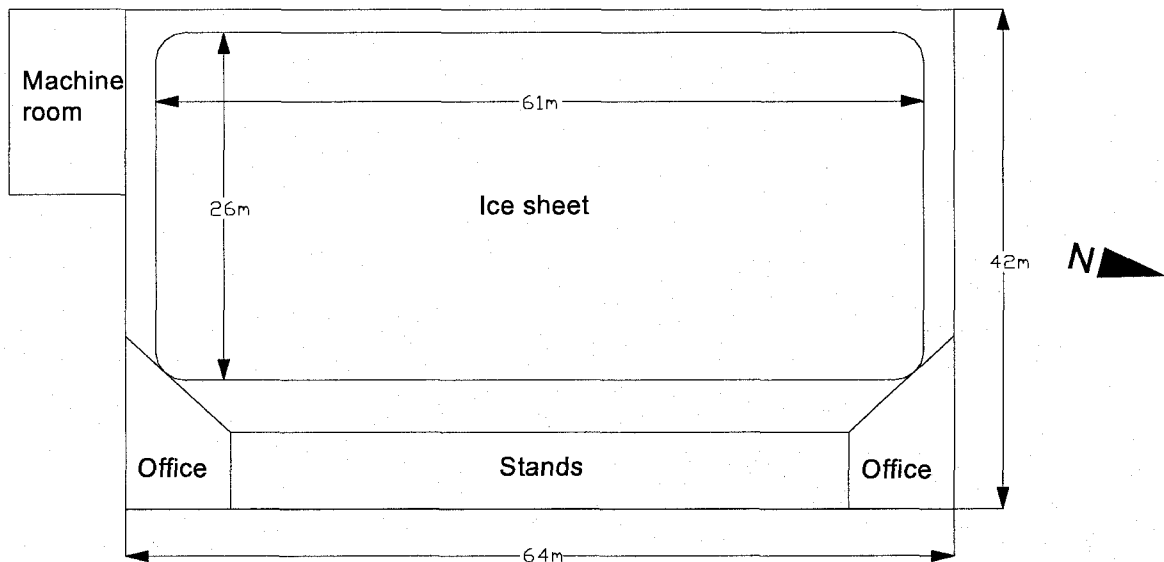
Figure 3.1: Layout of the Camillien-Houde ice rink (Ouzzane et al. 2006)

On the east side of the ice surface, six rows of stands run through entire length of the building with two offices at each extremity. There are about 200 seats for the public.

3.2.1 Refrigeration system

The Camillien-Houde refrigeration system is composed of two chillers that function with refrigerant R-22 and that are connected in series on the brine side. Each chiller has three semi-hermetic reciprocating compressors driven by a 22 kW electric motor rotating at 1750 rpm. Compressors are connected in parallel on the direct expansion evaporators. Each compressor has a capacity of 53 kW of refrigeration (15 tons), and is connected to an air-cooled condenser located on the roof of the building. Each of the six condensers has six 1.6 kW fans that draw air through the cooling coil.

Although there are six compressors installed, in order to limit the electric demand of the system, the maximum number of compressors in operation has been limited to five. Hence, modifications have been conducted on chiller #1 to reduce the maximum number of running compressors to two. To reach this goal, the third refrigerant line has been by-passed to be reconnected on the second compressor. This change of configuration has an impact on the refrigerating effect of the second compressor of chiller #1, since it operates with a double mass flow of refrigerant. The rest of the third line is identical to the others, i.e., passes by a condenser, an expansion valve and through the evaporator independently. The configuration of the Camilen-Houde's refrigeration system is presented in Figure 3.2.

The brine (calcium chloride (CaCl) solution with a 20% water concentration) circulates through the 32 mm polyethylene pipes in a four pass network within the concrete slab. An 11.2 kW pump is used to circulate the brine through the evaporators and the pipe network. The system operates approximately from 3:00 to 24:00.
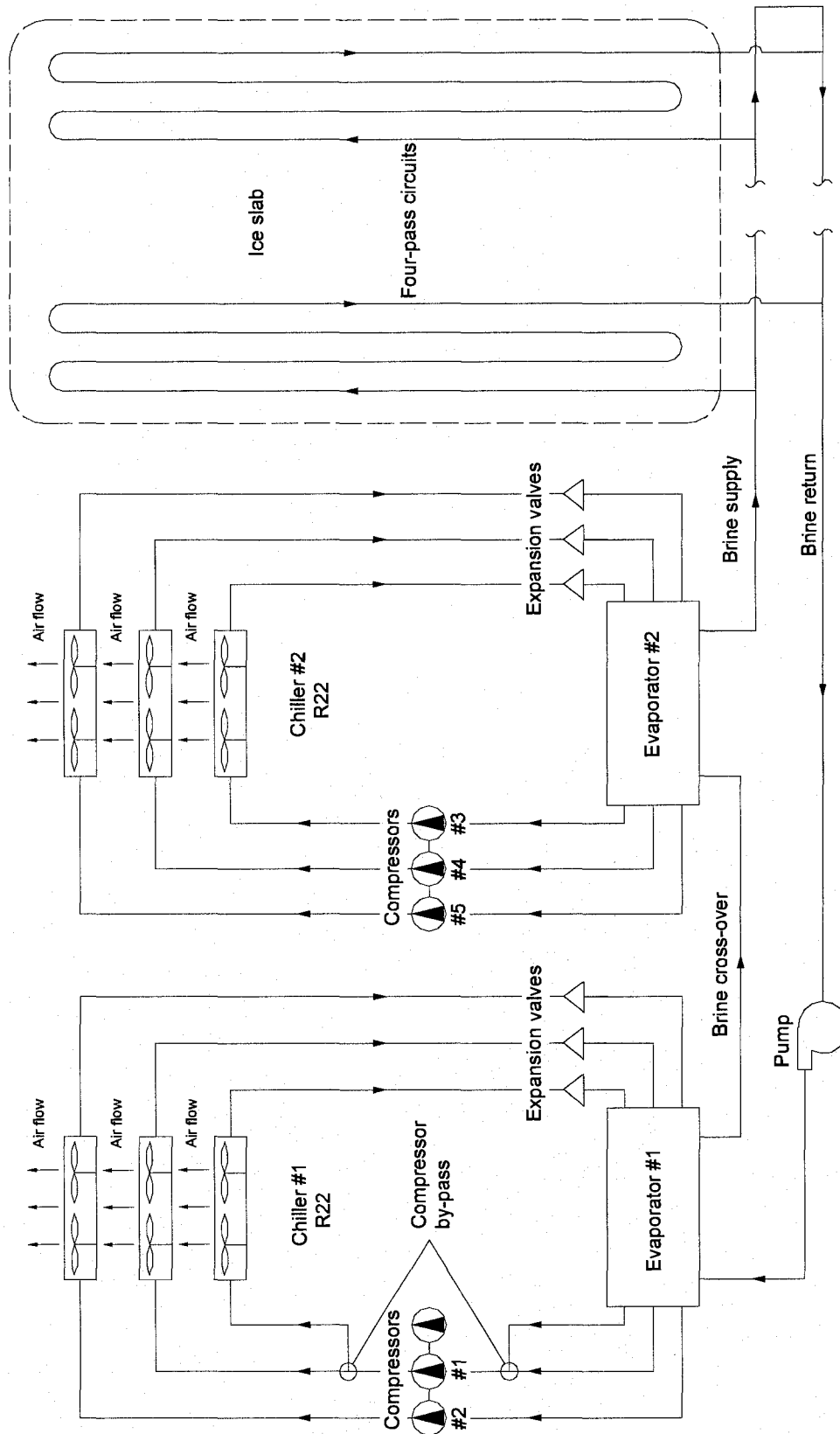
Figure 3.2: Layout of the Camillien-Houde refrigeration system

3.2.1.1 Description of components of the refrigeration system

Table 3.1 lists the main components with the corresponding description. Because the system has been installed more than 25 years ago, the information regarding the components of the refrigeration system was not always available.

Table 3.1: Main components of the Camillien-Houde refrigeration system

Component	Manufacturer	Model Number	Type
Compressors	Carlyle	5H40	Reciprocating
Evaporators	Stork Canada	unknown	Direct expansion
Condensers	Heatcraft Refrigeration - Larkin	RCX80768 R-22	Air
Expansion valve	Sporlan	OVE-15 and SVE-10	Unknown
Control system	Johnson control	unknown	Based on slab and return brine temperatures
Brine Pump	unknown	unknown	Centrifugal

Based on the manufacturer's information, a detailed description of the main components of the refrigeration system is presented.

3.2.1.2 Compressors

The six open reciprocating compressors installed at Camillien-Houde are sealed to avoid refrigerant leakage. Lubrication is provided by a large capacity pump equipped with a pressure regulator and an oil filtering system (Carrier 2001). The compressor suction pressure is approximately of 260 kPa, while the discharge pressure is of 1550 kPa. During normal operation of the system, the number of compressors in operation change depending on the brine temperature at the slab exit (return brine temperature).

3.2.1.3 Evaporators

The evaporators installed at Camillien-Houde are of the direct expansion (DX) type. Direct expansion evaporators are typically used in low temperature refrigeration

applications (below 0°C). The degree of superheating depends upon the thermostatic valve which is controlled by the bulb sensing at the exit of the coil.

3.2.1.4 Condensers

The air-fluid condensers mounted on the roof of the Camillien-Houde arena reject the heat previously absorbed by the refrigerant, by blowing outdoor air through the coils. As heat is released to the atmosphere, the refrigerant change from superheated vapour to compressed liquid. Each condenser has six direct drive fans of 1.6 kW each rotating at 830 rpm. Fans are staged by using pressure cycling controls leaving one or more fans to cycle as required. When a compressor is running, at least one fan of the connected condenser is turned on. The fan closer to the inlet heater runs continuously when the attached compressor is operating. This is done to prevent wide condenser temperature fluctuations that cause excessive expansion and contraction of the coil material and leaks due to metal fatigue. The condenser fan is set up using a 345 kPa (50 PSI) throttling range with the cut in set at 1379 kPa (200 PSI) and cut out set at 1034 kPa (150 PSI). This is the most economical method of controlling the head pressure, but it is also the most inefficient from an energy consumption point of view (Larkin 2006).

3.2.1.5 Expansion valve

The thermostatic expansion valve is mounted at the inlet of the coil evaporator. The expansion valve takes a high pressure liquid and throttles it down to a desired evaporator pressure. This pressure is maintained by a back pressure regulator mounted on

the evaporator outlet. The thermodynamic process in the expansion valves is assumed to be adiabatic; consequently the expansion process is isenthalpic.

3.2.1.6 Control system

The ice temperature is controlled by using a combination of the concrete slab temperature and the return brine temperature (Dumas 2004). For the start-up, two conditions are mandatory: if after 4:00 in the morning, the slab and the brine temperatures are beneath -5°C, the first compressor is turned on. Then, the controller increases in stages the number of compressors in operation in order to reach -9°C on the return brine temperature at 8:00. During the rest of the day, the controller changes the number of compressors to maintain the return brine temperature at approximately -9°C.

3.2.2 Heating and ventilation system

The primary ventilation system of the Camillien-Houde arena is composed of a 100% exhaust/make-up system with a capacity of 4000 l/s operating continuously (Ouzzane et al. 2006). In the dressing rooms, a gas-fired furnace is used to maintain the minimum temperature of the make-up air at 21°C. Local heating is provided to players and scorekeeper benches by eight natural gas high-intensity radiant heaters of a capacity of 140 kW. The radiant heaters above the spectator stands have a capacity of 176 kW and are activated by motion sensors in order to maintain the air temperature at 15°C. The combustion products from the gas fired-heaters are rejected to the outside of the building by using four roof-mounted exhaust fans. The hot water (sanitary and resurfacing) is prepared by a gas fired boiler.

3.2.3 Lighting system and resurfacing schedule

Lighting is provided above the ice sheet by several high density lights that have a power of 29 kW to ensure a lighting density of 18.3 W/m^2 (Ouzzane et al. 2006). The lights are switched on between 6:00 to 24:00. The ice is resurfaced at one-hour intervals, between 10:00 and 13:00 during weekdays and between 6:00 and 13:00 on weekends.

3.2.4 Distribution of total energy use

Figure 3.3 presents the distribution of the energy use at the Camillien-Houde ice rink (City of Montreal 2004). The graph shows that the refrigeration system (refrigeration and brine pump) combined with the heating needs (space heating and sanitary hot water) represents 91% of the total energy use.
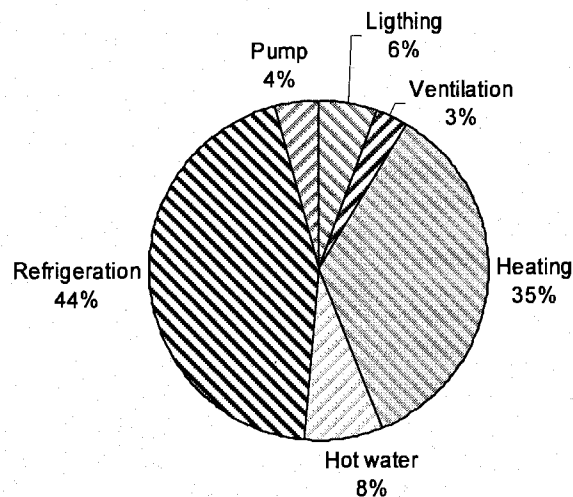
Figure 3.3: Energy distribution at the Camillien-Houde ice rink (City of Montreal 2004)

Knowing that part of the heating needs could be covered by recovering the heat rejected by the refrigeration system, the potential for energy savings is significant. By integrating various efficiency measures on the actual ice rink, the savings could reach 41% (Lavoie et al. 2000), leading to a CO_2 emissions reduction of 145 tons of per year.

3.3 Instrumentation and available data

Camillien-Houde arena was equipped with sensors and data loggers to collect information on the operating conditions of its refrigeration system. Long and short term measurements were conducted by the CANMET-Varennes Energy Technology Center (Ouzzane et al. 2006). The long-term measurements were collected at one-minute intervals during several days of different months by permanently installed sensors. They were then transferred to a computer though an Internet connection. In contrast, short-term measurements were realised by using portable instruments. These measurements were performed with five compressors in operation, outside the regular hours of use of the ice. Long and short terms measurements and corresponding instruments with their accuracies are presented in Table 3.2 and Table 3.3, respectively.

Table 3.2: Long-term measurements and instruments (Ouzzane et al. 2006)

Measurement	Variable name	Instrument	Accuracy
Surface temperature at several locations on the inside surface of walls and ceiling	T_{wall}	Thermocouple	± 0.1°C
Temperature of the ice surface	T_{ice}	Infrared temperature sensor	± 1.4°C
Dewpoint temperature at the dasher board	$T_{dew,point}$	Chilled mirror dew point transmitter	± 0.1°C
Brine temperature at the pump inlet and outlet	$T_{brine,in,pump}$ $T_{brine,out,pump}$	Thermocouple	± 0.1°C
Brine temperature at the outlet of evaporator #1, inlet of evaporator #2	$T_{brine,out,chill1}$	Thermocouple	± 0.1°C
Brine temperature supplied to the ice sheet	$T_{brine,out,chill2}$	Thermocouple	± 0.1°C
Refrigerant temperature leaving the evaporator	$T_{ref,out,evap}$	Thermocouple	± 0.1°C
Refrigerant temperature entering the expansion valve	$T_{ref,in,exp.valve}$	Thermocouple	± 0.1°C
Heat flux at four locations on the ice sheet	HF	Heat flux sensor	-
Outdoor air temperature	T_{air}	Thermocouple	± 0.1°C
Electric power demand	TPD	Power demand transmitter	-

Measurement	Variable name	Instrument	Accuracy
Suction and discharge pressures	P_1, P_2	Manometer	-
Refrigerant mass flow rate	$\dot{m}_{ref}$	Ultrasonic flow meter	$\pm\,0.1 - 2\%$
Brine mass flow rate	$\dot{m}_{brine}$	Ultrasonic flow meter	$\pm\,0.1 - 2\%$
Vertical profile of air temperature above the centre of ice surface and above stands	$T_{vert,air}$	Thermocouple	$\pm\,0.1°C$
Vertical profile of velocity of air above the centre of ice surface and above stands	$V_{air,ice}$	Air flow meter	-

Measurements on the refrigerant side of the system have been realised on the non-modified compressor of chiller #1. Figure 3.4 presents the location of the instruments on the refrigerant side of chiller #1.
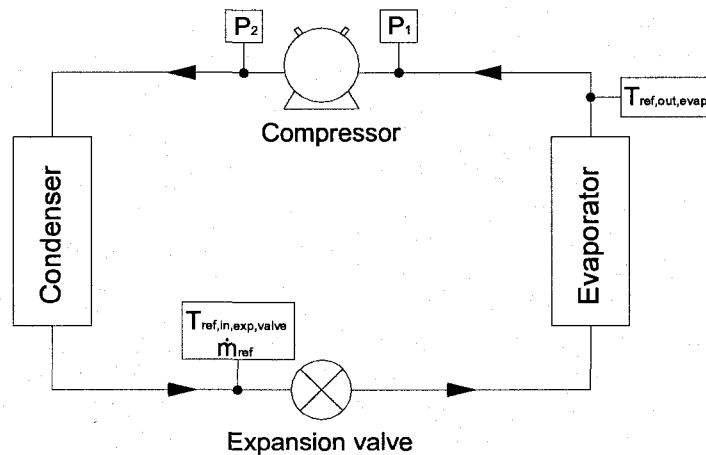
Figure 3.4: Location of the instruments on the refrigerant side

It is important to mention that temperature measurements on the refrigerant side have been conducted by measuring the temperature on the surface of the pipe. Therefore, the actual temperature of the refrigerant should be slightly lower than the measured one. Traditionally, the mass flow rate is measured by using intrusive instruments which require cutting the pipe to install the sensor. Cutting a pipe where refrigerant circulates is always a delicate operation because the system must be purged, and then refilled with

refrigerant. This operation usually results in a loss of refrigerant in the environment and sometimes leaves permanent leaks in the system. To avoid this problem, the refrigerant flow rate was measured by using a transit-time ultrasonic flow meter, based on the fluid sonic velocity and known pipe dimensions. This equipment can accurately measure the flow rate, resulting in high accuracy data without intruding into the flow stream (Scott 2003). The refrigerant volumetric volume flow of liquid was measured as 0.287 l/s, equivalent to a mass flow rate of 0.3348 kg/s (Ouzzane et al. 2006).

3.4 Analysis of the experimental measurements

The measurements taken on the refrigeration system were provided by CANMET-Varennes. The analysis of the monitored data is performed in this study in order to characterize the behaviour of the refrigeration system. Among all the measurements taken on the arena, the following are used to perform the analysis: ice temperature, electric demand, heat fluxes on the ice sheet, brine side temperature, and refrigerant side temperature and pressure.

3.4.1 Number of compressors in operation

The controller of the refrigeration system determines the number of compressors to use as a function of the brine temperature at the slab exit (return brine temperature). The number of compressors in operation at each time interval can be determined by analyzing the measured electric demand of the refrigeration system. Figure 3.5 plots the power input on December 7th, 2005 from about 2:35, which is a few minutes before start-up, until the system reaches five compressors in operation.
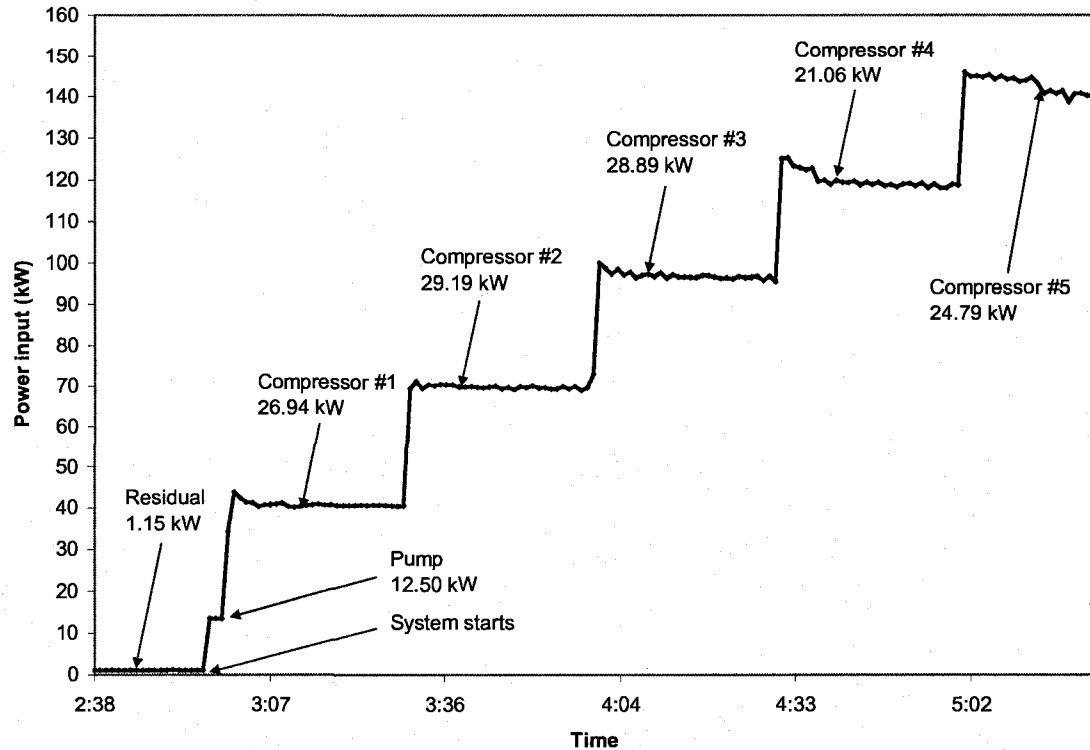
Figure 3.5: Power input during start-up: residual, pump and compressors on December 7th, 2005

As it can be observed, when the compressors, condensers and pump of the refrigeration system are stopped during the night, the power input transmitter records a constant power use of approximately 1.15 kW. This residual electric demand is caused by a source that is permanently turned on. Because the transmitter monitors the electric demand of the mechanical room, it is assumed that the residual electric demand is caused by the lights and the control panel of the mechanical room.

Three minutes before the system starts, the brine pump is switched on. The measured power input for the pump is of 12.5 kW. This value is 1.3 kW greater than the one provided by the manufacturer's catalogue, which is of 11.2 kW. At 3:00 the first compressor is turned on. The other compressors are switched on at an interval of 30 minutes.

Figure 3.5 shows that the compressors do not require the same power to operate. Indeed, while compressor #2 and #3 have approximately the same electric demand (about 29 kW), a large difference separates the three others compressors. Two factors can explain these differences. On one side, one compressor in chiller #1 is by-passed. This change results into an increase of the refrigerant mass flow, hence it is expected that this compressor would require a different power. On the other side, the power demand transmitter also measures the power input of the condensers. Because the fans are not always used simultaneously on all condensers, the power demand fluctuates and can be different from one condenser fan to another. However, the capacity of the condensers depends upon the outdoor air temperature. Since all the condensers operating simultaneously are exposed to the same air temperature, they are expected to operate with approximately the same number of fans. According to the manufacturer's catalogue, each condenser has six fans of 1.6 kW, hence it is assumed that in average three fans are used per condenser, which is equivalent to a power 4.8 kW. Thus, the approximated power demand of each compressor can be established as follows: compressor #1: 22.1 kW, compressor #2: 24.4 kW, compressor #3: 24.1 kW, compressor #4: 16.3 kW and compressor #5: 20.0 kW.

These results show a small difference, with respect to the electric demand, compared to the value provided by the manufacturer catalogue, i.e. 22.0 kW. Two compressors operate with a higher power while two others operate below the manufacturer's data.

Based on the analysis made from Figure 3.5, the number of compressors in operation is estimated from the total electric demand measured:

$$NCU = \frac{TED - PP}{PCC}$$

(3.1)

where: NCU = number of compressors in use;
TED = total electric demand (kW);
PP = power of the pump, the lighting system and the control panel of the mechanical room (12.5 kW+1.15 kW);
PCC = power of one compressor-condenser unit (22 kW+4.8 kW).

The numbers of compressors calculated with Equation 3.1 are rounded to the closer integer value. Figure 3.6 presents the variation of number of compressors in operation, as calculated by Equation 3.1 for March 16th, 2006. The maximum number of compressors is limited to five, while the minimum number of compressors in operation is limited to two.
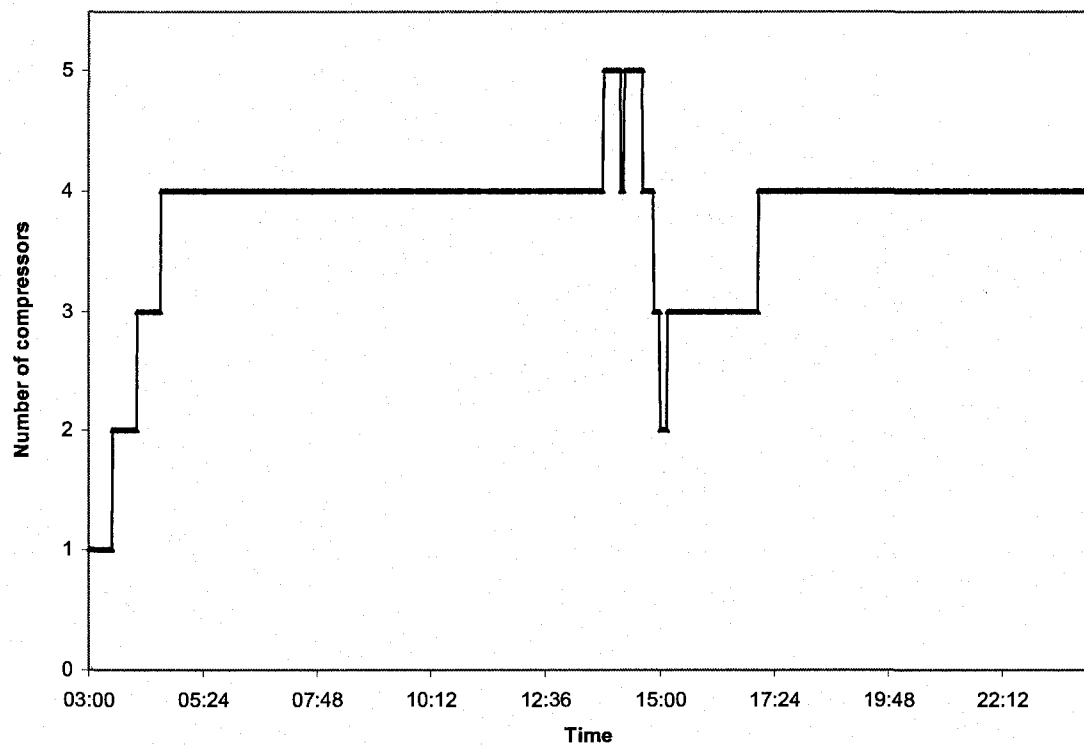
Figure 3.6: Number of compressors in operation on March 16th, 2006

3.4.2 Cooling load

The cooling load is affected by several factors such as the outdoor air temperature, the type of activity practiced on the ice surface, the presence of people in the stands, and the ice resurfacing. The thermal mass of the ice-concrete slab delays and reduces the peak cooling load. Therefore, the instantaneous cooling load felt by the chillers is different from the heat flowing through the ice sheet. To avoid confusion, ice sheet cooling load is referred to the heat flowing through the ice sheet while the system cooling load is referred to the heat extracted by the refrigeration system. The system cooling load is used to determine the refrigerating capacity of one compressor. The cooling capacity of one compressor can be evaluated with four different methods:

1- The heat balance equation on the brine side (HBB);
2- The heat balance equation on the refrigerant side (HBR);
3- The heat flux measurements (CHF);
4- The compressor manufacturer software called Carwin (Carlyle 2007).

3.4.2.1 Heat balance on the brine side

The heat balance on the brine side in the evaporator allows the determination of the cooling capacity of the refrigeration system. Applying the first law of thermodynamics for an open system under steady state, steady flow conditions, and by neglecting the change of potential and kinetic energy, the heat transferred is calculated with Equation 3.2. The brine specific heat ($c_{p.brine}$ = 2,957 J kg^{-1} °C^{-1}) is assumed to be constant and the measured brine mass flow is 34.324 kg/s (Ouzzane et al. 2006).

$$\dot{Q}_{HBB} = \dot{m}_{brine} \cdot c_{p,brine} \cdot (T_{brine,in} - T_{brine,out}) \qquad (3.2)$$

Figure 3.7 and Figure 3.8 presents the system cooling load based on the heat balance on the brine side for evaporator #1 and evaporator #2, respectively, on March 16th, 2006. The step fluctuations of cooling load correspond to changes in the number of compressors in operation of the corresponding chiller. The analysis of these graphs shows the sequence used by the controller to switch on and off the compressors. Analyzing the increase of the system cooling load during the start-up period between 3:00 and 5:00 helps understanding the sequence used by the controller for start-up. In Figure 3.7, it can be observed that between 3:00 to 4:00, two compressors are switched on in chiller #1 because the cooling load supplied by this chiller increases in two steps. During this period, no compressors are turned on in chiller #2 (Figure 3.8). However, between 4:00 and 5:00, the controller switches on two compressors in chiller #2 as observed in Figure 3.8. At the end of the start-up period, the system operates with four compressors (two in chiller #1 and two in chiller #2).

The sequence used by the controller after start-up can be observed in Figure 3.7 and Figure 3.8 after 5:00. While the cooling load provided by chiller #1 does not change by steps, indicating that the number of compressors in operation is constant, the cooling load provided by chiller #2 fluctuates. This shows that the controller maintains constantly two compressors in chiller #1, while chiller #2 is used to increase the refrigerating capacity of the system by adding one, two or three compressors to the system. This can be seen in Figure 3.8 between 13:45 and 17:45. At 13:45, one compressor is turned on; hence chiller #2 operates with three compressors until 14:40. Then, three compressors are switched off at an interval of 10 minutes until all compressors are turned off in chiller #2 at 15:00. Then, at 15:10 and 17:10, a compressor is turned on respectively.
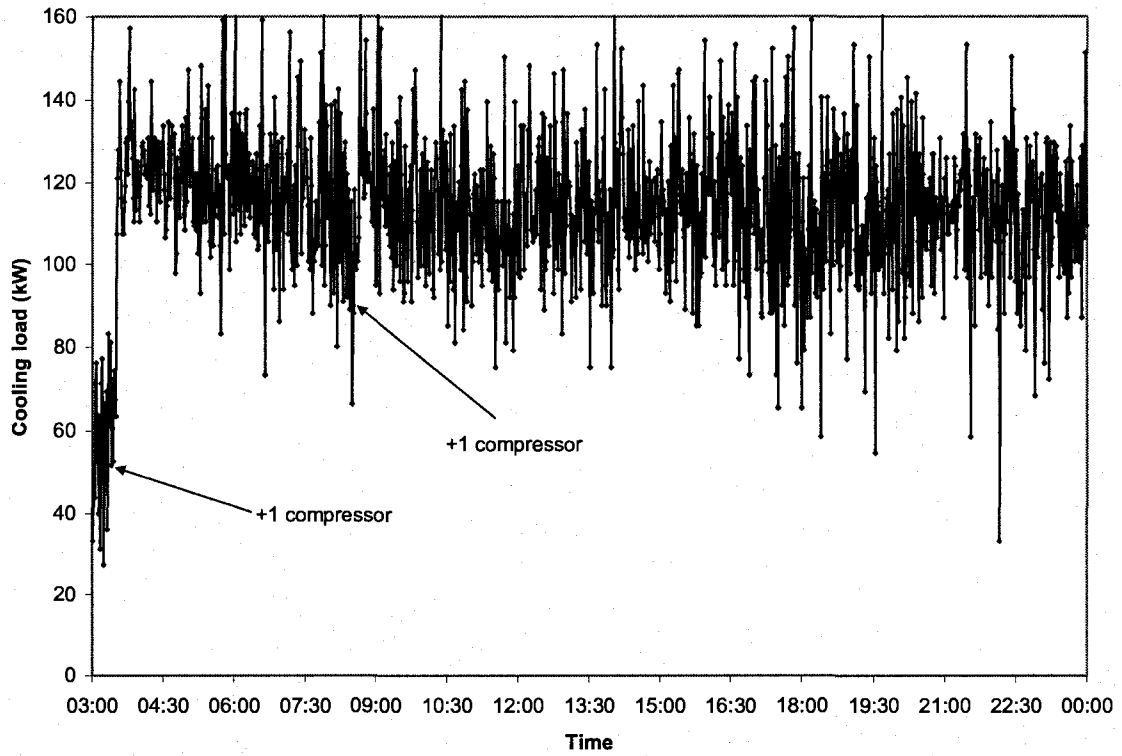
Figure 3.7: Cooling load based on heat balance on brine side for chiller #1 on March 16th, 2006
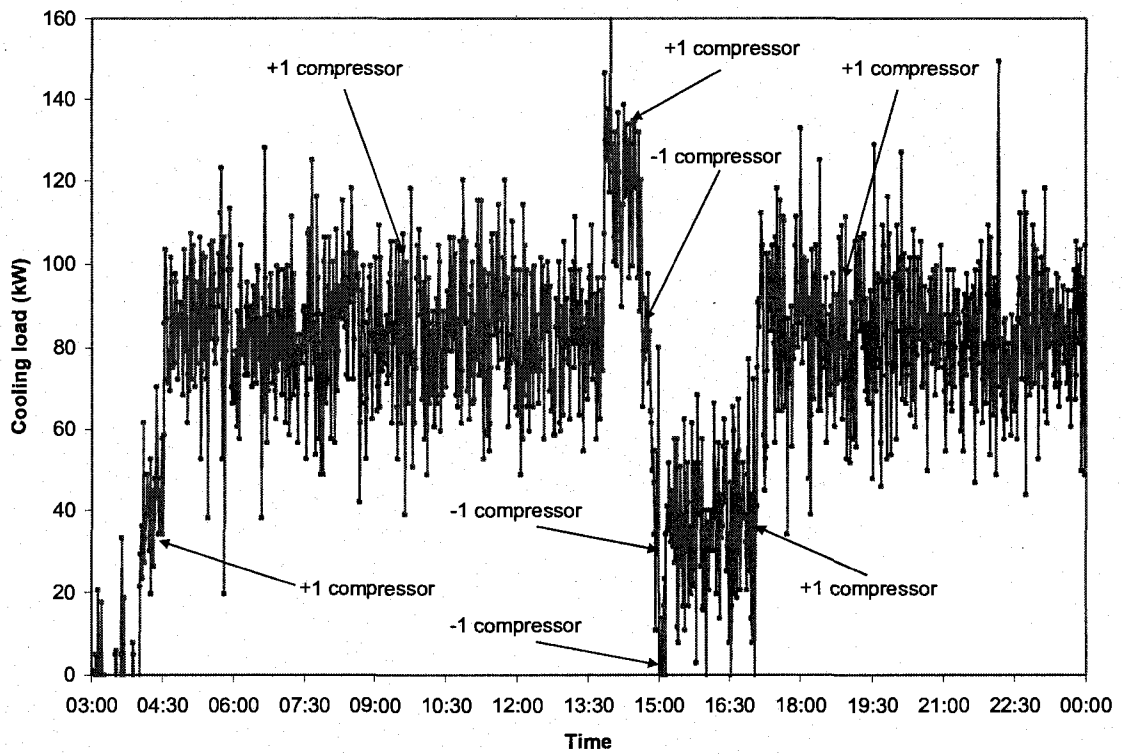
Figure 3.8: Cooling load based on heat balance on brine side for chiller #2 on March 16th, 2006

It can also be observed that when the chillers operate steadily with the same number of compressors (between 4:30 and 13:45, two compressors in chiller #1 and two compressors in chiller #2), the load on evaporators #1 and #2 are not equal. The average system cooling load on evaporator #1 is equal to 116 kW (58.5 kW per compressor) while for evaporator #2, the average system cooling load is of 83 kW (41.5 kW per compressor). This shows that the operating conditions of the compressors are different in chiller #1 and chiller #2.

However, due to the small brine temperature difference between inlet and outlet temperatures of the chillers, the HBB method is not precise. Ouzzane et al. (2006) suggest the use of enthalpy difference on the refrigerant side to obtain a more accurate measure of the cooling effect.

3.4.2.2 Heat balance on the refrigerant side

A procedure similar to the HBB is applied to determine the system cooling load with the heat balance on the refrigerant side. When the refrigerant undergoes a change of phase, the product between the temperature difference and specific heat (Equation 3.2) is replaced by an enthalpy difference in Equation 3.3. In this expression, the refrigerant mass flow rate measured by Ouzzane et al. ($\dot{m}_{ref}$=0.3348 kg/s) is used while the enthalpies are evaluated in terms of the temperature by using built-in routines from Engineer Equation Solver (Klein and Alvarado 1999).

$$\dot{Q}_{HBR} = \dot{m}_{ref} \cdot (h_{ref,in} - h_{ref,out}) \tag{3.3}$$

The refrigerant temperatures have only been monitored on the non-modified compressor of chiller #1 (compressor #2 in Figure 3.2). Thus, the heat balance on the refrigerant side only allows to evaluate the capacity of one compressor in one of the two chillers. Figure 3.9 presents the variations of the refrigeration capacity of compressor #2 during March 16th, 2006. The start-up period is not presented. The average cooling capacity of on compressor calculated by this method is 56.0 kW.
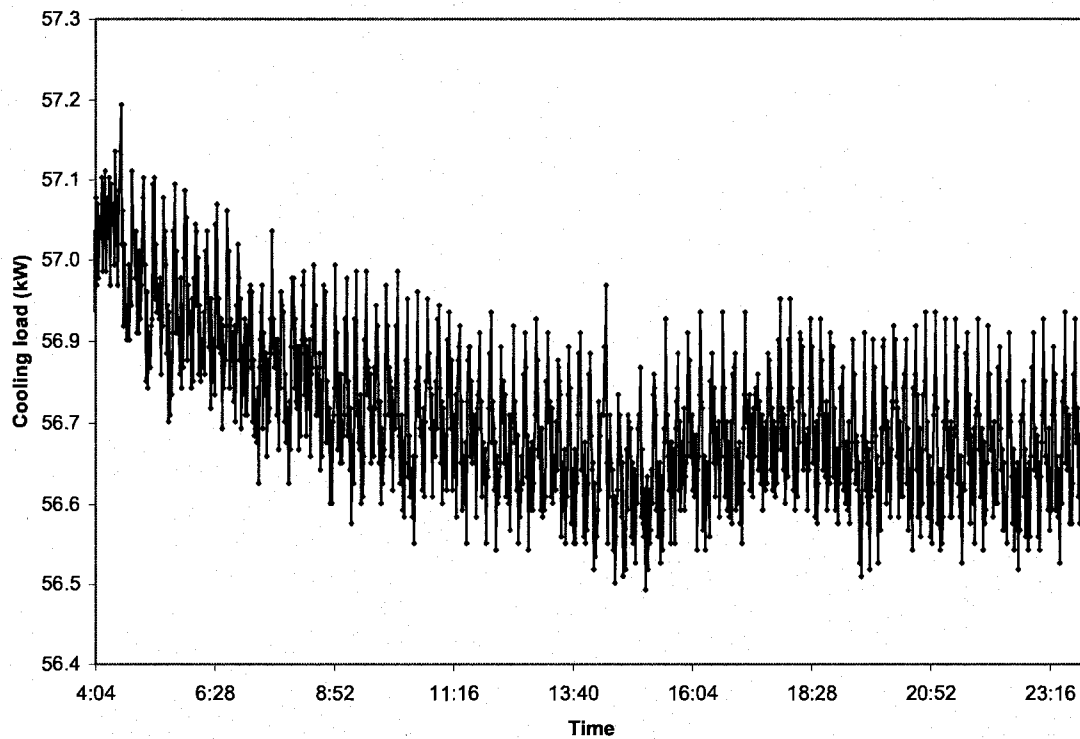
Figure 3.9: Cooling load of one compressor based on heat balance on the refrigerant side for chiller #1 on March 16th, 2006

From 4:00 to 13:40, the capacity of the compressor diminishes constantly. Then, the cooling load of the compressor reaches a constant level until the system is turned off. The constant fluctuations observed can be attributable to the noise of the instrumentation used during the monitoring of the refrigerant temperature.

3.4.2.3 Heat flux on the ice sheet

The third method consists in calculating the ice sheet cooling load based on the heat flux measurements. To this aim, an average value of the four heat flux sensors is used. The mean heat flux is then multiplied by the area of the ice surface (61 meters by 26 meters). Figure 3.10 plots the system cooling load calculated from the heat balance on the refrigerant side against the ice sheet cooling load calculated with the heat flux measurements for March 16th, 2006.
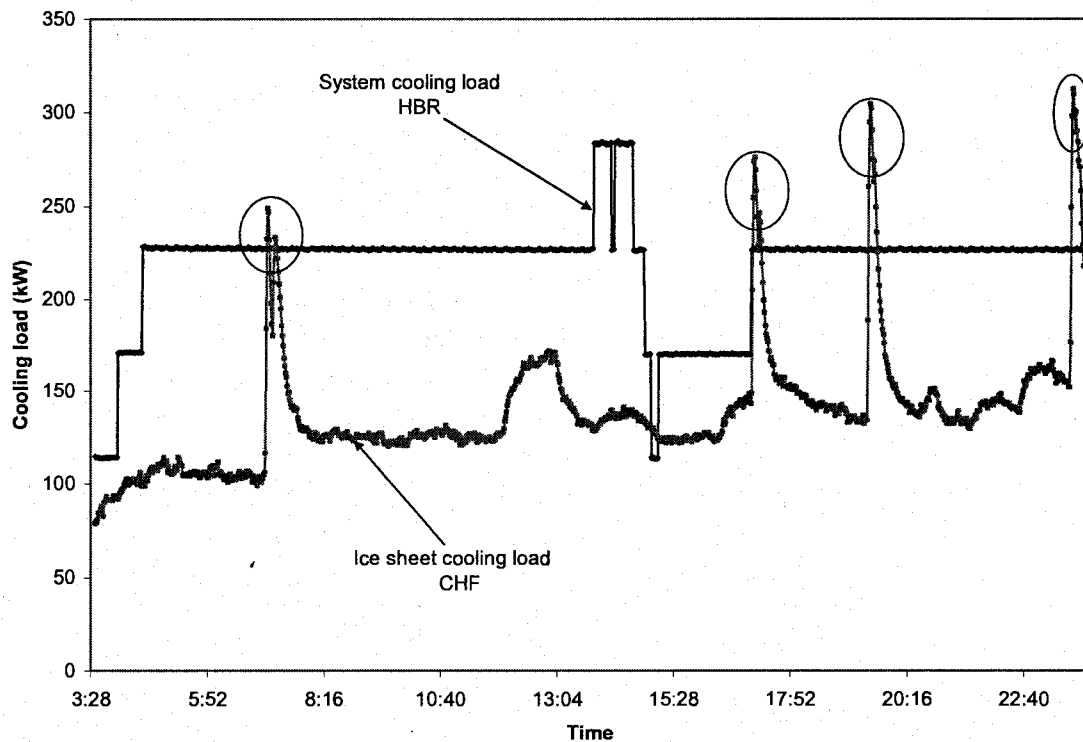
Figure 3.10: System cooling load from the energy balance on the refrigerant side and ice sheet cooling load from the heat flux measurements on March 16th, 2006

The encircled peaks observed on the CHF curve correspond to ice resurfacing periods. At this moment, the ice cooling load increases punctually while the system cooling load remains constant. As observed, the ice sheet cooling load is approximately half of the cooling load delivered by the refrigeration system. Based on the CHF method,

the capacity of one compressor is evaluated by considering a period where the number of compressors in operation is constant. During the interval between 8:00 and 12:00, four compressors are in operation (see Figure 3.6), and the average CHF is 124.8 kW; hence 31.2 kW of refrigeration per compressor.

3.4.2.4 Manufacture's software

The capacity of one compressor can also be evaluated by using the manufacturer's software. The compressor selection software called Carwin (Carlyle 2007) provides performance data on Carlyle compressors with commonly used refrigerants according to the operating conditions. The results obtained with the software can be considered as the most accurate because it was developed under laboratory conditions by the manufacturer. Based on the operating conditions at Camillien-Houde, the average refrigerating capacity calculated with the software for one compressor is of 56.3 kW

3.4.2.5 Comparing the four methods

A summary of the average refrigerating capacities obtained with the four different methods is presented in Table 3.4. Results from Ouzzane et al. (2006) are also presented, however, the paper does not mention for which chiller the capacity has been calculated.

Table 3.4: Refrigerating capacity per compressor calculated with four different methods

Method	Chiller #1 (kW)	Chiller #2 (kW)	Ouzzane et al. (2006) (kW)
HB, brine side	58.0	41.5	43.8
HB, refrigerant side	56.0	-	54.0
Heat flux ice sheet	31.2	31.2	Not calculated
Carwin	56.3	-	55.5

The results obtained in this study are very similar to those of Ouzzane et al. For the HBB method, the result from Ouzzane et al. is closer to the calculated load for chiller #2 than the one obtained for chiller #1. However, the results obtained for the HBR method are much closer: the difference is of 2.0 kW. This difference can be explained by the instruments setup used to measure the refrigerant temperatures. The Ouzzane et al. study used intrusive thermocouples, measuring directly the refrigerant temperature, while the calculations performed in this study are based on temperatures measured on the surface of the refrigerant pipes. Hence, the results obtained by Ouzzane et al. can be considered as more accurate. Table 3.4 also shows that the heat balance on the refrigerant side provides results slightly inferiors to those obtained with the compressor software. In light of these results, the heat balance on the refrigerant side method is considered to be the most accurate method.

3.4.3 Coefficient of performance

To evaluate the efficiency of refrigeration system, the coefficient of performance (COP) is used. The COP of the refrigeration system is defined as the ratio between the average cooling effect provided by one compressor (calculated with the heat balance on the refrigerant side) and the power of the compressor and connected condenser. The total electric demand (TED) measurements collected at Camillien-Houde are for the entire refrigeration system (compressors, condensers and pump) therefore, it is not possible to directly determine the power used by the condenser connected to the monitored compressor (compressor #2, in chiller #1). Hence, the average power input of the compressor-condenser unit (PCC) is determined by re-arranging Equation 3.1:

$$PCC = \frac{TED - PP}{NCU} \tag{3.4}$$

Equation 3.4 uses the number of compressor in operation calculated (NCU) to determine the electric demand of the compressor-condenser unit. This approach allows to obtain a variable COP, which reflects the real behaviour of the refrigeration system (compressor-condenser). Therefore, the COP is calculated as follows:

$$COP = \frac{\text{Refrigerating capacity (one compressor)}}{\text{Electric demand (one compressor - condenser unit)}} \tag{3.5}$$

Since the brine pump is not installed on the refrigerant side, it is not considered in the COP. Figure 3.11 plots the COP of one compressor-condenser unit, the number of compressors in operation and the ice sheet cooling load calculated with the heat flux sensors during a 21-hours interval on March 16th, 2006.
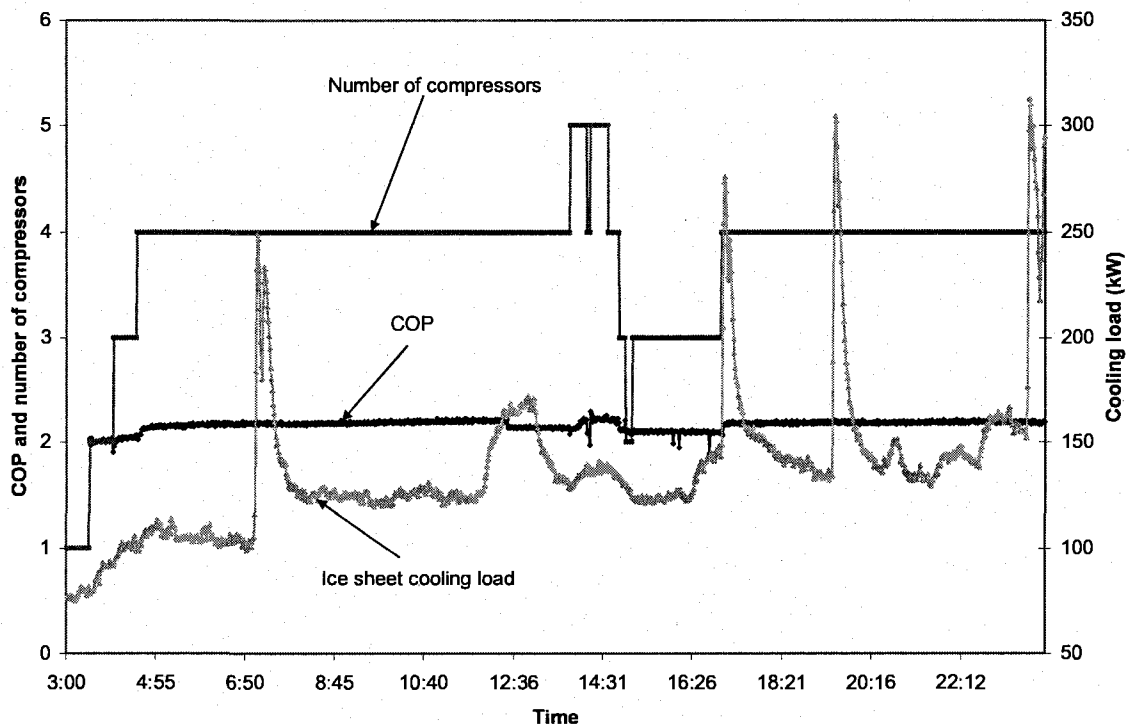
Figure 3.11: Number of compressors in operation, COP of the refrigeration system and ice sheet cooling load on March 16th, 2006

When the system starts (3:00 to 5:00), the controller turns on a compressor every 30 minutes. The slightly increase of the ice sheet cooling load in the morning is the due to the presence of people on the ice rink (activating the motion sensors which activates the radiant heating system) and the activities taking place on the ice. The peak ice sheet cooling loads correspond to resurfacing periods.

From 3:00 to 3:30, the COP is not calculated, since the monitored compressor is switched on at 3:30. Two minutes after start-up, the COP of the unit is about 2. During this period the refrigerant tends to accumulate in the heat exchangers, decreasing the cooling capacity of the compressor and the COP. Then, the COP slightly increases until 12:30. At that moment, the COP slightly decreases. This small variation as well as the others observed at 14:00, 15:00 and 17:00 are caused by an increase or decrease of the electric demand of the condenser. For that particular day, the daily average COP is 2.16. As observed in Figure 3.11, ice resurfacing has no significant effect on the COP of the system performance.

3.4.4 Ice resurfacing

The ice surface is redone almost every hour or after each activity to maintain its required quality. The resurfacing process consists of spreading a thin layer of about 0.25 mm of hot water on the ice surface. Figure 3.12 presents the power input to the refrigeration system (including the pump), the ice temperature, and the brine temperature at the slab exit (return brine temperature) for March 16th, 2006. The peaks of ice temperatures correspond to the resurfacing periods. However, the instantaneous increase

of the ice temperature observed at 18:45 can be considered as an error of lecture of the instruments.
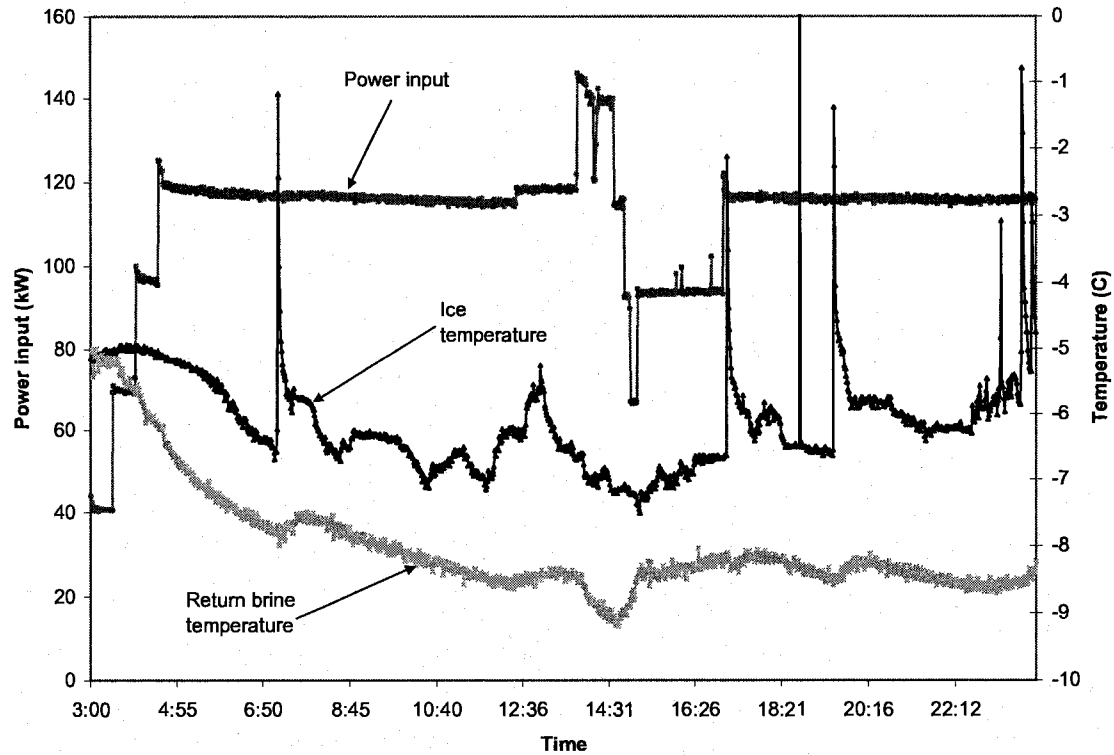
Figure 3.12: Power input, ice temperature, and return brine temperature on March 16th, 2006

When the ice is resurfaced (at 7:00, 15:00, 19:30 and 23:40), the ice temperature shows a sharp increase reaching almost -1°C. However, the increase of ice temperature does not increase in the same proportion the power input to the refrigeration system. Indeed, the controller maintains the same number of compressors in operation during resurfacing periods (see Figure 3.11). On the other hand, the ice resurfacing increases the return brine temperature. Due the thermal mass of the ice-concrete slab, the effect is smaller and it is delayed. As observed in Figure 3.13, the brine temperature increase is so small ($\approx 0.20°C$) that it probably falls in the dead band of the controller or measurement error. Therefore, there is no change in the number of compressors in operation.
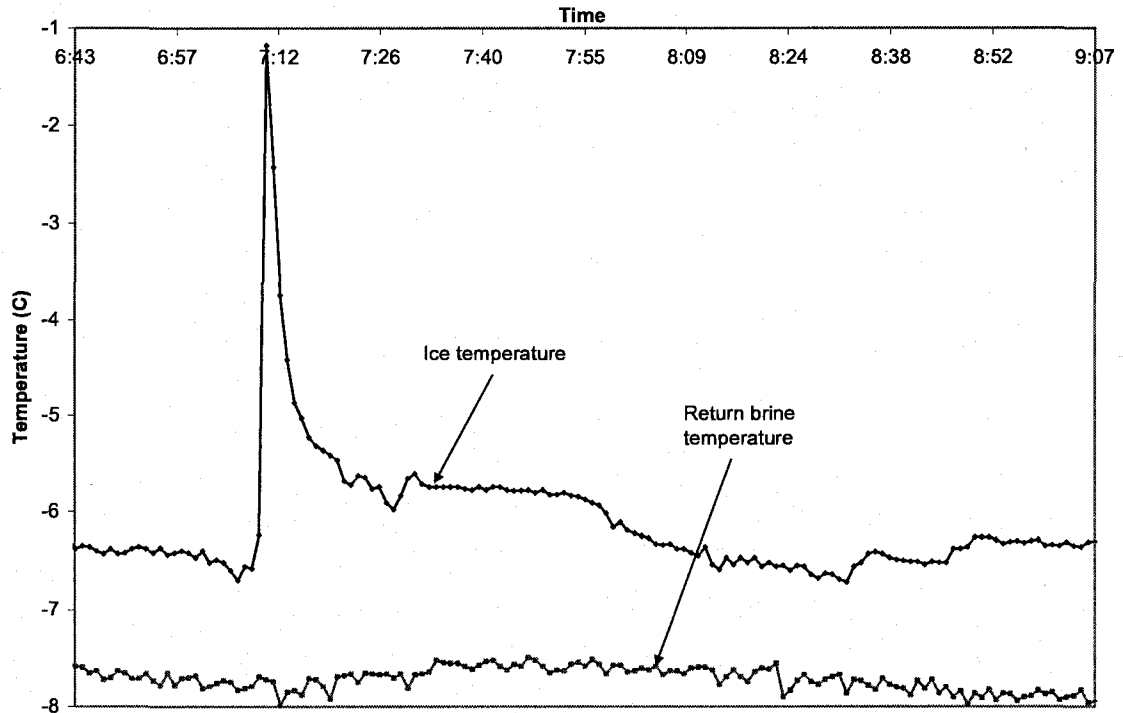
Figure 3.13: Effect of the thermal mass of the ice-concrete slab on the return brine temperature

The increase of the thermal mass of the ice-concrete slab would absorb the variations of the ice temperature, which would diminish the impact of the ice resurfacing on the return brine temperature. However, the control of the chillers, and therefore of the ice temperature, would be more difficult if the thermal mass is increased because the changes in the refrigerating capacity would be more filtered and delayed by the ice-concrete slab.

3.4.5 Exterior temperature

The exterior temperature has two major effects on the refrigeration system: (1) it influences the ice sheet cooling load due to the heat gain through the building envelope; and (2) as the exterior temperature increases, more fans are used by the condenser to compensate for reduction in temperature difference between the refrigerant in the

condenser and the outdoor air. This section analyzes the influence of the exterior temperature on the power used by the refrigeration system during the months of March and May 2006.

Figure 3.14 shows the COP of the refrigeration system (compressor-condenser unit), the electric demand and the exterior air temperature on March 16th, 2006. For this day, the average exterior temperature is of -0.9°C with a maximum of 2.1°C and a minimum of -2.8°C.
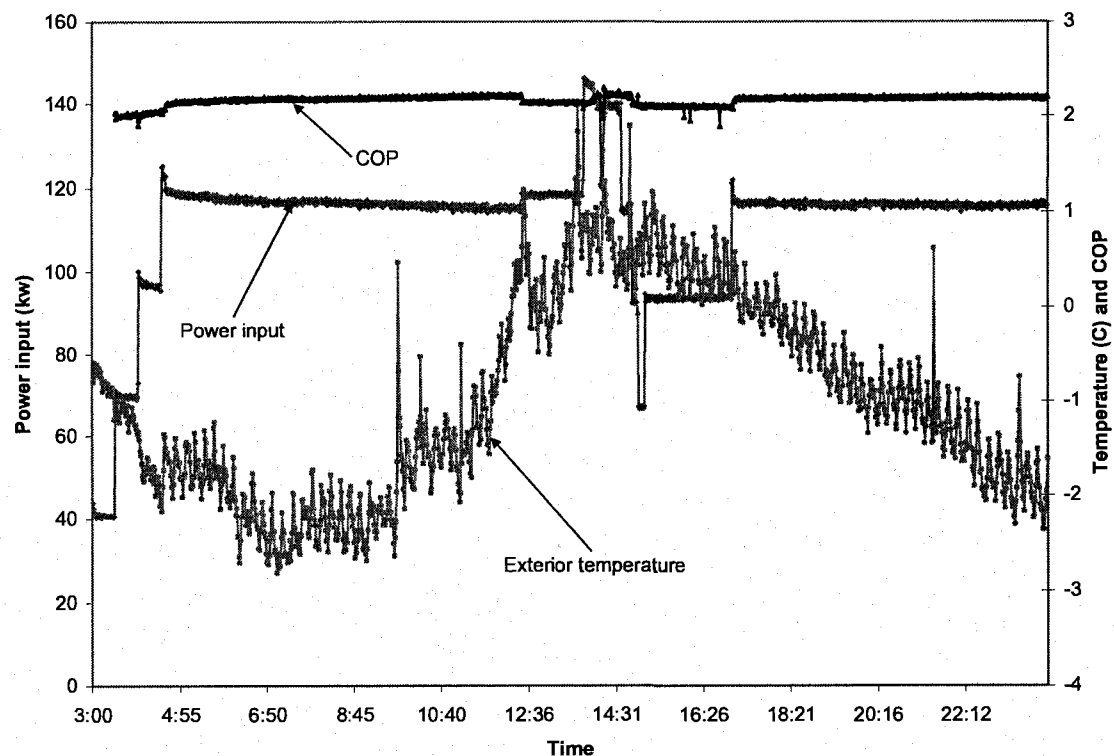
Figure 3.14: COP, power input and exterior temperature on March 16th, 2006

While the COP of the system is almost constant when the exterior temperature fluctuates, the highest power input (five compressors between 13:45 and 14:45) occurs when the exterior temperature reach a maximum. The increase in number of compressors

could be the consequence of an increase of the ice sheet cooling load due to infiltration in the building. However, by looking at Figure 3.11, it can be seen that during this period, the ice sheet cooling load does not increase. Hence, it is not possible to establish a direct relationship between the exterior temperature and the electric demand of the chiller.

The effects of the exterior temperature on the electric demand of the condensers are analyzed by looking at the COP. Because the operating conditions are almost constant (suction and discharge pressures are constants), the power input to a compressor and its refrigerating effect are also constant. Therefore, a fluctuation of the COP reflects a change in the power input to the condensers. Fluctuations are observed at 12:30, 14:00, 15:00 and, 17:00. Furthermore, by looking to the power input curve, it is possible to see that for a constant number of compressors in operation (four compressors between 4:30 and 13:50) the electric demand slightly varies, having an effect on the COP. For example, at 12:30, the electric demand increases of 3 kW, and the COP decreases of 0.1. At that moment, the exterior air temperature shows a sharp increase. This observation can be attributable to the start-up of two fans (1.6 kW per fan) on the condensers to compensate for the loss of heat transfer.

To obtain a better perspective of the effect of the exterior temperature, the same analysis is performed for a different day in a different month. Figure 3.15 presents the variations of the COP and the electric demand in function of the exterior temperature on May 14th, 2006.
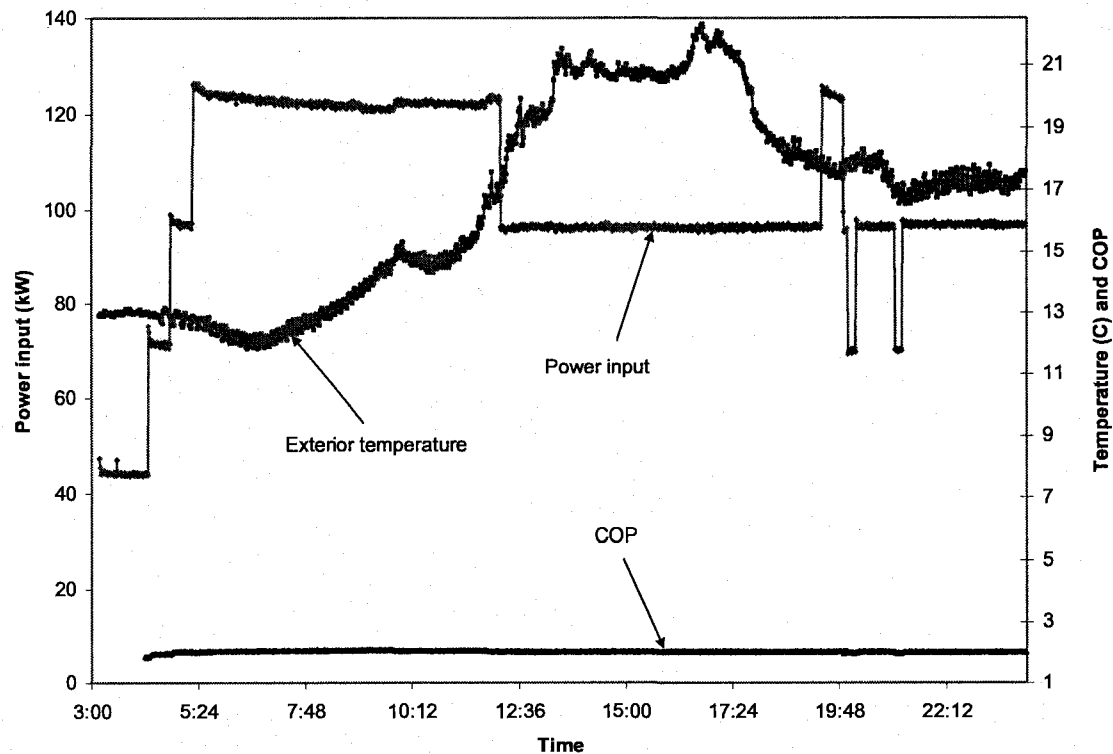
Figure 3.15: COP, power input and exterior temperature on May 14th, 2006

During this day, the average exterior temperature is of 16.6°C with a maximum of 22.3°C and a minimum of 11.8°C. The average COP is of 2.03, which is slightly less than the one calculated on March 16th, 2006 (COP = 2.16). The standard deviation of the COP during May 14th is equal to 0.03, while on March 16th, it is equal to 0.05. This indicates that the COP is practically constant during the day, and the difference between March and May is negligible.

From 5:20 to 12:10 the system operates with four compressors while the exterior temperature increases. When the exterior air temperature reaches a maximum at 16:40, three compressors are in operation. Then, at 19:30, the system increases the number of compressors in operation to four while the exterior temperature decreases. Therefore, in

59

light of the analysis performed on March 16th and May 14th, it is not possible to directly relate the exterior temperature with the number of compressors in operation.

Regarding the condensers, the COP is almost equal and constant for both months, even if the difference of the exterior air temperature is important. The small COP variation indicates that the power input to one compressor-condenser unit is greater if the exterior temperature is higher. In fact, during the month of March, the average electric demand of one compressor-condenser is of 27.5 kW while in May the same loop used 31 kW. Because the electric demand of a compressor is almost constant, the increase power input is related to the condensers. Indeed, the electric demand difference for these two days (3.5 kW) corresponds approximately to the power use of by two fans, i.e. 3.2 kW. Hence, it is possible to establish that the electric demand of the condenser is slightly higher if the exterior air temperature increases due to a higher number of fans in operation.

3.4.6 Operating characteristics of the refrigeration system

The operating characteristics of the refrigeration system are determined by analyzing the previous parameter for three different days. Table 3.5, Table 3.6 and Table 3.7 present a summary of the operating conditions at the Camillien-Houde arena for March 16th, May 14th and October 18th, 2006, respectively. Each parameter previously analyzed is presented with its corresponding average, maximum and minimum values and standard deviation. The night period, which corresponds to the moment when the refrigeration system is stopped, is not considered.

Table 3.5: Operating characteristics of the refrigeration system on March 16th, 2006

Parameter	Units	Average	Standard deviation	Minimum	Maximum
Heat flux cooling load	kW	136.8	34.6	74.7	312.2
Heat balance on the refrigerant side	kW	56.0	0.2	55.7	56.7
Ice temperature	°C	-6.1	0.8	-7.5	-4.8
Exterior temperature	°C	-0.9	1.0	-2.8	2.1
Return brine temperature	°C	-8.0	0.8	-9.2	-4.9
Electric demand	kW	111.5	16.2	40.2	146.1
COP	-	2.2	0.0	1.9	2.3

Table 3.6: Operating characteristics of the refrigeration system on May 14th, 2006

Parameter	Units	Average	Standard deviation	Minimum	Maximum
Heat flux cooling load	kW	149.3	7.9	111.8	162.7
Heat balance on the refrigerant side	kW	55.8	0.2	55.4	56.4
Ice temperature	°C	-7.0	0.8	-7.9	-5.2
Exterior temperature	°C	16.6	3.1	11.8	22.3
Return brine temperature	°C	-8.4	0.9	-9.4	-5.6
Electric demand	kW	102.0	19.6	43.6	126.6
COP	-	2.0	0.0	1.8	2.1

Table 3.7: Operating characteristics of the refrigeration system on October 18th, 2006

Parameter	Units	Average	Standard deviation	Minimum	Maximum
Heat flux cooling load	kW	171.9	25.3	115.9	259.2
Heat balance on the refrigerant side	kW	55.7	0.2	55.2	56.3
Ice temperature	°C	-5.8	0.9	-7.6	5.3
Exterior temperature	°C	14.6	2.2	9.8	19.7
Return brine temperature	°C	-8.6	1.0	-9.7	-4.8
Electric demand	kW	123.9	24.6	40.7	155.5
COP	-	2.0	0.6	1.77	2.32

The highest average electric demand, 123.9 kW occurs on October 18th when the average exterior temperature is of 14.6°C. However, on May 14th, the average exterior temperature is of 16.6°C and the average electric demand is decreased by 21.9 kW. The average energy demand on March 16th is greater (123.9 kW) even if the average exterior temperature is the lowest one among the three days (-6.1°C). Therefore, the analysis of

the average values of electric demand and exterior air temperature shows that there is not a direct relation between these two variables.

The average brine temperature at the slab exit for the three days is -8.3°C, while the average ice temperature is -6.3°C. It is interesting to see that the highest average ice temperature of the three days (-5.8°C on October 18th) occurs when the average return brine temperature is the lowest one among the three days (-8.6°C). This result is incoherent because the ice temperature should be proportional to the return brine temperature. However, variable factors such as the thickness of the ice layer and the heat absorbed by the brine from the ground could modify the heat exchange between the ice surface and the brine between the months. The average COP calculated for the compressor-condenser unit is almost equal to 2.0 for the three different days.

3.5 Conclusions

The collected data from the monitored ice rink have been analyzed in order to reach a better understanding of the operation and performance of the refrigeration system. The system cooling load felt by the compressors has been calculated following four different approaches. From the results obtained, the calculation of the cooling load based on the refrigerant energy balance is the most accurate method. The average refrigerating effect calculated with this approach for compressor #2 is 56 kW. The calculation of the capacity by using both the heat flux sensors and the heat balance on the brine side provide the worst results. The results obtained have been validated by using the compressor software and the results provided by Ouzzane et al. (2006).

The calculation of the heat balance on the refrigerant side has put in evidence the difference of refrigerating capacity of chiller #1 and chiller #2. Hence, a compressor operating in chiller #1 has an average refrigerating capacity of 58 kW, while in chiller #2 the cooling capacity of a compressor is of 41.5 kW. This difference between the two chillers will be considered during the development of the simulation model.

The analyses performed between the different variables have not allowed to make direct relations between them. This does not mean that the variables are independent, however other factors that have not been considered have an impact on the variables.

CHAPTER 4

MATHEMATICAL MODEL OF CHILLERS

The mathematical model of chillers used in the refrigeration system is presented in this chapter. The model is based on the ASHRAE Toolkit-I for Primary HVAC System (Bourdouxhe et al. 1997). This chapter begins with the presentation of the routine used for the identification of the compressor parameters. The equations and the procedure are presented in detail. The parameters identified are verified by using the Carwin compressor software. The chapter also presents the procedure proposed by the Toolkit for the identification of the heat exchangers parameters. The procedure is analyzed in detail and the limitations are discussed. The issues encountered during the identification procedure are explained and solutions are developed. At the end of the chapter, the routine proposed by the Toolkit for the simulation of the chillers is presented. Details on the modifications performed are also presented. These modifications led to a simplified simulation routine that is better adapted to the operating conditions of the refrigeration system installed at the Camillien-Houde ice rink.

4.1 Toolkit modelling approach

The mathematical model used to simulate the chiller is based on the ASHRAE Toolkit-I for Primary HVAC System (Bourdouxhe et al. 1997). The Toolkit contains a series of routines and subroutines written in Fortran to simulate the energy performance of several primary HVAC components. The models of the ASHRAE Toolkit-I are based

both on the thermodynamic analysis of the refrigeration process and on empirical equations. The thermal behaviour of each component of the refrigeration system is modeled separately and then connected together by the corresponding mass and heat transfer equations. The characteristic parameters of equipment are identified from the manufacturer's catalogue or measured data. Measurements collected at the monitored ice rink used in the development of the complete chiller model and in the identification process are presented in Figure 4.1.
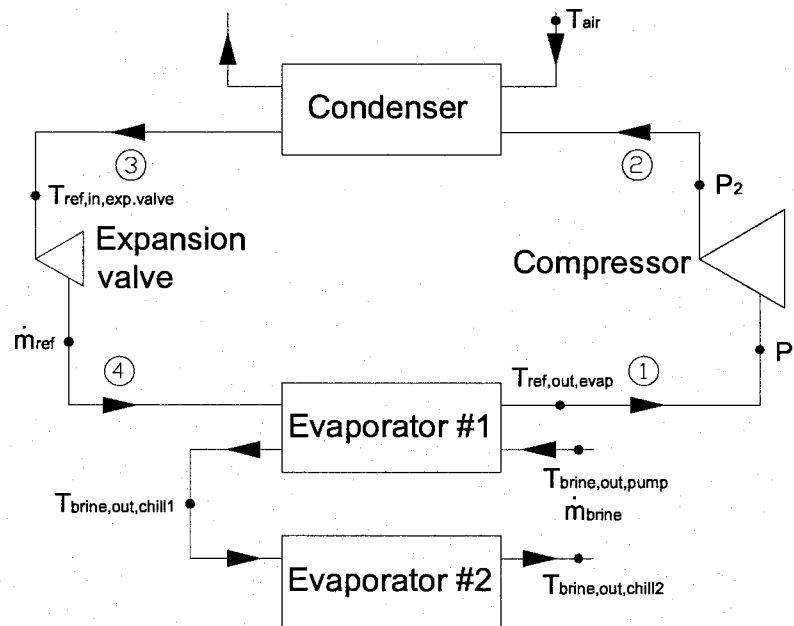
Figure 4.1: Simplified model of the refrigeration system and collected data

Each component is modeled in two steps. First, the characteristics of the components are identified based on the analytical model and the manufacturer's catalogue or measured data. The Toolkit provides the routine PISCOMP1 and the routine PISCHIL1 for the identification of the compressor and heat exchangers parameters. Then, the components are simulated by using the routine PISSIM1 for given operating conditions by using the analytical model along with the identified parameters.

4.2 Refrigerant properties

The thermodynamic properties of refrigerants are calculated in a subroutine called PROPERTY included in the Toolkit. The model assumes that a refrigerant is a perfect gas, a liquid or a mixture of both. This assumption is used to determine mean thermodynamic properties in a restrained domain of temperature. Concerning evaporation, the temperature range acceptable for accurate results is between 253.15 K and 283.15 K, while the acceptable condensation temperature covers a range between 303.15 K and 333.15 K. For the liquid phase, the enthalpy is defined as:

$$h = h_{fo} + \overline{c}_f \cdot (T - T_0) + v \cdot (P - P_0) \qquad (4.1)$$

where: h_{fo} = enthalpy of the saturated liquid at the reference temperature (J kg^{-1});
$\overline{c}_f$ = mean specific heat at constant volume (J kg^{-1} °C^{-1});
T = given temperature (K);
P = given pressure (Pa);
T_0 = reference temperature (273.15 K);
P_0 = reference pressure (Pa);
v = specific volume (m^3 kg^{-1}).

Because fluids are practically incompressible, the last term of Equation 4.1 can be neglected for the calculation of the liquid enthalpy leading to the following expression:

$$h = h_{fo} + \overline{c}_f \cdot (T - T_0) \qquad (4.2)$$

For instance, for refrigerant R-22: h_{fo} = 200,000 J kg^{-1}, $\overline{c}_f$ = 1,144 J kg^{-1} °C^{-1}. As for the vapour phase, the refrigerant is characterized by using the ideal gas approximation. The enthalpy of the superheated vapour is defined by the following relationship:

$$h = h_{fo} + h_{fgo} + \bar{c}_p \cdot (T - T_0) \qquad\qquad (4.3)$$

where: h_{fgo} = enthalpy of vaporization at the reference temperature (J kg^{-1});

$\bar{c}_p$ = mean specific heat at constant pressure (J kg^{-1}K^{-1}).

For example, for refrigerant R-22: h_{fgo} = 204,590 J kg^{-1}, $\bar{c}_p$ = 710.4 J kg^{-1} K^{-1}. The evaporation and condensation pressures (saturation pressures) are determined by means of the Clausius-Clapeyron equation:

$$P_{sat} = 1000 \cdot e^{\left(A + \frac{B}{T_{sat}} \right)} \qquad\qquad (4.4)$$

where A and B are the first and second coefficients in the Clausius-Clapeyron equation. Hence, for refrigerant R-22 A = 15.070 and B = -2,421.94 K. These values are valid for temperatures ranging from 253.15 K to 333.15 K.

4.3 Mathematical model of a reciprocating compressor at full load regime

Compressors at the Camillien-Houde ice rink are always operating at full load regime when there are in use. All four pistons of each compressor are running if the compressor is in operation. The part load regime, which occurs when a reduced number of pistons are in operation, would be an interesting measure to reduce the electric demand of the system. However, the actual control system does not have the capability to control directly the number of pistons in operation. The ASHRAE Toolkit presents models for both full and part load regimes.

4.3.1 Compressor model

For full load regime, the compressor is modeled as an ideal mechanical machine, i.e., irreversibilities are not taken into account. Therefore, an isentropic compression is assumed by the model. On the other hand, the simplified model of the compressor considers the losses due to the "motor-transmission" of the reciprocating compressor. To do this, the model analyzes the behaviour of the "motor-transmission" and the behaviour of the reciprocating compressor separately. The conceptual scheme of the power distribution and losses throughout the compressor is illustrated in Figure 4.2 (a) while Figure 4.2 (b) presents the evolution of the refrigerant across the compressor in a pressure-enthalpy diagram (Bourdouxhe et al. 1997).
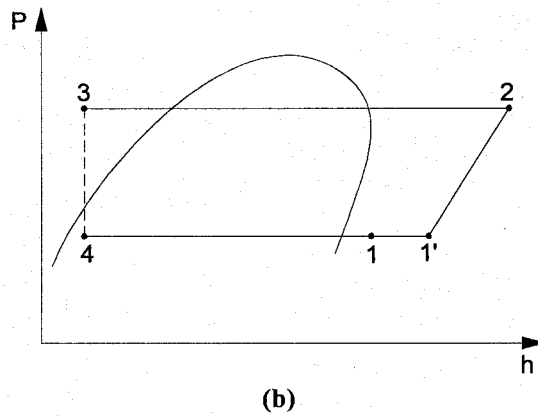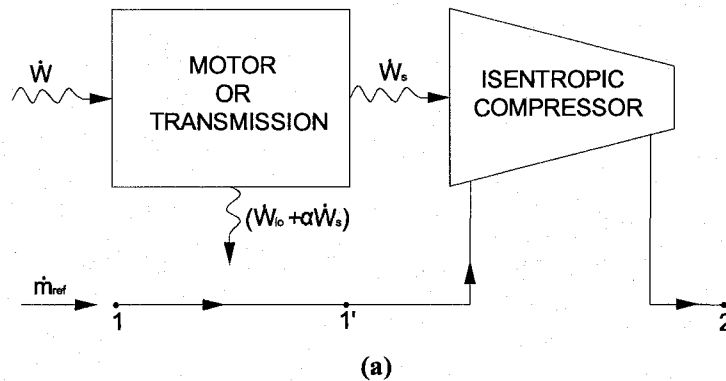
Figure 4.2: (a) Conceptual scheme of a compressor in full-load regime
(b) P-h diagram of compression process (points 1-2) (Bourdouxhe et al. 1997)

The model assumes that the refrigerant is heated-up by electromechanical losses (process 1 to 1' in Figure 4.2) before being compressed:

$$\dot{W} = \dot{W}_{lo} + \alpha \dot{W}_s + \dot{W}_s \qquad (4.5)$$

where: $\dot{W}$ = electrical shaft power (W);

$\dot{W}_{lo}$ = constant part of electromechanical losses (W);

α =loss factor;

$\dot{W}_s$ = compressor isentropic power (W).

A reciprocating compressor operates in a cyclic manner described by a series of four reversible processes as shown in the P-V diagram Figure 4.3.

- isobaric aspiration of the refrigerant into the cylinders (process a-b);
- isentropic compression (process b-c);
- isobaric expulsion of the refrigerant from the cylinder (process c-d);
- isentropic expansion of the refrigerant which remained in the clearance volume at the end of the expulsion process (process d-a).
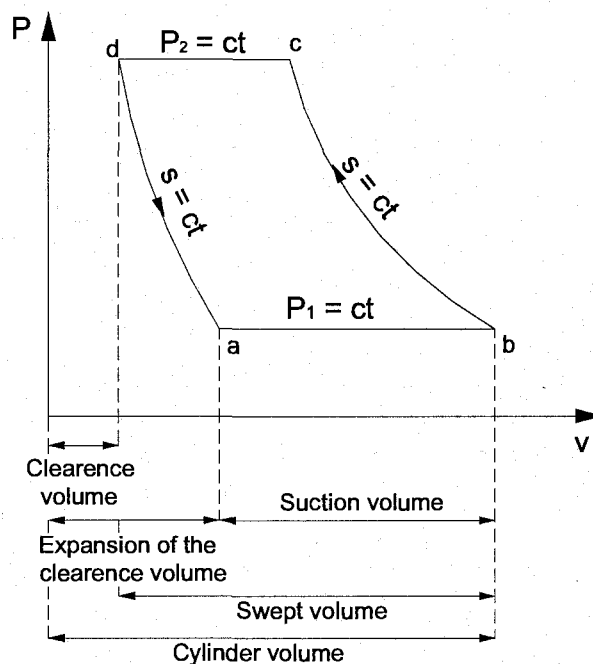
Figure 4.3: Reciprocating compressor cycle description (Bourdouxhe et al. 1997)

In order to relate the cyclic behaviour of the compressor with the suction and discharge pressures and volumes, the empirical Equation 4.6 is introduced:

$$\dot{V} = \dot{V}_s \left[1 + C_f - C_f \left(\frac{P_2}{P_1} \right)^{1/\bar{\gamma}} \right] \qquad (4.6)$$

where: $\dot{V}$ = volume flow rate entering the compressor (m³ s⁻¹);
$\dot{V}_s$ = swept volume flow rate (see Figure 4.3 for reference) (m³ s⁻¹);

C_f = clearance factor = $\left(\dfrac{V_{clearence}}{V_{swept}} \right)$ (see Figure 4.3 for reference);

$\dfrac{P_2}{P_1}$ = cylinder pressure ratio (discharge pressure over the suction pressure);

$\bar{\gamma}$ = mean isentropic coefficient.

According to ideal gas theory, the mean isentropic coefficient is obtained from:

$$\bar{\gamma} = \frac{\bar{c}_p}{\bar{c}_p - R} \qquad (4.7)$$

where: R = is the gas constant. For instance, for refrigerant R-22, $\bar{c}_p$ = 710.4 J kg⁻¹ °C⁻¹, R = 96.1426 J kg⁻¹ °C⁻¹ and $\bar{\gamma}$ = 1.114. Equation 4.6 can be rearranged and rewritten in a simplified form:

$$\dot{V} = \dot{V}_s - C_f \cdot \dot{V}_s \cdot pfactor \qquad (4.8)$$

where: $pfactor = \left(\dfrac{P_2}{P_1} \right)^{\frac{1}{\gamma}} - 1$

Equations 4.5 and 4.8 are used for the identification of four parameters: $\dot{W}_{lo}$, α, $\dot{V}_s$ and c_f to characterize the reciprocating compressor.

4.3.2 Identification of the compressor parameters

Based on the electromechanical model of the compressor and its cyclic description, the parameters of the reciprocating compressor are identified. The subroutine named PISCOMP1 is used to identify the four parameters of the compressor at full load regime. The subroutine considers the superheating in the evaporator and the sub-cooling in the condenser as illustrated on the P-h diagram in Figure 4.2 (b). The flow diagram presented in Figure 4.4 gives all the inputs and outputs used in this routine.
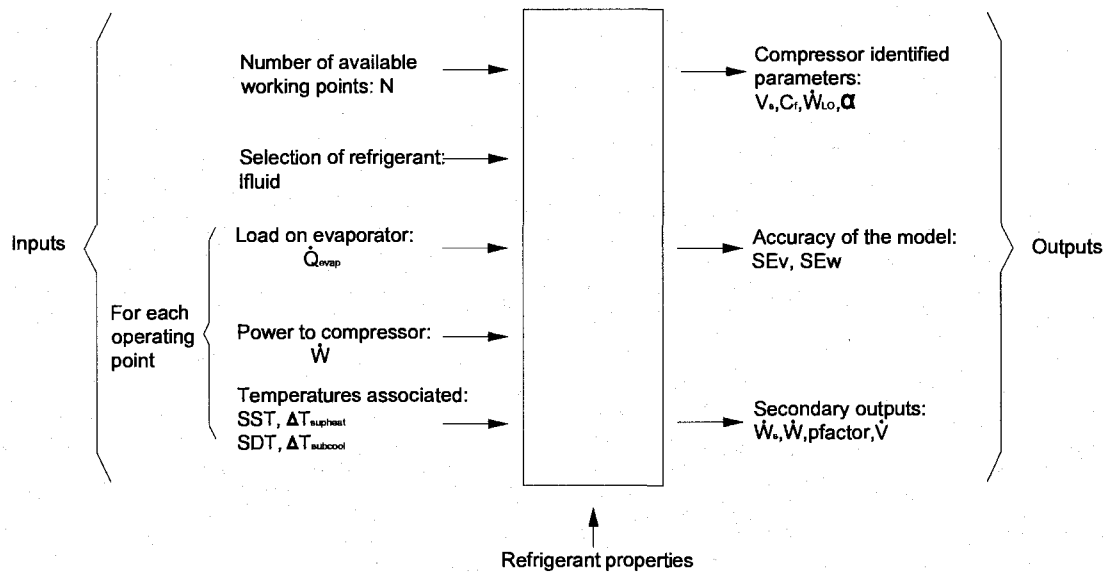
Figure 4.4: Information flow diagram of PISCOMP1 (Bourdouxhe et al. 1997)

4.3.2.1 PISCOMP1 mathematical description

Based on the given evaporation and condensation saturation temperatures (SST and SDT, respectively), the temperatures at the evaporator and condenser exit (points 1 and 3, respectively in Figure 4.2) are evaluated:

$$T_1 = SST + \Delta T_{sup\,heat} \tag{4.9}$$

$$T_3 = SDT - \Delta T_{subcool} \tag{4.10}$$

71

where the degrees of superheating ($\Delta T_{sup,heat}$) and of sub-cooling ($\Delta T_{sub,cool}$) are of 6°C and 12.5°C, respectively. Experts from CANMET-Varennes have recommended these values. The refrigerant mass flow rate is determined by dividing the given load at the evaporator by the enthalpy difference between the inlet and outlet of the evaporator:

$$\dot{m}_{ref} = \frac{\dot{Q}_{evap}}{h_1 - h_3} \qquad (4.11)$$

The isentropic work of the compressor is given by the following expression:

$$\dot{W}_s = \dot{m}_{ref} \cdot (h_{2s} - h_1) = \dot{m}_R \cdot \int_1^{2s} v dP \qquad (4.12)$$

For isentropic compression:

$$P \cdot v^\gamma = \text{constant} \qquad (4.13)$$

Therefore, Equation 4.12 becomes:

$$\dot{W}_s = \dot{m}_{ref} \cdot (h_{2s} - h_1) = \dot{m}_{ref} \cdot \frac{\gamma}{\gamma - 1} \cdot (P_{2s} \cdot v_{2s} - P_1 \cdot v_1) \qquad (4.14)$$

Assuming that the refrigerant is a perfect gas, a liquid or a mixing of both allows defining the product between the pressure and the volume by the equation of state for gases:

$$P \cdot v = \zeta \cdot R \cdot T \qquad (4.15)$$

where: ζ = mean compressibility factor and R = gas constant (J kg^{-1} K^{-1}).

Introducing the equation of state into Equation 4.14 leads to a reformulated form of the equation for the isentropic work:

$$\dot{W}_s = \dot{m}_{ref} \cdot \frac{\bar{\gamma}}{\bar{\gamma} - 1} \cdot \zeta \cdot r \cdot T_{1'} \cdot \left(\frac{T_{2s}}{T_{1'}} - 1 \right)$$

(4.16)

Assuming constant specific heats, the following relation is valid for an isentropic process of an ideal gas:

$$\frac{T_{2s}}{T_1'} = \left(\frac{P_2}{P_1} \right)^{\frac{\gamma-1}{\gamma}}$$

(4.17)

By introducing Equation 4.17 into Equation 4.16, the isentropic work becomes:

$$\dot{W}_s = \dot{m}_{ref} \cdot \frac{\bar{\gamma}}{\bar{\gamma} - 1} \cdot \zeta \cdot r \cdot T_{1'} \cdot \left(\left(\frac{P_2}{P_1} \right)^{\frac{\gamma-1}{\gamma}} - 1 \right)$$

(4.18)

where P_1 is the saturation pressure of evaporation and P_2 is the saturation pressure of condensation. When the refrigerant passes from state 1 to state 1' due to the electromechanical losses (see Figure 4.3), the enthalpy of point 1' after the heating-up is determined with the following expression:

$$h_{1'} = h_1 + \frac{\dot{W} - \dot{W}_s}{\dot{m}_{ref}}$$

(4.19)

By assuming a constant specific heat, Equation 4.19 is rewritten as:

$$T_{1'} = T_1 + \frac{\dot{W} - \dot{W}_s}{c_P \cdot \dot{m}_{ref}}$$

(4.20)

The volumetric flow rate of refrigerant suctioned by the compressor is determined from the ideal gas equation of state in terms of the temperature after the heating-up:

$$\dot{V} = \frac{\dot{m}_{ref} \cdot \varsigma \cdot R \cdot T_{1'}}{P_1}$$ (4.21)

For each working point, the refrigerant volumetric flow rate $\dot{V}$ is determined by means of Equation 4.21. Equation 4.8 is then fitted to the experimental results by means of the least square technique to provide the values of $\dot{V}_s$ and C_f in function of the pfactor (Figure 4.5 (a)). Equation 4.20 is then used into Equation 4.18 to determine $\dot{W}_s$. The values of $\dot{W}_{lo}$ and α (Figure 4.5 (b)) are estimated by using Equation 4.5 and the least square technique applied to experimental data.

(a)

(b)
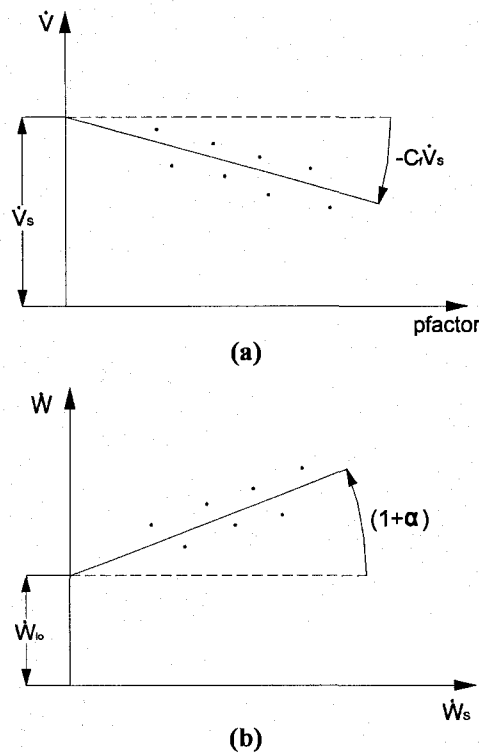
Figure 4.5: (a) Identification of $\dot{V}_s$, and C_f

(b) Identification of $\dot{W}_{lo}$ and α (Bourdouxhe et al. 1997)

4.3.2.2 Algorithm and flowchart of PISCOMP1

In order to reach a better understanding of the calculation steps of the routine, the algorithm is presented (Bourdouxhe et al. 1997).

i- First guess of the temperature after the heating-up (T_1')

ii- For each working point:

Calculate the evaporating and condensing pressures;

Calculate the temperature at the evaporator and condenser exit;

Calculate the enthalpy at the evaporator and condenser exit;

Calculate the refrigerant mass flow rate.

iii- Begin loop

1- Calculate the isentropic compression power;

2- Calculate a new estimated value of the temperature after the heating-up;

3- IF converged THEN leave loop; if not, then go to point 1.

iv- End loop

v- Final Calculations

Calculate the refrigerant volume flow rate entering the compressor;

Calculate the value of pfactor;

Calculate the four parameters of the compressor ($\dot{V}_s$ C_f $\dot{W}_{lo}$ α);

Calculate the dimensionless standard deviations (SEw, SEv).

To complement the algorithm, Figure 4.6 presents the iterative flowchart with the corresponding equations employed in the identification process for the reciprocating compressor in a full load regime. The subroutine ERROR is called to calculate the standard deviation of the linear regression obtained. The standard deviations are then provided as an output by the routine.

Start

INPUTS

Refrigerant, number of working points (N) and for each working point:

Refrigerating capacity $\dot{Q}_{evap}$
Power consumed by the compressor $\dot{W}$
Evaporating temperature   SST
Condensing temperature   SDT
Superheat in the evaporator $\Delta T_{supheat}$
Subcool in the condenser ΔT_{subool}

Subroutine PROPERTY

T_0, h_{fo}, h_{fgo}, $\overline{C_f}$, $\overline{C_p}$, r ,zeta ,gamma, Acl, Bcl

Equation 4.4 ──────▶ P_1, P_2

DO 20
I = 1,N

Equation 4.9 ────────▶ T_1
Equation 4.10 ──────▶ T_3
Equation 4.2 ────────▶ h_1
Equation 4.3 ────────▶ h_3
Equation 4.11 ──────▶ $\dot{m}_{ref}$

Guess of $T_{1'}$

Equation 4.18 ────────▶ $\dot{W}_s$
Equation 4.20 ────────▶ $T_{1'}$

Convergence

NO

YES

Equation 4.21 ────────▶ $\dot{V}$
Equation 4.8 ─────────▶ pfactor

20

OUTPUTS
$\dot{V}_s$,C_f,W_{Lo},α
SEw, SEv

End

Figure 4.6: Identification procedure flowchart of routine PISCOMP1 for the compressor (Bourdouxhe et al. 1997)

76

4.3.2.3 Application of PISCOMP1

The identification of the compressor parameters by means of the subroutine PISCOMP1 is not a simple task due to its iterative procedures. Attention must be given to the input data provided to the routine in order to obtain consistent outputs. Hence, several tests were necessary before obtaining coherent results. Because the routine is based on an iterative procedure, it is necessary to use input data representing a wide range of operating conditions. However, the collected data at the Camillien-Houde ice rink have very small fluctuations since the compressors operate at approximately constant conditions. Therefore, using the collected measures as input data in the routine PISCOMP1 provides inconsistent results such as negative work losses. To avoid this problem, an input data file for a wide range of operating conditions is constructed based on simulated results obtained from the manufacture's software called Carwin (Carlyle 2007). In order to create an input file based on the software, different compressor power and evaporation loads are calculated for different saturation suction and discharge temperatures. A superheating of 6°C at the evaporator and a sub-cooling of 12.5°C at the condenser are used for all operating conditions. An input file containing a total of 21 working points is created by selecting values of the saturated suction temperature (SST) between -10°C to 2°C and the saturated discharge temperature (SDT) between 30°C and 40°C. Calculations are performed by using a total of seven different SSTs and three different SDTs (30°C, 35°C and 40°C) for each SST. The input temperatures and the corresponding results (load on evaporator and electric demand) obtained from the manufacturer's software (Figure 4.7) are used as inputs in the routine PISCOMP1.
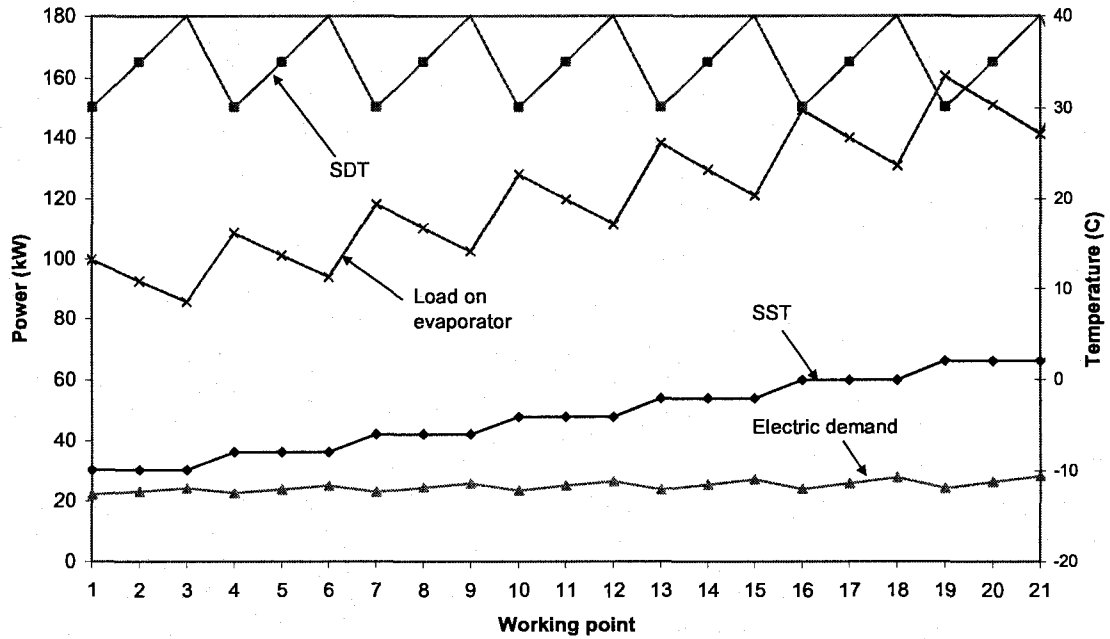
Figure 4.7: Results from the compressor software used to create the input file for PISCOMP1

The compressor parameters identified by means of PISCOMP1 are presented in Table 4.1.

Table 4.1: Identified parameters for the compressor with routine PISCOMP1

Parameter	Value
$\dot{W}_{lo}$	6330.472
α	-0.06780
C_f	0.70853
$\dot{V}_s$	0.045147

In order to verify the accuracy of the identified parameters, $\dot{W}_{lo}$ and α are used in Equation 4.5 to calculate the actual power of the compressor. Figure 4.8 shows the electric demand of the 21 working points obtained from the compressor software versus those calculated with the parameters identified.

78
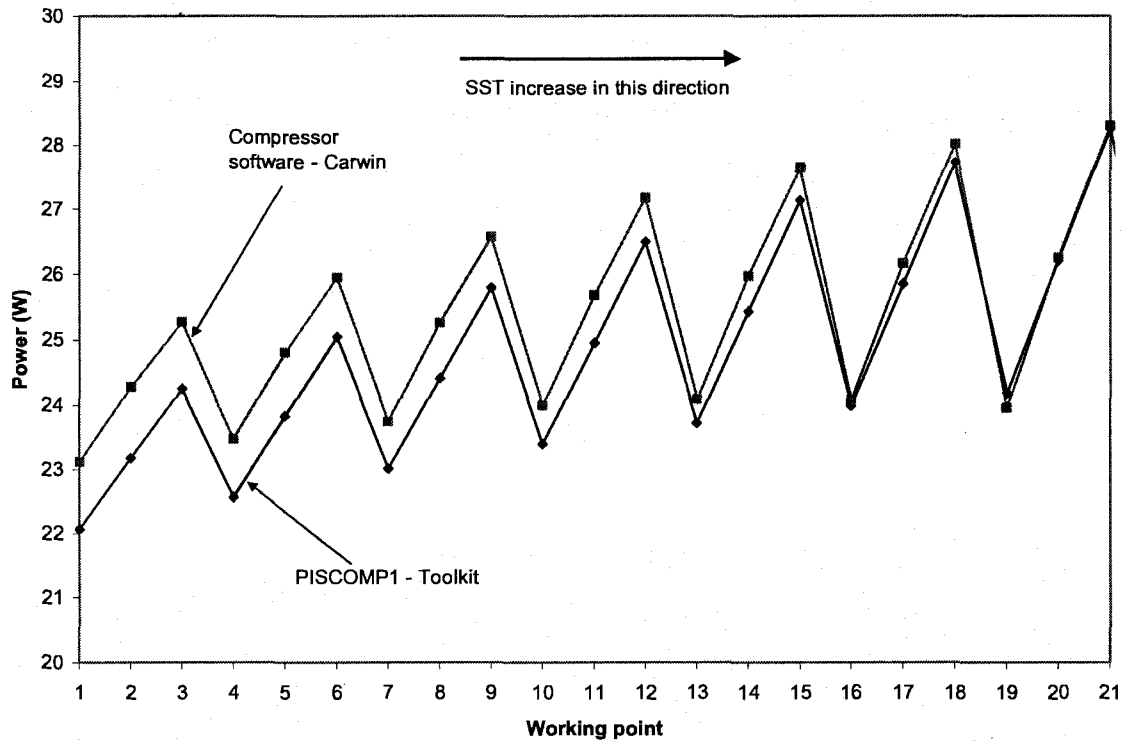
Figure 4.8: Validation of the compressor identified parameters with the Carwin software

As the saturated suction temperature increases, the difference between the electric demand calculated with the compressor software and the routine PISCOMP1 tend to diminish. Different factors could explain this tendency; however, the largest difference of power is about 1 kW, or less than 5%. Therefore, the parameters identified with the routine PISCOMP1 can be used with confidence. Moreover, if the Toolkit is used with high saturation suction temperatures, the compressor parameters will provide results with higher accuracy.

4.4 Mathematical model of heat exchangers

Two types of heat exchangers are installed at Camillien-Houde: fluid/fluid for the evaporator and fluid/air for the condenser. Heat exchangers can operate in transient or steady states. When a compressor is turned-on or off, a certain amount of refrigerant

tends to accumulate in the heat exchanger during a short period, leading to a variable refrigerant flow rate. The two compressors in chiller #1 at the Camillien-Houde ice rink are started once per day, while the three others in chiller #2 are switched on and off only few times per day. Thus, steady state operating conditions are assumed for the entire day.

4.4.1 Heat exchanger model

Both the evaporator and condenser models are based on the first principle of thermodynamics. Energy balance equations are applied on the refrigerant and brine/air sides to determine the heat flow rate between the two streams. The Toolkit heat exchanger model assumes that on the refrigerant side, the fluid has an infinite heat capacity, leading to an isothermal latent heat exchange. On the brine and air sides, the fluid is considered to experience an increase or decrease of temperature without phase change. Figure 4.9 summarizes the model proposed by ASHRAE Toolkit.

$$T_{ref,out,evap} = T_{ref,in,evap}$$
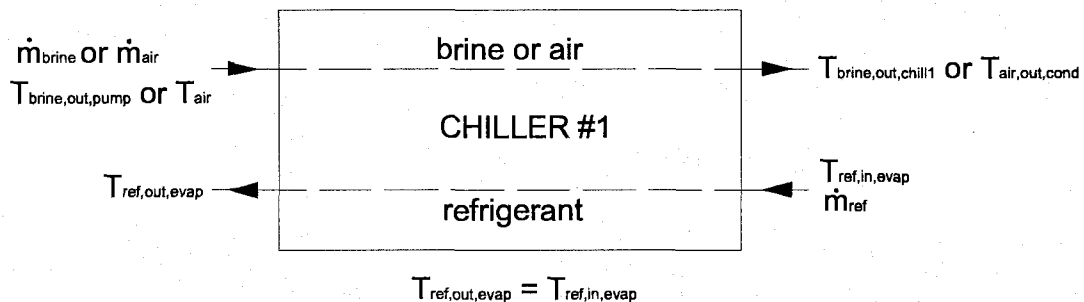
Figure 4.9: Heat exchanger model of the ASHRAE Toolkit

Based on the measured inlet and outlet refrigerant temperatures at the evaporator and condenser, the refrigerating capacity (Equation 4.22) and the heat rejected at the condenser (Equation 4.23) are determined by:

$$\dot{Q}_{evap} = AU_{evap} \cdot \Delta T_{ref,evap} \qquad\qquad (4.22)$$

$$\dot{Q}_{cond} = AU_{cond} \cdot \Delta T_{ref,cond} \qquad\qquad (4.23)$$

where $\dot{Q}_{evap}$ = heat exchanged in the evaporator (W);

$\dot{Q}_{cond}$ = heat exchanged in the condenser (W);

AU_{evap} = overall heat transfer coefficient of the evaporator (W °C^{-1});

AU_{cond} = overall heat transfer coefficient of the condenser (W °C^{-1});

$\Delta T_{ref,evap}$ = refrigerant temperature difference at the evaporator (°C);

$\Delta T_{ref,cond}$ = refrigerant temperature difference at the condenser (°C);

For the evaporator, the isothermal assumption is approximate but acceptable, since the amount of heat exchanged during the superheating of the refrigerant (sensible heat) is small compared to the latent heat exchanged during the evaporation. However, the hypothesis of an isothermal heat transfer on the refrigerant side in the condenser neglects all the effects of de-superheating and sub-cooling. Consequently, the mean temperature difference between the refrigerant and the air is underestimated by the Toolkit model at the condenser.

4.4.2 Identification of the heat exchanger parameters

The overall heat transfer coefficients (AU_{evap}, AU_{cond}) are identified as parameters characterizing the heat exchangers by using the collected data and a subroutine named PISCHIL1. Because the superheating in the evaporator and the de-superheating and sub-cooling in the condenser are neglected, the heat transfer coefficients identified with routine PISCHIL1 are only valid for latent heat exchange. These coefficients can be used if the assumption of sensible heat exchange is suitable. The information flow diagram of Figure 4.10 gives all the inputs and outputs used in this routine.
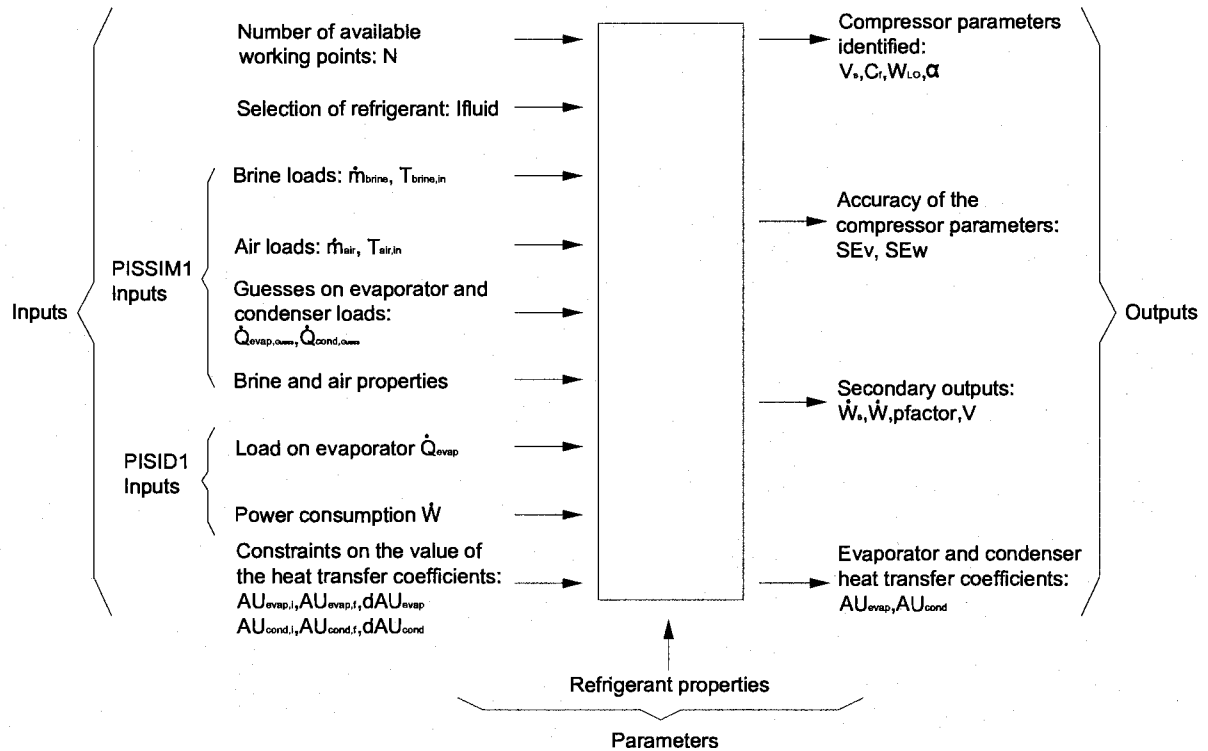
Figure 4.10: Information flow diagram of PISCHIL1 (Bourdouxhe et al. 1997)

Routine PISCHIL1 calls a subroutine named PISID1 to identify the compressor parameters. Subroutine PISID1 is similar to PISCOMP1 with the exception that the evaporator and condenser exit temperatures are equal to the evaporating and condensing temperatures. Subroutine PISID1 requires the same inputs as routine PISCOMP1, except the degrees of superheating and sub-cooling in the heat exchangers. The subroutine PISCHIL1 calls the subroutine PISSIM1 (section 4.5.1), which performs the numerical simulation of a chiller for steady state and full load regimes. This routine calculates the electric demand of the compressor, and the evaporating effect based on the parameters previously identified by PISSID1 and the heat transfer coefficient assumed during the iteration. The convergence is reached when the difference between the measured (input to the model) and calculated compressor power, as well as the difference between the measured and calculated refrigeration capacity is less than 0.0001.

82

4.4.2.1 PISCHIL1 mathematical description

Two values of heat transfer coefficients between the inferior and superior bounds provided to the routine are chosen so that the evaporator and condenser effectiveness as well as the evaporating and condensing temperatures can be calculated for each operating point by means of routine PISSIM1. More details regarding routine PISSIM1 are given in section 4.5.1. The evaporating and condensing temperatures determined in routine PISSIM1 are then used by the subroutine PISID1 to identify the four compressor parameters. The mathematical model of the PISID1 is exactly similar to the mathematical model previously described for PISCOMP1, except that the superheating and sub-cooling levels are equal to zero. Therefore, the identified parameters from PISID1 differ from those obtained from PISCOMP1. Based on the identified compressor parameters, the compressor power and the refrigerating capacity are calculated for each working point by means of subroutine PISSIM1. Then, the calculated electric input is compared with the actual ones. This is achieved by establishing the value of the function F (Equation 4.24):

$$F = \sum_{i=1}^{N} \left[\left(\frac{\dot{W}_i - \tilde{\dot{W}}_i}{\dot{W}_i} \right)^2 + \left(\frac{\dot{Q}_{evap,i} - \tilde{\dot{Q}}_{evap,i_i}}{\dot{Q}_{evap,i}} \right)^2 \right] \qquad (4.24)$$

where: $\dot{W}_i$ and $\tilde{\dot{W}}_i$ are the actual and calculated values of the compressor electric input, respectively (W);

$\dot{Q}_{evap,i}$ and $\tilde{\dot{Q}}_{evap,i_i}$ are the actual and calculated values of the refrigeration capacity, respectively (W).

During each iteration, the calculated value of F is compared against the minimal value stored during the previous iterations. When F reaches a minimal value, the heat transfer coefficients corresponding to the values of $\tilde{\dot{W}}_i$ and $\tilde{\dot{Q}}_{evap,i_i}$ are stored in memory.

4.4.2.2 Algorithm and flowchart of PISCHIL1

The different steps of routine PISCHIL1 are summarized in the algorithm described below (Bourdouxhe et al. 1997).

i- Begin loop

    1- Initial guess of two heat transfer coefficients ($AU_{evap,\text{inf}}$, $AU_{cond,\text{inf}}$);

ii- For each working point:

    2- Calculate the evaporator and condenser effectiveness (subroutine PISSIM1);

    3- Calculate the evaporating and condensing temperatures (subroutine PISSIM1);

    4- Identify the four compressor parameters (subroutine PISID1);

    5- Calculate the estimated values of the refrigeration capacity and electric input to the compressor (subroutine PSSIM1);

    6- Calculate the value of F (Equation 4.24);

    7- IF F is lower than the smallest value found so far, THEN store the value of the parameters associated with the two heat transfer coefficients considered. IF not, then go to point 1 and increment AU_{evap} and AU_{cond} of dAU_{evap}, dAU_{cond} respectively.

iii- End loop

iv- Final calculations

    Calculate the dimensionless standard deviations (subroutine ERROR) for the compressor coefficients

To clarify the procedure used by routine PISCHIL1, the flowchart is presented in Figure 4.11. The flowchart refers to subroutine PISSIM1, which is presented in section 4.5.1.

Figure 4.11: Identification procedure of routine PISCHIL1 for the heat exchangers (Bourdouxhe et al. 1997)

4.4.2.3 Application of PISCHIL1

The identification of the heat exchanger parameters by means of subroutine PISCHILL1 is not a simple task due to the complex iterative procedures. Several tests have been conducted with routine PISCHIL1 and convergence was never reached with data measured at the Camillien-Houde ice rink. In order to understand the convergence problem, the source codes of the three routines involved in the identification process (PISCHIL1, PISSIM1 and PISID1) have been analyzed. It has been noticed that the convergence problem was related to an infinite loop involving the value of the function F. In fact, as the number of iterations increase, the value of F tends to decrease, providing a minimum value during each iteration. Therefore, the convergence condition was never reached. As previously experienced with routine PISCOMP1, convergence is hard to reach if the input file is based on the operating conditions prevailing at Camillien-Houde ice rink. The convergence problem lies in the fact that the actual monitored conditions cover a reduced range of values. Iterative routines are unable to converge if the working points provided in the input file are approximately constant. Consequently, each working point provided to the routine must represent a different operating condition of the refrigeration system for the algorithm to converge.

An input file representing a wide range of operating conditions could be created by using the manufacturer's software. However, this approach was not used because routine PISCHIL1 does not consider the sensible heat exchange occurring in the evaporator and condenser. Thus, even by using appropriate input data, the heat transfer coefficients determined by means of PISCHIL1 would be only valid for heat exchangers

operating with latent heat exchanges. Since, the Toolkit procedure for the identification of heat exchangers parameters is not sufficiently accurate for this study it has not been used further.

Because the refrigerant, brine and air temperatures have been measured at the inlet and outlet of the heat exchangers, the identification of parameters can be achieved using an approach based on the logarithmic mean temperature difference. Therefore, based on this method, coefficients for the latent and sensible heat transfers can be determined separately. This procedure is more accurate and representative of the actual operating conditions than the identification routine PISCHIL1 provided by the Toolkit. The new identification procedure for heat exchangers is developed in Chapter 5. The coefficients that will be identified in Chapter 5 will be used along with the compressor coefficients determined with routine PISCOMP1 in the Toolkit simulation routine PISSIM1. This routine is presented in the next section.

4.5 Simulation of the refrigeration cycle

In this section, the equations used by the Toolkit for the simulation of reciprocating chillers are presented. Before this, it is interesting to analyze the actual vapour-compression refrigeration cycle in a temperature entropy (T-S) diagram as illustrated in Figure 4.12. The dashed lines stand for constant pressure lines (isobars).

Temperature

Sub-cooled region

Super-heated region

P = constant

P = constant

h = constant

P = constant

P = constant

Liquid-vapor region

Entropy
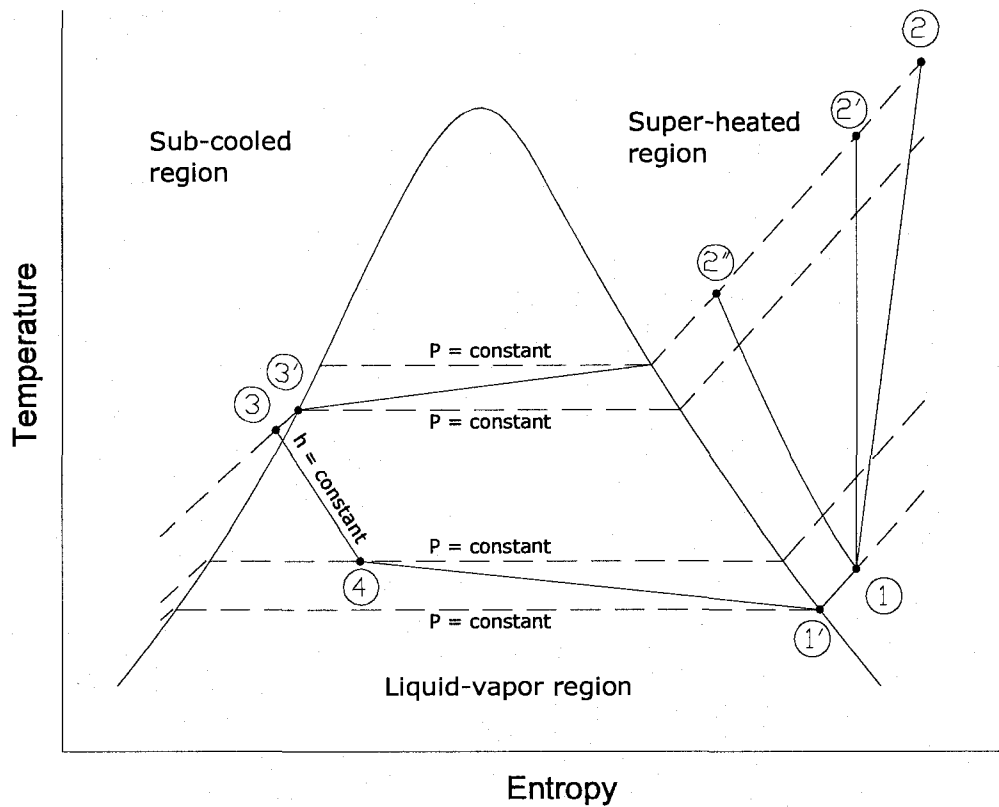
Figure 4.12: T-S diagram of the simulated refrigeration cycle

Starting the cycle from point 1, the superheated refrigerant is compressed to the actual point 2. The process from point 1 to point 2 is an irreversible compression process, and the entropy increases from state 1 to state 2. The compression process from point 1 to 2" may be even more desirable than the isentropic process from point 1 to 2'. In fact, process 1 to 2" requires less work than both the actual and the ideal compression processes. Therefore, when it is possible, the refrigerant should be cooled during compression to diminish the work input. Furthermore, compared to the actual condensing process (2-3), process 2" to 3 requires less condensing capacity which results in a smaller condenser, which might use less electricity. When passing through the condenser, the pressure drops due to the energy dissipation caused by the friction between the refrigerant and the heat exchanger. Since the pressure is not constant, the refrigerant experiences a

diminution of temperature while the pressure decreases. At the exit of the condenser, the refrigerant is sub-cooled, thus moving from point 3' to 3. At the exit of the condenser, the compressed liquid refrigerant is expanded through the expansion valve in order to reduce its temperature. The expansion valve is considered to be adiabatic, which indicates that the enthalpy is constant during the expansion. The irreversibility of the process is illustrated by the path between point 3 to point 4. From point 4 to point 1, the refrigerant is evaporated while passing through the evaporator. The refrigerant experiences a pressure drop due to the friction between the refrigerant and the heat exchanger. Thus, the temperature at the exit of the evaporator (point 1') is lower than the temperature at the inlet of the evaporator (point 4). To ensure that the refrigerant is completely evaporated, the refrigerant is superheated from point 1' (saturated vapour) to point 1 (superheated vapour).

Mandatory conditions have to be respected while designing a refrigeration system. On one side, the refrigerant that flows in the compressor must be empty of liquid to avoid cavitations that reduces the total life of the machine. Thus, the refrigerant has to be superheated in the evaporator. The degree of superheating is calculated in function of the heat losses occurring in the pipe separating the compressor from the evaporator. If the length of the pipe is long, condensation can occur resulting into the aspiration of liquid bubbles by the compressor. On the other hand, a higher degree of superheated vapour at the exit of the evaporator results into a higher electric demand by the compressor, leading to a smaller COP for the system (Koury, 2001). Furthermore, the transfer of sensible heat into the refrigerant requires more heat exchange area in the evaporator than the transfer of

latent heat. The degree of superheated vapour is controlled by opening or closing the expansion valve which results into a decrease or increase of the evaporator pressure, thus changing the proportions of latent and sensible heat transferred.

The second mandatory condition that needs to be respected is to have sub-cooled liquid at the exit of the condenser (point 3 in Figure 4.12). On one side, the expansion valve cannot deal with vapour, since expanding vapour is in practice difficult. On the other side, a higher degree of sub-cooled refrigerant allows to increase the temperature drop while the refrigerant passes through the expansion valve. Consequently, a higher degree of sub-cooled refrigerant increases the potential of heat absorption in the evaporator.

4.5.1 Modified PISSIM1 mathematical description

For the simulation of the whole refrigeration system, the Toolkit provides the routine PISSIM1. However, modifications were brought to the routine in order to adapt the simulation to the specific operating conditions of the Camillien-Houde ice rink. The original routine PISSIM1 has been modified to use the identified parameters as inputs. The compressors parameters have been identified in section 4.3.2. The heat exchangers parameters will be identified in Chapter 5 using the logarithmic mean temperature difference technique. Moreover, the refrigerating capacity of the compressors is known, since it has been calculated in Chapter 3 based on the heat balance on the refrigerant side (section 3.4.2.2). Therefore, modifications have also been brought to consider the evaporating load as an input value. Finally, the original routine has been adapted to

consider the measured refrigerant mass flow rate as an input to the model. These modifications led to a simplified routine PISSIM1 requiring less calculation time. The modified routine PISSIM1 calculates the temperatures of the brine and air at the heat exchangers exit as well as the electric demand of the compressor. The flowchart of the modified routine PISSIM1 is presented in Figure 4.13.
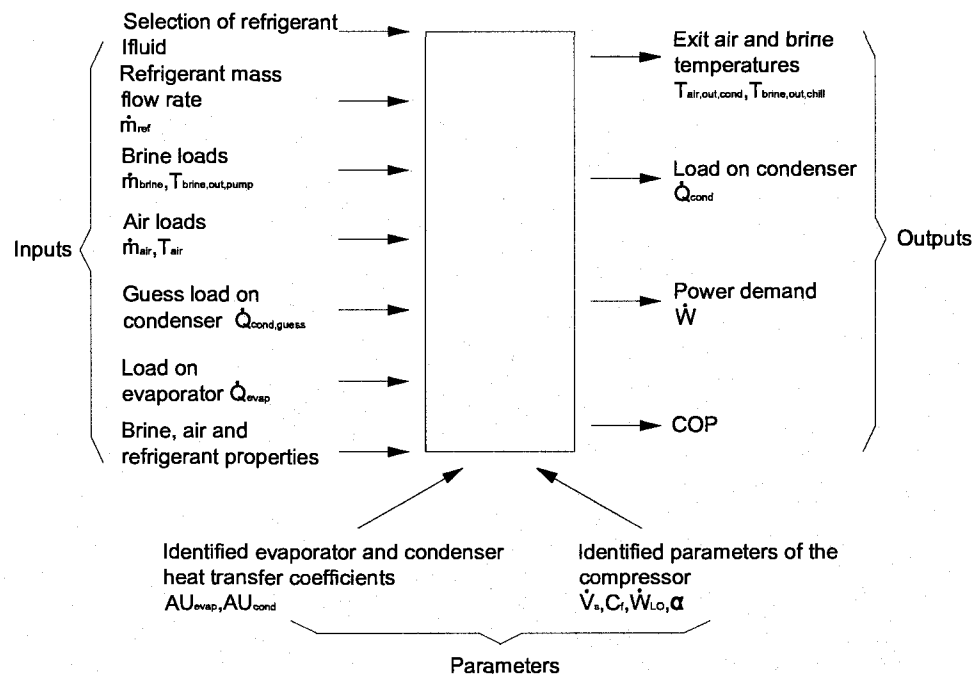
Figure 4.13: Information flowchart for the modified PISSIM1

4.5.1.1 Simulation of compressors

The simulation of the compressor is performed by using the parameters provided by the routine PISCOMP1 along with the saturation temperatures (Equations 4.37 Equation 4.38). The compressor simulation is based on an iterative process in order to determine the refrigerant temperature after the heating-up due to the electromechanical losses (Point 1', Figure 4.2). The evaporation and condensing pressures are determined by means of the Clausius-Clayperon equation (see Equation 4.4). The volumetric

effectiveness of the compressor is defined by rearranging the volume flow equation (Equation 4.8), reintroducing the definition of pfactor along with the identified parameter C_f:

$$\varepsilon_{vol} = \frac{\dot{V}}{\dot{V}_s} = 1 + C_f - C_f \cdot \left(\frac{P_2}{P_1}\right)^{1/\gamma}$$

(4.25)

The volumetric effectiveness can be used to determine the refrigerant mass flow rate:

$$\dot{m}_{ref} = \frac{\varepsilon_{vol} \cdot \dot{V}_s}{v_{1'}}$$

(4.26)

where $v_{1'} = \dfrac{\varsigma \cdot r \cdot T_{1''}}{P_1}$ is the volumetric flow and $T_{1''}$ is the guessed temperature after the heating up. For the first iteration, $T_{1''}$ is set equal to the saturation temperature determined by Equation 4.37. However, in this study the refrigerant mass flow rate measured on site is input to the model. Thereafter, the isentropic compression power is calculated as:

$$\dot{W}_s = \dot{m}_{ref} \cdot \frac{\gamma}{\gamma - 1} \cdot \varsigma \cdot r \cdot T_{1''} \cdot \left(\left(\frac{P_2}{P_1}\right)^{\frac{\gamma-1}{\gamma}} - 1\right)$$

(4.27)

Equation 4.27 is used along with the parameter $\dot{W}_{lo}$ in order to determine the actual electric input to the compressor:

$$\dot{W} = \dot{W}_{lo} + \alpha \dot{W}_s + \dot{W}_s$$

(4.28)

The temperature after the heating-up is then recalculated by applying the energy balance between the inlet and the outlet of the compressor:

$$T_{1'} = T_1 + \frac{\dot{W}_{lo} + \alpha \cdot \dot{W}_s}{\overline{c}_p \cdot \dot{m}_{ref}} \qquad (4.29)$$

The simulation converges when the relative error between the temperature after the heating up calculated in Equation 4.28 and the temperature after the heating up guessed is less than 10^{-5}:

$$Error = \frac{(T_{1'} - T_{1''})}{T_{1''}} \leq 10^{-5} \qquad (4.30)$$

4.5.1.2 Simulation of heat exchangers

The simulation of heat exchangers proposed by PISSIM1 is based on a combination of the effectiveness-number of transfer units method (ε-NTU) along with the corresponding parameter AUs that will be identified in Chapter 5. The ε-NTU method is based on a dimensionless parameter called the heat transfer effectiveness ε, defined as (Holman, 1997):

$$\varepsilon = \frac{\dot{Q}_{evap}}{\dot{Q}_{evap,\max}} \qquad (4.31)$$

where $\dot{Q}_{evap}$ represents the actual heat transfer rate while $\dot{Q}_{evap,\max}$ represents the maximum possible heat transfer rate. The actual heat transfer is obtained by calculating either the energy released by the hot fluid or absorbed by the cold fluid. To determine the maximum heat transfer rate in a heat exchanger, the maximum temperature difference must be used. The maximum temperature difference corresponds to the difference between the inlet temperatures of the cold and hot fluids, thus:

$$\Delta T_{\max} = T_{hot,in} - T_{cold,in} \tag{4.32}$$

The fluid that might undergo the maximum temperature difference is the fluid that has the smaller heat capacity rate. The heat capacity rate is defined as followed (Holman, 1997):

$$C_{cold} = c_{p,cold} \cdot \dot{m}_{cold} \text{ and } C_{hot} = c_{p,hot} \cdot \dot{m}_{hot} \tag{4.33}$$

When a fluid experiences a latent heat exchange (evaporation or condensation at a constant temperature) the value of the heat capacity tends to infinity. Hence, during latent heat exchange, the following ε-NTU expression is used by Bourdouxhe et al. (1997):

$$\varepsilon = 1 - \exp(-NTU) \tag{4.34}$$

where $NTU = \dfrac{AU}{C_{min}}$. Equation 4.33 is only valid for vaporization and condensation. Therefore, the coefficient AU used in the NTU expression must correspond to the latent heat transfer of the evaporator and condenser. This is considered during the identification of the heat exchangers. By rearranging Equation 4.33, the evaporator and condenser effectiveness can be written as (Bourdouxhe et al. 1997):

$$\varepsilon_{evap} = 1 - \exp\left(\frac{AU_{evap,lat}}{C_{p,brine} \cdot \dot{m}_{brine}} \right) \tag{4.35}$$

$$\varepsilon_{cond} = 1 - \exp\left(\frac{AU_{cond,lat}}{C_{p,air} \cdot \dot{m}_{air}} \right) \tag{4.36}$$

From Equation 4.30, the following formulation is obtained:

$$\dot{Q}_{evap} = \varepsilon \cdot \dot{Q}_{evap,max} = \varepsilon \cdot C_{min} \cdot (T_{h1} - T_{c1}) \qquad (4.37)$$

where C_{min} is either equal to $c_{p_{brine}} \cdot \dot{m}_{brine}$ for the evaporator or $c_{p_{air}} \cdot \dot{m}_{air}$ for the condenser. Thus, the evaporating and condensing temperatures can be determined by rearranging Equation 4.36:

$$SST = T_{brine,out,pump} - \frac{\dot{Q}_{evap}}{\varepsilon_{evap} \cdot c_{p,brine} \cdot \dot{m}_{brine}} \qquad (4.38)$$

$$SDT = T_{air} + \frac{\dot{Q}_{cond}}{\varepsilon_{cond} \cdot c_{p,air} \cdot \dot{m}_{air}} \qquad (4.39)$$

This procedure allows obtaining the evaporating and condensing temperatures by means of the inlet brine and air temperatures and by determining the actual heat transfer in the heat exchangers. Once the condensing load and the refrigerant mass flow are determined, the brine and air temperatures at the exit of the heat exchangers are determined:

$$T_{brine,out,chill1} = T_{brine,in,out,pump} - \frac{\dot{Q}_{evap}}{c_{p,brine} \cdot \dot{m}_{brine}} \qquad (4.40)$$

$$T_{air,out,cond} = T_{brine,in} + \frac{\dot{Q}_{cond}}{c_{p,air} \cdot \dot{m}_{air}} \qquad (4.41)$$

Written in this form, Equations 4.37 and 4.39 are for chiller #1, however they are also valid for chiller #2 if the related brine temperature at the evaporator inlet is used.

4.5.1.3 Algorithm and flowchart of PISSIM1

The modified routine PISSIM1 consists of two imbricated loops. The first loop applies to the heat rejected by the condenser, and the second loop applies to the refrigerant temperature after the heating-up. The following operations are performed:

i-   For each working point:

Select of the refrigerant (subroutine PROPERTY);

Calculate the evaporator and condenser effectiveness;

Calculate the evaporating temperature and pressure as well as the enthalpy at the evaporator exhaust from the evaporating capacity;

ii-   Begin first loop – Calculation of the heat rejected in the condenser

A - Calculate the condensing temperature and pressure as well as the enthalpy at the condenser exhaust;
B - Calculate the volumetric effectiveness of the compressor;

iii-   Begin second loop – Calculation of the temperature after heating-up

1 - Calculate the refrigerant mass flow rate and the isentropic compression power;

2 - Calculate a new temperature after heating-up;

3 - IF converged THEN leave second loop. IF not, then go to point 1 and use the new temperature after heating-up calculated at point 2.

iv-   End second loop

C - Calculate the power consumed by the compressor

D - Calculate a new heat rejected in the condenser

E - IF converged THEN leave first loop. IF not, then go to point A and use the recalculated temperature after the heating-up

v-   End first loop

vi-   Final calculations

-Calculate the other outputs

The corresponding flow chart is presented in Figure 4.14.

Start

INPUTS AND PARAMETERS
Refrigerant mass flow rate $\dot{m}_{ref}$
Brine mass flow rate $\dot{m}_{brine}$
Brine inlet temperature $T_{brine,in,chill}$
Air mass flow rate $\dot{m}_{air}$
Air inlet temperature T_{air}
Evaporator load $\dot{Q}_{evap}$
Condenser guess load $\dot{Q}_{cond,guess}$
Evaporator heat transfer coefficient AU_{evap}
Condenser heat transfer coefficient AU_{cond}
Compressor parameter V_s, C_f, W_{lo}, α

Subroutine PROPERTY
T_0, h_{fo}, h_{fgo}, $\overline{C}_f$, $\overline{C}_p$, r, zeta, gamma, Acl, Bcl
Equation 4.4 ⟶ P_{evap}, P_{cond}
Equation 4.37 ⟶ T_{evap}
Equation 4.38 ⟶ T_{cond}
Equation 4.3 ⟶ h_1
Equation 4.2 ⟶ h_3
Equation 4.25 ⟶ ε_{vol}

Guess of $T_{1'}$

Equation 4.27 ⟶ W_a
Equation 4.28 ⟶ $T_{1'}$

Convergence
NO
YES

Equation 4.5 ⟶ $\dot{W}$
$\dot{Q}_{evap} + \dot{W}$ ⟶ $\dot{Q}_{cond}$

Convergence
NO
YES

OUTPUTS
Equation 4.39 ⟶ $T_{brine,out,chill}$
Equation 4.40 ⟶ $T_{air,out,cond}$
Equation 4.5 ⟶ $\dot{W}$

End

Figure 4.14: Simulation of the refrigeration system with the modified routine PISSIM1 flowchart (adapted and modified from Bourdouxhe et al. 1997)

4.6 Conclusions

The models developed by the Toolkit are for steady state operating conditions; hence they are not valid immediately after compressor's start-up. The routine PISCOMP1 was used for the compressor identification along with 21 working points corresponding to the actual compressor created with compressor software Carwin. The parameters identified from the new input file have been validated by using Carwin, and a good agreement was observed between the results. For the identification of the heat exchangers parameters, the Toolkit proposes the routine PISCHIL1. This iterative routine allows to determine the overall heat transfer coefficient by neglecting the sensible heat exchanges. This approximation is very crude for the current application. Therefore, based on the monitored temperatures, a modified approach will be used where the heat exchangers parameters will be identified by using the logarithmic mean temperature difference. This procedure will be developed in Chapter 5 by using the software EES. The simulation of the refrigeration system is described by the routine PISSIM1. Important modifications have been brought to routine PISSIM1 in order to consider the latent and sensible heat exchanges. Moreover, because the parameters are identified prior to the simulation, the routine has also been modified to use the compressor and heat exchangers as inputs instead of calculating them. A loop corresponding to the calculation of the evaporator load has also been modified to consider the refrigerating load calculated in Chapter 3 as an input to the model. The modified routine PISSIM1 will be programmed in C++ and incorporated as an external DLL into TRNSYS for the simulation of the refrigeration system in Chapter 7.

CHAPTER 5

DEVELOPMENT OF THE REFRIGERATION MODEL USING THE ENGINEERING EQUATION SOLVER

As presented in chapter 4, the sensible heat transfer in the evaporator and air-cooled condenser is neglected by the Toolkit for the identification of the overall heat transfer coefficients of those heat exchangers. The logarithmic mean temperature difference method is used in this chapter to evaluate the overall heat transfer coefficients depending on the type of heat exchange occurring in the exchanger (e.g., sensible or latent). The overall heat transfer coefficients are calculated from temperature measurements of both fluids flowing through the heat exchanger. The measurements cover several days of operation of different months, and finally an average value of the overall heat transfer coefficients are used further in simulation. This chapter covers the development of the model, which is based on the measurements collected at the monitored ice rink. At the exit of each component of the chiller, the properties of the refrigerant are determined by using thermodynamic equations.

5.1 Objectives of the refrigeration model

The model is developed with two main objectives: to identify the parameters of the heat exchangers, and to have a reference model for comparison purposes during simulations in TRNSYS by providing the temperature of the refrigerant at the exit of each component. The model uses thermodynamic equations and empirical relations to describe the behaviour of the refrigeration system.

5.2 Development of the refrigeration model

The model is developed using the Engineering Equation Solver (EES) (Klein and Alvarado 1999). This is a non-linear equation solver presenting the capability to calculate thermodynamic properties of commonly found substances such as air, water and several refrigerants. The EES environment allows to model thermodynamics processes such as refrigeration cycles.

5.2.1 Model assumptions

The model assumes that the temperature and pressure at the condenser exit are equal to the measured temperature and pressure at the expansion valve inlet. The heat losses and pressure drop in the pipe between the condenser outlet and the expansion valve are neglected. At the evaporator inlet, the conditions are assumed to be equal to those at the expansion valve exit. This assumption is realistic since the expansion valve is directly connected to the evaporator. It is also assumed that the chiller operates steadily.

5.2.2 Mathematical model

Among all measurements available from the Camillien-Houle ice rink (see section 3.3), the following data are used by the EES model:

- Refrigerant temperature at the inlet of the expansion valve ($T_{ref,in,\exp.valve}$);
- Refrigerant temperature at the exit of the evaporator ($T_{ref,out,evap}$);
- Refrigerant mass flow ($\dot{m}_{ref}$);
- Compressor suction pressure (P_1);
- Compressor discharge pressure (P_2);

- Brine temperature at the inlet of the pump ($T_{brine,in,pump}$);
- Brine temperature at the exit of the pump ($T_{brine,out,pump}$);
- Brine temperature at the exit of chiller #1 ($T_{brine,out,chill1}$);
- Brine temperature at the exit of chiller #2 ($T_{brine,out,chill2}$);
- Brine mass flow ($\dot{m}_{brine.}$);
- Exterior air temperature (T_{air}).

Based on the monitored data, the proposed model calculates the refrigerant properties at the inlet and outlet of each component (evaporator, compressor, condenser and expansion valve).

5.5.2.1 Evaporator

The saturation suction temperature (SST), which is also the evaporation temperature, is directly evaluated from the pressure measured at the inlet of the compressor because the pressure is considered constant during evaporation. Hence, for a saturation suction pressure P_1 = 263.4 kPa (Ouzzane et al. 2006), the corresponding saturation temperature is of -18.14°C on March 16th, 2006. Although the refrigerant temperature is reduced as the refrigerant passes through the tubes of the evaporator due to pressure drop (see Figure 4.12), the SST is considered to be constant. At the end of the evaporation of the saturated mixture, the refrigerant is superheated. Based on measured data, the average refrigerant temperature at the exit of the evaporator is -12.32°C for March 16th, 2006. The average degree of superheating for the same day (Equation 5.1) is of 5.8°C. A rounded value of 6°C is used as an average value for several days.

$$\Delta T_{sup\,heat} = T_{ref,out,evap} - SST \tag{5.1}$$

5.5.2.2 Compressor

Due to the pipe length separating the evaporator and compressor, some heat gain from surroundings takes place. The corresponding increase of temperature was evaluated by CANMET at about 3°C. Hence, the temperature at the compressor inlet (point 1 in Figure 4.12) is calculated as:

$$T_{ref,in,comp} \equiv T_1 = T_{ref,out,evap} + 3 \qquad (5.2)$$

The average compressor inlet temperature is of $T_{ref,in,comp}$ = -9.32°C on March 16th 2006. Therefore, the average enthalpy and entropy at the compressor inlet are determined based on the estimated temperature and measured pressure (h_1 = 403.0 kJ/kg and s_1 = 1.79 kJ/kgK). Because the compressor operates practically with constant suction and discharge pressures, the compression ratio is assumed to be constant. From the suction and discharge pressures measured on the monitored refrigeration system (Ouzzane et al. 2006), the mean compression ratio is evaluated as r = 5.8808.

The isentropic work of the compressor is determined by assuming that the entropy during the compression process is constant (process 1-2' in Figure 4.12):

$$\dot{W}_s = \dot{m}_{ref} \cdot (h_{2'} - h_1) \qquad (5.3)$$

By using the measured discharge pressure P_2 = 1549 kPa (Ouzzane et al. 2006), the temperature and the enthalpy at the exit of the isentropic compression are determined ($h_{2'}$ = 449.9 kJ/kg and $T_{2'}$ = 77.64°C). The mean isentropic work for March 16th, 2006 is evaluated at 15.68 kW. In order to determine the actual work done by the compressor, an empirical relation published by the Air-Conditioning and Refrigerating Institute (ARI

2004) is used. This third degree polynomial relation relates the brake-horse power (BHP) of the compressor with the saturation suction and discharge temperatures (SST and SDT):

$$BHP = P_1 + P_2 \cdot SST + P_3 \cdot SST + P_4 \cdot (SST^2) + P_5 \cdot SST \cdot SDT +$$
$$P_6 \cdot SDT^2 + P_7 \cdot SST^3 + P_8 \cdot SDT \cdot SST^2 + P_9 \cdot SST \cdot SDT^2 + P_{10} \cdot SDT^3 \qquad (5.4)$$

The coefficients used in Equation 5.4 are determined from the manufacturer catalogue for the 5H40 reciprocating compressor used in the ice-skating rink (Carrier Corporation 2001). The actual mean compressor power input is evaluated at 20.6 kW.

The isentropic efficiency allows to evaluate how far an irreversible mechanical system is from the equivalent reversible system. It is defined as the ratio between the ideal required work and the actual required work (Equation 5.5). The mean isentropic efficiency calculated for compressor #2 of chiller #1 is of $\eta_s = 0.77$.

$$\eta_s = \frac{\dot{W}_s}{\dot{W}} \qquad (5.5)$$

Two approaches can be used to determine the temperature at the exit of the compressor. The first method consists of using Equation 5.4 to determine the power input to the compressor and then determining the outlet enthalpy (h_2) by applying the energy balance of the compressor; it is assumed that the whole work input is transferred to the refrigerant. This method is not accurate since the empirical relation 5.4 gives the actual electric demand of the compressor, but does not allow determining the energy transferred directly to the refrigerant. The second approach consists of employing an empirical equation provided by the manufacturer, which relates the discharge temperature (T_2 in ° C), with the suction temperature T_1 (°C) (Carrier Corporation 2001):

$$T_2 = \left[(T_1 + 273.33) \cdot C\right] - 273.33 \tag{5.6}$$

Because Equation 5.6 was developed by the manufacturer, the discharge temperature calculated with this method is more accurate than the result obtained from the combination of the energy balance and the empirical relation 5.4. Constant C is calculated by combining the compression ratio with the compression exponent of refrigerant gas (Carrier Corporation 2001):

$$C = \left(\frac{P_2}{P_1}\right)^{\frac{N-1}{N}} \tag{5.7}$$

For instance, for a compressor operating with refrigerant R-22 and without water-cooled heads, the compression exponent N is equal to 1.23224, leading to a constant $C = 1.395232$ (Carrier Corporation 2001). Therefore, by using Equation 5.6, the average discharge temperature of the compressor T_2 is evaluated at 93.63°C.

5.5.2.3 Condenser

At the exit of the compressor, the superheated refrigerant is condensed by passing through the condenser. The saturation pressure of condensation (P_2) was measured by Ouzzane et al. (2006) as 1549 kPa. The saturation discharge temperature (SDT) is directly evaluated from the pressure as 40.4°C. If pressure drop is neglected, the SDT can be considered as the condensing temperature during latent heat exchange. The temperature at the condenser exit is assumed to be equal to the measured temperature at the inlet of the expansion valve (Point 3 in Figure 4.12). For March 16th 2006, the average temperature is of 28.17°C. From the difference between the condensing

temperature and the temperature at the exit of the condenser, the degree of sub-cooling is evaluated to be of 12.23°C, rounded to 12.5°C.

5.5.2.4 Expansion valve

Because of the pressure drop that occurs when the refrigerant flows through the evaporator, the refrigerant temperature at the exit of the expansion valve is not exactly equal to the SST. Based on discussions with experts from CANMET-Varennes, they recommended to adjust this temperature to better fit the actual conditions at Camillien-Houde. The refrigerant temperature at the exit of the expansion valve is evaluated to be equal to the SST plus one degree (Equation 5.8). From the measured SST, the mean temperature at the exit of the expansion valve is estimated at -17.14°C on March 16th, 2006.

$$T_{ref,out,exp.valve} = SST + 1 \qquad (5.8)$$

5.5.2.5 Calculation of thermal loads of heat exchangers

The evaporation and condensing thermal loads are computed from the refrigerant enthalpy difference between the inlet and outlet of each heat exchanger. In order to identify the parameters of heat exchangers, the load is divided into latent load and sensible load. For instance, the latent evaporation load is of 54.6 kW and the sensible load of 1.3 kW leading to a total evaporation load of 55.9 kW. For the condenser, the mean de-superheating load is 15.7 kW, while the latent load is 55.3 kW and the sub-cooling load is 5.7 kW. The total average condensing load is 76.7 kW.

The coherence of the model is evaluated by applying the first law of thermodynamics on the chiller. The heat rejected by the condenser as calculated above (76.7 kW) is almost equal to the sum of the heat absorbed by the evaporator (55.9 kW) and the energy supplied to the compressor (20.6 kW). The small difference between these two values (76.7 kW vs. 76.5 kW) can be caused by an over-estimation of the sub-cooling at the condenser; the temperature at the condenser exit is not exactly equal to the temperature at the inlet of expansion valve.

5.2.3 Verification of the EES model

The results from the EES model are compared with the simulation performed with the Carwin software made by Carlyle (Carlyle 2007). The average values measured on the chiller along with the compressor characteristics are used in the Carwin software to simulate the chiller. A short presentation of input and output from Carwin software is given below. Table 5.1 presents the input values used to simulate the chiller with the manufacturer's software.

Table 5.1: Input values used in Carwin software

Inputs	Values
Compressor model	5H40
Refrigerant	R22
Voltage	460 Volts
Shaft speed	1750 RPM
Saturated suction temperature (SST)	-18.1°C
Saturated discharge temperature (SDT)	40.4°C
Temperature leaving the condenser	28.1°C
Temperature entering expansion valve	28.1°C
Superheat level	6.0°C
Return gas temperature (RGT)	-9.3°C

The Carwin software calculates the power input to the compressor, the compressor capacity, the refrigeration effect, the heat rejected at the condenser, the temperature of the refrigerant at the compressor exit, the refrigerant mass flow rate, and the COP of the chiller.

The compressor capacity, a terminology frequently used by compressor manufacturers, must be carefully defined. The actual useful heat transfer occurs in the evaporator (refrigeration effect), which is almost completely unrelated to the compressor. The capacity of a refrigeration system depends on the mass flow of refrigerant and the enthalpy difference between the inlet and the exit of the evaporator. If any of the parameters that define the capacity change, the capacity of the compressor must be adjusted to account for this change. The maximum mass flow of a compressor occurs when the inlet gas is saturated vapour. Therefore, the manufacturer specifies the nominal conditions used to establish the capacity of the compressor: (i) 8.3°C of superheating in the evaporator, (ii) 0°C of sub-cooling in the condenser, and (iii) a saturated discharge temperature of 40.5°C.

A good agreement is observed between results from Carwin and EES model for March 16th, 2006 (Table 5.2).

Table 5.2: Comparison between results of EES and Carwin models

Outputs	Carwin	EES	Absolute/relative error
Evaporator refrigerating effect	56.29 kW	55.90 kW	0.39 kW (0.7%)
Compressor capacity	56.91 kW	-	-
COP	2.60	2.70	0.1 (3.8%)
Refrigerant mass flow	0.335 kg/s	0.3348 kg/s	0.0002 kg/s (0.5%)
Compressor power input	20.57 kW	20.55 kW	0.03 kW (0.1%)
Discharge temperature	97.5°C	93.6°C	3.9°C (4%)

5.3 Identification of parameters of heat exchangers

The EES model is used to identify parameters of heat exchangers by using the logarithmic mean temperature difference (*LMTD*) method. The temperature variation of fluids flowing through the evaporator and condenser, respectively, is presented in Figure 5.1. The names used to identify the intermediate temperatures are also presented.

T ├────── Latent ──────┬ Sensible ┤

In

$T_{brine,out,pump}$

Out ● Brine $T_{brine,out,sens}$

$T_{brine,out,chill1}$

Out

In ● $T_{ref,out,evap}$

SST Refrigerant SST

Length ──▶

(a)

T ├ Sensible ──┬── Latent ──┬── Sensible ──┤

In ●

$T_{ref,out,comp}$

SDT SDT

Refrigerant

$T_{ref,in,exp,valve}$

Out ● Out

$T_{air,out,cond}$ $T_{air,out,lat}$ Air In

$T_{air,out,subcool}$ T_{air}

Length ──▶

(b)
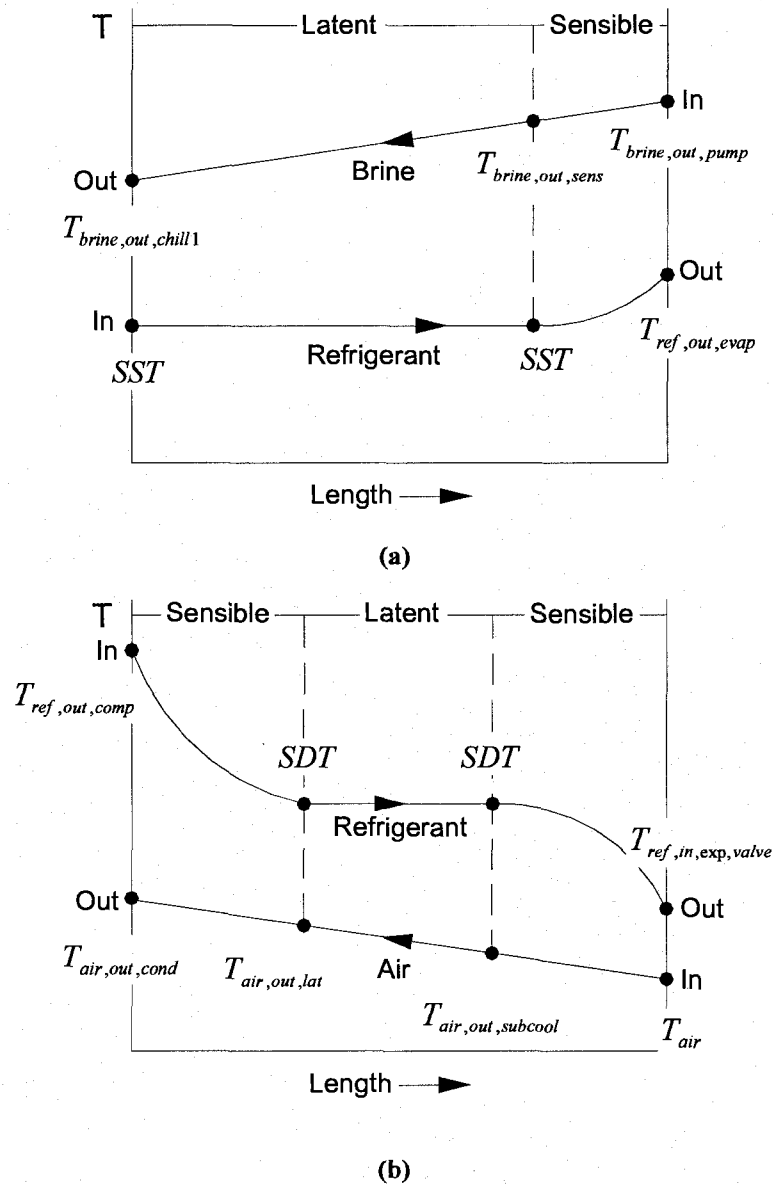
Figure 5.1: (a) Temperature variation of the refrigerant and brine in the evaporator
(b) Temperature variation of the refrigerant and air in the condenser

In the evaporator, the saturated mixture refrigerant is evaporated at constant temperature (latent heat) and at the end, slightly superheated (sensible heat). During this process, brine temperature decreases constantly (sensible heat). In the condenser, the vapour refrigerant is first de-superheated (sensible heat), then condensed (latent heat) to finally be sub-cooled (sensible heat) while the air temperature increases constantly (sensible heat).

5.3.1 Definition of the overall heat transfer coefficient

Heat exchangers are characterized by their overall heat transfer coefficient (U). By definition, the overall heat transfer coefficient is the inverse of the total thermal resistance between two mediums, for instance the refrigerant and the brine or air. This parameter considers both the convective and conductive heat transfer mechanisms. Both heat flows depend on several operating characteristics such as fluid properties, materials and design of the exchanger. Two methods can be used to determine the overall heat transfer coefficient. One choice is to use an analytical model to calculate the total thermal resistance to heat flow across the surface between the inside and outside flows. This method provides satisfactory results if proper relations are used to determine the conductive and convective coefficients. However, when dealing with two phase fluids, the calculation of the total thermal resistance is complex. Furthermore, if the heat exchanger is fouled with accumulation of deposits, an additional thermal resistance must be evaluated to take into account this effect.

The alternative is to calculate the overall heat transfer coefficient by means of an inverse approach. Based on the collected data on the monitored ice rink, the logarithmic

mean temperature difference (ΔT_m) between the hot and cold fluids over the entire length

of the heat exchanger is estimated as:

$$\Delta T_m = \frac{\Delta T_1 - \Delta T_2}{\ln(\Delta T_1 / \Delta T_2)}$$
(5.9)

where ΔT_1 and ΔT_2 are the temperature differences between the two fluids at each end

of the heat exchanger. Because the heat load on the evaporator and on the condenser is

known, the overall heat transfer coefficient can be defined by the following relation

(Holman, 1997):

$$U = \frac{\Delta T_m}{A \cdot Q}$$
(5.10)

where: A = the total heat transfer area (m^2);
$\quad\quad\quad U$ = average overall heat transfer coefficient (W m^{-2} °C^{-1})

5.3.2 Calculation of the overall heat transfer coefficient

The ASHRAE Toolkit uses parameter AU to characterize the evaporator and

condenser respectively because the area of heat exchanger is constant. The same notation

is used in this study. It is important to note that the overall heat transfer coefficient is

variable along the heat exchanger. The variation is more important when the fluid

experiences a change of phase (latent heat). For calculations, the heat exchanger is

divided into one part that experiences sensible heat transfer and another part with latent

heat transfer. Thus, two parameters AU are determined for the evaporator, and three

parameters AU are determined for the condenser. The intermediate temperatures of the

refrigerant, brine and air (Figure 5.1) must be determined in order to apply Equation 5.9.

5.3.2.1 Evaporator

For the evaporator, the coefficients AU are determined as follows:

1- Calculation of the total evaporation effect of one compressor loop by applying the heat balance on the refrigerant side:

$$\dot{Q}_{evap} = \dot{m}_{ref} \cdot (h_{ref,out,evap} - h_{ref,in,evap})$$
(5.11)

2- Calculation of the sensible evaporation load of one compressor loop provided to superheat the refrigerant:

$$\dot{Q}_{evap,sens} = \dot{m}_{ref} \cdot (h_{ref,out,evap} - h_{ref,sat,vap,evap})$$
(5.12)

3- Calculation of the latent evaporation load of one compressor loop:

$$\dot{Q}_{evap,lat} = \dot{Q}_{evap} - \dot{Q}_{evap,sens}$$
(5.13)

4- Calculation of the brine temperature after the latent heat exchange:

$$T_{brine,out,sens} = T_{brine,out,chill1} + \frac{2 \cdot \dot{Q}_{evap,lat}}{\dot{m}_{brine} \cdot c_{p,brine}}$$
(5.14)

Because the measured temperature correspond to effect of two compressors of chiller #1 (see Chapter 3), the latent load is multiplied by two in Equation 5.14.

5- Calculation of the logarithmic mean temperature difference (Equation 5.9 and Figure 5.1 (a)) for the evaporator latent load, where:

$$\Delta T_1 = T_{brine,out,sens} - SST$$

$$\Delta T_2 = T_{brine,out,chill1} - SST$$

6- Calculation of the logarithmic mean temperature difference (Equation 5.9 and Figure 5.1 (a)) for the evaporator sensible load, where:

$$\Delta T_1 = T_{brine,out,sens} - SST$$

$$\Delta T_2 = T_{brine,out,pump} - T_{ref,out,evap}$$

7- Calculation of coefficients AU_{latent} and $AU_{sensible}$ by using Equations 5.15, 5.16. The load is multiplied by two in order to account for the two compressors in operation, and thus to obtain the overall heat transfer coefficient corresponding to one compressor:

$$AU_{evap,lat} = \frac{2 \cdot Q_{lat}}{\Delta T_{m,evap,lat}} \qquad (5.15)$$

$$AU_{evap,sens} = \frac{2 \cdot Q_{sens}}{\Delta T_{m,evap,sens}} \qquad (5.16)$$

5.3.2.2 Condenser

The mass air flow passing through the air-cooled condenser was not measured at the ice rink. The number of condenser fans in operation is variable depending on the condenser load and outdoor conditions. Therefore, based on the manufacturer's catalogue, an average constant air flow rate of 8.2 kg/s is used in the simulations. The coefficients AU_{cond} are estimated as follow:

1- Calculation of the condensing latent load of one compressor loop by using the saturated refrigerant enthalpy difference:

$$\dot{Q}_{cond,lat} = \dot{m}_{ref} \cdot (h_{ref,sat,vap,cond} - h_{ref,sat,liq,cond}) \qquad (5.17)$$

2- Calculation of the sensible load corresponding to the de-superheating load of one compressor loop:

$$\dot{Q}_{cond,sens-de\,sup\,heat} = \dot{m}_{ref} \cdot (h_{ref,out,comp} - h_{ref,sat,vap,cond})$$ (5.18)

3- Calculation of the sensible load corresponding to the sub-cooling load of one compressor loop:

$$\dot{Q}_{cond,sens-subcool} = \dot{m}_{ref} \cdot (h_{ref,sat,liq,cond} - h_{ref,in,exp.valve})$$ (5.19)

4- Calculation of the air temperature after the de-superheating process:

$$T_{air,out,subcool} = T_{air} + \frac{2 \cdot \dot{Q}_{cond,sens-subcool}}{\dot{m}_{air} \cdot c_{p,air}}$$ (5.20)

5- Calculation of the air temperature after the latent heat exchange

$$T_{air,out,lat} = T_{air,out,subcool} + \frac{2 \cdot \dot{Q}_{cond,lat}}{\dot{m}_{air} \cdot c_{p,air}}$$ (5.21)

6- Calculation of the air temperature at the exit of the condenser:

$$T_{air,out,cond} = T_{air,out,lat} + \frac{2 \cdot \dot{Q}_{cond,sens-de\,sup\,heat}}{\dot{m}_{air} \cdot c_{p,air}}$$ (5.22)

8- Calculation of the logarithmic mean temperature difference (Equation 5.9 and Figure 5.1 (b)) for the de-superheating load, where:

$$\Delta T_1 = SDT - T_{air,out,lat}$$

$$\Delta T_2 = T_{ref,out,comp} - T_{air,out,cond}$$

9- Calculation of the logarithmic mean temperature difference (Equation 5.9 and Figure 5.1 (b)) for the latent load, where:

$$\Delta T_1 = SDT - T_{air,out,lat}$$

$$\Delta T_2 = SDT - T_{air,out,subcool}$$

10- Calculation of the logarithmic mean temperature difference (Equation 5.9 and Figure 5.1 (b)) for the sub-cooling load, where:

$$\Delta T_1 = SDT - T_{air,out,subcool}$$

$$\Delta T_2 = T_{ref,in,exp,valve} - T_{air}$$

11- Calculation of coefficients AU_{latent} and $AU_{sensibles}$ by using Equations 5.23, 5.24, 5.25.

$$AU_{cond,lat} = \frac{2 \cdot Q_{cond,lat}}{\Delta T_{m,cond,lat}} \tag{5.23}$$

$$AU_{cond,sens-de\,sup\,heat} = \frac{2 \cdot Q_{cond,sens-de\,sup\,heat}}{\Delta T_{m,sens-de\,sup\,heat}} \tag{5.24}$$

$$AU_{cond,sens-subcool} = \frac{2 \cdot Q_{cond,sens-subcool}}{\Delta T_{m,sens-subcool}} \tag{5.25}$$

5.3.3 Average overall heat transfer coefficient

The calculation of the AU values is conducted for different days of different months to determine average coefficients for the evaporator and condenser. The results for the evaporator and the condenser, with the corresponding average exterior air temperature are presented in Table 5.3, and Table 5.4, respectively. The daily average sensible and latent heat exchange in the evaporator and condenser are presented as well.

114

Table 5.3: AU$_{evap}$ for latent and sensible loads of the evaporator for different days

		Date				Average
		2005-12-07	2006-03-16	2006-05-14	2006-10-18	
$AU_{evap,lat}$ (W/°C)	Average	14,752	11,336	11,360	12,294	13,238
	Std. Dev	1190	728	868.5	692.6	
	Min	11,140	8668	8636	9451	
	Max	16,775	12,857	12,443	13,656	
$AU_{evap,sens}$ (W/°C)	Average	313.5	359.7	308.9	369.9	337
	Std. Dev	49.4	43.03	39.9	47.18	
	Min	190.8	262.5	231.3	273.5	
	Max	432.8	481.2	554.5	533.8	
$Q_{evap,lat}$ (kW)	Average	54.8	54.8	54.8	54.8	54.8
$Q_{evap,sens}$ (kW)	Average	0.8	1.3	1.1	1.2	1.1
T_{air} (°C)	Average	-1.74	-0.97	13.03	15.03	

Table 5.4: AU$_{cond}$ for latent and sensible loads of the condenser for different days

		Date				Average
		2005-12-07	2006-03-16	2006-05-14	2006-10-18	
$AU_{cond,lat}$ (W/°C)	Average	3,265	3,372	5,981	6,829	4,862
	Std. Dev	250.4	112.5	187.6	857.6	
	Min	2,906	3,187	5,550	5,353	
	Max	3,975	3,719	6,557	9,698	
$AU_{cond,sens-desup\,heat}$ (W/°C)	Average	1179	1283	1473	1606	1,385
	Std. Dev	32.02	43.58	71.62	114.2	
	Min	1124	1204	1366	1450	
	Max	1,288	1,453	1,720	2,129	
$AU_{cond,sens-subcool}$ (W/°C)	Average	204.7	333.7	554.8	597.4	423
	Std. Dev	15.62	13.74	15.86	62.71	
	Min	156.7	302.7	514.8	460.3	
	Max	247.6	426.4	608	796.8	
$Q_{cond,lat}$ (kW)	Average	55.3	55.3	55.3	55.3	55.3
$Q_{cond,sens}$ (kW)	Average	18.8	21.3	21.0	21.0	20.5
T_{air} (°C)	Average	-1.74	-0.97	13.03	15.03	

The difference of $AU_{evap,lat}$ between the maximum of 14,752 W/°C (December 7th) and minimum of 11,360 W/°C (May 14th) is of 2458 W/°C, or about 23%. The average value of $AU_{evap,lat}$ over four different days is 13,238 W/°C. The results show that the $AU_{cond,lat}$ value is slightly more variable. The difference between the highest value of 6829 W/°C (October 10th) and lowest of 3265 W/°C (December 7th) is of 3564 W/°C, or about 52%. The, $AU_{cond,lat}$ value increases when the exterior air temperature increases.

The average value of $AU_{cond,lat}$ = 4862 W/°C. The average latent heat transfers in the heat exchangers are constant for all the days because the condensing pressure is assumed to be invariable. The latent heat exchange is constant throughout the days, because the evaporation and condensing pressures (P_1 and P_2, respectively) are considered constant in the calculations. The sensible heat exchange is very small for the evaporator, since the superheating is of 6°C, while in the condenser, the sensible heat corresponds to the de-superheating and sub-cooling of the refrigerant. The average values of sensible heats will be used in the chiller simulation (modified routine PISSIM1) as presented in Chapter 7.

5.4 Conclusions

Based on the experimental data, a refrigeration model was developed by using EES. The results obtained with the EES program were compared with the results from the compressor manufacturer software. A good agreement between the values was found. The EES model was used to identify two important parameters of the evaporator and condenser: the AU_{evap} and AU_{cond}, respectively. These coefficients are more accurate than those that could be calculated from the Toolkit since they are specifically calculated for the type of heat exchange occurring in the heat exchanger. Because the Toolkit equations are only valid for latent heat exchanges, the overall latent heat transfer coefficients determined for the evaporator and the condenser will be used during the simulation of the modified Toolkit model presented in chapter 4 (modified routine PISSIM1). It is important to mention that the coefficients calculated are based on the refrigerant temperatures collected on compressor #2 in chiller #1 (Chapter 3). It is assumed that the other compressors operate in similar conditions than those measured on compressor #2.

CHAPTER 6

MODEL DEVELOPMENT FOR THE SLAB
AND THE CONTROLLER

This chapter begins with the presentation of the slab model. The slab is thoroughly described and analyzed. Two types of models are developed: (1) an analytical model which is adjusted by using the experimental data; and (2) a correlation-based model between the return brine temperature and the ice and the slab inlet brine temperatures. The results obtained from both slab models are compared together by using measurements of four different days. The monitored brine and ice temperatures are analyzed along with the power input to chillers to understand the behaviour of the controller. Empirical rules are then determined and tested with measurements of two different days.

6.1 Slab description and analysis

The slab is composed of a 25 mm thick ice sheet with a surface area of 1586 m^2 (Figure 6.1). Below the ice sheet, a 25 mm thick concrete slab covers polyethylene brine pipes that have 25 mm diameter at 100 mm centre-to-centre distance. Beneath the 100 mm concrete slab, a 100 mm thick rigid polystyrene insulation is used. Under the polystyrene insulation, a layer of 1200 mm of sand covers the gravel. Heating pipes are placed at 300 mm below the insulation. This piping system, which carries warm brine independently of the cold brine, is designed to prevent frost heave at the subgrade.
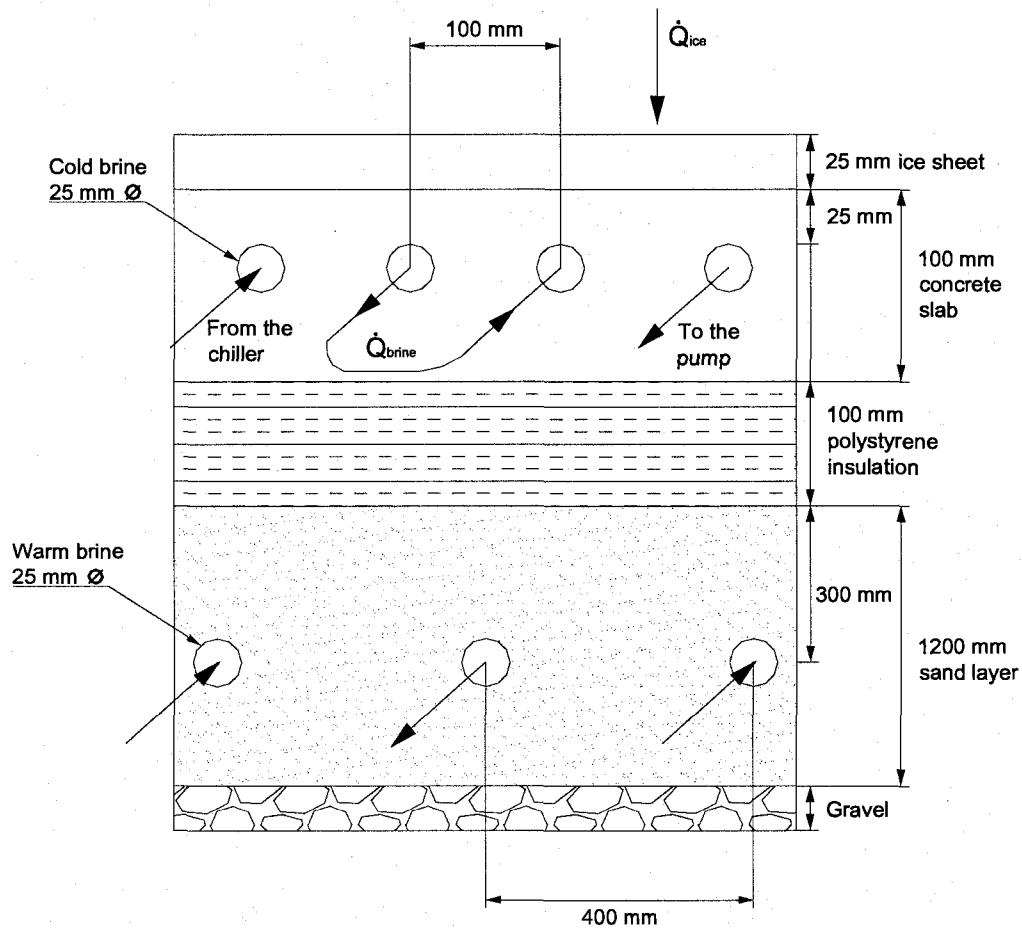
Figure 6.1: Ice rink floor description

Heat is conducted from the surface of the ice sheet to the surface of the cold brine pipes. The brine temperature increases by removing heat from the ice-slab structure. The brine delivered by the chiller circulates inside a four passes network before returning to the pump. Insulation is used between the concrete slab and the sand to minimize the heat flux from ground and from the heating pipes toward the cold brine. Table 6.1 summarizes the thermal properties of components.

Table 6.1: Properties of principal elements of the ice-concrete slab

Property	Units	Ice	Concrete	Brine
Conductivity (k)	W m^{-1} °C^{-1}	2.6	1.1	-
Specific heat (C_p)	J kg^{-1} °C^{-1}	4,186	665.7	2,957
Density (ρ)	kg m^{-3}	917	2,428.4	1,200

6.1.1 Mathematical model of the slab

Different mathematical models can be used to describe the thermal performance of the ice-slab structure. The performance of the slab model is defined by the accuracy of the calculated return brine temperature, based on the ice and the inlet brine temperatures compared with the measured value, under the same conditions. One option is to use an analytical solution to describe the thermal performance of the slab. The accuracy of this type of model strongly depends on the assumptions used and on the thermal characteristics of the system. Another option is to define a correlation-based model using the measured variables. This type of model can provide accurate results; however, it is only applicable to the operative conditions of Camillien-Houde ice rink.

6.1.2 Analytical model

The accuracy of the analytical model is not always related to the precision of the mathematical description. In some cases, a crude approximation of the heat transfer processes can be sufficient to estimate the performance of a thermal system. Hence, the use of valid assumptions can lead to calculation time savings without affecting the accuracy of results.

6.1.2.1 Assumptions

It is assumed that the cooling load of the brine is equal to the cooling load at the ice sheet; therefore, no heat losses or gains from the bottom surface of the slab are added to the brine. Furthermore, there is no heat transferred from one pipe to another, nor in the

119

direction of the circulation of brine in pipes. The model does not consider the transient behaviour of the ice. This assumption is used because the ice layer is very thin and it is two times more conductive than the concrete. The concrete slab is modeled using a lumped-capacitance, with homogenous properties and no temperature gradient.

6.1.2.2 Mathematical description

The energy transfer between the concrete slab and the brine is calculated by using the heat exchanger effectiveness method. The effectiveness approach is a helpful simplification of the complex piping configuration and the heat transfer. The effectiveness of a heat exchanger is defined as the actual energy transferred divided by the maximum possible heat transfer between the two mediums (Holman 1997):

$$\varepsilon = \frac{actual\ heat\ transfer}{maximum\ possible\ heat\ transfer} = \frac{\dot{Q}_{actual}}{\dot{Q}_{max}} \tag{6.1}$$

The maximum possible heat transfer would occur if the brine exits the slab at the slab temperature or if the slab temperature decreases to the brine inlet temperature. The medium undergoing the maximum energy transfer is the one with the minimum capacitance because the energy balance requires that the energy received by one medium be equal to the energy given by the other medium. The capacitance is defined as the product between the mass flow rate and the heat capacity of the medium. The minimum capacitance is given by the following expression (TRNSYS Type 653, Klein et al. 2000):

$$C_{min} = MIN((\dot{m}_{brine} \cdot c_{p,brine}),(m_{slab} \cdot c_{p,slab})) \tag{6.2}$$

The maximum heat transfer corresponds to the product between the minimum capacitance and the temperature difference between the slab and brine at the inlet of the slab ($T_{brine,out,chill2}$):

$$\dot{Q}_{max} = C_{min} \cdot (T_{slab} - T_{brine,out,chill2})$$ (6.3)

The actual heat transfer is calculated by applying the energy balance on the brine side between the inlet ($T_{brine,out,chill2}$) and outlet ($T_{brine,in,pump}$) of the slab:

$$\dot{Q}_{actual} = \dot{m}_{brine} \cdot c_{p,brine} \cdot (T_{brine,in,pump} - T_{brine,out,chill2})$$ (6.4)

Combining Equations 6.1, 6.3 and 6.4 leads to the following expression for the effectiveness of the slab heat exchanger:

$$\varepsilon = \frac{\dot{m}_{brine} \cdot c_{p,brine} \cdot (T_{brine,in,pump} - T_{brine,out,chill2})}{C_{min} \cdot (T_{slab} - T_{brine,out,chill2})}$$ (6.5)

The minimum capacitance of the slab heat exchanger is given by:

$$C_{min} = \dot{m}_{brine} \cdot c_{p,brine}$$ (6.6)

Thus, the effectiveness formulation can be rewritten in a simplified form:

$$\varepsilon = \frac{(T_{brine,in,pump} - T_{brine,out,chill2})}{(T_{slab} - T_{brine,out,chill2})}$$ (6.7)

Since the value of the effectiveness depends on the slab temperature, which is not monitored at Camillien-Houde, it is assumed that the slab temperature is equal to the ice temperature. This assumption is only used for the calculation of the effectiveness.

Because the ice temperature fluctuates with time, the average effectiveness is calculated for March 16th, 2006 by using measurements collected at one-minute interval (Figure 6.2).
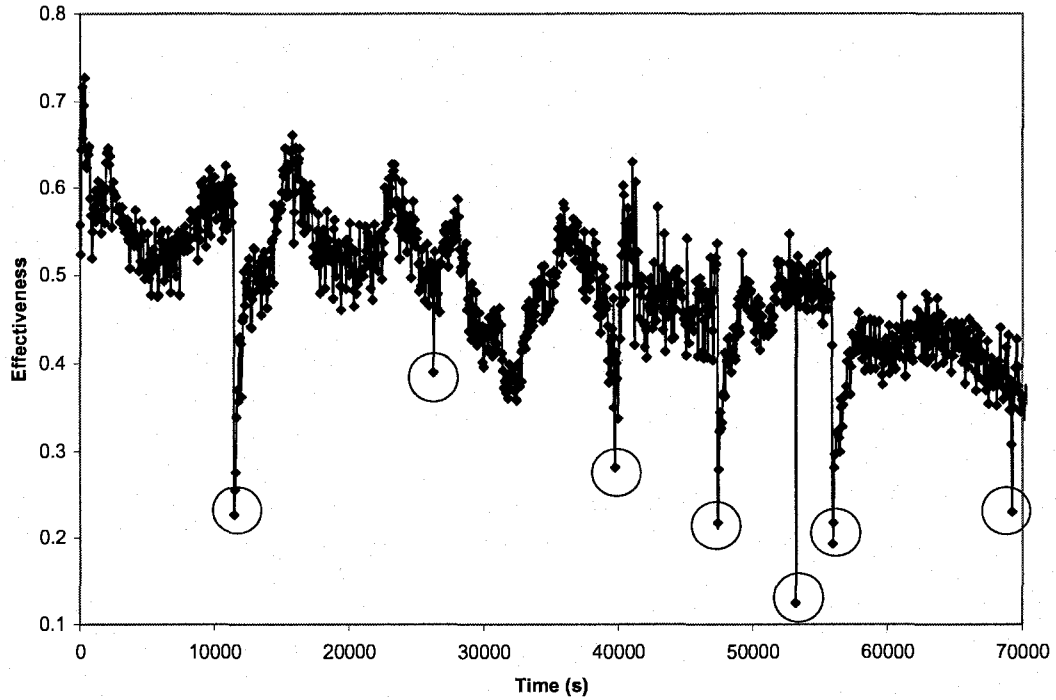
Figure 6.2: Effectiveness of the slab on March 16th, 2006

During resurfacing (circled points in Figure 6.2), the ice temperature increases rapidly to a higher temperature, leading to a low effectiveness. In order to calculate the average effectiveness, the resurfacing and the recovering periods are not considered. The daily mean effectiveness is estimated at $\varepsilon = 0.49$ for March 16th, 2006.

By applying the energy balance on the system presented in Figure 6.1, the following expression is obtained:

$$\dot{Q}_{ice} - \varepsilon \cdot \left(\dot{m} \cdot c_p \right)_{brine} \cdot \left(T_{slab}(t) - T_{brine,out,chill2} \right) = \left(\rho \cdot V \cdot c_p \right)_{slab} \frac{dT_{slab}}{dt} \qquad (6.8)$$

In this expression, the ice load ($\dot{Q}_{ice}$) is calculated from the heat conducted through the ice layer. Since the ice layer is thin, the thermal storage in ice is neglected. Mathematically, this is expressed in function of the temperature difference between the ice and slab at each time t. A thermal conductivity equal to $k = 2.3$ W m^{-1} °C^{-1}, an ice area equal to A = 1586 m^2 and an ice thickness equal to 25 mm have been used in Equation 6.9 to estimate $\dot{Q}_{ice}$:

$$\dot{Q}_{ice} = (kA)_{ice} \frac{(T_{ice} - T_{slab}(t))}{\Delta x_{ice}} \qquad (6.9)$$

Equation 6.8 is a first order differential equation, of the form $dT_{slab}/dt = aT_{,slab} + b$, where a and b are two constants defined as:

$$a = \frac{-(kA/\Delta x)_{ice} - \varepsilon(\dot{m}c_p)_{brine}}{(\rho V c_p)_{slab}} \qquad (6.10)$$

$$b = \frac{(kA/\Delta x)_{ice} \cdot T_{ice} + \varepsilon(\dot{m}c_p)_{brine} \cdot T_{brine,out,chill2}}{(\rho V c_p)_{slab}} \qquad (6.11)$$

Equation 6.8 is solved analytically leading to an exponential-type solution that is function of time, and constants a and b:

$$T_{slab}(t) = e^{(at)} \cdot (-5 + b/a) - b/a \qquad (6.12)$$

An initial condition is necessary to resolve the differential equation. In this case, it is assumed that the temperature of the concrete slab at the time $t = 0$ is equal to brine temperature at the time $t = 0$. The temperature of -5°C is used as the initial condition by

123

selecting from measurements the ice temperature when the system starts. Therefore, Equation 6.4 can be rewritten in the following form:

$$T_{brine,in,pump} = T_{brine,out,chill2} + \frac{\dot{Q}_{actual}}{(\dot{m} \cdot c_p)_{brine}} \qquad (6.13)$$

Equation 6.13 is further developed by using Equation 6.5 and replacing $\dot{Q}_{actual}$:

$$T_{brine,in,pump} = T_{brine,out,chill2} + \varepsilon \cdot \left(T_{slab}(t) - T_{brine,out,chill2}\right) \qquad (6.14)$$

Equation 6.14 allows to determine the return brine temperature ($T_{brine,in,pump}$) in function of the brine temperature at the slab inlet ($T_{brine,out,chill2}$), the slab temperature and the effectiveness of the heat exchanger. This relation considers the effect of the thermal mass of the slab and the variation of slab temperature in terms of the ice temperature.

6.1.2.3 Ice resurfacing

During resurfacing, a thin layer of hot water at approximately 70°C is spread on the ice sheet. The hot water melts the ice shavings and fills the cracks and holes created by the blades. As reported in Figure 6.2, the ice resurfacing influences the thermal behaviour of the slab during a short period. The increase of ice temperature has only a small effect on the actual thermal load felt by the refrigeration system. This additional load is calculated by using the mass of hot water spread and the temperature difference between the ice after and before the resurfacing (Table 6.2). From the analysis of measured data, the impact on the ice temperature lasts approximately 20 minutes.

Table 6.2: Water characteristics used for resurfacing

Characteristic	Value
Water temperature	Between 60°C to 80°C
Volume of water	379 L
Thickness of the layer	0.25 mm

Equation 6.15 is introduced to calculate the load corresponding to the increase of ice temperature during resurfacing:

$$\dot{Q}_{resurf} = \frac{m_{water,resurf} \cdot c_{p,water} \cdot (T_{ice,after} - T_{ice,before})}{60} \qquad (6.15)$$

The load is divided by 60 seconds, because the data was collected at one-minute intervals. The resurfacing load calculated with Equation 6.15 is added to the left side of Equation 6.8 resulting into a modified differential equation that leads to a new definition of constant b:

$$b = \frac{(kA/\Delta x)_{ice} \cdot T_{surface,ice} + \varepsilon(\dot{m}c_p)_{brine} \cdot T_{brine,in} + \dot{Q}_{resurf}}{(\rho V c_p)_{concrete,slab}} \qquad (6.16)$$

Therefore, when resurfacing occurs, $\dot{Q}_{resurf}$ is not zero, while the rest of the time it is equal to zero. In order to detect ice resurfacing periods, a routine is developed that calculates the value of two ice temperature slopes:

$$Slope1 = T_{ice}(t) - T_{ice}(t-2) \qquad (6.17)$$

$$Slope2 = T_{ice}(t-1) - T_{ice}(t-2) \qquad (6.18)$$

Slope1 is the difference between the actual ice temperature (t) and the ice temperature collected two minutes before, at (t-2). The routine detects the ice resurfacing when both *Slope1* and *Slope2* are greater than 2°C, based on observation of the monitored

ice temperatures. When ice resurfacing is detected, Boolean variables called Surf1 to Surf20 are equals to one to take into account the effect during 20 minutes. In that case, the model uses into the differential equation (6.12) the redefined constant b (Equation 6.16) for a period of 20 minutes. The value of ice temperature, which is stored before the resurfacing, is increased by 0.03°C after each iteration during the 20 minute interval in order to reach a total ice temperature increase of 0.6°C after resurfacing. Those two values, 0.03 °C and 0.6 °C, are based on observations of the measured ice temperature.

6.1.2.4 Verification of the analytical model

The model is verified by comparing the measured and simulated return brine temperatures (inlet of the pump), as presented in Figure 6.3 for March 16th, 2006. The ice temperature is also plotted since it is used by the slab model as input data.
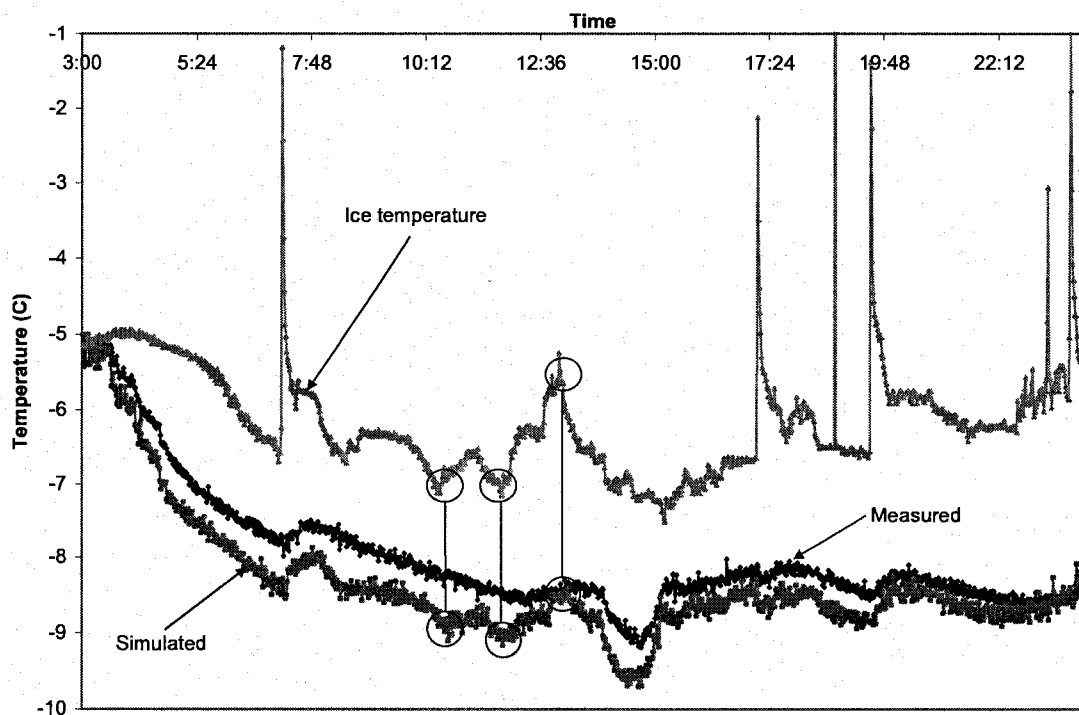
Figure 6.3: Measured against simulated return brine temperatures, and ice temperature on March 16th, 2006 ($\varepsilon = 0.49$)

The results provided by the slab model are coherent with the measured return brine temperature; however, simulated temperatures are lower by about 4.6%, on average. The difference between the measured and simulated brine temperature increases from the start-up of the system at 3:00 in the morning until 7:00. Then, the difference between the measured and simulated temperatures fluctuates around 0.37°C. This error is lower than the thermocouple accuracy (see section 3.3).

As illustrated by the encircled areas in Figure 6.3, small ice temperature fluctuations have almost no effects on the measured return brine temperature while the modeled return brine temperature is more sensitive. The higher fluctuation of the simulated return brine temperature could lead to instable solutions of the refrigeration system. Greater sensitivity to variation of ice temperatures might be caused by an under-estimation of the thermal mass of slab.

The difference between simulated and measured results can be in part due to the transient behaviour of the slab after the start-up. In fact, when the system starts, the slab is at a temperature near -5°C. As time goes by, the temperature of the slab decreases until it practically reaches a constant temperature. Equation 6.12 considers that the transient regime only occurs at the start-up. In fact, the slab behaves transiently at the start-up and each time the ice temperature varies. Thus, the equation developed provides the solution for a transient slab with a constant boundary condition, while the actual boundary condition is not constant. The equation fitting is good immediately after start-up but it tends to provide lower temperatures as time pass. Because the boundary condition (ice

temperature) continually changes and cannot be predicted, it is very difficult to resolve this problem analytically. However, during normal operations (no start-up, no resurfacing) ice temperatures variations are less than 0.8°C. Since the variations of the boundary conditions are small, they are only responsible of a fraction of the difference observed between simulated and measured return brine temperature.

Part of the difference can also be explained by the assumptions used in the energy balance equation (Equation 6.8). This equation considers that the flux from the ground is null. Simulation by Patil and Zmeureanu (2006) concluded that the heat flux from the warm pipes corresponds approximately to 14% of the total load absorbed by the cold brine. Increasing the actual load on the brine by adding heat from below increases the slab effectiveness from 0.49 to 0.57.

The actual ice and concrete thermal conductivity might slightly differ from those provided in Table 6.1, since they have not been directly measured. Furthermore, the ice thickness is not constant throughout the ice rink (see Figure 6.1), because it depends of the activity, and it also varies after each resurfacing.

In order to adjust the model based on the measured data, a correction factor Z is introduced. This factor multiplies the right hand term of Equation 6.9 and corrects the ratio between the ice thermal conductivity (k_{ice}) and the ice thickness (Δx). The introduction of the correction factor Z results into a new definition of the two constants of the differential equation 6.8:

$$a = \frac{-Z \cdot (kA/\Delta x)_{ice} - \varepsilon(\dot{m}c_p)_{brine}}{(\rho V c_p)_{concrete,slab}}$$

(6.19)

$$b = \frac{Z \cdot (kA/\Delta x)_{ice} \cdot T_{surface,ice} + \varepsilon(\dot{m}c_p)_{brine} \cdot T_{brine,in} + \dot{Q}_{resurf}}{(\rho V c_p)_{concrete,slab}}$$

(6.20)

where Z is equal to 1.7. The value of Z has been determined to obtain the best fitting between the simulated and measured brine temperature. Figure 6.4 shows the return brine temperature calculated by the adjusted analytical model, the monitored return brine temperature, and the ice temperature.
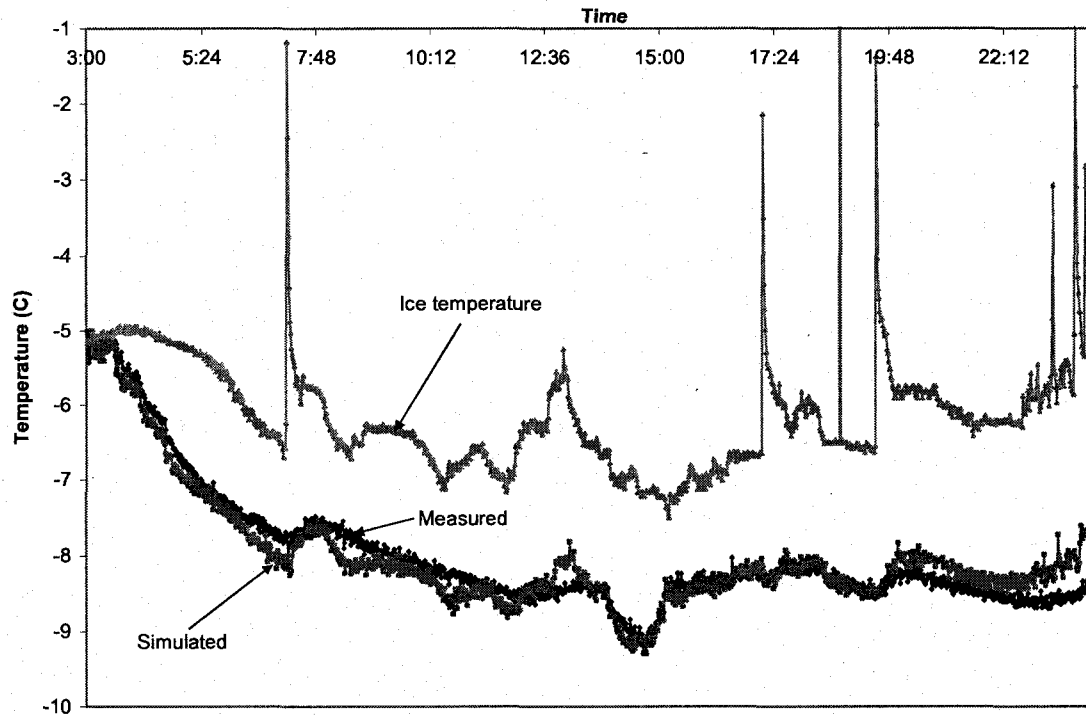
Figure 6.4: Measured against corrected simulated return brine temperatures, and ice temperature on March 16th, 2006 ($\varepsilon = 0.57$)

Compared to the initial model, the corrected model provides more accurate results by diminishing the difference between the measured and simulated return brine temperatures. The model closely follows the trend of measurements. Indeed, the average error between the simulated and measured temperatures is of 0.18°C (2.25%).

129

6.1.3 Inverse model

An inverse approach can also be used to predict the return brine temperature. This approach is interesting because it does not require the mathematical description of the thermal phenomena occurring in the slab. The correlation-based model reflects the relationship between inputs and output.

6.1.3.1 Analysis of the measured data

A relationship is developed in this section that predicts the return brine temperature (dependent variable) in terms of the ice temperature and the inlet brine temperature (independent variables). Figure 6.5 presents the return brine temperature versus the ice temperature from measurements taken at one-minute interval on March 16th, 2006. The encircled areas present three different regimes of operation: the start-up of the system, the steady operation, and the ice resurfacing.
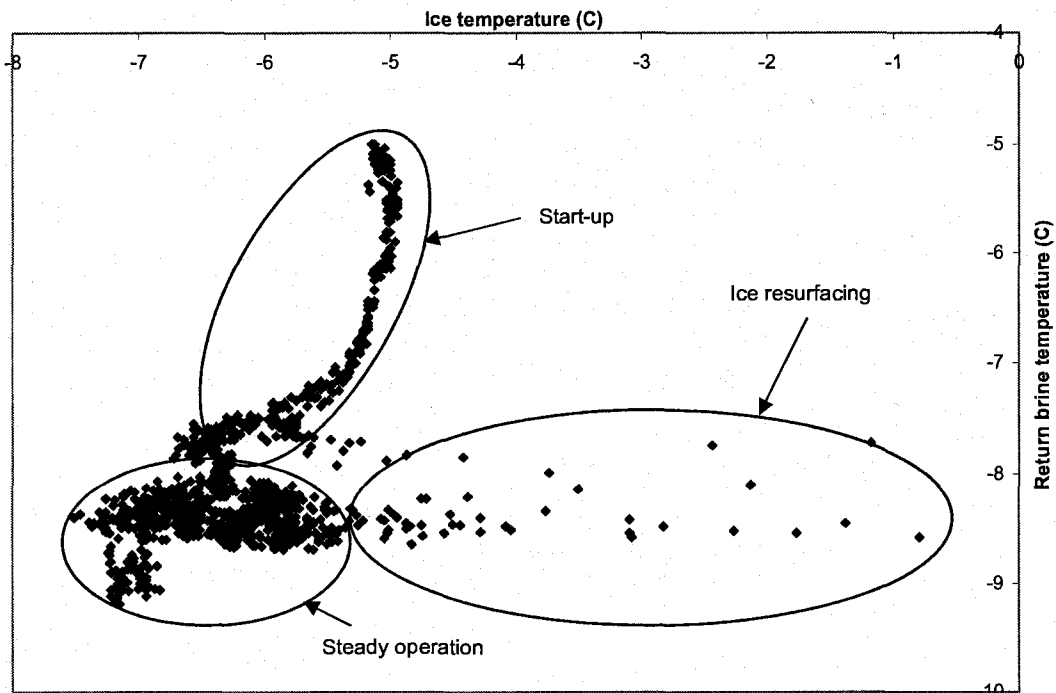
Figure 6.5: Return brine temperature versus the ice temperature on March 16th, 2006

During the steady operation, the return brine temperature ranges between -8°C and -9°C while the ice temperature fluctuates between -5°C and -7°C. Thus, the relation between the two variables can be described by a nonlinear model or by linearizing the dependent variable with a proper transformation.

Figure 6.6 presents the return brine temperature versus the inlet brine temperature from measurements taken at one-minute intervals on March 16th, 2006.
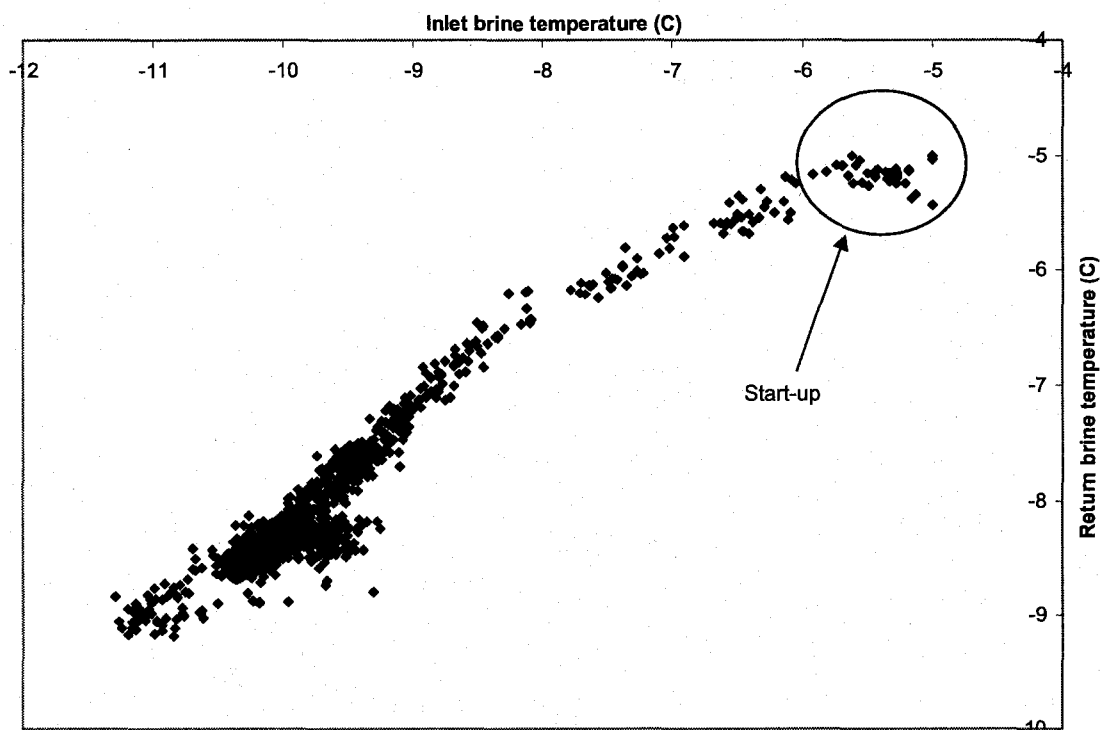
Figure 6.6: Return brine temperature versus the inlet brine temperature on March 16th, 2006

It can be observed that the relationship between the two variables is almost linear. However, the return brine temperature is equal to the inlet brine temperature when it fluctuates between -5°C and -6°C. This corresponds to the start-up period of the system. During steady operation, the relation is positive, meaning that if one variable tends to increase, the other one will also tend to increase. Thus, a positive coefficient should be used to relate the two variables.

131

6.1.3.2 Developing a correlation based on one day of operation

In this section, a correlation-based model is developed based on the measurements collected on March 16th, 2006. Because the relationship between the inlet and the return brine temperatures is linear, only one coefficient is used to relate the two variables. On the other hand, the relation between the ice temperature and the return brine temperature is not linear. Hence, a polynomial equation of third degree is used. The polynomial correlation proposed has the following form:

$$T_{brine,in,pump} = A \cdot T_{brine,out,chill2} + B \cdot T_{ice} + C \cdot T_{ice}^{2} + D \cdot T_{ice}^{3} + E \qquad (6.21)$$

where A, B, C, D and E are coefficients that have to be determined. The correlation is derived by using multiple correlation techniques in the Statgraphics program (Statgraphics 2006). Table 6.3 lists the regression coefficients, standard errors, T-Statistics and P-Values obtained from the program.

Table 6.3: Regression coefficients, standard error, T-Statistic and P-Value for March 16th, 2006

Parameter	Estimate	Standard Error	T-Statistic	P-Value
A	0.708352	0.00663615	106.741	0.0000
B	-0.127861	0.0216395	-5.90868	0.0000
C	0.0166354	0.00583716	2.84991	0.0044
D	0.00484019	0.000688604	7.02899	0.0000
E	-1.40321	0.121146	-11.5827	0.0000

As expected, the coefficient A relating the return brine temperature with the inlet brine temperature is positive indicating a positive relation between these two variables as observed in Figure 6.5. The standard errors are very small for all coefficients, and therefore the values given can be considered as accurate. The T-Statistic (Student) is used to test the hypothesis that two variables are correlated. The T-Statistic can range between minus infinity to plus infinity. A T-Statistic value near zero indicates that there is no

correlation between the two variables. On the other hand, a T-Statistic far from zero (either positive or negative) is evidence that there is correlation between the variables. Since all T-Statistics are significatly greater or less than zero, the correlation between variables is statistically significant. The P-Value indicates if the model can be simplified by removing a term without significantly degrading the accuracy. Since all P-Values are less than 0.05, each term is statistically significant at 95.0% confidence level. Thus, all coefficients and related variables should be kept in the model. Equation 6.21 takes now the form of:

$$T_{brine,in,pump} = 0.708352 \cdot T_{brine,out,chill2} - 0.127861 \cdot T_{ice} + 0.0166354 \cdot T_{ice}^{2} + 0.00484019 \cdot T_{ice}^{3} - 1.40321 \tag{6.22}$$

An analysis of variance (ANOVA) is conducted by using Statgraphics program. The analysis of variance consists of a decomposition of the variability of the dependent variable Y into a model sum of squares and a residual or error sum of squares (Table 6.4).

Table 6.4: Analysis of variance for the slab correlation for March 16th, 2006

Source	Sum of Squares	Degree of freedom	Mean Square	F-Ratio	P-Value
Model	838.909	4	209.727	5022.43	0.0000
Residual	50.5273	1210	0.0417581		
Total (Corr.)	889.436	1214			

In Table 6.4, the F-Ratio is defined as follows:

$$F\text{-}Ratio = \frac{Actual\ variation\ of\ the\ group\ averages}{Expected\ variation\ of\ the\ group\ averages} \tag{6.23}$$

It is interesting to analyze the F-test (Fisher test) and the associated P-Value. In multiple regressions, F-test indicates if one of the coefficients is equal to zero. The null

hypothesis states that all coefficients are equal to zero, while the alternative hypothesis simply states that at least one of the coefficients is not equal to zero. If the null hypothesis is valid, an F-Ratio around one is expected. Since the F-Ratio is much larger (5022.43) it is possible to reject the null hypothesis. Furthermore, because the P-Value in the ANOVA table is less than 0.05, there is a statistically significant relationship between variables at a confidence level of 95.0%.

Further statistical information is obtained from the Statgraphics program, including the R-Squared (R^2), the adjusted R-Squared, the standard error of estimate (SEE), the mean absolute error (MAE), the Durbin-Watson Statistic (DWS) and the Lag 1 residual autocorrelation (Table 6.5).

Table 6.5: Statistical information for the slab correlation for March 16th, 2006

Statistic information	Value
R-squared	0.943
R-squared adjusted for the degree of freedom	0.943
Standard error of estimate	0.204
Mean absolute error	0.168
Durbin-Watson autocorrelation	0.422 (P = 0.0000)
Lag 1 Residual Autocorrelation	0.787

The R^2 indicates that the model as fitted explains 94.3% of the variability of the brine temperature at the outlet of the slab. The remaining 5.7% is attributable to deviations from the model, which may be caused by other factors such as measurement errors or simply by a failure of the current model to fit the data adequately. The adjusted R-Squared, which considers the number of coefficients in the model, is used to compare models with different numbers of coefficients. The adjusted R-squared is more suitable in this case because the model uses four coefficients. In this case, it is also of 94.3%. The standard error of estimate is an evaluation of the deviation of the residuals. This value is

usually used to create prediction limits for new observations. The standard error of the estimate shows the standard deviation of residuals to be 0.204°C. The mean absolute error of 0.168°C represents the average absolute value of the residuals.

To detect outliers, which are values that are numerically distant from the rest of the data, the studentized residuals are used. Because the variances of the residuals are not constant, studentization is necessary to obtain residuals with equal variance. Studentized residuals take into account the change of variability by dividing the observed residual by an estimate of the standard deviation of the residual at that point. Figure 6.7 plots the studentized residuals versus the return brine temperature as predicted by the model.
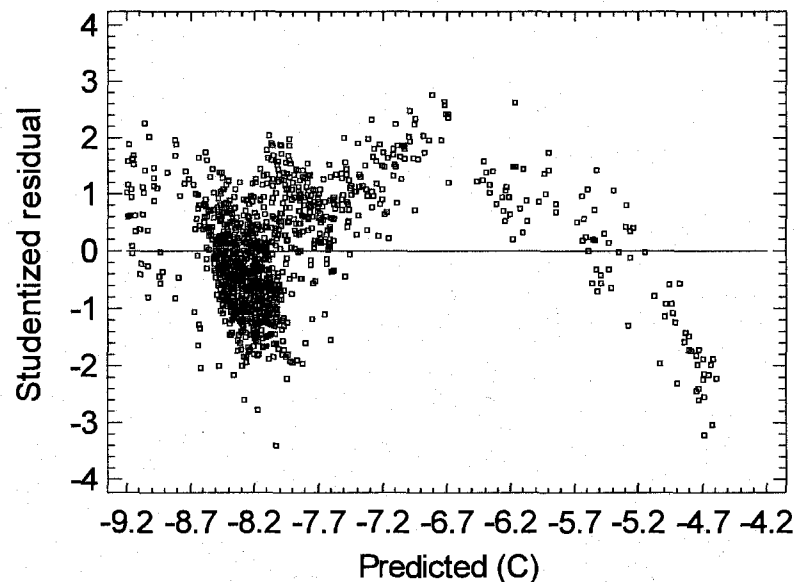
Figure 6.7: Studentized residuals versus predicted return brine temperature

The studentized residuals are approximately homogeneously spread about zero, and only few exceed the absolute value of two. The four studentized residuals exceeding the absolute value of three can be considered as outliers (Statgraphics 2006). These outliers probably correspond to the ice resurfacing.

The Durbin-Watson (DW) Statistic is a measure of serial correlation in the residuals. If the residuals vary randomly, this value is close to 2. The actual value of 0.422 (see Table 6.5) signifies that residuals are related to the predicted brine temperature. Since the P-Value is less than 0.05, some trend or possible serial correlation of the residuals can be established at a 95% of level.

The Lag 1 residual autocorrelation allows to estimate the correlation between the consecutive residuals on a scale of -1 to 1. Values far from zero indicate that significant structures remains unaccounted by the model. Because the Lag 1 residual autocorrelation is of 0.787, some structure is not considered by the model.

6.1.3.3 Verification of the correlation-based model

The measured return brine temperature is compared against the predicted value based on the correlation-based model built for March 16th, 2006 (Figure 6.8). Overall, the model predicts accurately the experimental data.
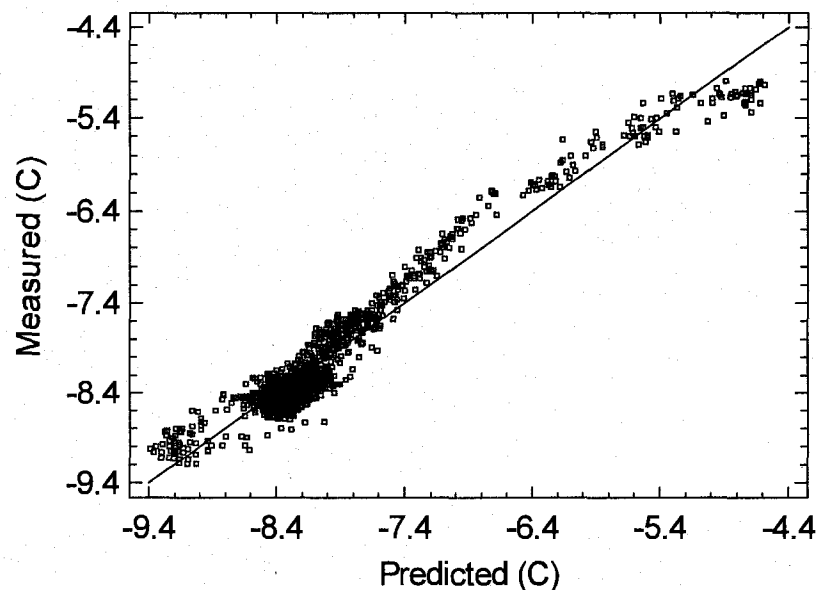
Figure 6.8: Measured versus predicted return brine temperatures on March 16th, 2006

The return brine temperature calculated and measured are compared in Figure 6.9 for March 16th, 2006.
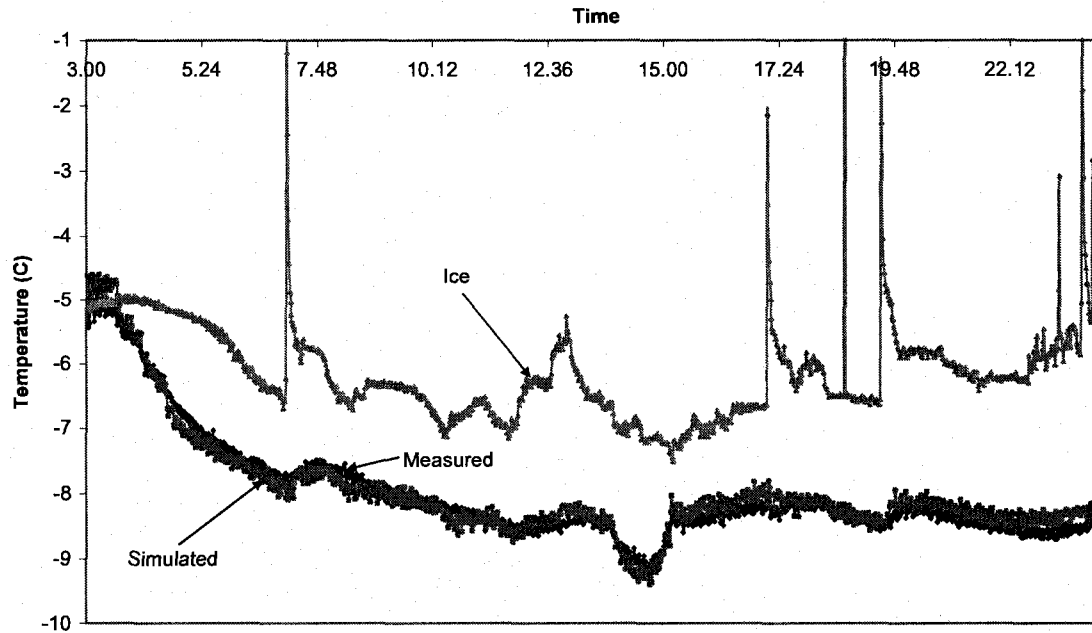
Figure 6.9: Measured and simulated return brine temperatures based on the correlation-based model, and ice temperature on March 16th, 2006

The agreement between the measured and simulated return brine temperatures is good. The average error of temperature is of 0.15°C (1.90%).Compared to the analytical model (Figure 6.4), the predicted values based on the correlation-model are less sensitive to the variation of ice temperature.

6.1.3.4 Calculation of coefficients based on several days of operation

In this section, new coefficients are determined for the same correlation-based model (Equation 6.21) by using measurements collected during five different days of different months: March 16th, May 14th, September 2nd, October 18th and November 10th,

2006. Table 6.6 lists the regression coefficients, standard errors, T-Statistics and P-Values obtained from Statgraphics for the five days analyzed.

Table 6.6: Regression coefficients, standard error, T-Statistic and P-Value for five days of operation

Parameter	Estimate	Standard Error	T-Statistic	P-Value
A	0.696435	0.00298536	233.284	0.0000
B	-0.0174158	0.0103714	-1.67921	0.0931
C	-0.0103419	0.000772722	-13.3837	0.0000
D	0.00052341	0.000108861	4.80808	0.0000
E	-0.929877	0.0508188	-18.2979	0.0000

The new correlation-based model is written as follows:

$$T_{brine,in,pump} = 0.696435 \cdot T_{brine,out,chill2} - 0.0174158 \cdot T_{ice} - 0.0103419 \cdot T_{ice}^{2} + 0.00052341 \cdot T_{ice}^{3} - 0.92877$$

(6.24)

In Table 6.6, the standard error for all the coefficients is very small, indicating that the estimated values are accurate. The T-Statistic, which indicates if two variables are correlated or not, is far from 0 (either positive or negative) for all coefficients. This indicates that the correlation between the dependent and independents variables is statically significant. However, it is interesting to note that the T-Statistic of parameter B is the one nearest zero (-1.67921).In determining whether the model can be simplified, it is possible to note that the highest P-Value is 0.0931. Since the P-Value is greater than 0.05, the corresponding term is not statistically significant at the 95% confidence level. Therefore, the term $B \cdot T_{ice}$ should be removed from the model.

The statistical analysis indicates that parameter B is less significant if it is determined using five days operation (Table 6.6) instead of one day (Table 6.3). Therefore, no further statistical analysis is conducted, because this would only confirm that coefficient B should be removed from the correlation. Hence, the correlation-based model developed in section 6.1.3.2 will be used in further analysis.

6.1.4 Comparing the slab models

The results previously presented show that the average error given by the analytical model for March 16th, 2006 is about 0.18°C (2.25%), while the correlation-based model leads to 0.15°C (1.90%) (see Figure 6.4 and Figure 6.9). It is of greater interest to test both models using collected data from different days. Therefore, both analytical and correlation-based models are tested by using three others days: May 14th, September 2nd and October 18th, 2006.

Figure 6.10 and Figure 6.11 presents the results obtained from the analytical and the correlation-based models for May 14th, 2006, respectively. As observed, both models provide similar results: the average error of the analytical model is 0.10°C (1.26%) while it is of 0.15°C (1.81%) for the correlation-based model. However, when looking to the ice temperature it is possible to see that it is approximately constant during this day. Therefore, the effect of the ice resurfacing cannot be analyzed during this day.

Figure 6.12 and Figure 6.13 presents the results obtained from the analytical and the correlation-based models for September 2nd, 2006, respectively. For this day, the

average error corresponding to the analytical model is of 0.16°C (2.04%), while for the correlation-based model it is of 0.18°C (2.22%). Hence, the difference between predictions of those two models is negligible. The correlation-based model is more sensitive to the ice resurfacing than the analytical model. At 11:15 and 11:40, the sudden increase of ice temperature has a greater effect on the predicted return brine temperature.

Figure 6.14 presents the results from the analytical model while Figure 6.15 presents the results from the correlation-based model using as input data measurements from October 18th, 2006. During that day, the ice is resurfaced several times. Both results follow the trend of the measured return brine temperature. However, the correlation-based results are more accurate. The average error is 0.38°C (4.36%) for the analytical model, while it is of 0.22°C (2.55%) for the correlation-based model.

Several factors explain the differences observed between the results of analytical and correlation-based models. The assumptions used for the analytical model only represent part of the actual heat transfer occurring (e.g. horizontal heat transfer is not considered), while the correlation directly takes into account all the thermal processes because it is completely based on the measured data. The correlation model is therefore chosen to be used in the next chapter for the ice rink refrigeration model, due to its greater capacity to reproduce the measured data. However, if the model is applied for another ice slab, the analytical model should be used instead because this model is independent of the measured data.
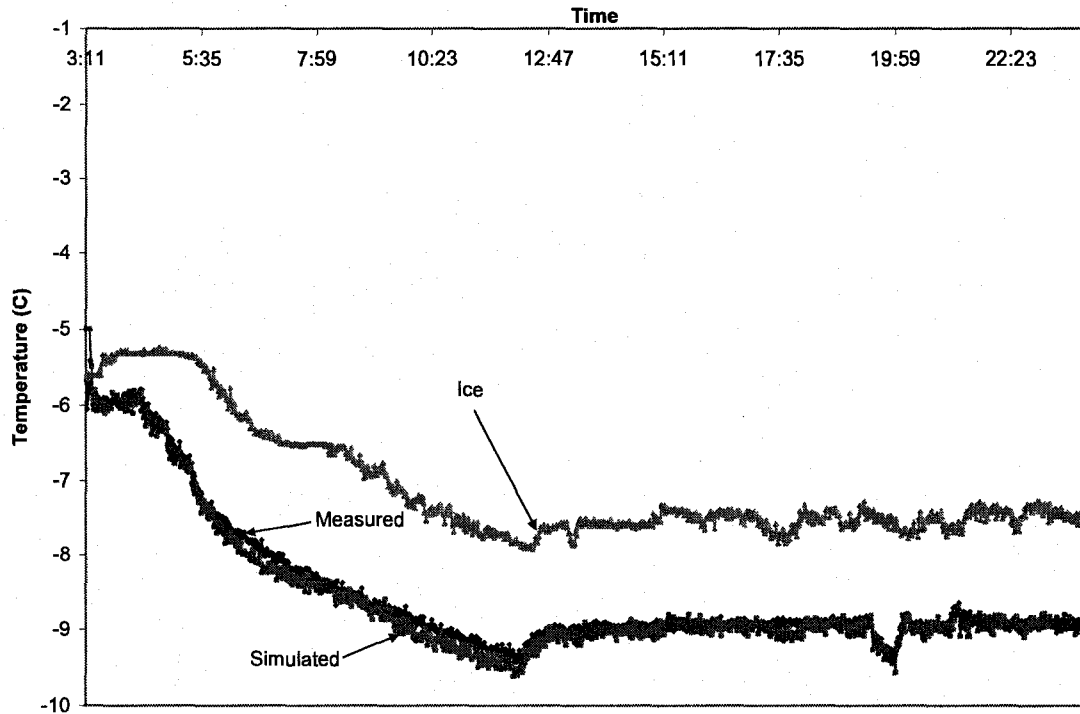
Figure 6.10: Measured and calculated return brine temperatures based on the analytical slab model on May 14th, 2006
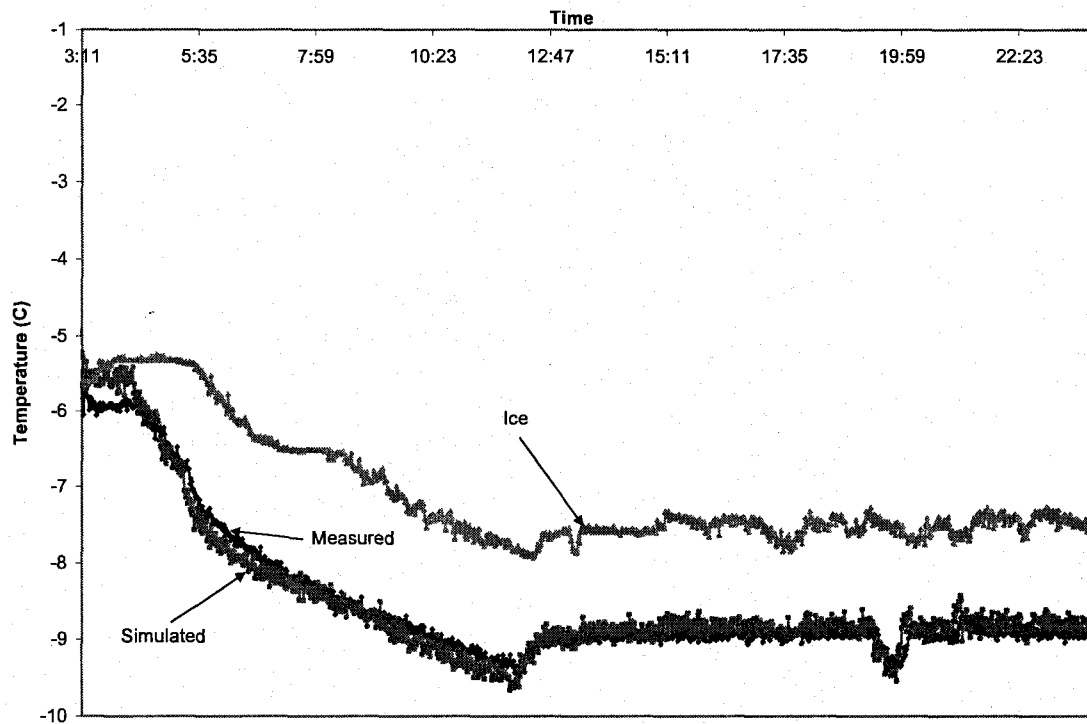
Figure 6.11: Measured and calculated return brine temperatures based on the correlation-based slab model on May 14th, 2006

141
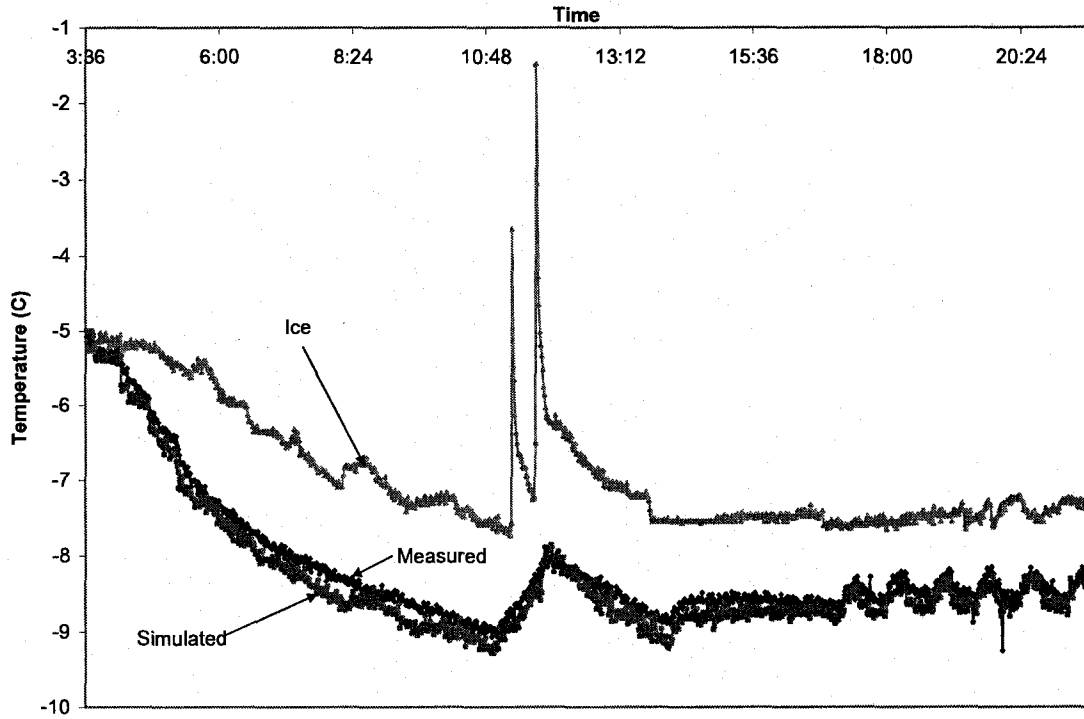
Figure 6.12: Measured and calculated return brine temperatures based on the analytical slab model on September 2nd, 2006
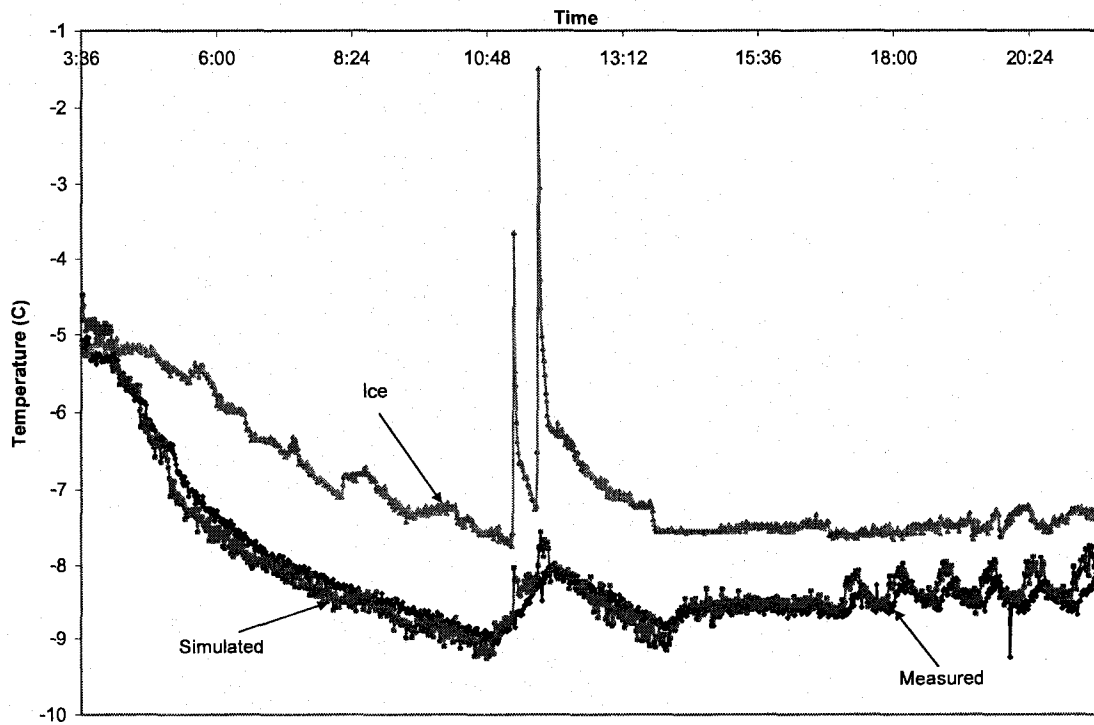
Figure 6.13: Measured and calculated return brine temperatures based on the correlation-based slab model on September 2nd, 2006
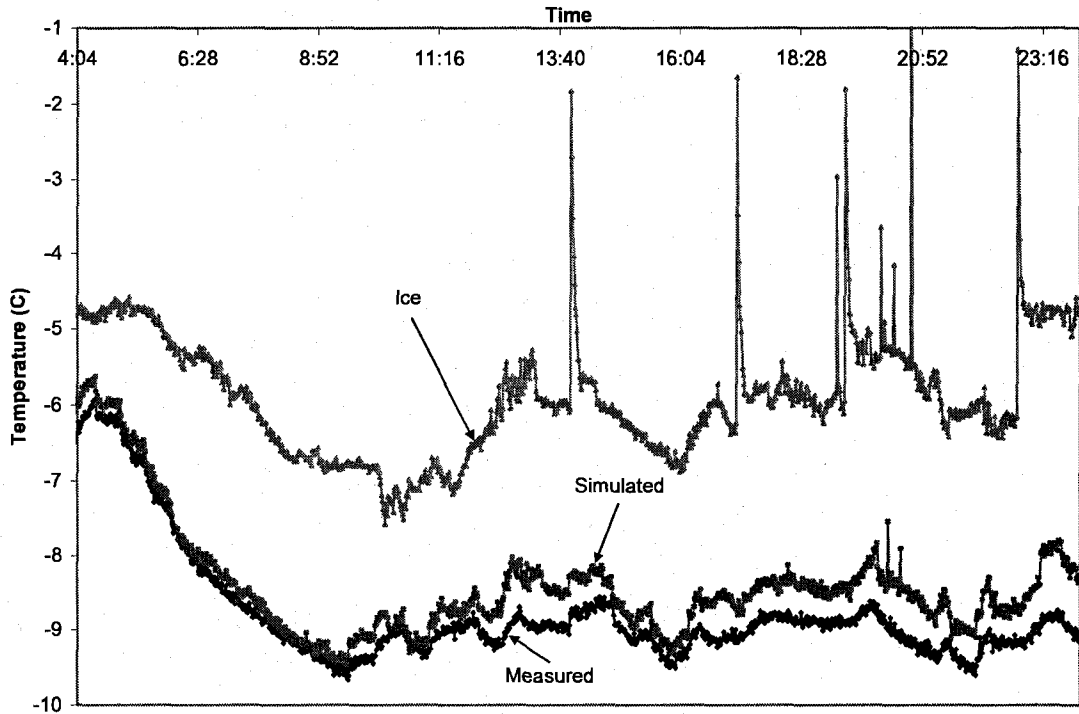
Figure 6.14: Measured and calculated return brine temperatures based on the analytical slab model on October 18th, 2006
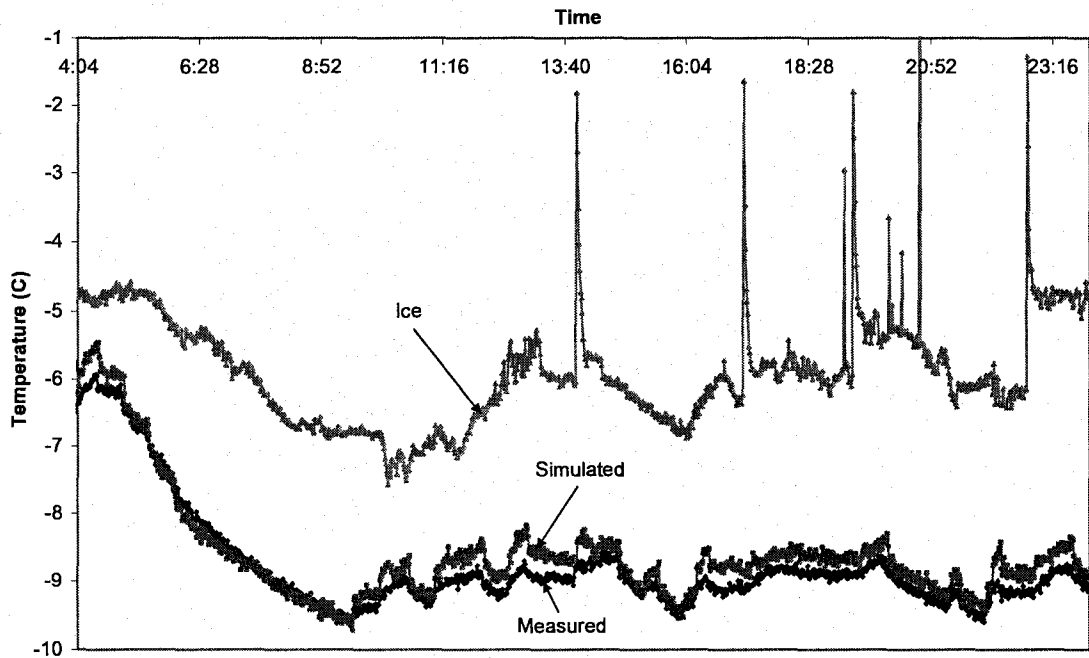
Figure 6.15: Measured and calculated return brine temperatures based on the correlation-based slab model on October 18th, 2006

6.2 Controller description and analysis

Traditionally, ice rink refrigeration systems are controlled through the temperature of the brine returning from the slab or the temperature of the underlying slab measured at one or several locations. The brine or floor temperature is continually adjusted to a level that ensures a satisfactory ice temperature. Recent developments in the ice-skating rink industry have led to improvements in the ice quality control domain. One of the leaders in this field, CIMCO refrigeration, has developed an infrared control system (CIMCO 2006). By instantly measuring the ice temperature, the control system signals to the refrigeration plant to modify the supply brine temperature and therefore maintain the ice temperature within its set point. This new way of controlling rink's refrigeration systems has led to energy savings. However, this type of controller is not used in this study.

6.2.1 Actual controller

At Camillien-Houde ice rink, the ice temperature is controlled using a combination of the concrete slab temperature and return brine temperature (Dumas 2004). In the morning, the system starts if after 3:00 the slab and the brine temperatures are above -5°C. Then, the controller increases the number of compressors in operation in order for the return brine temperature to reach approximately -9°C at 8:00. During the rest of the day, the controller adjusts the number of compressors in order to maintain the return brine temperatures at the set point.

6.2.2 Model description

The model of the controller is based on the analysis of three monitored variables: the power input to the chillers and pump, the ice temperature, and the return brine

temperature. Empirical relations are determined between the return brine temperature and the power input while the measured ice temperature is employed to determine ice resurfacing periods (section 6.2.3). Figure 6.16 presents the return brine temperature, the power input and the ice temperature variations during the day of March 16th, 2006.
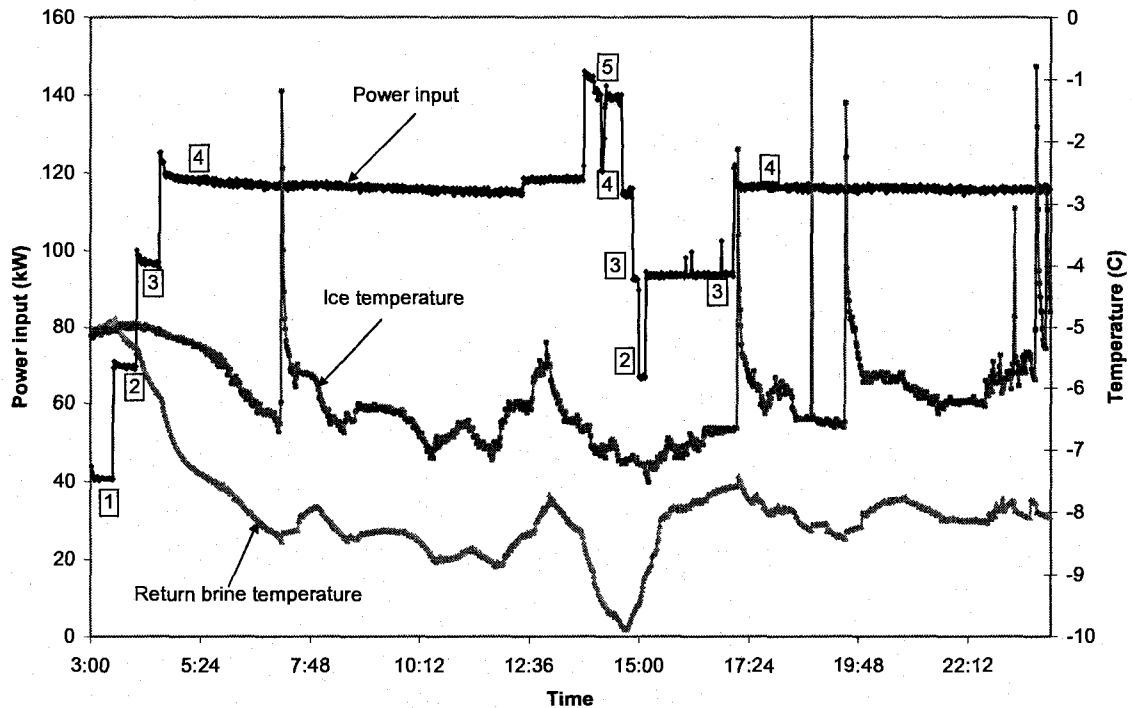
Figure 6.16: Return brine temperature, ice temperature, and power input on March 16th, 2006

The step variations of power input correspond to changes in the number of compressors in operation. This number of compressors is identified beside the power input curve inside small boxes. When the system starts, compressors are switched on, one at a time at 30-minutes intervals, until the adequate return brine temperature is reached. Then, the number of compressors is adjusted following the variations of the return brine temperature. It can be noticed that between 7:00 and 13:50, when four compressors are in operation, the power input slightly varies. These variations are caused by variations of the condenser operating conditions due to changes of air temperature. The controller modeled in this study is only used to determine the number of compressors in operation.

145

Ice resurfacing, that is presented by the peak of ice temperature at about 7:10, 17:10 and 19:30 (Figure 6.12), has a reduced and delayed effect on the return brine temperature. The electric demand of the refrigeration plant is not affected by the small increase of the return brine temperature. Hence, the cooling load added by the hot water spread on the ice sheet does not increase the number of compressors in operation. Due to the thermal mass of the concrete slab and of the brine circuit including the evaporator, the chillers do not react to the additional resurfacing cooling load.

The method used by the actual controller is not available and is not easy to understand, since it is based on a combination of the return brine temperature (measured), the slab temperature (not measured) and human interaction. This section presents a new controller model by relating the number of compressors and the return brine temperature as presented in Figure 6.17. The encircled numbers roughly represent how the controller increases or decreases the number of compressors in function of the return brine temperature. The controller model is tested with measurements at the Camillien-Houde ice rink.
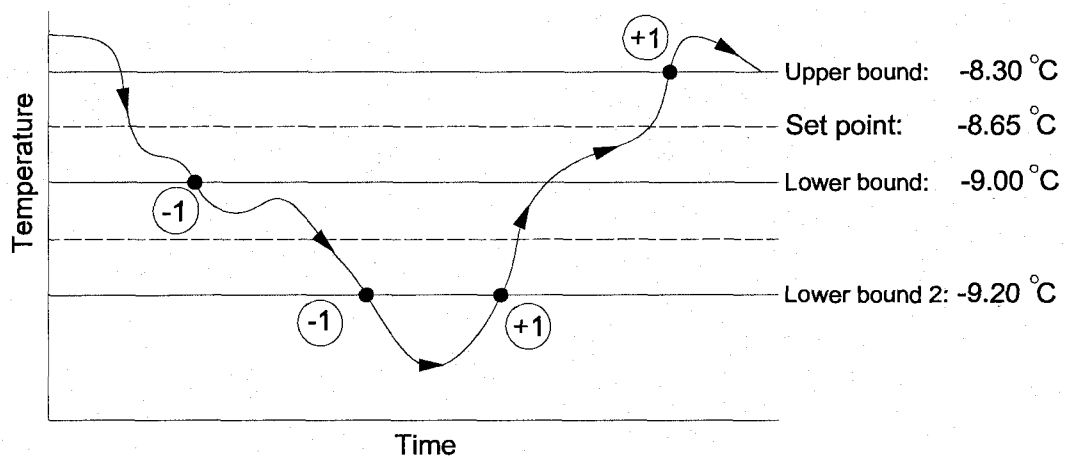
Figure 6.17: Controller sequences in function of the return brine temperature

When observing the variations of the return brine temperature, it is noticed that the controller set point is around -8.65°C. The controller does not instantly react when the return brine temperature fluctuates around the set point. Hence, a dead band with an upper limit at -8.30°C and a lower limit at -9.00°C is defined (Figure 6.17). If the temperature is within the dead band and leaves through the upper or lower bound, one compressor is turned on (+1 in Figure 6.17) or off (-1), respectively. However, if the temperature is outside the dead band and crosses the boundaries towards the set point value, the number of compressors in operation is maintained constant. Further analysis allows to define a second temperature range, comprised between the lower bound of the dead band (-9.00°C) and a second lower bound defined at -9.20°C. If the brine temperature crosses with a negative slope the second lower bound, a compressor is turned off (-1). If it crosses with a positive slope, a compressor is turned on (+1). When the return brine temperature is maintained within the second temperature range, the number of compressors decreases every 10 minutes until a minimum of three compressors is reached. However, if the return brine temperature is below the second lower bound, the number of compressors is decreased every 10 minutes until it reaches a minimum of two compressors. Regardless of the brine temperature fluctuations, if the number of compressors is changed, the controller always waits for 10 minutes before changing again the number of compressors in operation. For the start-up of the system, the controller turns on a compressor every 30 minutes until the return brine temperature reaches -6°C (Figure 6.16). Based on the defined temperature boundaries, controller decisions are set based on a number of rules. Some of the rules are based on the calculations of brine temperature slope, which is a generic term used to define a tendency. More details on the controller algorithm are provided in section 6.2.3.

Rule 1

IF the return brine temperature is within the upper and the lower bounds, the number of compressors is kept CONSTANT. However, IF the brine temperature has a negative slope (Slope1 & Slope2 & Slope3 < 0) ONE compressor is turned OFF.

Rule 2

IF the return brine temperature crosses the lower bound with a negative slope (Slope1 < 0), ONE compressor is turned OFF.

Rule 3

IF the return brine temperature crosses the upper bound with a positive slope (Slope1 > 0), ONE compressor is turned ON.

Rule 4

IF the return brine temperature is within the lower bound and the lower bound 2, and IF the temperature has a negative slope (Slope1 < 0), ONE compressor is turned OFF every 10 minutes until a MINIMUM of THREE compressors is reached.

Rule 5

IF the return brine temperature is between the lower bound and the lower bound 2, and IF the temperature has a positive slope, ONE compressor is turned ON every 10 minutes until a MAXIMUM of THREE compressors is reached.

Rule 5

IF the return brine temperature is below the lower bound 2, ONE compressor is turned OFF.

Rule 6

IF the number of compressors changes, the controller WAITS 10 minutes before making any new change.

Rule 7

Except during the start up of the system, the MAXIMUM and MINIMUM number of compressors that can operate at the same time is either FIVE or TWO, respectively.

6.2.3 Controller algorithm

The controller takes into account current (at time t) and past (at time t-j) brine temperatures in order to determine the adequate number of compressors in operation. The controller stores in memory the brine temperature of the last eight minutes before the current reading at time t. The stored temperatures are used by the controller to calculate three parameters.

$$Slope1 = T_{brine,in,pump}(t) - T_{brine,in,pump}(t-5) \tag{6.25}$$

$$Slope2 = T_{brine,in,pump}(t) - T_{brine,in,pump}(t-8) \tag{6.26}$$

$$Slope3 = T_{brine,in,pump}(t) - T_{brine,in,pump}(t-2) \tag{6.27}$$

A Boolean variable named *wait* is used by the controller to identify any variations in the number of compressors in operation. When the number of compressors changes, the variable *wait* is equal to one and the controller waits 10 minutes before bringing any new changes to the system (Rule 6). The variable *wait* is also equal to one if the return brine temperature enters negatively the upper bound or positively the lower bound. Since at that moment the temperature fluctuates near the bounds, the controller waits for the system to stabilize. Another Boolean variable named *start* is utilized to identify the start-up period. When *start* is equal to one, the start-up period is finished. From that moment, the rest of the controller algorithm is applied to make new changes. The Boolean variable *out* is used to recognize when the return brine temperature crosses the upper bound of the dead band. If *out* = 1, the temperature has crossed the upper bound and the controller must add one compressor to the system. However, this compressor is only turned on if only the three slopes (Equations 6.25, 6.26, 6.27) are less than 0.0001. This ensures that

149

the change is brought when the temperature profile has stop rising and has reached a local maximum. Finally, Boolean variables *ok1* and *nogo1* are employed to identify when the brine temperature is within lower bound and lower bound 2 or below lower bound 2. These variables are used to ensure that the order of changes is respected when the brine passes from the upper bound to a temperature below the lower bound 2. The following algorithm summarizes the different conditions of the controller model.

Brine temperature exiting the upper bound

IF $(T_{brine,in,pump}(t) > Upper\ bound$ AND $T_{brine,in,pump}(t-1) > Upper\ bound$ AND $T_{brine,in,pump}(t-2) > Upper\ bound$ AND $T_{brine,in,pump}(t-3) > Upper\ bound$ AND $T_{brine,in,pump}(t-4) \leq Upper\ bound$ AND $T_{brine,in,pump}(t-5) < Upper\ bound$ AND $Slope1 < 0.1)$
  THEN out = 1
IF $(out = 1$ AND $Abs(Slope1) < 0.0001$ AND $Abs(Slope2) < 0.0001$ AND $Abs(Slope3) < 0.0001)$
  THEN Rule 3 is TRUE and ONE compressor is turned ON
    Wait = 1

Brine temperature entering negatively the upper bound

IF $(T_{brine,in,pump}(t) < Upper\ bound$ AND $T_{brine,in,pump}(t-1) < Upper\ bound$ AND $T_{brine,in,pump}(t-2) < Upper\ bound$ AND $T_{brine,in,pump}(t-3) < Upper\ bound$ AND $T_{brine,in,pump}(t-4) \geq Upper\ bound$ AND $T_{brine,in,pump}(t-5) > Upper\ bound)$
  THEN NO changes to the number of compressor
    Wait = 1

Brine temperature exiting negatively the lower bound

IF $(T_{brine,in,pump}(t) > Lower\ bound$ AND $T_{brine,in,pump}(t-1) > Lower\ bound$ AND $T_{brine,in,pump}(t-2) > Lower\ bound$ AND $T_{brine,in,pump}(t-3) \leq Lower\ bound$ AND $T_{brine,in,pump}(t-4) < Lower\ bound$ AND $T_{brine,in,pump}(t-5) < Lower\ bound)$
  THEN Rule 2 is TRUE and ONE compressor is turned OFF
    Wait = 1

Brine temperature entering positively the lower bound

IF $(T_{brine,in,pump}(t) < Lower\ bound$ AND $T_{brine,in,pump}(t-1) < Lower\ bound$ AND $T_{brine,in,pump}(t-2) \geq Lower\ bound$ AND $T_{brine,in,pump}(t-3) > Lower\ bound$ AND $T_{brine,in,pump}(t-4) > Lower\ bound$ AND $T_{brine,in,pump}(t-5) > Lower\ bound)$

        THEN NO changes to the number of compressor
                Wait = 1

Brine temperature between the upper and the lower bounds

IF $(T_{brine,in,pump}(t) > Lower\ bound$ AND $T_{brine,in,pump}(t) < Upper\ bound$ AND *Slope1*<0 AND *Slope2*<0 AND *Slope3*<0

        THEN ONE compressor is turned OFF
                Wait = 1

Brine temperature between lower bound and lower bound 2

IF $(T_{brine,in,pump}(t) < Lower\ bound$ AND $T_{brine,in,pump}(t) => Lower\ bound2)$

      THEN

                IF *(Slope1<0)*
                      THEN rule 4 is true and ONE compressor is turned OFF
                IF *(Slope1>0)*
                      THEN rule 5 is true and ONE compressor is turned ON
      Wait = 1

Brine temperature below lower bound 2

IF $(T_{brine,in,pump}(t) < Lower\ bound2)$

        THEN Rule 5 is TRUE and ONE compressor is turned OFF
                Wait = 1

The controller verifies if the minimum or the maximum number of compressors is reached. If the number of compressors is greater than five or less than two, the controller maintains either five or two compressors in operation, respectively. When the controller ends the calculation process at each time step, it distributes the total number of compressors in operation between Chiller #1 and Chiller #2. The following algorithm is used to distribute the compressors between Chiller #1 and Chiller #2

IF (number of compressors = 2)
      THEN two compressors in Chiller #1
IF (number of compressors = 3)
      THEN two compressors in Chiller #1, one compressor in Chiller #2
IF (number of compressors = 4)
      THEN two compressors in Chiller #1, two compressors in Chiller #2
IF (number of compressors = 5)
      THEN two compressors in Chiller #1, three compressors in Chiller #2

6.2.4 Calibration and validation of the controller

The model is calibrated by comparing the number of compressors in operation as calculated from measurements against the number predicted by the controller model. The controller model uses the return brine temperature calculated by the correlation-based model of slab (section 6.1.3.2). Figure 6.18 compares the simulated and measured number of compressors along with the return brine temperature measured and simulated with the correlation-based model for March 16th, 2006.
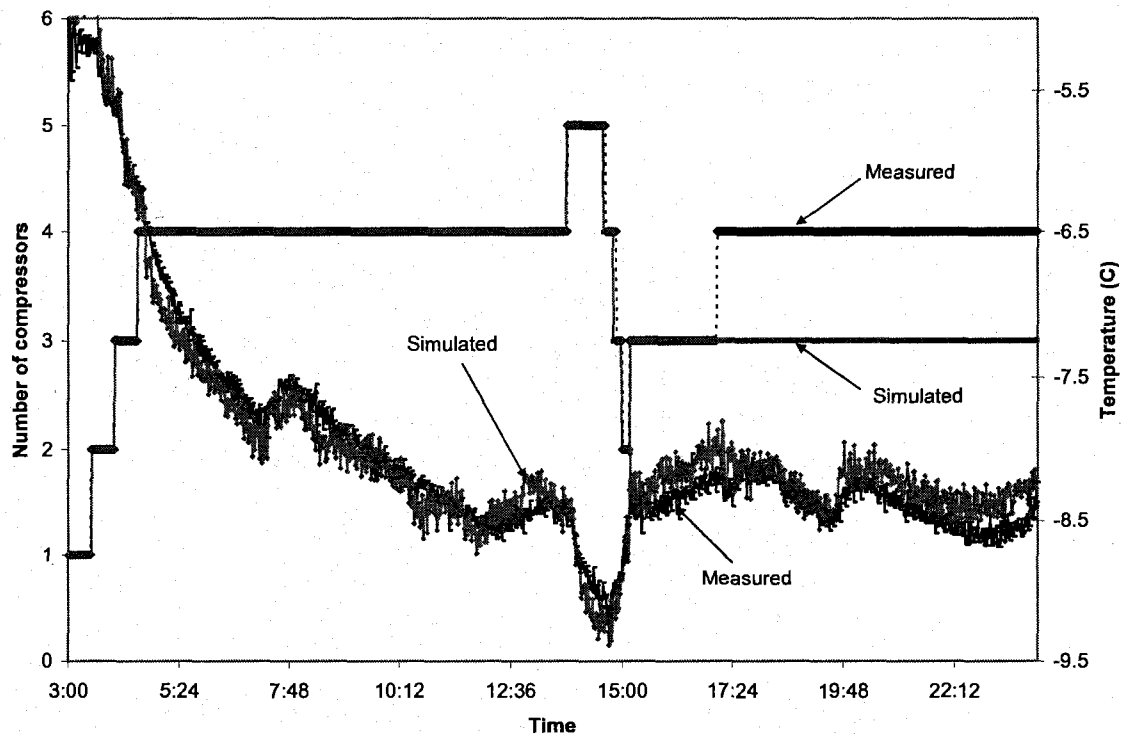
Figure 6.18: Number of compressors and return brine temperature. Measured versus simulated results on March 16th, 2006

At the start-up, the controller switches on one compressor every 30 minutes until the return brine temperature reaches the set point. The simulated number of compressors in operation is equal to the measurements until about 17:00. At that time, the controller is supposed to start a compressor to reduce the return brine temperature; however, it does not. This error of the simulated controller is due to an overestimation of the return brine temperature by the slab model. The results of the controller model are compared with measurements from another day, chosen randomly, May 14th, 2006 (Figure 6.19).
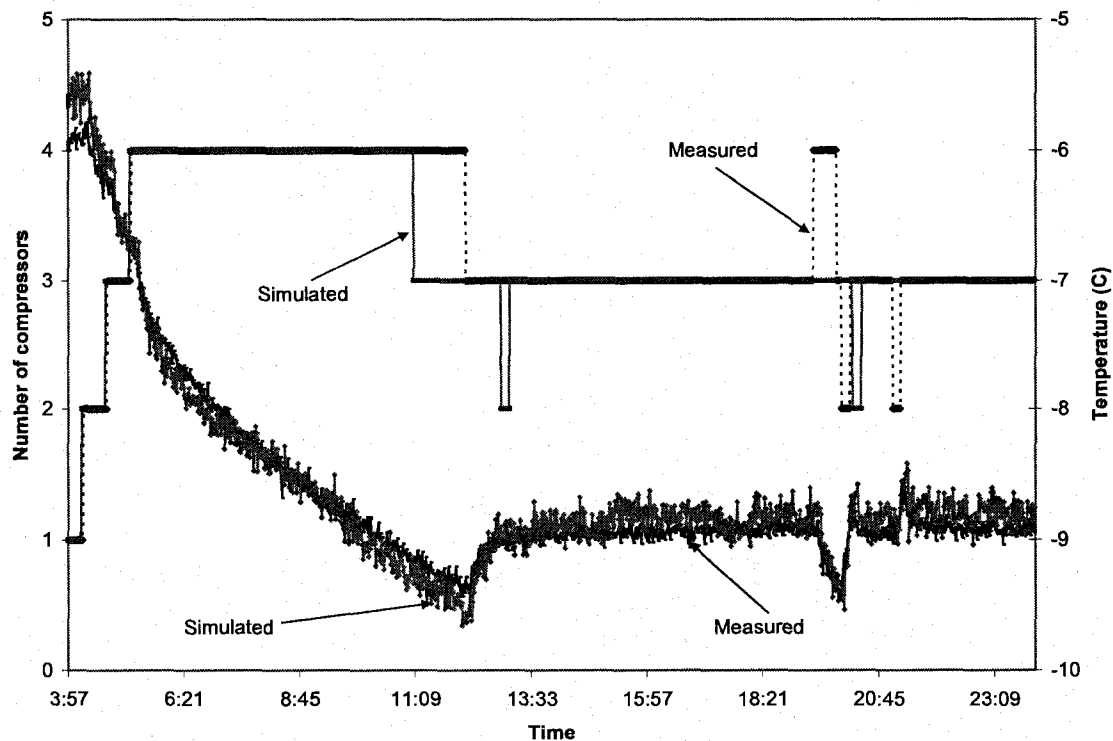
Figure 6.19: Number of compressors and return brine temperature. Measured versus simulated results on May 14th, 2006

On May 14th, the controller starts and stops compressors several minutes before or after these changes should occur. At 11:00, the controller model shuts off one compressor while the actual controller switches off one compressor around one hour later. At 12:50, the simulated controller turns off a compressor for about 10 minutes, while the system

maintains three compressors in operation. At 19:30, the controller model keeps the number of compressors constant while the actual controller turns on one compressor for 30 minutes because of a small increase of the return brine temperature. These results demonstrate that the accuracy of the controller is not very good. The principal factor affecting the errors in the estimation of the number of simulated compressors in operation is the small fluctuations of the return brine temperature. Because the controller mechanisms are based on a set of rules depending on the return brine temperature, variations near the limits defined lead to sudden changes in the number of compressors.

6.2.4.1 Noise reduction

Most measuring instruments are affected by noise at different frequencies. Thermocouples are particularly sensitive to noise because the signal output is generally low. Noise has an impact on the quality of measurements by adding significant oscillations when a series of measures are taken. Adequate instrument set-up can be useful to reduce it. It is generally convenient to employ a filter to remove the noise.

Low frequency noises have affected the collected data at Camillien-Houde ice rink for the ice, brine and refrigerant temperatures. In some cases, noise is responsible for oscillations of 0.1°C. Moreover, by using the correlation-based slab model to determine the return brine temperature, noise is amplified and reaches levels fluctuating around 0.3°C. This is shown in Figure 6.18 and Figure 6.19. The presence of noise in the brine temperature leads to wrong decisions by the controller. When the temperature fluctuates near the boundaries of the controller model (Figure 6.17), the noise generates instabilities for the controller. In order to reduce these interferences, a low-pass filter is applied.

6.2.4.2 Low-pass filter

Noise usually falls into the high frequency range of the signal. Hence, low-pass filters are appropriate to clean the signal from the high frequency components. A second order low-pass filter is considered in the current study. The transfer function between the signal and the output in the Laplace space is given by (Antoniou 1979):

$$H(s) = \frac{w_c^2}{s^2 \cdot T^2 + 2 \cdot \xi \cdot w_c \cdot s + w_c^2} \tag{6.28}$$

where $w_c = 2 \cdot \pi \cdot f_c$ (center frequency), f_c is the cut-off frequency, T is the period and ξ is the damping coefficient. Transforming the S space into the Z space leads to the following expression:

$$s = \frac{2}{T} \cdot \frac{(z-1)}{(z+1)} \tag{6.29}$$

Hence, the square of the S space is then given by:

$$s^2 = \frac{4}{T^2} \cdot \frac{(z-1)}{(z+1)} \tag{6.30}$$

Considering that the product of the damping coefficient (2ξ) is equal to $\sqrt{2}$, the transfer function of the signal in the Z space is given by the following relation:

$$\frac{O}{I} = \frac{w_c^2 \cdot T^2 z + w_c^2 \cdot T^2}{(w_c^2 \cdot T^2 + 1.41 \cdot 2 \cdot w_c \cdot T + 4) \cdot z - (4 + 1.41 \cdot 2 \cdot w_c \cdot T - w_c^2 \cdot T^2)} \tag{6.31}$$

or

$$\frac{O}{I} = \frac{a \cdot z + a}{b \cdot z - c} \tag{6.32}$$

where $a = w_c^2 \cdot T^2$, $b = w_c^2 \cdot T^2 + 1.41 \cdot 2 \cdot w_c \cdot T + 4$ and $c = 4 + 1.41 \cdot 2 \cdot w_c \cdot T - w_c^2 \cdot T^2$.

Rearranging Equation 6.32 brings to the following equation relating the filtered output signal (O_t) in terms of the three constants (a, b, c), the past input I_{t-1} and filtered output O_{t-1}, and the actual input I_t :

$$O_t = \frac{[a \cdot (I_t + I_{t-1}) + c \cdot O_{t-1}]}{b} \qquad (6.33)$$

Before applying Equation 6.33, parameters and constants have to be defined. The period T is equal to the interval separating two measurements (60 seconds), while the cutting frequency is usually defined with respect to the frequency of the collected measures ($f = 1/60$ Hz). However, noise in temperature measurements obtained from the correlation-based slab model have a higher frequency oscillating near $f_c = 0.15/60$ Hz. Hence, the center frequency, which is given by $w_c = 2 \cdot \pi \cdot f_c$, is equal to 0.016 Hz. Then, the three constants can be calculated and defined as followed: $a = 0.888$, $b = 7.546$ and $c = 5.769$.

Figure 6.20 presents the filtered return brine temperature against the temperature directly obtained from the correlation-based model of slab for March 16th, 2006. The low-pass filter presented in this section increases the smoothness of the temperature curve by eliminating the noise. This filter is used at the exit of the slab model in order to obtain less temperature fluctuations, for the benefit of the controller.
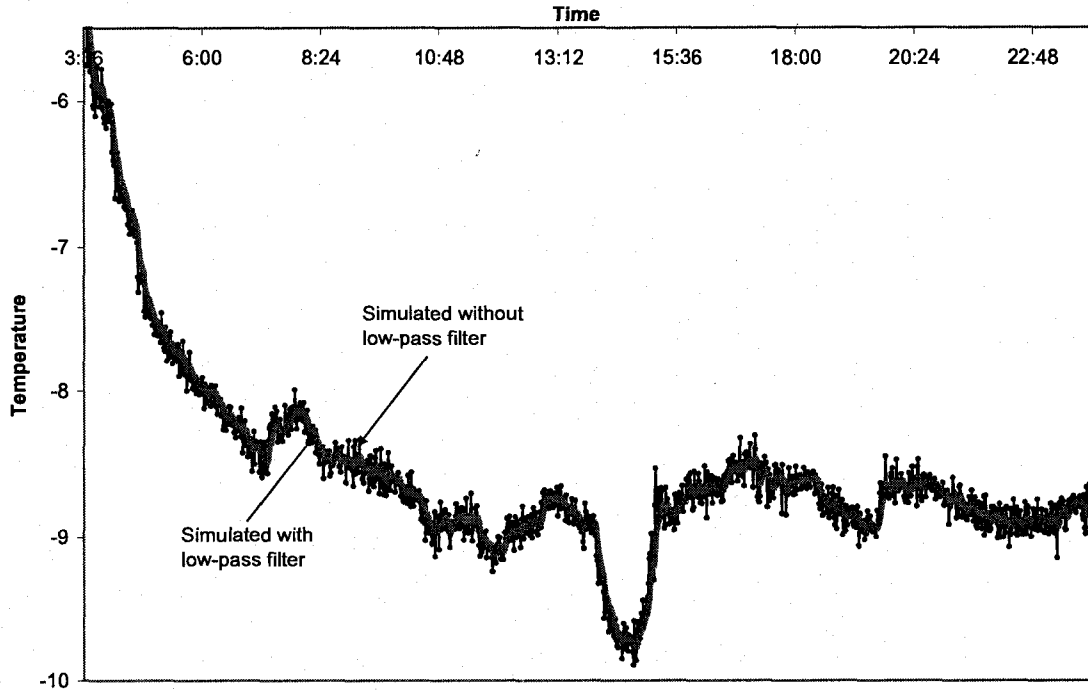
Figure 6.20: Return brine temperature simulated with the correlation-based model of slab with and without low-pass filter on March 16th, 2006

6.2.4.3 Results with low-pass filter

The controller model is tested using the predicted filtered brine temperature at the exit of the slab. Figure 6.21 plots the measured number of compressors in operation and the return brine temperature versus the simulated number of compressors in operation, and the filtered return brine temperature for March 16th, 2006. The agreement between the measured and simulated numbers of compressors in operation is increased when the simulated brine temperature is filtered. The change of number of compressors around 17:00 follows better the measurements than in the case without a filter (Figure 6.18). Similar results are obtained for May 14th (Figure 6.22). One compressor is turned off about 30 minutes earlier (around 11:30), and the simulated controller does not turn on and off a compressor around 19:30. On the other hand, by looking to the brine temperature, it is not possible to justify the decision of adding a compressor at 19:30.

157
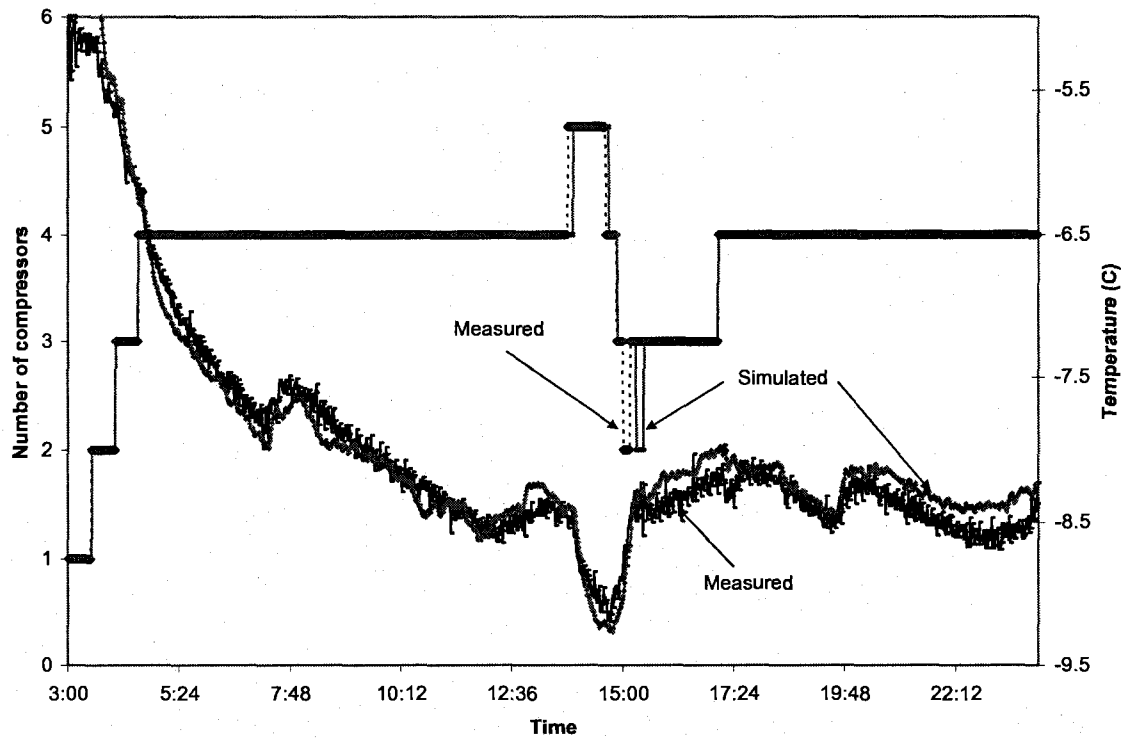
Figure 6.21: Number of compressors and return brine temperature. Measured versus simulated filtered results on March 16th, 2006
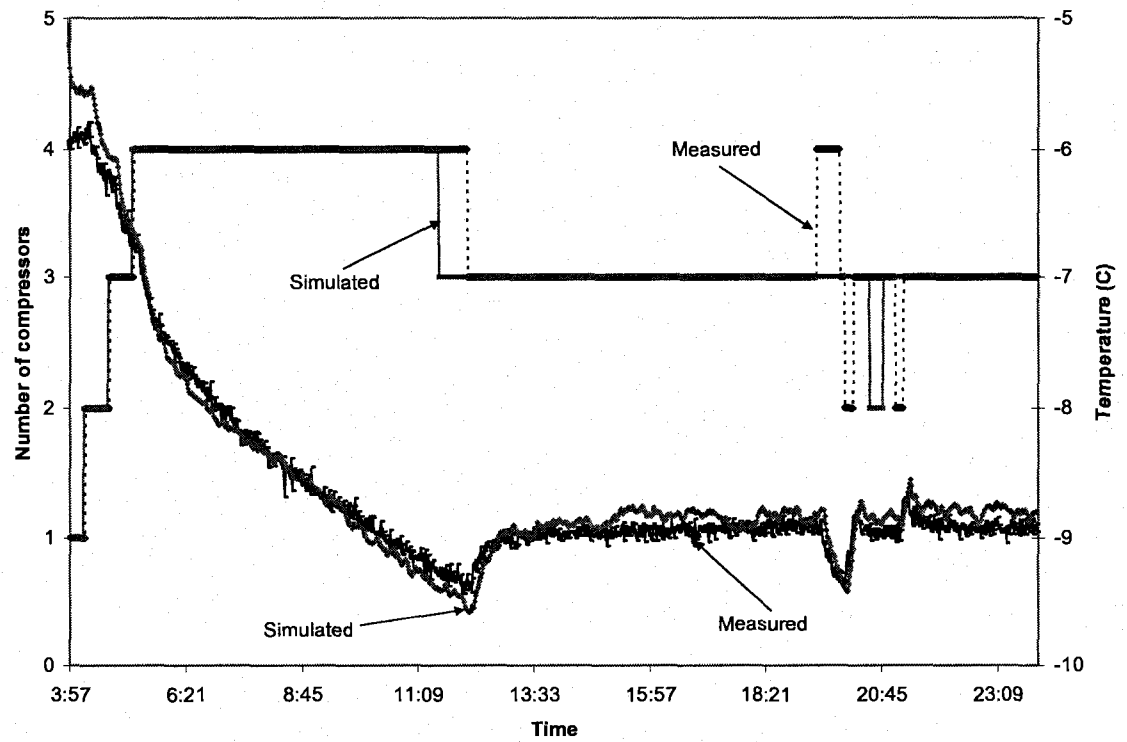
Figure 6.22: Number of compressors and return brine temperature. Measured versus simulated filtered results on May 14th, 2006

158

6.3 Conclusions

The analytical slab model developed has allowed to evaluate the difficulties in describing accurately the heat transfer occurring between the ice sheet and the brine. In fact, parts of the differences between simulated and measured temperatures are caused by assumptions used to describe the model. Actual heat exchanges are far more complex and would need a deeper analysis to be modeled analytically. Even though, the analytical model provides good results. The correlation-based model developed for the slab is more accurate because it is completely based on the experimental measurements. The statistical investigation of the correlation has demonstrated its validity. The correlation-based model has been tested using four different days of operation. The analytical and correlation-based models have been compared together by evaluating their ability to reproduce measured brine temperatures on several days. In light of the analysis, the correlation-based model has provided better agreement with the measurements. Therefore, due to its higher accuracy (average error of 0.21°C (2.48%) for analytical model versus 0.18°C (2.12%) for the correlation-based model), the correlation-based model will be used throughout the simulations of the refrigeration system presented in Chapter 7. The controller model presented is based on a set of empirical rules allowing to determine the number of compressors in function of the brine temperature exiting the slab. Combined with the low-pass filter, the results obtained have shown good accuracy. The low-pass filter and the controller model will be integrated into TRNSYS environment to perform the simulation of the refrigeration system. Therefore, both models will be programmed in C++ and exported as DLLs.

CHAPTER 7

SIMULATION OF THE ICE RINK REFRIGERATION

SYSTEM WITH TRNSYS ENVIRONMENT

In this chapter, the mathematical models of the components described in Chapters 4 and 6 are coupled in the TRNSYS environment. The overall flowchart is presented where the computer models are integrated. Particular programming characteristics of the software are discussed: variable *time* management and values retrieve. The procedure used to import a DLL is also presented. The compressor parameters identified with the Toolkit (Chapter 4) and the heat exchangers coefficients identified with the EES model (Chapter 5) are defined and used into the chiller proformas. Each new component is described by presenting the inputs, parameters and outputs used.

Open system simulations are performed by connecting all components together except the link between the chiller #2 model and the slab model. This arrangement allows to verify the performance of the mathematical model of the components. Closed system simulations are conducted by connecting all components together to verify the stability of the system. Simulated brine temperature and power demand are compared for both simulations. Finally, the heat recovery from the condenser is estimated. The reduction of electricity use for sanitary hot water by using the heat recovered from the condenser is estimated along with the corresponding reduction of equivalent CO_2 emissions.

7.1 Modeling approach with TRNSYS

A component approach is used for the simulation of the refrigeration system. Each component is described by a mathematical model, and all components are linked together by the corresponding energy and mass transfer equations. The complete refrigeration system is modeled based on the components available in the library of TRNSYS environment and by integrating new developed components presented in previous chapters: chillers, slab, and controller.

7.1.1 TRNSYS structure

The modular structure of TRNSYS is the key point of its flexibility. Each component is independent of the kernel and the source code is provided to the user if modifications are necessaries to fit the user's needs. The dynamic link library (DLL) based structure allows users to integrate new component to the existing library by using any common programming languages (C, C++, Fortran, etc.). TRNSYS facilitates the integration of new components by generating a Fortran or a C++ template and a compiler project. The TRNSYS project includes all the settings required to generate a DLL.

7.1.2 TRNSYS overview

The main visual interface of TRNSYS is called the Simulation Studio. A project is setup by dragging iconographical representations of components, referred as Types, from the components library into the Simulation Studio and connecting them together. The Studio creates and saves a project as a Trnsys Project File (*.tpf). Graphical connections between components give an easy overview of the interactions between the

selected Types. The mathematical model of each Type is incorporated into the TRNSYS simulation engine by a set of grey-boxes called Proformas. Proformas contain a brief description of the components by identifying the inputs, outputs and parameters. They establish the link between the user and the source code of the component. Parameters are inputs that do not change with time, while inputs are referred as time dependent variables. All outputs are assumed to be time dependent. When the user runs a simulation, the Studio creates a TRNSYS input file (text file) which contains all the information regarding the simulation. Users can control global simulations parameters (start time, stop time, time step, tolerances, etc.) by accessing to the Control Cards menu. The Simulation Studio also includes an output manager which facilitates the control of the variables printed and integrated.

7.1.3 TRNSYS framework for the simulation

The flowchart presented in Figure 7.1 helps identifying the variables and parameters used to drive the simulation. The inputs are based on the collected data from the monitored ice rink, while parameters are used for the compressors and the heat exchangers to characterize their behaviours. The compressor and heat exchangers coefficients have been determined in Chapter 4 and Chapter 5, respectively.
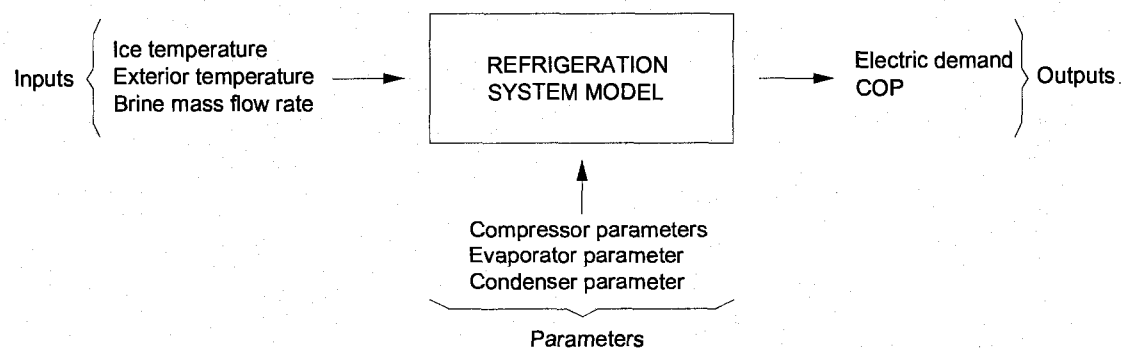
Figure 7.1: Flowchart for the simulation of the refrigeration system

Based on the inputs and parameters provided to the refrigeration system model, which includes the new components developed in this study and TRNSYS components, the temperature in key points of the refrigerant and brine circuits are estimated, and compressor and brine pump power input are calculated. The power used by the condensers is considered to be constant because the control of the fans is not modeled. The flowchart of the computer model of the refrigeration system is presented in Figure 7.2. The brine temperature is written as *Tb*, and the number of compressors in operation is represented by *n*.
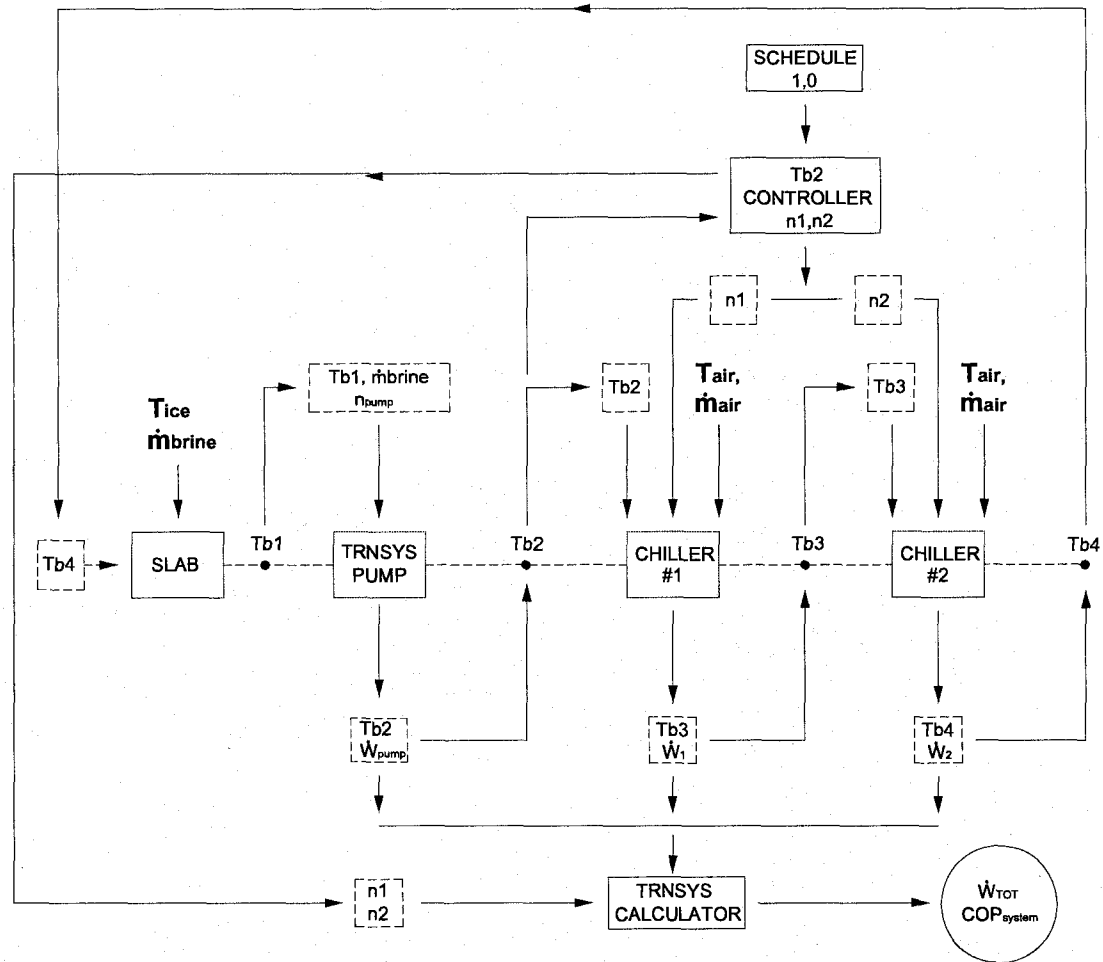
Figure 7.2: Flowchart of the simulation with TRNSYS

The input values from the monitored ice rink are in bold, while internal variables exchanged between the components are written inside dashed boxes. The components used to simulate the refrigeration system are in solid boxes. The outputs are encircled. Among all refrigeration system components, the pump and the calculator are used from the TRNSYS library while the rest of the components have been developed in the present study. The measured ice temperature and brine mass flow rate along with the predicted inlet brine temperature ($Tb4$) are provided to the slab model, which calculates the return brine temperature ($Tb1$) from the slab. This temperature is then used, along with the pump efficiency and the brine mass flow rate, by the TRNSYS pump model to calculate the brine temperature entering the first chiller ($Tb2$). The chillers model uses the predicted inlet brine temperatures ($Tb2$ and $Tb3$), and the measured air temperature along with the air mass flow rate to obtain the exit brine temperatures ($Tb3$ and $Tb4$) and the electric demand ($\dot{W}_1$ and $\dot{W}_2$). The chillers are connected in series on the brine side, and they are controlled by a controller that determines the number of compressors in operation ($n1$ and $n2$) for each chiller. In addition, the controller is also driven by a schedule which decides whether the refrigeration system is in operation or not. At the exit of the second chiller, the calculated brine temperature ($Tb4$) is returned to the slab to complete the refrigeration loop. Finally, the total electric input to chillers ($\dot{W}_{TOT}$) and the coefficient of performance (COP) of chillers are calculated in the Type called calculator.

7.1.4 Creating new components

The TRNSYS modular structure allows the user to integrate self-written components into the standard library. Compared to other simulation software, TRNSYS

has the particularity that the kernel does not impose any hierarchy between the Types called during a simulation. The kernel treats equally the new components and the standard components: they are linked to the kernel as external DLLs. At the beginning of each simulation, TRNSYS loads all files with an extension *.dll corresponding to the Types used in the project. Thus, the user only needs to drop the new Type into the appropriate directory to be integrated into TRNSYS. The source code related to a DLL has to follow a particular syntax in order to be compatible with TRNSYS. Understanding the TRNSYS manipulations can be time consuming due to the kernel subroutines that are called by the components.

This step can be avoided by directly using the New Component menu that is accessible in TRNSYS. This feature begins with the creation of a Proforma for the new component. The user defines the inputs, parameters and outputs that will be manipulated by the component. Then, the Studio: (1) creates a Fortran or C++ skeleton for the new Type; and (2) generates a project accessible by using Compaq Visual Fortran or Microsoft Visual C++ compilers; the project includes all the required TRNSYS settings to build the external DLL, along with the inputs, outputs and parameters defined in the Proforma. Then, the user writes the source code corresponding of the new component. The project must be compiled in order to build and export the external DLL into the right directory. The new component is accessible throughout the standard library components of TRNSYS and can be dragged and dropped into the studio as other components.

At the beginning of the study, new components of the refrigeration system, based on ASHRAE Toolkit, where developed in Fortran since the routines of Toolkit are

written in this programming language as well as the TRNSYS kernel. TRNSYS manual ensures that the Fortran projects generated with the Studio are compatible with the Compaq Visual Fortran 6.6 (CVF). However, this compiler is discontinued and was replaced by the Microsoft Power Station (MPS), also discontinued, and ultimately by the Intel Visual Fortran (IVF). The migration path between the compilers is complex and an excellent knowledge of Fortran language is necessary. The quality of the migration depends upon different factors such as the internal settings, the version of IVF used and the complexity of the project. The MPS compiler was not able to compile the CVF workspace (*.dsp) because of several linking issues. After this, the migration from the Compaq Visual Fortran to the Intel Visual Fortran was tested. The IVF does not have a direct interface. It is accessible using Microsoft Visual Studio .NET (MVS). The IVF Version 9.1 was used with the MVS 2002 to convert the CVF workspace (*.dsp). This combination also engendered different conversion and linking problems during the compilation of the project. The difficulties encountered to access and convert the CVF project skeleton into a MPS or IVF workspace were time consuming and frustrating. Finally, the new component models where re-written in C++. Therefore, a C++ skeleton was generated in the Studio for each new component (chillers, slab, and controller) and a Microsoft Visual C++ Version 6.0 (MVC) compiler was used to open and compile the workspace files (*.dsw). Compilation of the project with the added code was successful, and DLLs where exported to the corresponding directory without any problem. It is important to note that the problems were met during the development of DLLs for individual new components. No attempt was made to generate the whole DLL of TRNSYS augmented with the new components.

7.1.5 Special programming considerations

Special precautions are necessary when writing new components for TRNSYS. Since simulations are performed for certain time intervals, it is essential to understand how TRNSYS manages the value of time throughout iterations. The variable time is used by both TRNSYS kernel and by the self-written components, thus a perfect agreement of its value is necessary.

7.1.5.1 Managing the variable *time*

When performing simulations in TRNSYS, the user is prompted to enter, in the Control Cards menu, the starting and the ending time along with the time step of the simulation. Time can be specified in seconds, hours, days or any other unit defined by the user. In the current application, simulations are performed using 60 second time step to be consistent with the interval at which the measurements were collected at the Camillien-Houde ice rink. However, even if the time step of simulation is specified in seconds or minutes, the TRNSYS *time* variable is always defined in fractions of hours. Handling values of time in fraction of hours can be confusing. Consequently, a variable *time* in seconds is used by the new components, which were created and incorporated in the Studio. To do this, each new time dependent component calls an external file containing the value of *time* in seconds for each time step. This method permits to simplify the time management by components and reduce the possibility of errors.

7.1.5.2 Storing and retrieving values

Another characteristic of TRNSYS is the method employed by the software to store and recall values between the time steps. In the conventional programming

languages, values can be stored into a user defined array. In TRNSYS special precautions are necessary to ensure proper manipulations of values between iterations. A subroutine named *getStorageVars* is used by TRNSYS to retrieve stored values that are needed in calculations. This subroutine must be called before the component. During calculations, variables can be stored by the subroutine *setStorageVars*. Therefore, by using these two subroutines, values can be stored and recalled at each time interval. However, this procedure does not allow the control of number of times a variable is retrieved or on how long the component should wait before retrieving a variable. This major inconvenient is in fact a limitation for the user who needs to handle variables through time.

In order to control the time separating each variable recall, Type 93 of the standard component library is used. This component allows recalling variables previously calculated at different user-defined time steps. Type 93 is also very useful in adding time delays to components that are sensitive to input changes or that are unstable. This component is widely used throughout the simulation of the refrigeration system to recall values of Boolean variables and to store variables during certain time periods.

7.2 New components

New components for the ice rink refrigeration system are created and added to the Simulation Studio. For each component, a Proforma containing the corresponding inputs, outputs and parameters is created. Then, a skeleton containing all the required settings is built and compiled using the C++ language. A Type number is assigned to each component following the TRNSYS nomenclature. Therefore, in order to avoid conflicts with the existing components, a number in the [201; 300] range is assigned to each

component. Several components were written during the development of the refrigeration system model. However, throughout different analyses, simplifications where possible, and the number of components was reduced. This section presents the variables defining the Proformas of each new component created.

7.2.1 Type 203 - Chiller

Based on the modified chiller model of the ASHRAE Toolkit (routine PISSIM1) described in Chapter 4, the new Type 203 for this component is created in TRNSYS. The total power input to all chillers is determined by multiplying the power of one compressor by the number of compressors in operation for the corresponding chiller, which is determined by the controller. The Proforma of Type 203 includes seven inputs. Six of them are presented in Table 7.1.

Table 7.1: Inputs for Type 203 - Chiller

Given name	Dimension	Description	Units	Default value
Mbrine	Mass flow	Mass flow rate of brine circulated through the evaporator	kg/s	31.32
Mair	Mass flow	Mass flow rate of air circulated though the condenser	kg/s	8.22
Tbrine_in	Temperature	Temperature of the brine entering the evaporator	°C	-5
Tair_in	Temperature	Air temperature entering the condenser	°C	5
Ncomp	Dimensionless	Number of compressors in operation	-	1
QcdG	Power	Guessed capacity of the condenser	W	80,000

As already discussed in Chapter 3, the capacity of the five compressors are not equal to each other. Based on the heat balance on the brine side, the capacity difference between compressors operating in chiller #1 and chiller #2 is important. Therefore, the capacity of each compressor is defined separately for chiller #1 (Qev1) and chiller #2 (Qev2) (Table 7.2).

Table 7.2: Capacity input for Type 203 – Chiller

Given name	Dimension	Description	Units	Default value
Qev1	Capacity	Capacity of one compressor for chiller #1	W	55,000
Qev2	Capacity	Capacity of one compressor for chiller #2	W	41,000

Type 203 calculates the power input to one compressor in operation for the specified chiller, the brine temperature leaving the evaporator, the leaving air temperature from the condenser, and the COP of the system (Table 7.3). It is important to mention that this COP does not consider the power input to condensers and brine circulating pump; therefore, it does not reflect the efficiency of the entire refrigeration system. It is the COP of chillers in operation. Furthermore, in order to validate the chiller model, the mass flow rate of refrigerant is calculated, hence agreement can be verified with field measurements.

Table 7.3: Outputs from Type 203 - Chiller

Given name	Dimension	Description	Units	Default value
Mref	Mass flow	Refrigerant mass flow	kg/s	-
Wcomp	Power	Compressor power input	W	-
COP	Dimensionless	Coefficient of performance	-	-
Tair_out	Temperature	Air temperature leaving the condenser	°C	-
Tbrine_out	Temperature	Brine temperature leaving the evaporator	°C	-

Table 7.4 presents the parameters used by Type 203. Parameters of heat exchangers are identified in Chapter 5 based on the EES model while compressor parameters are identified by means of the ASHRAE Toolkit routines in Chapter 4. Several parameters are also necessary to establish the properties of refrigerant R-22.

Given name	Dimension	Description	Units	Default value
AUev	Heat transfer coefficient	Evaporator overall heat transfer coefficient (latent) (Chapter 5)	W/°C	13,238
AUcd	Heat transfer coefficient	Condenser overall heat transfer coefficient (latent) (Chapter 5)	W/°C	4,862
DTsupheat	Temperature	Superheating level in the evaporator	°C	6
DTsubcool	Temperature	Sub-cooling level in the condenser	°C	12.5
Qev_sens	Capacity	Average sensible heat transfer in the evaporator (Chapter 5)	W	1,100
Qcd_sens	Capacity	Average sensible heat transfer in the condenser (Chapter 5)	W	20,500
Losses	Power	Constant part of the electromechanical losses	W	6,330.472
Alpha	Dimensionless	Loss factor defining another electromechanical loss	-	-0.0678
Cf	Dimensionless	Clearance factor of the compressor		
VsFL	Volumetric flow	Geometric displacement of the compressor	m³/s	0.045147
CpBrine	Specific heat	Brine specific heat	J/(kg°C)	2,957
CpAir	Specific heat	Air specific heat	J/(kg°C)	1,005
CpRefVap	Specific heat	Specific heat of vapour refrigerant	J/(kg°C)	710.4
CpRefLiq	Specific heat	Specific heat of liquid refrigerant	J/(kg°C)	1,144
To	Temperature	Reference temperature	K	273.15
hfo	Enthalpy	Enthalpy of saturated liquid of refrigerant	J/kg	200,000
hfgo	Enthalpy	Enthalpy of vaporization of refrigerant	J/kg	204,590
R	Dimensionless	Gas constant	J/(kgC)	96.1426
Zeta	Dimensionless	Compressibility factor	-	0.93
Acl	Dimensionless	Clausius-Clapeyron constant	-	15.07
Bcl	Dimensionless	Clausius-Clapeyron constant		-2,421.94

7.2.2 Type 205 - Controller

The empirical rules used by the controller are based on the return brine temperature leaving the slab. Type 205 uses a combination of inputs at current and past time steps. In order to recall previous values, two Type 93 components are connected to the controller. The first Type 93 is used to recall values at one time step, while the second one is used to conserve information during 10 minutes. More details on the connections between Type 93 and Type 205 are provided in section 7.3. Table 7.5 presents the inputs used by this component. Refer to Chapter 6 for an explanation on the Boolean variables used by the controller.

Table 7.5: Inputs for Type 205 - Controller

Given name	Dimension	Description	Units	Default value
Tbrine_outslab_t	Temperature	Brine temperature at the exit of the slab	°C	-5
Tbrine_outslab_t1 to Tbrine_outslab_t10	Temperature	Brine temperature at one to ten minutes time step prior to the current time	°C	-5
Ncomp_tot	Dimensionless	Number of compressors in operation at one time step prior to current time	-	1
wait1 to wait 10	Boolean	Values of wait at one time step prior to the current time	-	0
out	Boolean	1 minute time step prior the current time	-	0
ok1-ok2	Boolean	Value of ok at one and two time step prior current time	-	0
nogo1-nogo2	Boolean	Value of nogo one and two time step prior current time	-	0
Time1	Time	Actual time t	s	0

The main outputs of Type 205 are the number of compressors in operation of chiller #1, chiller #2, and total of the system (Table 7.6). In addition, a Boolean variable is exchanged to identify if the chillers are in configuration of chiller #1 or chiller #2. The others outputs are internally used by the routine. The controller dead bands are defined as parameters in the Proforma (Table 7.7). The upper bound, the lower bound and the lower bound 2 are specified as parameters following the analysis presented in Chapter 6.

Table 7.6: Outputs from Type 205 - Controller

Given name	Dimension	Description	Units	Default value
Ncomp_chill1	Dimensionless	Number of compressors operating in chiller 1	-	1
Ncomp_chill2	Dimensionless	Number of compressors operating in chiller 2	-	0
Ncomp_tot	Dimensionless	Total number of compressors in operation	-	1
Chill1	Dimensionless	Identification of chiller #1	-	1
Chill2	Dimensionless	Identification of chiller #2	-	2
wait	Boolean	Value of variable wait for resurfacing	-	0
out	Boolean	Value of out, if the upper bound is crossed	-	0
ok1	Boolean	Value of ok1	-	0
nogo1	Boolean	Value of nogo1	-	0

Table 7.7: Parameters for Type 205 - Controller

Given name	Dimension	Description	Units	Default value
Upper_bound	Temperature	Upper bound of the dead band	°C	-8.30
Lower_bound	Temperature	Lower bound of the dead band	°C	-9.00
Lower_bound2	Temperature	Lower bound 2 below the dead band	°C	-9.20

7.2.3 Type 207 - Analytical slab model

The analytical slab model is accessible in TRNSYS as Type 207 (Table 7.8). This component uses the ice temperature and the brine temperature entering the slab to determine the return brine temperature. The coefficients of the differential equation are calculated internally by the routine. In order to consider the ice resurfacing, the component uses several inputs provided by two Types 93. More details on the connections are provided in the next section 7.3. Type 203 does not use any parameter, because all the variables used are function of time.

Table 7.8: Inputs for Type 207 – Analytical slab model

Given name	Dimension	Description	Units	Default value
Time1	Time	Current time in seconds	s	0
Tice_t	Temperature	Temperature of ice at current time	°C	-5
Tice_t1 and Tice_t2	Temperature	Ice temperature at one and two time step prior the current time	°C	-5
Tbrine_in_slab_t	Temperature	Brine temperature entering the slab at current time	°C	-5
Tbrine_in_slab_t1 and Tbrine_in_slab_t2	Temperature	Brine temperature entering the slab at one and two time step prior the current time	°C	-5
Tice_stdby	Temperature	New ice temperature after resurfacing	°C	0
Tice_surf	Temperature	Ice temperature at one time step prior to resurfacing	°C	0
Tslab_t1	Temperature	Slab temperature at one minute prior to current time	°C	0
Surf1 to Surf20	Boolean	Variable used to detect ice resurfacing	-	0

The outputs of analytical slab component consist of the brine temperature exiting the slab and the different variables stored in Type 93 (Table 7.9). Refer to Chapter 6 for a more complete description of the variables used by this component.

Table 7.9: Outputs from Type 207 - Analytical slab model

Given name	Dimension	Description	Units	Default value
Tbrine_outslab_t	Temperature	Current brine temperature at the slab exit	°C	-5
Surf	Boolean	Value of Surf (1 if resurfacing, else 0)	-	0
Tice_stdby	Temperature	Ice temperature if resurfacing	°C	-5
Tice_t	Temperature	Ice temperature at current time	°C	-5
Tice_surf	Temperature	Ice temperature before resurfacing occurs	°C	-5
Tslab_t	Temperature	Slab temperature at current time	°C	-50

7.2.4 Type 208 - Correlation-based slab model

The correlation-based slab model is simpler than Type 207 and requires fewer inputs (Table 7.10). Type 208 determines the brine temperature leaving the slab in terms of the ice temperature and the brine temperature entering the slab. Table 7.11 presents the coefficients of the correlation-based slab model, as calculated in Table 6.3. Table 7.12 shows the only output provided by Type 208, which is the brine temperature leaving the slab, also called return brine temperature.

Table 7.10: Inputs for Type 208 – Correlation-based slab model

Given name	Dimension	Description	Units	Default value
Tbrine_in_slab	Temperature	Current brine temperature entering the slab	°C	-5
Tice	Temperature	Current ice temperature	°C	-5

Table 7.11: Parameters for Type 208 – Correlation-based slab model

Given name	Dimension	Description	Units	Default value
A	Dimensionless	Coefficient of the correlation	-	0.708352
B	Dimensionless	Coefficient of the correlation	-	-0.127861
C	Dimensionless	Coefficient of the correlation	-	0.0166354
D	Dimensionless	Coefficient of the correlation	-	0.00484019
E	Dimensionless	Coefficient of the correlation	-	-1.40321

Table 7.12: Output from Type 208 – Correlation-based slab model

Given name	Dimension	Description	Units	Default value
Tbrine_out_slab	Temperature	Brine temperature exiting the slab	°C	-5

7.2.5 Type 212 - Low-pass filter

Type 212 reduces the variation of the brine temperature leaving the slab to increase the accuracy of the controller (Table 7.13). The second order low-pass filter process the signal using brine temperature at the current and previous time leaving the slab. Refer to Chapter 6 for the explanation of the equations used by the low-pass filter. Table 7.14 presents the parameters while Table 7.15 shows the output of the component.

Table 7.13: Inputs for Type 212 – Low-pass filter

Given name	Dimension	Description	Units	Default value
Time1	Time	Current time	s	0
Tbrine_outslab	Temperature	Current ice temperature	°C	-5
Tbrine_outslab_t1	Temperature	Brine temperature leaving the slab one time step prior current time	°C	-5
Tbrine_outslab_filter_t1	Temperature	Brine temperature leaving the filter one time step prior current time	°C	-5

Table 7.14: Parameters for Type 212 – Low-pass filter

Given name	Dimension	Description	Units	Default value
T	-	Period	s	60
Fc	-	Cut-off frequency	Hz	0.0025

Table 7.15: Output for Type 212 – Low-pass filter

Given name	Dimension	Description	Units	Default value
Tbrine_outslab_filter	Temperature	Brine temperature filtered	°C	-5

7.3 Connecting components

Components are connected together using the Link tool from the TRNSYS studio. The Link tool allows to connect components by connecting outputs of one component to inputs of another component. Careful attention is necessary when connecting components with Type 93 for data retrieving. Confusions regarding the information provided by this component can lead to errors during the simulation.

7.3.1 Connecting Type 203 - Chiller

In order to respect the actual configuration of the refrigeration system, two Chillers (Type 203) are connected in series on the brine side (Figure 7.3). The brine temperature and mass flow rate are exchanged between these two Types.
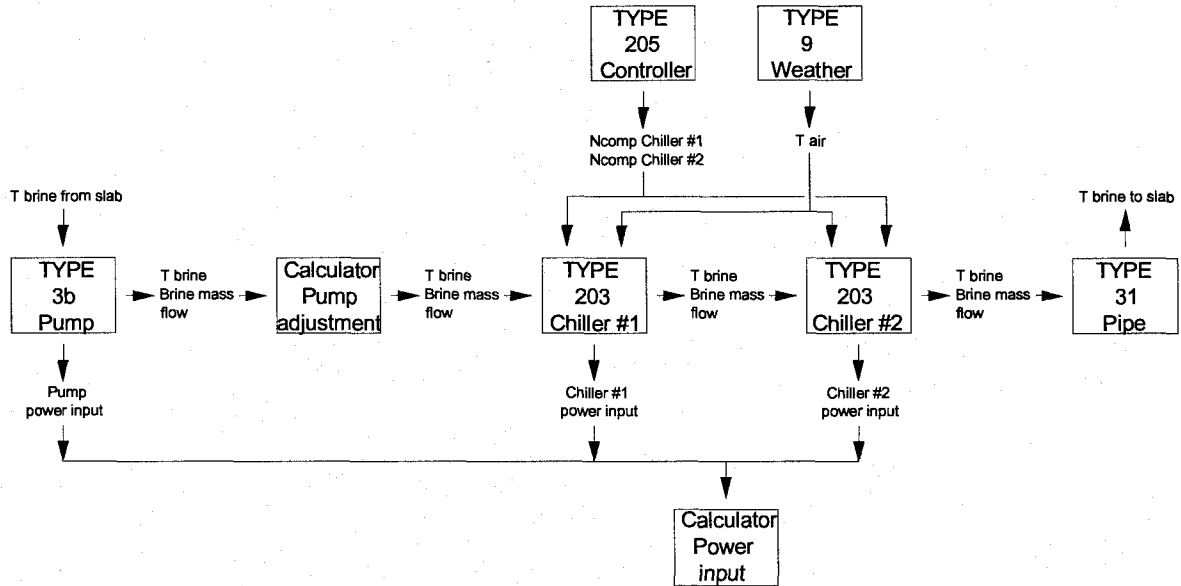
Figure 7.3: Connections for Type 203 - Chiller

The 12.5 kW brine pump is simulated by using Type 3b from the standard library component. The pump is controlled by two parameters: the conversion coefficient and the power coefficient. The conversion coefficient (f) is the fraction of pump power converted into fluid thermal energy. Due to mechanical losses, the brine temperature increases while flowing through the pump. This is calculated in terms of the conversion coefficient:

$$T_{out,pump} = T_{in,pump} + \frac{(f \cdot Power)}{\dot{m}_{brine} \cdot c_{p,brine}} \tag{7.1}$$

The power coefficient is employed to specify a non-linear relationship between pump power input and brine flow rate. Since the pump operates at constant speed, this

176

coefficient is set to one. In order to take into account some small heat gains occurring between the exit of the pump and the inlet of chiller #1, a calculator (a special Type of TRNSYS) is utilized to increase the brine temperature by 0.1°C.

The controller output (Type 205) is connected to both chillers to control the number of compressors in operation. Type 9 (data reader) is used to read the exterior air temperature from the weather file, which was developed by CANMET. The chiller model uses the exterior air temperature to calculate the condensing temperature and the temperature of refrigerant leaving the condenser.

At the exit of chiller #2, the brine circulates through a pipe before passing below the slab. The brine mass flow rate and temperature are used as inputs in Type 31 to model the pipe connecting the chiller and the slab. A heat transfer coefficient equal to 3,000 J hr^{-1} m^{-2} °C^{-1}) is used to simulate the thermal losses to the environment. The use of Type 31 helps reducing the temperature fluctuations in the brine loop. The total power input to the refrigeration plant is computed by a calculator which adds the power input to the pump, chiller #1 and chiller #2.

7.3.2 Connecting Type 205 - Controller

The controller (Type 205) decisions are based on the brine temperature at the exit of the slab and the time of simulation. Two Types 93 are used to recall past values of internal variables. More details on the connections between the components used with Type 205 are presented in Figure 7.4.

TYPE
9
Time1

wait

Time1

TYPE
93
10 min. recall

wait1 to
wait10

TYPE
205
Controller

Ncomp total
Ncomp chiller #1
Ncomp chiller #2

TYPE
93
1 min. recall

Ncomp tot.
out, ok1, ok2
nogo1, nogo2
Time2, Time3

Ncomp tot.
out, ok1, nogo1
Time2, Time3

T brine (t)
to (t-8)

TYPE
93
8 min. recall

T brine (t-45)

TYPE
93
45 min. recall

T brine
from slab
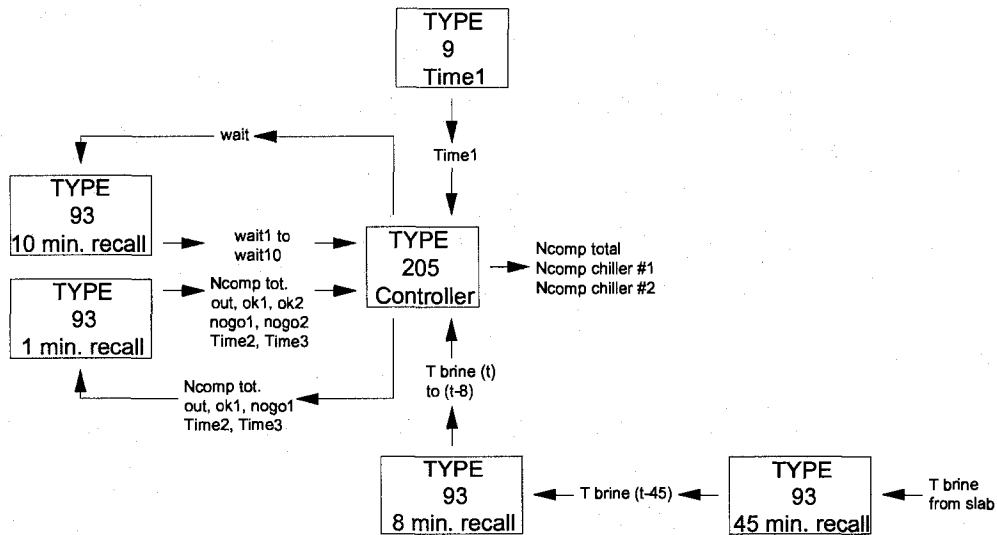
Figure 7.4: Connections for Type 205 – Controller

Internal values used by the controller are handled by one Type 93 using a ten minute delay and another Type 93 using a one minute delay. Details on the interval values manipulated by the controller are provided in Chapter 6. Analysis of measurements shows that the controller decisions are delayed by 45 minutes when the return brine temperature crosses a boundary. In order to take into account this delay, the return brine temperature used by the controller is delayed by 45 minutes. The controller decisions are based on the delayed return brine temperatures at the current time (t) and on the temperatures of the eight minutes before the current time. Type 9 (data reader) is used to read the values of the variable *time* from an external file. The values of *time* are in seconds and they increase by 60 seconds at every time step. Time is used by the controller to determine if the system is in the start-up period.

7.3.3 Connecting Type 207 - Analytical slab model

The analytical slab model (Type 207) determines the brine temperature at the exit of the slab in function of the ice temperature and the inlet brine temperature (Table 7.8). Because the analytical model resolves a differential equation, the value of *time* is provided in seconds. To do this, Type 9 (Data reader) reads the value of *time* from an external file. Details on the connections of Type 207 are presented in Figure 7.4.
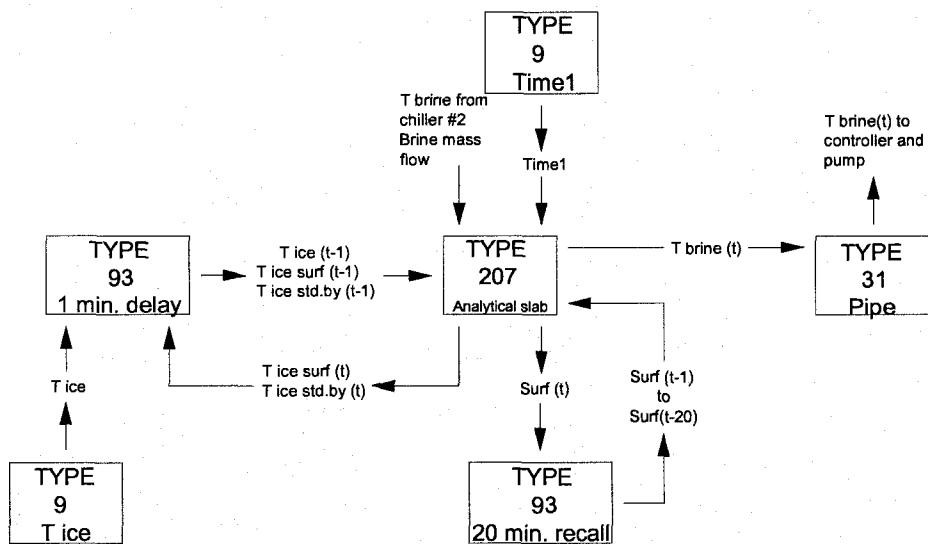
Figure 7.5: Connections for Type 207 – Analytical slab

Type 9 is also used to read the ice temperatures from an external file. This Type is connected to Type 93 to provide the current and past values of the ice temperature to the slab model. Type 93 also handles two variables of Type 207, in order to store, during one time step, the values of the ice temperature if resurfacing occurs (*Tice,surf*) and the new ice temperature increased after the resurfacing (*Tice,std.by*). Another Type 93 is employed to store the value of the variables *Surf1* to *Surf20* during twenty minutes. When resurfacing occurs, the variables *Surf1* to *Surf20* are equal to one and the model uses the modified constants to consider the effects of resurfacing. At the exit of the slab, the brine

passes through a pipe before being pumped to the evaporator of chiller #1. The pipe

between the slab and the evaporator is modeled by Type 31. A heat transfer coefficient

equal to 3,000 J hr^{-1} m^{-2} °C^{-1} is used.

7.3.4 Connecting Type 208 and Type 212 - Correlation-based slab model and low-pass filter

The correlation-based slab model (Type 208) uses the supply brine temperature

and mass flow rate provided by chiller #2 and the ice temperature to determine the return

brine temperature from the slab. The input brine temperature is simulated while the ice

temperature is red from a file containing the measured ice temperature. Figure 7.6 shows

the details of the connections between the components.
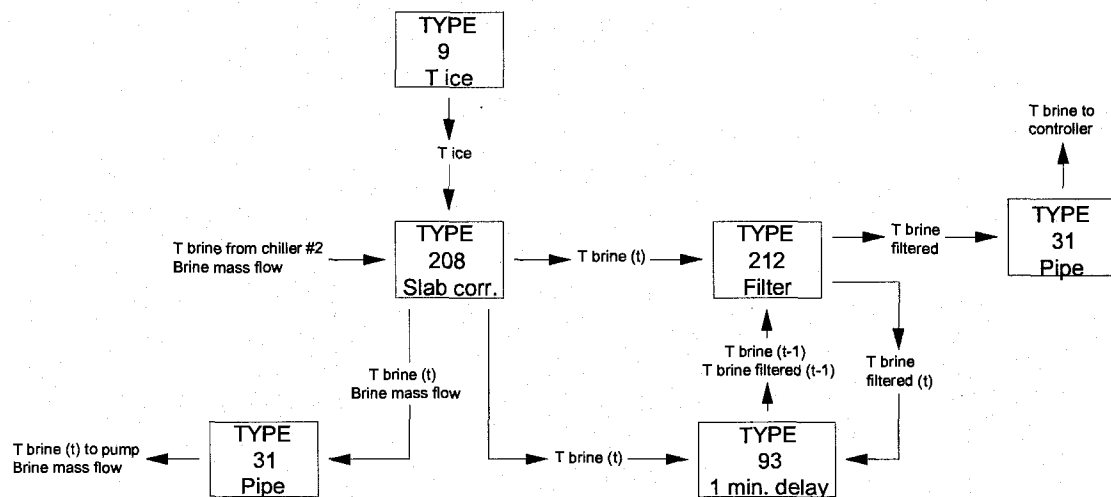
Figure 7.6: Connections for Type 208 and Type 212 – Slab correlation and low-pass filter

The slab uses as inputs the brine temperature at the exit of chiller #2 and the ice

temperature. Type 9 (data reader) is utilized to read the ice temperatures from an external

file. At the exit of the slab, the brine passes through a pipe before being pumped to the

evaporator. A heat transfer coefficient equal to 3,000 J hr^{-1} m^{-2} °C^{-1} is used to simulate the thermal losses to the environment in Type 31. The brine temperature calculated by the slab is employed by the controller to determine the number of compressors in operation. However, this brine temperature is filtered by Type 212 before being used by the controller. Type 212 requires the current and precedent brine temperatures calculated by Type 208 and the precedent brine temperature filtered to obtain the current brine temperature filtered. Current brine temperatures are stored during one time step by Type 93 before being provided to Type 212. The filtered brine temperature also passes through a pipe before being analyzed by the controller. A heat transfer coefficient equal to 3,000 J hr^{-1} m^{-2} °C^{-1} is used as well.

7.4 Simulation of the refrigeration system

Once the components are connected together in the Studio, the simulation can be performed. Depending on the user's preferences, outputs can be printed to the screen or/and into an external file. Proper connections are necessary between the component outputs variables and the appropriate plotter or/and printer (Type 65, Type 25). By turning to the Output manager, the organization of simulation results is facilitated. This feature is particularly useful when several components are interconnected in Studio. A friendly-user interface summarizes the connections and the possible outputs available.

Tolerances must be defined in the Control Cards menu to control the iterations. The following tolerances are used throughout the simulations: tolerance integration = 0.001 and tolerance convergence = 0.01. The Successive method is used as internal solver

method. The user must set the limits on the number of iterations that TRNSYS can perform during a time step before it determines that the differential equations and/or the algebric equations do not converge. If during a time step the limit is reached, a WARNING message is printed out. Simulations are conducted with a limit of 30 iterations. The user must also specify the limits on the number of warnings that simulation can tolerate before TRNSYS terminates the simulation and print out an ERROR message. This limit is set to 30 warnings.

In order to evaluate the quality of results from the refrigeration system model, two types of simulation are performed: open system and closed system simulations. The open system simulation assesses the component behaviours when interacting together. Once the components are validated, closed simulation is performed to verify the stability and the auto-regulation of the system. Throughout the simulations, the slab is modeled with Type 208 (correlation-based model) because, as discussed in Chapter 6, it provides more accurate results than Type 207.

7.4.1 Open system simulations

The open system simulations are performed to asses the accuracy of components when connected together. As shown in Figure 7.7, the open system simulation consists of simulating the refrigeration system composed only of the correlation-based model of slab, pump and chillers and leaving open the brine connection between the exit of chiller #2 and the inlet of the slab.

Schedule

Pump

Chiller #1

Chiller #2

Correlation slab

T_{ice}

$T_{brine, inlet slab}$

② ③ ④ ①
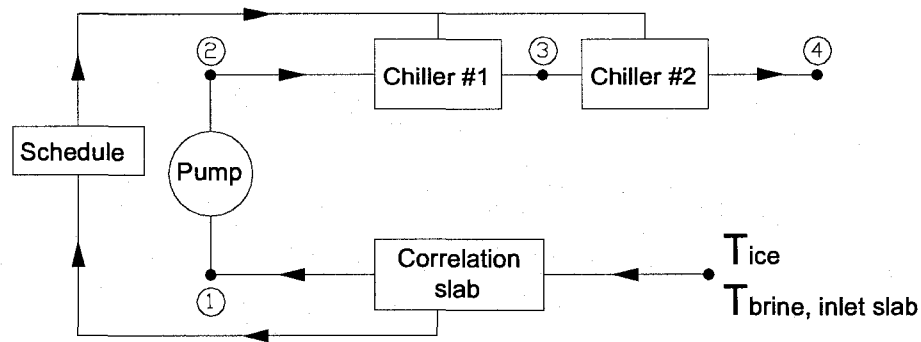
Figure 7.7: Open system simulation

The measured ice temperature and brine temperature entering the slab are used as inputs. The resulting brine temperature is compared with collected data at the exit of each component (encircled numbers in Figure 7.7). Hence, differences between measured and simulated results can be identified for each particular component. A schedule is input, instead of a controller, to reproduce the exact variation of refrigeration load provided by the chiller, regardless of the brine temperature variation. Therefore, when comparing the calculated brine temperature at the exit of each component against the measured data, both are at the same refrigeration load and differences are only due to the component model. By using a schedule, the results are not affected by the controller or by the number of compressors in operation.

7.4.1.1 Verification of the pump model

The pump model is verified by comparing simulated against measured brine temperatures exiting the pump. Based on the brine temperature calculated with the correlation-based slab model, the pump slightly increases the temperature of the brine. As presented in Figure 7.8, the simulated brine temperature at the exit of the pump fits well with the monitored temperatures for March 16th, 2006 (point 2 in Figure 7.7).
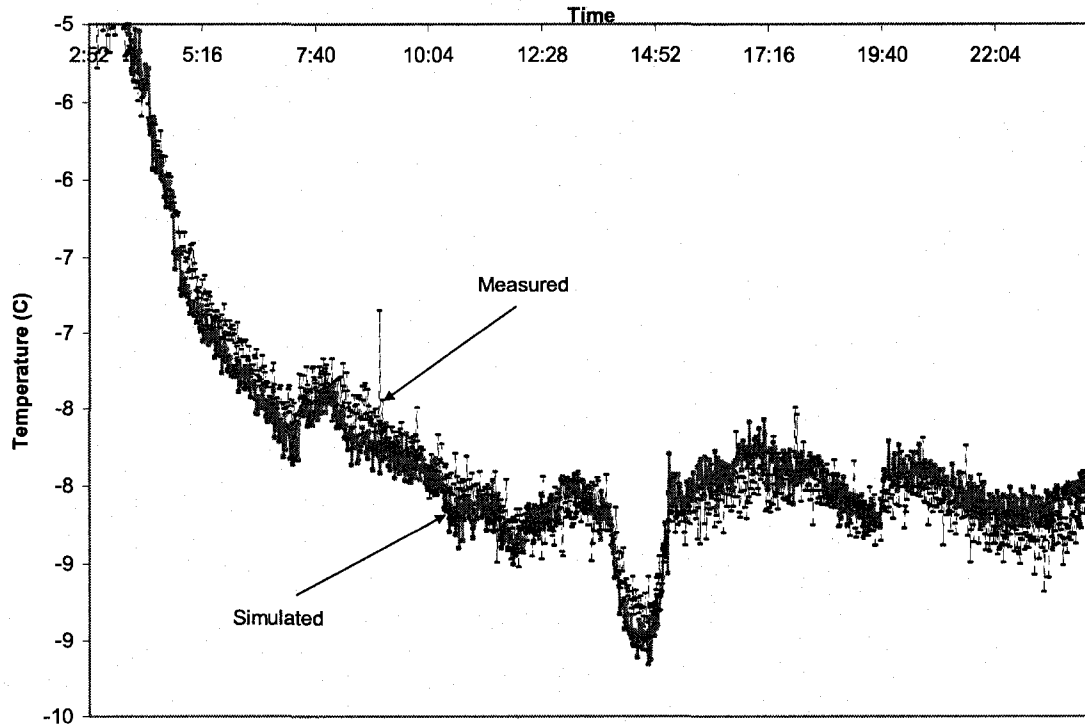
Figure 7.8: Open system simulation with schedule – Measured and simulated brine temperatures at the pump exit on March 16th, 2006

The small differences between the measured and simulated temperatures are caused by a small error in the evaluation of the brine temperature exiting the slab by the correlation model (see Chapter 6). Noise is also amplified by the correlation explaining the oscillations observed in Figure 7.8. The average error between measured and simulated temperatures is of 0.18°C (0.03%), indicating an excellent agreement.

7.4.1.2 Verification of the chiller model

Open-system simulations are particularly useful to validate the chiller model. Because the controller is replaced by a schedule, it is possible to obtain a real measure of accuracy of the chiller model for a given number of compressors in operation. The analysis of the simulated and measured brine temperatures leads to assessment of the

184

effect of thermal inertia and the cooling capacity of compressors. The compressor power input, calculated by the chiller model, can also be verified with measurements. Figure 7.9 presents the simulated brine temperature at exit of chiller #1 (point 3 in Figure 7.7), along with the number of compressors in operation in chiller #1 for March 16th, 2006.
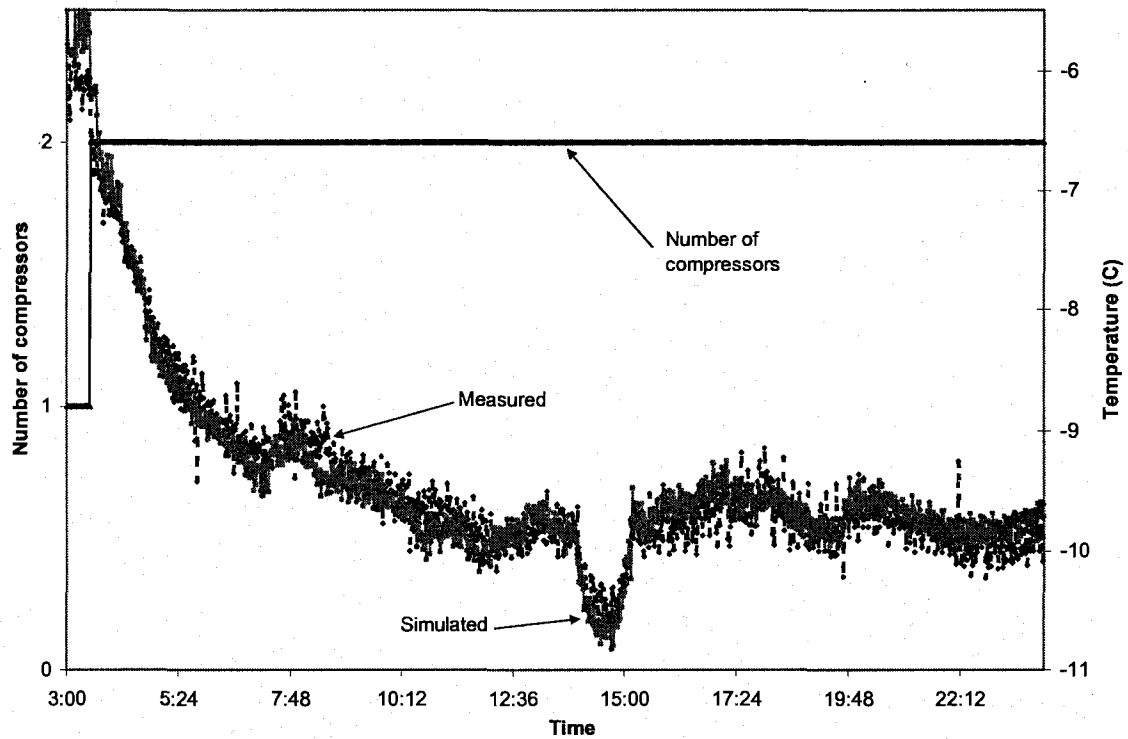
Figure 7.9: Open system simulation with schedule – Measured and simulated brine temperatures leaving the chiller #1, and number of compressors in operation on March 16th, 2006.

When the first compressor is switched on, the simulated temperature is higher than the measured temperature for about 30 minutes. This might be the effect of the transient behaviour of the compressor, which is not taken into account by the model. After the start-up period, chiller #1 operates steadily. The error of the average temperatures difference between the two curves is of 0.16°C (1.89%), demonstrating a good agreement.

Chiller #2 is evaluated in Figure 7.10, where the simulated brine temperature leaving the chiller #2 is plotted against the measured temperature (point 4 in Figure 7.7). The number of compressors in operation in chiller #2 is shown as well.
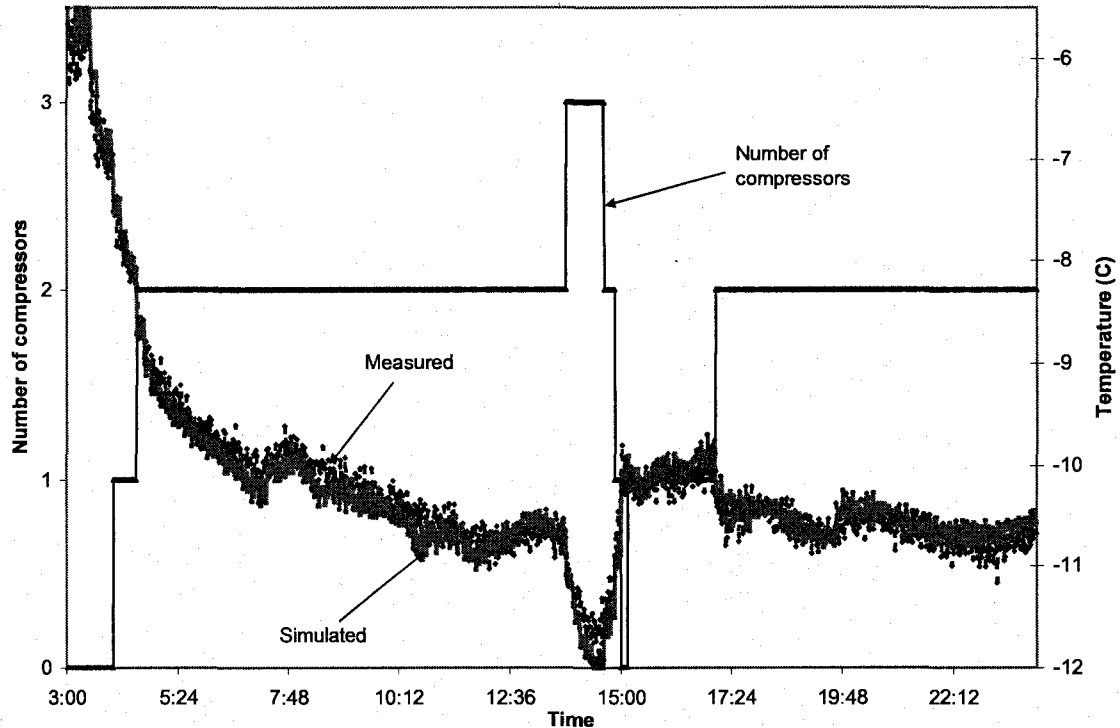
Figure 7.10: Open system simulation with schedule – Measured and simulated brine temperatures leaving the chiller #2, and number of compressors on March 16th, 2006

At 14:35, the difference of about 0.3°C between the calculated and measured brine temperature at the exit of chiller #2 might be the result of the transient behaviour of the chiller when the number of compressors in operation changes. As observed, the transient effect seems to be more important when compressors are switched off. This difference can also be explained by the difference between the capacity of the third compressor compared to others. The estimates show that the capacity of the third compressor is slightly inferior to others. For chiller #2, the average error between the simulated and measured temperatures is 0.15°C (1.59%). Therefore, the model reproduces the actual brine temperature with a good accuracy.

The model used to estimate the compressor power input is verified by comparing the simulation results of both chillers against the measured power input. The data acquisition system installed in the arena measures simultaneously the power input to compressors, pump and fans of air-cooled condensers. Because no measurements on the condensers have been collected, each condenser is considered to use a constant power input of 7 kW when the connected compressor is in operation. Thus, the total power input simulated takes into account the compressor power calculated by the chiller model, the power of the TRNSYS pump model and the approximated condenser power input.

Figure 7.11 compares the simulated power input to the measured input for March 16th, 2006. As one can observe, both curves are practically identical.
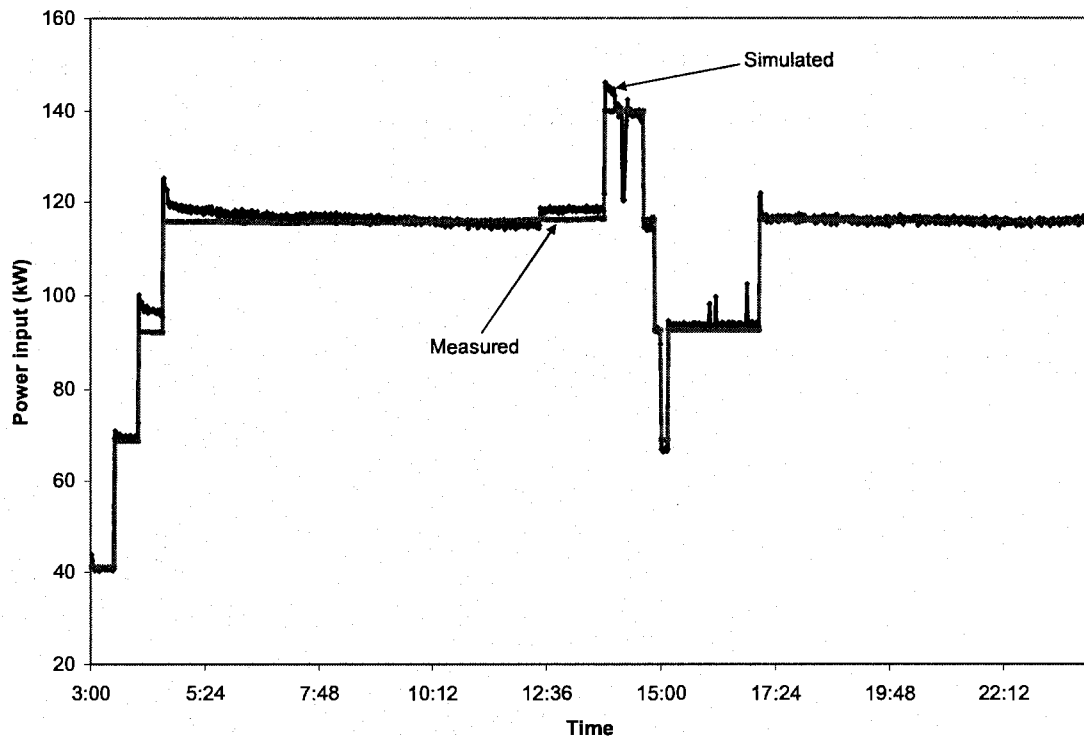
Figure 7.11: Open system simulation with schedule – Measured and simulated power input on March 16th, 2006

For the entire day, the simulated electricity use of the refrigeration system is of 2,322 kWh/day while the measured electricity use is of 2,338 kWh/day. The average difference between the simulated and measured energy use is of 16.1 kWh/day (0.69%), showing an excellent agreement between the results.

The open-system simulation also allows to verify the accuracy of the Toolkit model used for the chillers. The simulated power input of each compressor can be compared with the results obtained with the compressor Carwin software (Carlyle 2007). The average simulated power input to one compressor in chiller #1 is of 20.60 kW while in chiller #2 it is of 16.60 kW. The power input to one compressor as calculated with the manufacturer's software is of 20.57 kW (see Chapter 5). For chiller #1, the simulated results are practically the same as those obtained with the manufacturer's software since the error is only of 0.03 kW (0.15%). This indicates that the Toolkit method for the identification of the compressor parameters provide accurate results. Furthermore, the results show that the Toolkit compressor model reproduces very well the actual behaviour of the compressor. However, the simulated power input for one compressor in chiller #2 (16.60 kW) is quite different from the result obtained with the compressor software (20.57 kW). Two factors explain this difference. First, the results from the compressor software are based on the measures collected on compressor #2, in chiller #1. Secondly, based on the heat balance on the brine side, it has been demonstrated in Chapter 3 that the refrigerating capacity of compressors operating in chiller #2 was inferior to those operating in chiller #1 (56,000 kW for chiller#1 versus 41,000 kW for chiller #2). Because no data was collected on the refrigerant side of the second chiller, the power input to the compressor could not be evaluated and verified with the compressor

software. However, since the evaporation effect is inferior in chiller #2, the related power

demand per compressor is also expected to be inferior. Therefore, the results obtained

from the model are coherent with existing operating conditions.

7.4.2 Closed system simulations

Once the components are verified with the open configuration, the closed system

simulation is performed. This arrangement consists of a closed refrigeration loop, by

connecting the brine temperature leaving the chiller #2 to the brine temperature entering

the slab (Figure 7.12). For the closed loop, the ice temperature is supplied to the

refrigeration system model from an external file based on measurements. The encircled

numbers show the points where the simulated brine temperature is compared to the

measured one.
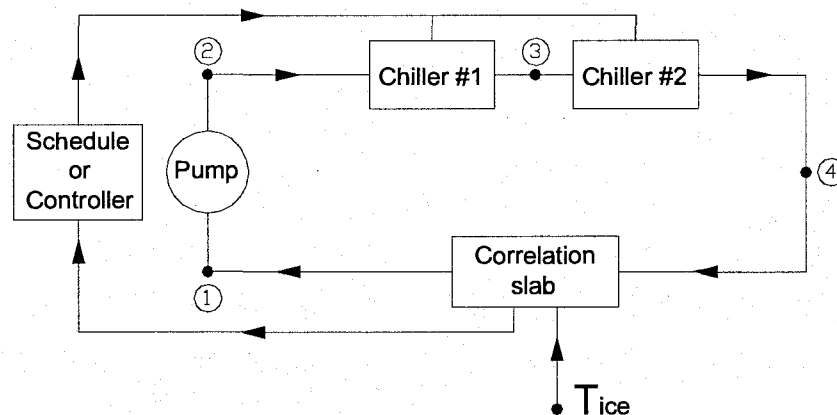
Figure 7.12: Closed system simulation

Simulations are performed under two scenarios. First, the closed system

simulation is performed employing a schedule of operation to test the stability of the

numerical system. The temperature difference between measured and simulated results

can lead to numerical instability that can be more easily identified if a common schedule

is used instead of a controller. In the second scenario, the closed system simulation is performed by using the controller model instead of the given schedule of operation. This type of configuration allows the evaluation of the auto-regulation of the refrigeration system when the only input supplied to the model is the ice temperature. The limits of the controller can then be tested.

7.4.2.1 Closed system with schedule

The response of the system is evaluated by comparing the temperatures of simulated brine leaving the slab, the chiller #1 and the chiller #2 with the measurements for March 16th, 2006. Figure 7.13 presents the simulated brine temperature against the measured temperature at the slab exit as well as the total number of compressors in operation as input by the schedule.
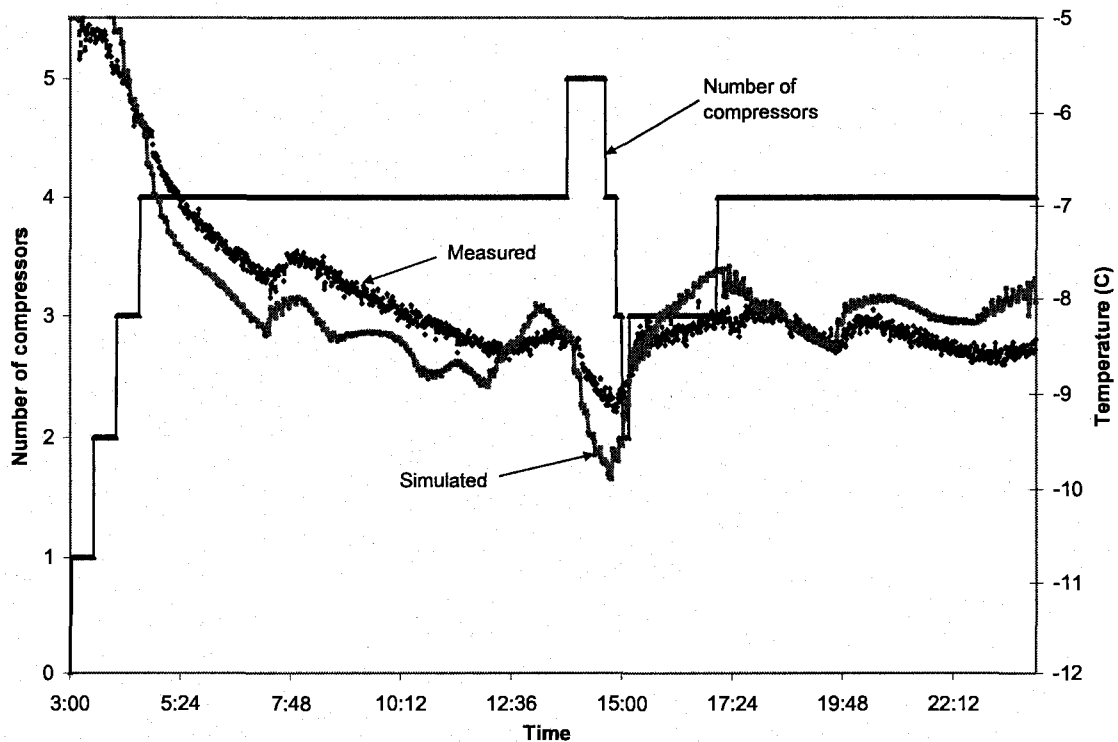
Figure 7.13: Closed system simulation with schedule - Measured and simulated brine temperatures leaving the slab, and total number of compressors in operation on March 16th, 2006

The difference between the measured and simulated temperature at the slab exit in a closed system arrangement is slightly greater than those observed in an open configuration. For closed system, the average error is of 0.35°C (4.45%), while in the open system (see section 6.1.3.3) it is of 0.15°C (1.90%). The difference in errors is negligible.

Figure 7.14 compares the simulated brine temperature leaving chiller #1 to measurements for March 16th, 2006. The number of compressors in operation for chiller #1 is also plotted. The average error between the simulated and measured brine temperature leaving the chiller #1 is of 0.34°C (3.97%), while it is of 0.16°C (1.89%) in open system configuration. After start-up, chiller #1 operates steadily with two compressors. The difference is also negligible.
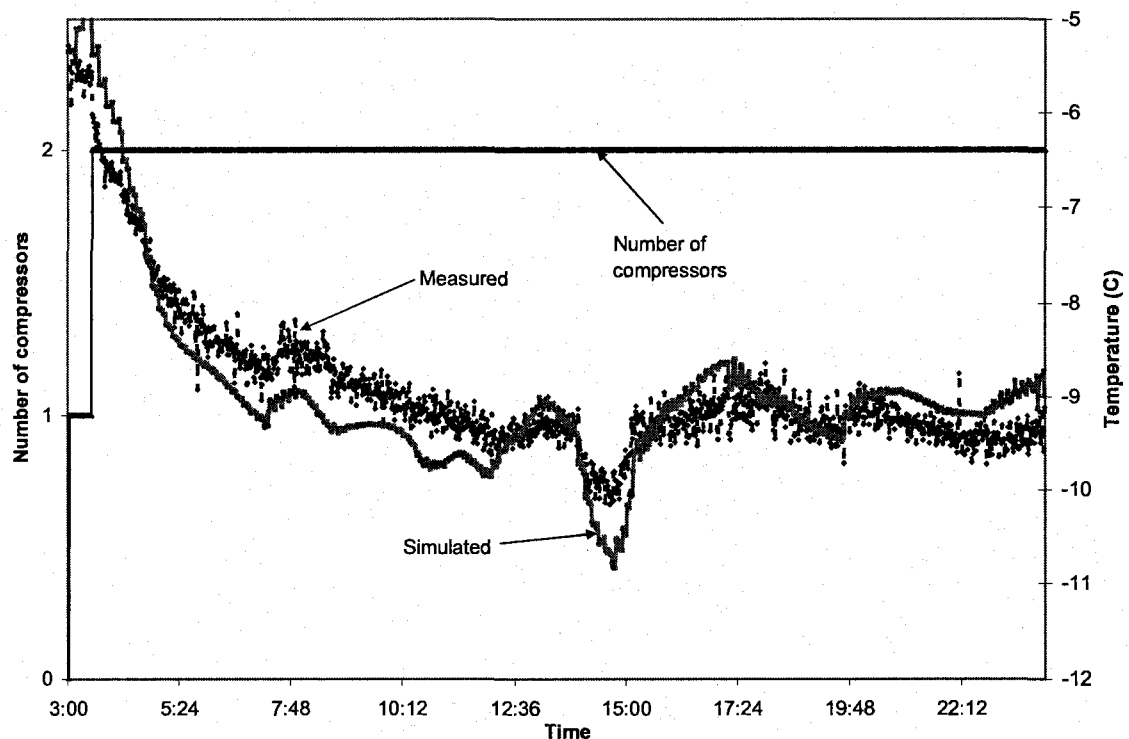
Figure 7.14: Closed system simulation with schedule - Measured and simulated brine temperatures leaving chiller #1, and number of compressors in operation on March 16th, 2006

Figure 7.15 compares the simulated brine temperature leaving chiller #2 to measurements for March 16th, 2006. The number of compressors in operation for chiller #2 is also plotted.
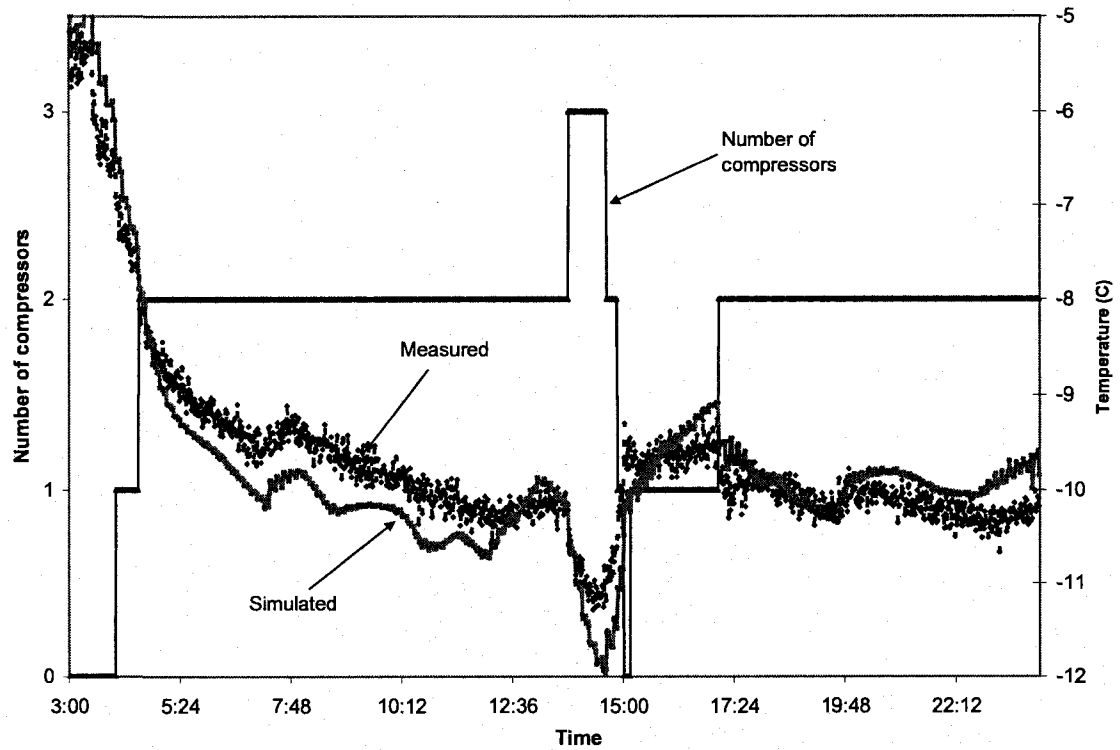
Figure 7.15: Closed system simulation with schedule - Measured and simulated brine temperatures leaving chiller #2, and number of compressors in operation on March 16th. 2006

By superposing the temperatures exiting chiller #1 (Figure 7.14) with those exiting chiller #2 (Figure 7.15), it can be observed that the shape of the curves is quite different. This difference is particularly evident in the interval between 13:45 and 15:00 when the number of compressors in chiller #2 changes several times. This result is coherent, because by switching on or off compressors in chiller #2, it decreases or increases the brine temperature. The average error between the simulated and measured brine temperatures leaving chiller #2 is of 0.33°C (3.54 %) in closed arrangement, while in an open system configuration it is of 0.15°C (1.59%).

Table 7.16 summarizes the absolute and relative errors calculated at the components exit between measured and simulated temperatures for open and closed system arrangements. The absolute errors are very small for both configurations; they are all equal or inferior to 0.35°C while the relative errors are all les than to 4.50%.

Table 7.16: Absolute and relative errors at the components exit between measured and simulated temperatures

Component	Open-system	Closed-system
Slab	0.15°C (1.90%)	0.35°C (4.45%)
Chiller #1	0.16°C (1.89%)	0.34°C (3.97%)
Chiller #2	0.15°C (1.59%)	0.33°C (3.54%)

Although the errors are negligible, a short discussion might be of some interest. In open system configuration, the errors are only attributable to the corresponding component. In the closed system, it is more difficult to determine which component is responsible for the increase of the errors. As observed in Table 7.16, in both open and closed configurations, the errors are more important at the slab and chiller #1 exits. As seen in Figure 7.15, the number of compressors in operation of chiller #2 changes several times during the day. These changes can result into a transient response of the evaporator and compressor. Transient regimes are characterized by amplification and delay effect. As explained in Chapter 4, the Toolkit chiller model was developed for steady state regimes; hence when the system behaves transiently, the model provides less accurate results. When compressors are turned on or off, the effect of the refrigerant's temperature variation is delayed on the brine side due to the thermal mass of the evaporator. Dynamic behaviour of the heat exchanger due to variations of the inlet temperature is a topic widely discussed in the literature as by Manish et al. (2006). Several solutions have been developed for heat exchangers submitted to step variations of inlet temperature, however, the models are complex and require deeper measurements on evaporators. Consequently,

no model is developed to take into account the transient effect of chillers. As observed,
transient response is more evident when the system is simulated in a closed loop
configuration than in an open one. Transient effects also occur in open system; however,
the effects are less apparent. By closing the refrigeration loop, the temperature exiting
chiller #2 is fed back into the system itself, creating a feedback effect. Feedback
amplifies the errors, hence the transient effect is amplified and reused as system input.

7.4.2.2 Closed system with controller

In this section, the simulation is performed in a closed configuration along with a
controller instead of a schedule. Figure 7.16 presents the number of compressors in
operation calculated versus the number simulated, while Figure 7.17 illustrates the
simulated and measured brine temperatures leaving the slab for March 16th, 2006.
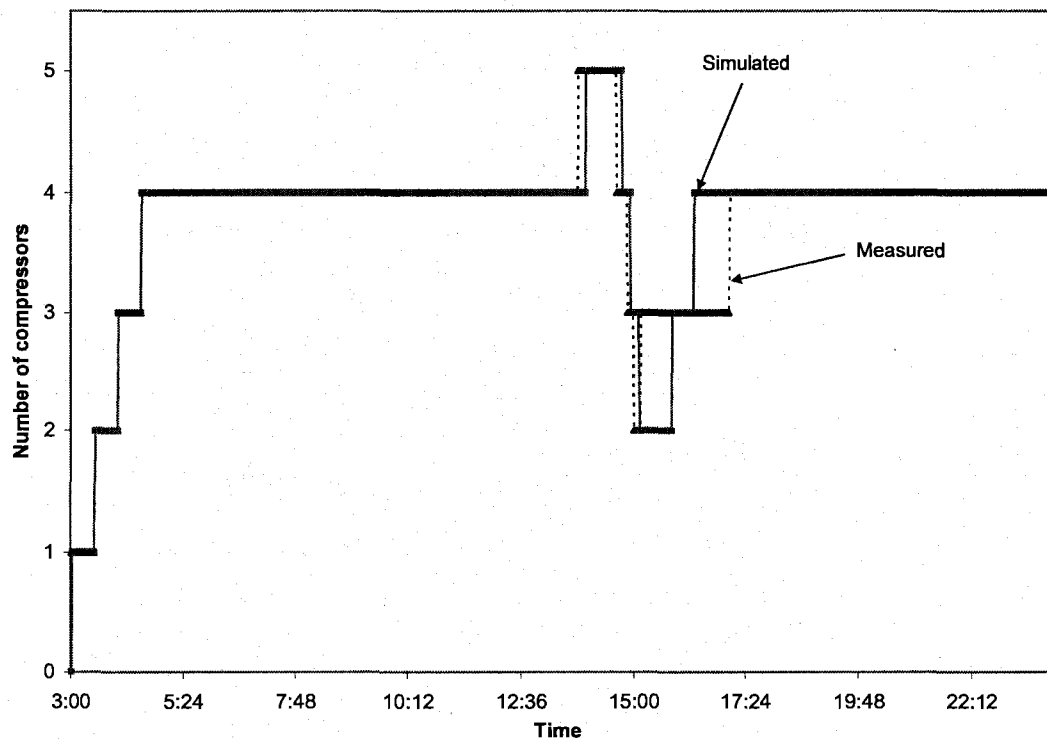
Figure 7.16: Closed system simulation with controller – Measured and simulated number of compressors in operation on March 16th, 2006
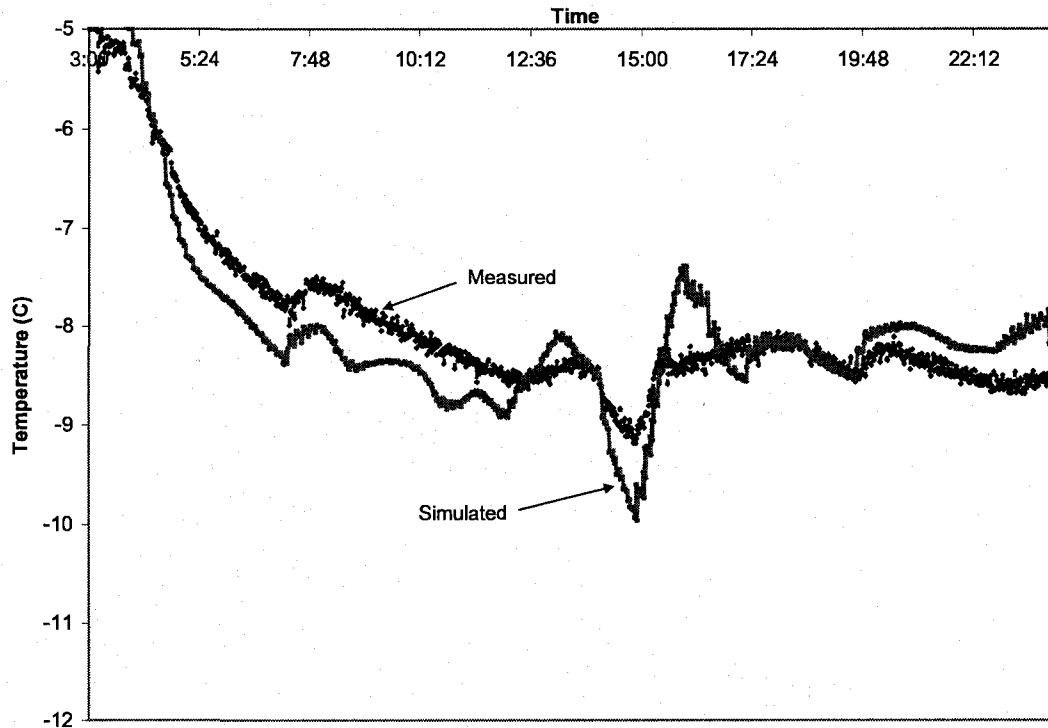
Figure 7.17: Closed system simulation with controller– Measured and simulated brine temperatures leaving the slab on March 16th, 2006

Although the simulated brine temperature leaving the slab experiences significant fluctuations (Figure 7.17), the resulting number of compressors determined by the controller approximately fits the actual number (Figure 7.16). At the start-up, the simulated controller turns four compressors on, at the same time intervals as those observed in the measurements. The controller switches on the fifth compressor (around 13:00) and then turns off in sequence three compressors by following accurately the actual variation. The brine temperature during this interval fluctuates near the defined boundaries; hence, the controller makes good decisions. However, when only two compressors are in operation (around 15:00), the simulated brine temperature exiting the slab experiences an important drop that is larger than measurements (about 0.9°C). At that moment, the controller is not able to turn off more compressors because the

minimum number of compressors is limited to two. After the increase of brine temperature, the controller switched on two compressors. Even so, the brine temperature continues to increase but the controller waits until the temperature is stabilized. The error with respect to measured brine temperature at the slab exit is of 0.35°C (4.48%). Hence, the results obtained with the controller in a closed loop arrangement are satisfactory even if the simulated brine temperature does not follow exactly the measurements. On the other hand, this shows that the controller is able to provide good results based on brine temperature having greater fluctuations. More accurate results would be possible by re-calibrating the controller for closed loop configuration. However, re-calibrating the controller based on bad simulated brine temperatures without trying to correct them (e.g. by considering transient regimes) would constitute a contradiction.

When simulated and measured power input to the refrigeration system are compared for March 16th, 2006 (Figure 7.18), the computer model provides excellent results. The total power input includes the compressors, condensers and brine pump. Because the power input depends on the number of compressors in operation, the differences noticed in Figure 7.16 are also observed in Figure 7.18 between the measured and simulated power input. The total simulated electricity use by the refrigeration system is of 2353 kWh/day while the measured electricity use is of 2338 kWh/day. The average absolute difference is of 15.37 kWh/day and the average relative difference is of 0.60%. This difference shows a good agreement between simulation and measurements.
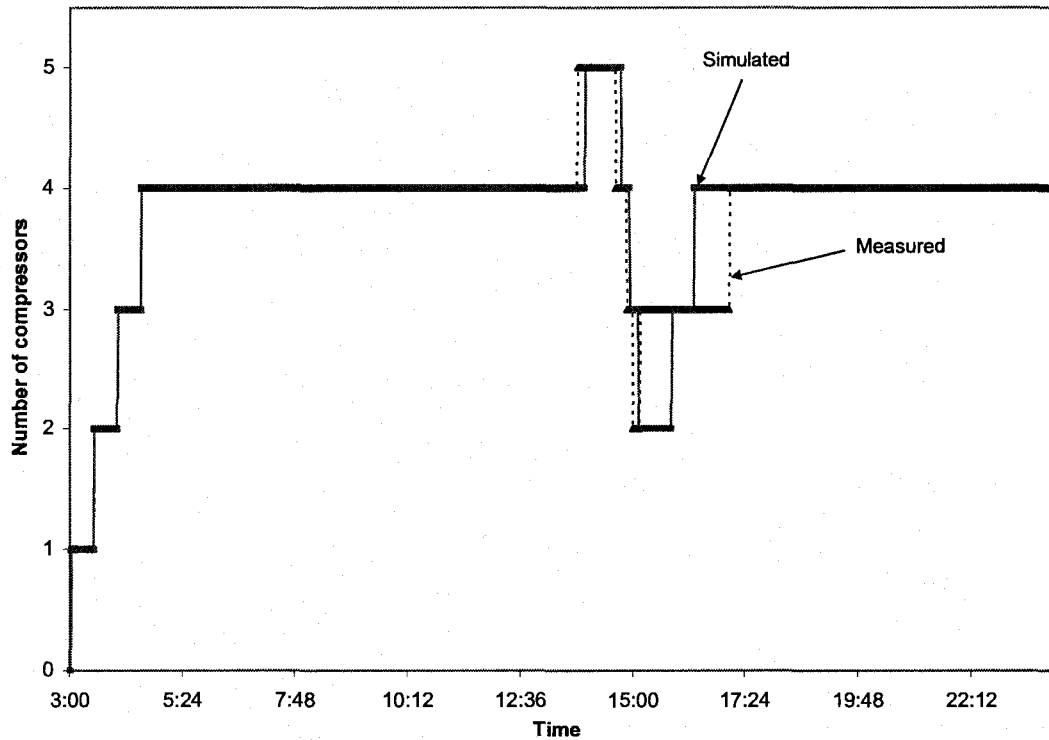
Figure 7.18: Closed system simulation with controller– Measured and simulated power input exiting the slab on March 16th, 2006

7.5 Heat recovery from condensers

At Camillien-Houde ice rink, condensers reject to the environment the heat previously absorbed by the refrigerant during the evaporation and compression processes. Releasing heat to the outside air constitutes a waste of energy because, at the same time, electricity and gas are used to heat the building, the domestic hot water and the water used for resurfacing. Therefore, important energy savings are possible if the heat rejected by the condensers is recovered to be used for other heating applications.

197

7.5.1 Evaluation of the energy rejected by condensers

To determine the potential heat recovery per compressor, it is necessary to establish the duration of operation of each compressor during one day. Table 7.17 presents for each compressor, the average number of hours of operation for four different days of different months.

Table 7.17: Daily operating hours of each compressor for different days

Day	Chiller #1		Chiller #2		
	Comp. #1 (hours)	Comp. #2 (hours)	Comp. #3 (hours)	Comp. #4 (hours)	Comp. #5 (hours)
March 16th, 2006	20.98	20.48	19.83	17.28	0.82
May 14th, 2006	20.25	19.75	18.90	7.43	0
October 18th, 2006	20.05	19.57	19.07	16.08	6.75
November 10th, 2006	19.65	19.17	16.05	5.38	1.02
Average	20.23	19.74	18.46	11.55	2.15

Compressor #1 has the highest average number of hours of operation per day. As long as the refrigeration system is switched on (for approximately 21 hours per day), compressor #1 operates. Compressor #2 and compressor #3 also operate during approximately the whole day (19.74 hours/day and 18.56 hours/day, respectively). However, compressor #4 and compressor #5 are used during short intervals to increase the refrigerating capacity of the system when it is necessary. This is particularly true for compressor #5, which in average operates only 2.15 hours/day. Moreover, results in Table 7.17 confirm that this compressor is not uniformly used: it is not used on May 14th, while it is used for 6.75 hours on October 10th. This can be explained by the variation of the ice cooling load during different days.

Based on the first law of thermodynamics, the total heat rejected by the compressor is equal to the work supplied to the compressor and the heat absorbed through the evaporator:

$$\dot{Q}_{cond} = \dot{W}_{comp} + \dot{Q}_{evap} \tag{7.2}$$

At Camillien-Houde ice rink, the evaporation and condensation pressures are practically constant. Hence, the amount of heat rejected by each compressor-condenser unit is also constant. However, as revealed by the energy balance on the brine side (see Chapter 3), the refrigerating effect of each compressor is quite different. Therefore, as shown in section 7.4.1.2, the power input of a compressor is different if it operates in chiller #1 or in chiller #2. By multiplying the heat rejected at each condenser by the corresponding number of hours of operation of the connected compressor (Table 7.17), the energy released to the environment by the connected condenser is determined. Table 7.18 summarizes the power input, the refrigerating effect and the total heat rejected per day by each compressor-condenser package. In this calculation, the heat loss through the pipes is neglected.

Table 7.18: Power input, refrigerating effect and heat rejected for each compressor-condenser unit

	Chiller #1		Chiller #2		
	Comp. #1	Comp. #2	Comp. #3	Comp. #4	Comp. #5
Power input (kW)	20.6	20.6	16.6	16.6	16.6
Refrigerating effect (kW)	56.0	56.0	40.0	40.0	40.0
Heat rejected (kW)	76.6	76.6	56.6	56.6	56.6
Energy rejected (kWh/day)	1549.62	1512.08	1044.84	653.73	121.69

The average amount of heat rejected to the environment by the five condensers is of 4882 kWh/day. This amount of energy is considerable in the perspective that part of it could be re-used and therefore reduce the total energy used by the building.

7.5.2 Heat recovery

Chillers are used in several applications where refrigeration needs occur at the same time as heating needs. Hence, the recovery of the heat rejected by the condensers is a common energy efficient measure used by the industry. Heat released by the chillers is commonly recovered to heat the hot water, which can be used for heating the building, or for preheating domestic hot water. Because the amount of energy released by the air-cooled condensers installed at Camillien-Houde is significant, it is proposed to recover this energy to preheat the domestic hot water. To do this, a simplified system is used where part of the energy necessary to heat the water is provided by the recovery system, while the rest of the heating is supplied by an electric heating tank. Figure 7.19 shows the components of the recovery system proposed:
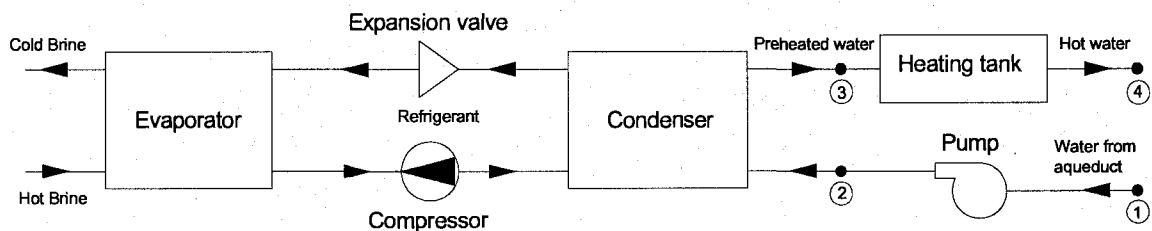
Figure 7.19: Heat recovery system

The water from the aqueduct (point 1) is pumped to the condenser where it is preheated (point 3). The heat gains from the pump are not considered; hence the temperature at point 1 is equal to the temperature at point 2. Then, the water is stored in a tank where heat is supplied to reach 60 °C (point 4). The water supplied by the city's aqueduct has a variable temperature depending on the time of the year. Dumas et al. (2004) have conducted measurements of the water temperature in Montreal's aqueduct for several years. Figure 7.20 presents data for two years only. During the summer, the

water reaches a temperature of 23°C, while in the winter time, the temperature drops to 2°C. The average temperature of the water supplied by Montreal's aqueduct is of 11°C. In the current study, the average temperature will be used and considered constant.
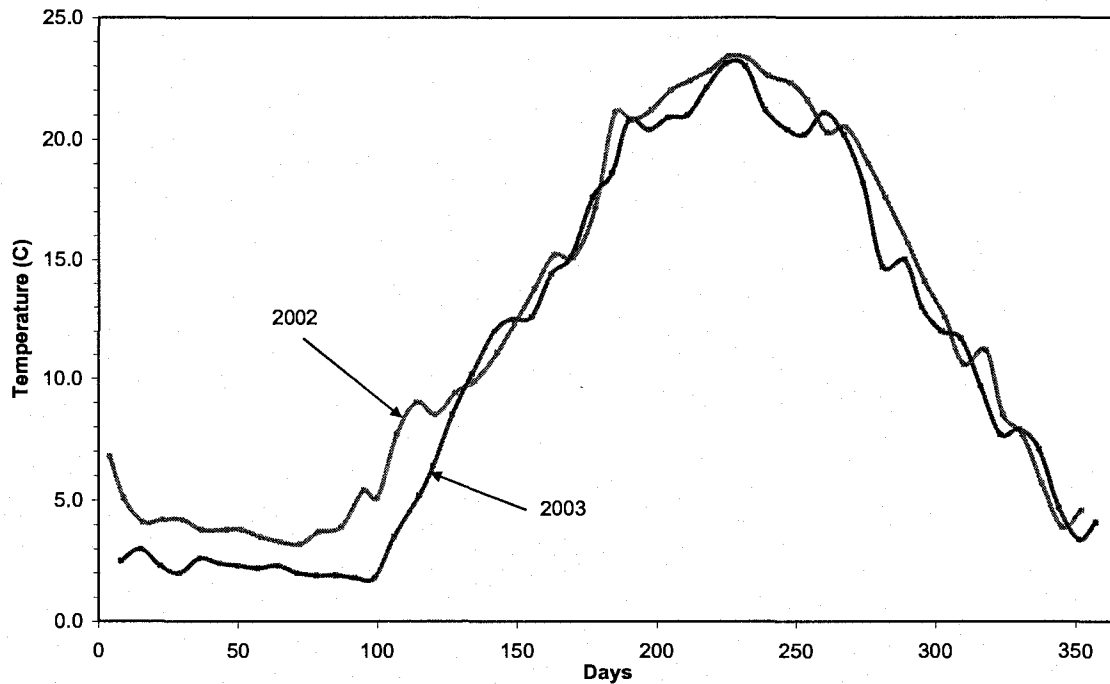
Figure 7.20: Temperature variations of the water from Montreal's aqueduct (Dumas et al. 2004)

For the present purpose, the domestic hot water is considered to only be used for the showers in dressing rooms. Because the volumetric flow of the hot water was not directly measured at the ice rink, the water consumption is based on recommended values for gymnasiums (ASHRAE 2007). It is assumed that the ice rink has 18 showers, each consuming 10 l/min of warm water at 45°C. Each shower is used during a period of 10 minutes six times per day. Warm water is produced by mixing cold water from the aqueduct with hot water provided by the heating tank at 60°C. Therefore, a volumetric flow of 5.9 l/min of hot water at 60°C is necessary to obtain warm water at 45°C if the cold water is considered to be at 11°C. The heat required to increase the water

temperature from the aqueduct temperature up to the tank set point temperature is given by the following relation:

$$\dot{Q}_{water} = \dot{m}_{water} \cdot c_{p,water} \cdot (T_{tank} - T_{aqueduct})$$ (7.3)

where: $\dot{Q}_{water}$ = heat supplied to the water (kW);

$\dot{m}_{water}$ = mass flow of water (5.9 kg min^{-1});

$c_{p,water}$ = specific heat of water (4,181 J kg^{-1} °C^{-1});

T_{tank} = set point temperature of water in the tank (60 °C);

$T_{aqueduct}$ = aqueduct temperature (11 °C).

Therefore, for one shower, 20.15 kW of heat is necessary to increase its temperature to 60 °C. For a shower that it is used six times per day during a period of ten minutes each time, the energy required is of 20.15 kWh per shower per day. For the 18 showers installed, the total energy required is of 362.61 kWh per day.

The actual heating tank uses electricity to provide this energy to the water. However, by using the recovery system, part of this energy can be provided by the condenser. In order to evaluate the potential for energy savings, it is necessary to determine the contribution of the condenser in the preheating process. Because the temperature of the sanitary water leaving the condenser (point 3, Figure 7.19) is not known, a sensitivity analysis is conducted to determine the contribution of the recovery system in terms of different water temperatures at the condenser exit. It is important to mention that the water temperature increases at the condenser exit is limited by the temperature of the refrigerant. Hence, the water cannot reach a temperature greater than the refrigerant temperature. The refrigerant temperatures during the condensation process

are of 93.6°C at the condenser inlet, 40.4°C during the latent heat exchange and of 28.2°C at the end of the sub-cooling (see Chapter 5). Because the main heat exchange occur when the refrigerant condense (latent heat), the maximum temperature of the water at the condenser exit is set to 40°C. Therefore, electrical heating is always necessary to reach 60°C. Table 7.19 presents the different energy contributions of the condenser for different water temperatures at the condenser exit for an entire day. The related energy supplied to the heating tank is also presented.

Table 7.19: Sensitivity analysis of the water temperature at the condenser exit for heat recovery

Energy (kWh/day)	Water temperature at the condenser exit (°C)				
	20	25	30	35	40
Energy recovered from the condenser	66.60	103.61	140.61	177.61	214.61
Energy supplied to the tank	296.01	259.01	222.01	185.01	148.01

As it can be observed in Table 7.19, independently of the water temperature at the condenser exit, the energy recovered is always less than to the total energy rejected by the condenser determined in section 7.5.1. The maximum potential energy recovered is of 214.61 kWh/day while the total amount of energy rejected by the condenser is of 4882 kWh/day (see Table 7.18). In the worst case, the energy savings are of 66.60 kWh/day, while in the best case, the economies are of 214.61 kWh/day.

7.5.3 CO_2 emissions

Due to the large amounts of energy used by the refrigeration system of the ice rink, the CO_2 emissions are considerable. Furthermore, the refrigerant used in the refrigeration system also contributes to the total equivalent CO_2 emissions. At Camillien-Houde ice rink, the system operates with refrigerant R-22, a fluid having an important

global warming potential. Each kilogram of refrigerant leaking from the system is equivalent to 1900 kg of CO_2. CANMET (2004) has calculated that a typical ice rink emits in average 278 tons of CO_2 per year. This evaluation includes the emissions from the leaks of refrigerant and those from the use of energy from electricity and fossil fuels. A possible way to diminish the total emissions is to decrease the energy use in the building. Therefore, it is interesting to analyze the possible reductions that could result from the use of a recovery system to preheat the sanitary hot water. Different criteria have been developed to evaluate the CO_2 emissions of refrigeration systems such as the ozone depletion potential and the global warming potential. However, the total equivalent warming impact (TEWI), is the most complete and accurate criterion (Falcon 2000) because it considers both the direct and indirect impacts of the refrigerant over the lifetime of the system. This coefficient is used to evaluate the total emissions from the refrigeration and sanitary hot water systems.

Two coefficients TEWI are calculated: one for the actual system installed at Camillien-Houde ice rink, and another for the modified system which use a heat recovery system to preheat the domestic hot water. The direct impacts are calculated by multiplying the global warming impact of the refrigerant by the mass of refrigerant assumed to leak from the refrigeration system. The indirect impacts are evaluated by considering the energy used to operate the system over its lifetime. This is obtained by multiplying the energy used by a coefficient that relates the CO_2 emissions per kWh used. For instance, for Canada, this coefficient is equal to 0.26 kg of CO_2/kWh. The software developed by Falcon (2000) is used to evaluate the TEWI. Table 7.20 presents the inputs used in the program.

Table 7.20: Input values used in TEWI

Input	Value
COP of the refrigeration system	2.7
Power input to compressor	Depends on the compressor
Refrigerating capacity	Depends on the compressor
Refrigerant	R-22
Mass of refrigerant	100 kg
Annual leak rate	12%
End of life charge loss	20%
Number of total leaks	0
Lifetime of the system	25 years
Annual operating time	Depends on the compressor

Based on the results obtained in Chapter 5 with the EES model (and verified with the compressor software), the COP of the refrigeration system is set to 2.7. This COP is based on the ratio between the refrigerating capacity and the power input to one compressor. All compressors are considered to operate with the same COP. In Table 7.20, a power input of 20.6 kW is used for compressors in chiller #1, while for compressors in chiller #2 a power input of 16.6 kW is used instead. Depending on the chiller, the refrigerating capacity is also different (see Chapter 3): the refrigerating capacity is of 56 kW for compressors in chiller #1, and of 40 kW for compressors in chiller #2. The refrigeration system operates with approximately 500 kg of refrigerant R-22. Thus, each compressor-condenser unit use 100 kg of refrigerant. Based on discussions with experts from CANMET-Varennes, the annual leak rate is evaluated at 12%, while the end of life charge loss is of 20%. The lifetime of the refrigeration system is considered to be of 25 years. The annual operating time is different for each compressor. Therefore, calculations for the TEWI have been conducted for each compressor by multiplying the average daily time of operation of each compressor (Table 7.17) by the 335 days (11 months). Table 7.21 presents the direct and indirect CO_2

emissions calculated for each compressor. The annual operating time of each compressor is also presented.

Table 7.21: Annual operating time, direct and indirect emissions of each compressor over lifetime

	Chiller #1		Chiller #2		
	Comp. #1	Comp. #2	Comp. #3	Comp. #4	Comp. #5
Annual operating time (hours)	6,778.17	6,613.46	6,184.94	3,867.85	718.85
Direct emissions (Tons of CO_2)	608	608	608	608	608
Indirect emissions (Tons of CO_2)	1,028	1,003	670	419	77
Total emissions (Tons of CO_2)	1636	1611	1278	1027	685

The total emissions for both chillers over the entire lifetime of the system are of 6237 tons of CO_2. The emissions corresponding to the hot water heating system are determined by multiplying the lifetime energy use by the coefficient of emissions (0.26 kg of CO_2/kWh). As previously determined, the total energy use per day by the domestic hot water system is of 363 kWh/day (all showers). Therefore, on a daily base, the total emissions are of 94.38 kg of CO_2/day. Over the entire lifetime of the system (335 days per year (11 months), during 25 years), the total emissions are of 790 tons of CO_2. The total emissions for the refrigeration system and for the hot water system are obtained by adding both emissions during the lifetime of the system. Hence, the total emissions at Camillien-Houde ice rink during 25 years are of 7028 tons of CO_2.

If the heat recovery system is used, new emissions are calculated for the part of additional heating supplied by electricity to the hot water tank during the lifetime of the system (see Table 7.19). The part of energy recovered does not engender any new emissions, assuming that the recovering process does not modify the operation of the chillers. Because the temperature of the water at the exit of the condenser is not known,

206

the reduction of emissions is calculated for different water temperatures. Table 7.22 presents the CO_2 emissions associated to the domestic hot water heating tank if the recovery heating system is used with different water temperature at the condenser exit. The corresponding total CO_2 emissions of refrigeration and hot water tank during the lifetime of the system are also presented.

Table 7.22: CO_2 emissions of the domestic hot water with heat recovery and total emissions of the refrigeration and hot water systems over the lifetime

	Water temperature at the condenser exit (°C)				
	20	25	30	35	40
CO_2 emissions of heating tank with recovery (Tons)	644.57	564.00	483.43	402.86	322.29
Total CO_2 emissions (Tons)	6882.56	6801.99	6721.42	6640.85	6560.28

If the temperature of the preheated water only reaches 20°C, the reduction of emissions is only of 7028 - 6882.56 = 145.44 tons. However, if the temperature of the water at the condenser exit reaches 40°C, the reductions of emissions are of 7028 − 6560.28 = 467.72 tons, which is equivalent to 1.5 years of operation of the ice rink. Thus, the reduction of emissions is less important than the reduction of energy.

Therefore, heat recovery should be considered as a measure to reduce the energy use and the total emissions of the ice rink. Even with a low efficiency heat exchanger, it is better to recover the heat at the condenser than to reject to the exterior when heating is necessary for the domestic hot water.

7.6 Conclusions

A detailed description of TRNSYS has been presented at the beginning of this chapter. The software overview allowed to present its characteristics and the procedure used to integrate new components. Based on the chiller simulation model (Chapter 4), the slab and the controller models (Chapter 6), proformas were developed by using the inputs, parameters and outputs of each component.

Both open and closed system simulations were conducted. Open system simulations have shown that the mathematical model used to simulate the chillers and the slabs were accurate. Therefore, these components can be used with good confidence. However, as discussed in Chapter 6, the results provided by the controller are limited due to its algorithm, which is based on empirical rules using temperature boundaries.

Closed system simulations were performed by using a schedule and a controller. Simulations with this type of arrangement and a schedule have shown that the fluctuations of the brine temperature at the exit of each component were greater than in open system configuration. In particular, the errors of the brine temperature at the exit of the slab and of chiller #2 were greater than in open system simulations. The fluctuations observed could be related to the transient behaviour of the slab and of the chiller #2, since these two components operate under variable conditions (variable ice temperature and variable number of compressors, respectively). The amplifications of the fluctuations observed could be explained by a feedback effect when simulating the system in a closed loop arrangement. The closed system simulation using the controller has provided good results. Moreover, the higher brine temperature fluctuations observed in closed system

simulations has only a slightly effect on the accuracy of the controller. The combinations of the controller and chiller models have lead to accurate evaluation of the electricity use during simulation in closed loop. For the entire refrigeration system, the difference is of 0.66%.

Because heat is rejected by the condenser to the exterior air, a heat recovery system was developed to use this energy to heat the domestic hot water. The calculations performed have shown that a recovery system would be an interesting measure to diminish the electricity use of the ice rink and the total equivalent CO_2 emissions. Based on the TEWI criterion, the total emissions during the lifetime of the system are of 7028 tons of CO_2. The use of a recovering system could decrease the emissions by 467 tons of CO_2 during the entire lifetime of the system.

CHAPTER 8

CONCLUSIONS

8.1 Conclusions

As one of the most important pieces of equipment in an ice rink, refrigeration systems performance highly affects the energy consumption of the building. Different models using different approaches are available to evaluate the energy performance of chillers used in buildings. However, models predicting the performance of ice rink refrigeration systems have not been researched as much.

Therefore, a refrigeration system model of an existing ice rink has been developed in this study. Monitoring measurements were available from an ASHRAE project carried out by CANMET-Varennes. A component approach was used for the modelling. Hence, the rink's refrigeration system was divided into three components: chillers, ice-concrete slab and controller. Each component has been developed and programmed separately.

The reciprocating chiller model is based on the ASHRAE Toolkit-I for primary HVAC system. By employing a component approach, the Toolkit combines thermodynamic equations and empirical relations to model the compressor and the heat exchangers. Each component is modeled in two steps: identification and simulation.

The compressor parameters have been identified by combining the manufacturer software and the Toolkit procedures. The identified parameters have been validated by using the Toolkit compressor model and the manufacturer compressor software.

210

Due to crude approximations in the identification procedure of heat exchangers, the Toolkit was not used. A much more accurate identification method was developed by using the EES environment. Based on the collected measurements, a thermodynamic model was developed allowing to calculate the logarithmic mean temperature difference for each heat exchangers. Therefore, the evaporator and condenser overall heat transfer coefficients were determined for the latent and sensible heat exchanges separately.

The simulation model of the chiller use a procedure that is based on a modify method provided by the Toolkit. Changes have been brought to consider the particular operating conditions of the monitored ice rink refrigeration system: superheating at the evaporator, de-superheating and sub-cooling at the condenser, and constant evaporation load. The modify Toolkit procedure use the identified parameters for the compressor and heat exchangers as inputs instead of calculating them.

Two ice-concrete slab models were developed: analytical and correlation-based models. The analytical model is based on a differential equation to describe the heat transfer, while the correlation-based model use a polynomial equation based on the ice and brine temperature measurements. The validities of both slab models have been tested using several days of measurements. It appears from the results that the correlation-based model have higher accuracy.

The controller model developed use a series of empirical rules that have been determined by analyzing measurements of the brine temperature and of the electric demand. The controller model was defined by using three temperature boundaries that

allows to determine the number of compressors in operation by means of the brine temperature at the slab exit. The model has been tested by using two different days of operation and has provided satisfactory results. However, because the model uses a set rules based on pre-defined boundaries, stronger temperature fluctuations than those observed can lead to incoherent results.

By exporting the chiller, slab and controller models as DLLs, components have been integrated into TRNSYS simulation program. The software was used to connect the components with a brine pump used from the component library of TRNSYS. Simulations have been performed using two types of configuration: open and closed system. In open system arrangement, the connection between chiller #2 and the slab was left open, while in closed system configuration all the components were connected together. Open system simulations were performed by using a schedule to evaluate the performance of each component. For the correlation slab-model, an error of 0.15°C (1.90%) was obtained between the measured and simulated brine temperatures for March 16th, 2006. This error was of 0.16°C (1.89%) at the exit of chiller #1 and of 0.15°C (1.59%) at the exit of chiller #2 for the same day. Closed system simulations have been conducted by using a schedule and the controller model. In closed system simulations with a schedule, it was remarked that the relative error at the exit of all the components was greater of approximately 0.19°C (2.20%). Simulations in closed configuration with the controller model have shown that the relative error for the electricity use was of 0.66%, indicating a good agreement between the simulated and measured values.

An evaluation of the energy savings that could result from the use of a heat recovery system at the condenser have shown that the savings in electricity use would be in the best case of 214.61 kWh/day. The corresponding CO_2 emissions reduction based on the TEWI criterion would be of 467 tons for the complete refrigeration-hot water system over the lifetime of the system.

The research accomplished in this study could be used to simulate another ice rink operating with reciprocating compressors. However, because the chillers, the ice-concrete slab and the controller models have been developed by using measurements collected at the Camillien-Houde ice rink, the identified parameters of the components are specifically valid for this arena. Hence, to perform the simulation of another ice rink, new parameters characterizing the compressors and the heat exchangers should be identified by using measurements from the refrigeration system studied. On the other hand, the analytical ice-concrete slab model should be used instead of the correlation-based model, since the coefficients of the polynomial equation developed are only valid for the Camillien-Houde ice rink. Finally, because the controller model is based on the analysis of the measured return brine temperature, the rules defined are exclusively valid for the Camillien-Houde ice rink. Therefore, if the controller model is used to simulate another ice rink, simulated results might be different from collected measurements.

8.2 Recommendations for future work

The mathematical model used to simulate the chillers was developed by the Toolkit for steady state regimes. Hence, this model is valid when the compressors and the

heat exchangers do not experience changes in their operating conditions. However, as observed in the measurements, the ice rink refrigeration system starts and stops compressors several times per day, thus the transient response of the system should be taken into account. The simulation of the refrigeration system in a closed loop arrangement has led to an increase of the errors in the evaluation of the brine temperatures. This indicates that the models did not consider some thermal effects. Part of these errors could provide from the transient response of the system.

All the mathematical models developed for the components have provided good results. However, to really test the performance of the refrigeration system, it would be necessary to use a better controller. Furthermore, it would be interesting to develop a series of energy efficient measures by using different types of ice temperature control. Finally, it would be interesting to integrate into TRNSYS new components to recover the heat rejected by the condensers.

REFERENCES

American Refrigerating Institute (ARI) 2004, 'Performance rating of positive displacement refrigerant compressors and compressor units - Standard 540', Arlington. Virginia.

Antoniou, A. 1979. *Digital Filters: Analysis and Design*, New York, McGraw-Hill Book Company.

Aprea, C. and Renno, C. 2004, 'An experimental analysis of a thermodynamic model of a vapour compression refrigeration plant on varying the compressor speed' *International Journal of Energy Research*, Vol. (28), pp. 37-49.

Arias, J. and Lundqvist, P. 2005, 'Modeling and experimental validation of advanced refrigeration systems in supermarkets', *Process Mechanical Engineering*, Vol. 219(E), pp. 149-56.

ASHRAE 1998a, 'Secondary coolants in refrigeration systems' *1998 ASHRAE Handbook*, Atlanta: American Society of Heating, Refrigerating and Air-Conditioning Engineers, Inc.

ASHRAE 1998b, 'Ice rinks', *1998 ASHRAE Handbook*, Atlanta: American Society of Heating, Refrigerating and Air-Conditioning Engineers, Inc.

ASHRAE 2005, 'Energy estimating and modeling methods', *2005 ASHRAE Handbook*, Atlanta: American Society of Heating, Refrigerating and Air-Conditioning Engineers, Inc.

ASHRAE 2007. 'Service water heating', *2007 Fundamentals*, Atlanta: American Society of heating, Refrigerating and Air-Conditioning Engineers, Inc.

Bourdouxhe, J.P., Grodent, M. and Lebrun, J.J. 1997, '*HVAC1 Toolkit: Algorithms and Subroutines for Primary HVAC System Energy Calculations*'. Atlanta: America Society of Heating, Refrigerating and Air Conditioning Engineers, Inc.

Brownell, A.K. 1998, 'Fixed and floating head pressure comparison for Madison ice arena'. Energy Center of Wisconsin.

Buzelin, L.O.S, Amico, S.C., Vargas, J.V.C, and Parise, J.A.R. 2005, 'Experimental development of an intelligent refrigeration system' *International Journal of Refrigeration*, Vol. 28, pp. 165-75.

Calm, J.M. and Hourahan, G.C. 2001, 'Refrigerant Data summary'. *Engineered Systems*, vol. 18, pp. 74-88. Retrieved November 7, 2007, from
http://www.acca.org/tech/articles/ref_summary.pdf

Canadian Centre for Occupational Health and Safety (CCOHS) 2003, 'Heath Effects of Ammonia Gas', Retrieved November 7, 2007, from
http://www.ccohs.ca/oshanswers/chemicals/chem_profiles/ammonia/working_ammonia.html

CANMET 2003a, 'Management of Ice Temperature-Ice and Curling Rinks'. Retrieved November 7, 2007, from
http://cetc-varennes.nrcan.gc.ca/fichier.php/codectec/En/2003-066-6/2003-066-6e.pdf.

CANMET 2003b, 'Optimization of ice and concrete slab thickness-Ice and Curling Rinks', Retrieved November 7, 2007, from
http://cetc-varennes.nrcan.gc.ca/fichier.php/codectec/En/2003-066-8/2003-066-8e.pdf.

CANMET 2003c, 'The secondary coolant and pumping power relation-Ice and Curling Rinks'. Retrieved November 7, 2007, from http://cetc-varennes.nrcan.gc.ca/fichier.php/codectec/En/2003-066-2/2003-066-2e.pdf.

CANMET 2006, 'Buildings', Retrieved November 7, 2007, from http://cetc-varennes.nrcan.gc.ca/en/b_b.html

Carlyle Compressor Company 2007, 'Carwin compressor selection software', Version 3.0.

Carrier Corporation 2001, 'Open-Drive Compressors and 09RH Water-Cooled Condensers', Catalogue No. 510-505 for 5F,H.

Çengel, Y.A. and Boles, M.A. 2002, (4th ed), *Thermodynamics An Engineering Approach*. New York: McGraw-Hill Book Company.

Center for Energy and Environment 1998, 'Cost-effective energy efficient improvements for Minnesota's public ice arenas: overview of 20 options', Retrieved November 7, 2007, from http://www.mncee.org/ceedocs/ice_fact.pdf

CIMCO Refrigeration 2006, 'Ecosense Sense 500E and 1000E', Retrieved November 7, 2007, from http://www.cimcorefrigeration.com/ec_ecosense.asp

City of Montreal 2004, 'Bilan énergétique de l'aréna Camillien-Houde avec système a 4 passes', Internal report.

DOE-2 1982, 'Engineers Manual' Lawrence Berkeley Laboratory and Los Alamos National Laboratory.

Dumas, C. 1996, 'Energy-Saving Technology for Skating rinks', *Heating, Piping and Air Conditioning*, Vol. 68, pp. 127-135.

Dumas, C. 2004, 'Système frigorifiques des arrondissements de l'ancienne ville de Montréal - arrêt du système frigorifique la nuit', Internal report, Ville de Montreal.

Dumas, C. and Marcoux, C. 2004, 'Water temperature of montreal aqueduct', Retrieved November 7, 2007, from http://www.ashrae-mtl.org/text/f_babillard.html

Energyplus 2001, 'Engineering Document – The reference to EnergyPlus Calculations', The Ernest Orlando Lawrence Berkeley National Laboratory.

Environmental Protection Agency (EPA) 2007, *Ozone depletion glossary*, Retrieved November 7, 2007, from http://www.epa.gov/ozone/defns.html

Environnement Canada 2005, *Climate change overview: The protocol. The Green Lane: Climate change 2005*, Retrieved November 7, 2007, from http://www.ec.gc.ca/climate/kyoto-e.html.

Falcon, B. 2000, 'Dossier de conception de TEWI', Centre technique des industries aéronautiques et thermiques, France.

Friedman, S.J. and Homer-Dixon, T. 2004, 'Out of the energy box', *Foreign affairs*, vol. 83 p. 6.

Ge, Y.T. and Tassou, S.A. 2000, 'Mathematical of supermarket refrigeration systems for design, energy prediction and control', *Journal of Power and Energy*, Vol. 214(A) pp. 101-114.

Hittle, D.C. 1977, 'BLAST (The Building Loads Analysis and System Thermo-Dynamics)', Construction engineering research lab. Program. Volume II. Reference Manual.

Holman, J.P. 1997. (8th ed) *Heat transfer*, New York: McGraw-Hill Book Company.

Jolly, P.G., Tso, C.P., Wong, Y.W. and Ng, S.M. 2000, 'Simulation and measurement on the full-load performance of a refrigeration system in a shipping container', *International Journal of Refrigeration*, Vol. 23, pp. 112-126.

Klein, S.A. and Alvarado 1999, Engineer Equation Solver (EES), F-Chart Software.

Klein, S.A., Beckman, W.A., Mitchell, J.W., Duffie, J.A., Duffie, N.A., Freeman, T.L., Mitchell J.C., Braun, J.E., Evans, B.L., Kummer, J.P., Urban, R.E., Fiksel, A., Thornton, J.W., Blair, N.J., Williams, P.M., Bradley, D.E., McDowell, T.P., Kummert, M. and Arias, D.A. 2000, TRNSYS. Solar Energy Laboratory. University of Wisconsin-Madison. Version 16.01.002.

Koury, R.N.N., Machado, L. and Ismail, K.A.R. 2001, 'Numerical simulation of variable speed refrigeration system', *International Journal of Refrigeration*, vol. 4, pp. 192-200.

Larkin 2006, 'Condenser Fan Cycling', Retrieved November 7, 2007, from http://www.heatcraftrpd.com/resources/techtopics/Tech%20Topics%2061544E.pdf

Lavoie, M., Sunyé, R. and Giguère, D. 2000, 'Potentiel d'économies d'énergie en réfrigération dans les arénas du Québec', *Programme d'interventions en réfrigération dans les arénas du Québec(PIRAQ)*, Vol. 1.

Manish, M., Das, P.K. and Sarangi, S. 2006, 'Transient behaviour of crossflow heat exchangers due to perturbation in temperature flow', *International Journal of Heat and Mass Transfer*, Vol. 49 pp. 1083-89.

McQuay 2002, 'Series Chillers - What's old Is New Again' *Engineering system solutions*.

Natural Resources Canada (NRCan) 2003, 'Commercial and institutional building energy use survey 2000: Summary Report'.

Ng, K.C., Chua, H.T., Ong, W., Lee, S.S. and Gordon, J.M. 1997, 'Diagnostics and optimization of reciprocating chillers: theory and experiment', *Applied Thermal Engineering*, Vol. 17(3), pp. 263-276.

Outtagarts, A., Haberschill, P. and Lallemand, M. 1995, 'Comportement dynamique d'un évaporateur de machine frigorifique soumis à des variations de débit'. *International Congress of Refrigeration*, IIIa: 412-20. La Haye. Netherlands.

Ouzzane, M., Sunyé, R., Zmeureanu, R., Giguère, D., Scott, J. and Bellache, O. 2006, 'Cooling load and environmental measurements in a Canadian indoor ice rink', *ASHRAE Transactions*, Vol. 112(2), pp. 538-545.

Pacific Gas and Electric 2001, 'CoolTools: a Toolkit to Optimize Chilled Water Plants', San Francisco, CA, Retrieved November 7, 2007, from http://www.hvacexchange.com/cooltools/.

Patil, R., Zmeureanu, R. and Giguère, D. 2007, 'Computer modeling of cold storage under the concrete slab in ice skating rinks', Internal report. Centre for Building Studies, Department of Building, Civil and Environmental Engineering. Concordia University, Canada.

PRISM (PRInceton Scorekeeping Method) 1986, Princeton University.

Scott, J. 2003, 'Ultrasonic Chiller Validation: Liquid flow vs. Refrigerant Flow', Seminar 19, ASHRAE Winter Meeting, Chicago.

Sreedharan, P. 2001, 'Comparison of Chiller Models for use in Model-Based Fault Detection'. Master Thesis. University of California.

Sreedharan, P. and Haves, P. 2001, 'Comparison of Chiller Models for use in Model-Based Fault Detection', International Conference for Enhanced Building Operations, Austin, Texas.

Statgraphics, 2006, Centurion XV Version 14.2.00, StatPoint. Inc.

Tremblay, G. 2001, 'Nouvelles technologies destinées aux arénas', *Climapresse*, novembre-décembre.

United Nations Environment Program (UNEP) 2006, 'Handbook for the Montreal Protocol on Substances that Deplete the Ozone Layer'. Retrieved November 7, 2007, from http://ozone.unep.org/Publications/MP_Handbook/index.shtml

World Meteorological Organization (WMO) 1999, 'Scientific Assessment of Stratospheric Ozone', *Global Ozone Research and Monitoring Project*, Report No. 44.